IMPROVEMENTS IN TEST METHODOLOGY AND CHARACTERISATION OF LONG-TERM FLEXURE BEHAVIOUR OF FIBRE-REINFORCED CONCRETE

Aitor Llano Torre

DOCTORAL THESIS

Supervised by

Pedro Serna Ros, PhD.
José Rocío Martí Vargas, PhD.

UNIVERSITAT POLITÈCNICA DE VALÈNCIA

UNIVERSITAT
POLITÈCNICA
DE VALÈNCIA

DOCTORAL THESIS

Improvements in test methodology and characterisation of long-term flexure behaviour of fibre-reinforced concrete

by
Aitor Llano Torre

Supervised by
PhD. Pedro Serna Ros
PhD. José Rocío Martí Vargas

València, Spain
December 2022

A mi Madre (in memoriam).

Agradecimientos

Quisiera agradecer a mis directores de tesis doctoral Pedro Serna y José Rocío Martí todo su apoyo durante el largo proceso de desarrollo de este trabajo, tanto durante las campañas experimentales, como en el asesoramiento y revisión de este y el resto de los trabajos que hemos compartido. En especial a Pedro que durante estos 10 años ha sido como un padre y referente que me ha guiado e inculcado la pasión por el hormigón y las fibras. Gracias también por asumir el reto de dirigir el Comité Técnico de RILEM CCF-261 sobre fluencia que tanto me ha aportado. Asumir el rol de coordinador del comité técnico me ha permitido conocer a grandes profesionales del hormigón reforzado con fibras de todo el mundo y poder contribuir con mis aportaciones derivadas de la tesis doctoral de manera muy temprana y directa en el desarrollo y avance de una metodología de ensayo consensuada.

A mis compañeros del laboratorio y grupo de investigación Paco, Juanan, Emili, Marta(s) y Hessam entre otros, que siempre que han podido, me han ayudado con las amasadas, ensayos e interpretación de resultados. Les deseo mucha suerte tanto para culminar sus proyectos profesionales y académicos como en su vida personal ya que se merecen lo mejor. Gracias Dani por estar siempre disponible para ayudarme a configurar los *fieldpoints* y adecuarlos a mis raras peticiones para poder completar con éxito cada una de las complejas campañas experimentales de fluencia. Tu soporte técnico y personal han sido imprescindibles para mí.

A mis amigos doctores, que poco a poco han ido dando el salto de becarios a profesionales de la investigación y el hormigón. Gracias Pau, Sergio, Tati, Pablo, Yasna y Manolo, por compartir tantos almuerzos, risas y experiencias durante mi tiempo dentro y fuera del ICITECH. Un agradecimiento especial para Roberta, Vicente y Javi que empezaron siendo compañeros de laboratorio y acabaron siendo compañeros de todo y un soporte y apoyo esencial para poder culminar este proyecto personal. A Roberta por su labor policial recodándome en cada *deadline* que tenía que seguir avanzando y cumpliendo objetivos. A Vicente (*Lokris* and Matlab consulting) por animarme a adentrarme en el mundo de la programación en Matlab y LaTex que tanto me ha ayudado en la recta final del doctorado. A Javi (el *Traidor*) porque fue él quien me invitó a mirar por primera vez dentro de la amasadora para enseñarme cómo se cuece el hormigón. Desde ese día fuiste, conocido, compañero, amigo y hermano. Ojalá la vida nos vuelva a acercar y poder compartir más momentos juntos.

No puedo terminar mis agradecimientos sin acordarme de Carol, mi gran amor y más importante compañera de vida y mi mejor apoyo en esos momentos en los que uno pierde la esperanza y la confianza. Si bien, durante todo este tiempo he progresado y

evolucionado mucho en mi faceta profesional, muchos más logros destacables he conseguido en mi faceta personal de su mano. En todo este tiempo nos hemos casado, hemos formado nuestro hogar y hemos descubierto lo que es el verdadero amor incondicional gracias a nuestra hija Uxue. Muchas gracias a ellas y a mi familia que, desde la distancia, siempre han creído en mí.

A todos ellos, gracias.

Aitor Llano-Torre

Abstract

Creep testing methodology on fibre-reinforced concrete is a long and complex process involving multiple variables. On the one hand, creep testing parameters such as pre-cracking level and creep index or stress sustained level, as well as boundary and environmental conditions, can be found among other variables. Variations on these parameters, together with the intrinsic variability of FRC due to the random fibre distribution of FRC, have a significant impact on the experimental results obtained among the existent methodologies. The long duration of the creep test and the required space in the facilities laboratories as the environmental conditions to keep during the creep test entail a significant challenge and outlay in terms of both space and expense resources that have reduced the research investment on this topic. Thus, after an exhaustive analysis of the state-of-the-art and starting from an existent creep testing methodology, several experimental programmes were developed to assess the effect of main creep testing parameters and the influence of creep frame construction as well as different procedure steps on the experimental results when the flexure creep testing methodology is applied. This work intends to define test parameters focused on characterising the effect of creep in the service limit state (SLS), as well as to unify criteria and processes of creep test, developing a procedure that can be standardised.

On the other hand, it is difficult to understand what happens within the cross-section during the creep test beyond the crack opening variation. The stress redistribution within the cross-section during the creep test is still unknown. This work also aims to shed some light by studying both the evolution of the crack opening and the compressive deformations in the compressed concrete zone. Experimental campaigns have been designed to assess both the tensile (crack opening) and compression (compressive strains) creep simultaneously that, allow to determine the contribution of compressive creep in the concrete area in the delayed crack opening and to assess the evolution of the neutral fibre position of the cross-section during the flexure creep test duration.

In this context, the result of this PhD research is a new flexure creep methodology proposal able to characterise long-term behaviour in flexure of cracked fibre-reinforced concrete, as well as some valuable tools such as the creep database that will help to understand experimental results and to contribute to consider delayed deformations in the international standards in the service state limit design.

Resumen

El procedimiento de ensayo de fluencia es un proceso muy complicado, largo y que envuelve muchas variables. Por una parte, están las variables relativas al proceso de ensayo de fluencia como condiciones de contorno, condiciones ambientales, parámetros de ensayo como nivel de carga o prefisura inicial, entre muchos otros. Estas variables influyen ya de por si lo suficiente en los resultados experimentales obtenidos en los ensayos sumado a la variabilidad intrínseca del hormigón reforzado con fibras. La duración mínima requerida en este tipo de ensayos y el espacio físico necesario, así como asegurar las condiciones ambientales, supone muchas veces un importante reto y consumo de recursos y espacio, lo que ha frenado hasta ahora la inversión en investigación para abordar este tema. Para ello, tras un exhaustivo estudio del estado del arte y partiendo de una metodología a flexión existente, se han desarrollado varias campañas experimentales para evaluar el efecto de los parámetros básicos de ensayo, la construcción del bastidor y el análisis de los resultados experimentales obtenidos de aplicar la metodología. Con todo ello se pretende obtener parámetros de ensayo diseñados para caracterizar el efecto de la fluencia en estado límite de servicio, así como unificar criterios y procesos del ensayo diseñando un procedimiento que pueda ser estandarizado.

Por otra parte, existe la dificultad añadida de entender qué sucede dentro de la sección durante el ensayo de fluencia más allá de la variación en abertura de fisura. La redistribución de esfuerzos que se produce dentro de la sección fisurada durante el ensayo de fluencia a flexión es una incógnita. Este trabajo pretende también arrojar algo de luz estudiando tanto la evolución de la abertura de fisura como las deformaciones en la zona comprimida del hormigón. Se han diseñado campañas experimentales para evaluar simultáneamente las deformaciones de tracción (abertura de fisura) y las deformaciones de compresión (zona comprimida del hormigón) de modo que permitan evaluar tanto la contribución de la fluencia a compresión sufrida por la zona comprimida de hormigón en las mediciones de abertura de fisura como la evolución de la profundidad de la fibra neutra de la sección fisurada durante el ensayo a flexión.

En este contexto, el resultado es una nueva propuesta metodológica de fluencia a flexión consensuada y capaz de caracterizar el comportamiento a flexión de hormigones reforzados con fibra en estado fisurado, así como algunas herramientas como la base de datos de fluencia que ayudan a la interpretación de los resultados experimentales y puedan contribuir a la consideración de estas deformaciones por las distintas normativas internacionales en su fase de diseño.

Resum

El procediment d'assaig de fluència és un procés molt complicat, llarg i que embolica moltes variables. D'una banda, estan les variables relatives al procés d'assaig de fluència com a condicions de contorn, condicions ambientals, paràmetres d'assaig com nivell de càrrega o prefissura inicial, entre molts altres. Aquestes variables influeixen ja de per si prou en els resultats experimentals obtinguts en els assajos sumat a la variabilitat intrínseca del formigó reforçat amb fibres. La duració mínima requerida en aquesta mena d'assajos i l'espai físic necessari, així com assegurar les condicions ambientals, suposa moltes vegades un important repte i consum de recursos i espai, la qual cosa ha frenat fins ara la inversió en investigació per a abordar aquest tema. Per a això, després d'un exhaustiu estudi de l'estat de l'art i partint d'una metodologia a flexió existent, s'han desenvolupat vàries campanyes experimentals per a avaluar l'efecte dels paràmetres bàsics d'assaig, la construcció del bastidor i l'anàlisi dels resultats experimentals obtinguts d'aplicar la metodologia. Amb tot això es pretén obtindre paràmetres d'assaig dissenyats per a caracteritzar l'efecte de la fluència en estat límit de servei, així com unificar criteris i processos de l'assaig dissenyant un procediment que puga ser estandarditzat.

D'altra banda, existeix la dificultat afegida d'entendre què succeeix dins de la secció durant l'assaig de fluència més enllà de la variació en obertura de fissura. La redistribució d'esforços que es produeix dins de la secció fisurada durant l'assaig de fluència a flexió és una incògnita. Aquest treball pretén també llançar una mica de llum estudiant tant l'evolució de l'obertura de fissura com les deformacions en la zona comprimida del formigó. S'han dissenyat campanyes experimentals per a avaluar simultàniament les deformacions de tracció (obertura de fissura) i les deformacions de compressió (zona comprimida del formigó) de manera que permeten avaluar tant la contribució de la fluència a compressió patida per la zona comprimida de formigó en els mesuraments d'obertura de fissura com l'evolució de la profunditat de la fibra neutra de la secció fisurada durant l'assaig a flexió.

En aquest context, el resultat és una nova proposta metodològica de fluència a flexió consensuada i capaç de caracteritzar el comportament a flexió de formigons reforçats amb fibra en estat fisurado, així com algunes eines com la base de dades de fluència que ajuden a la interpretació dels resultats experimentals i puguen contribuir a la consideració d'aquestes deformacions per les diferents normatives internacionals en la seua fase de disseny.

Table of Content

List of Figures

Glossary

FRC	fibre-reinforced concrete
SyFRC	synthetic fibre-reinforced concrete
SFRC	steel fibre-reinforced concrete
FRS	fibre-reinforced shotcrete
FR-SCC	fibre-reinforced self-compacting concrete
CMOD	crack mouth opening displacement
CTOD	crack tip opening displacement
COD	crack opening displacement
δ	deflection
$CMOD_{pn}$	nominal CMOD in the pre-cracking stage
$CMOD_p$	maximum CMOD reached in the pre-cracking stage
$CMOD_{pri}$	elastic CMOD recovery when the pre-cracking test unloading process ends
$CMOD_{prd}$	residual CMOD 10 minutes after unloading in the pre-cracking stage
$CMOD_{ci}$	instantaneous CMOD immediately after reaching the reference load
$CMOD_{ci}^{10'}$	short-term CMOD deformation 10 minutes after reaching the reference load
$CMOD_{ci}^{30'}$	short-term CMOD deformation 30 minutes after reaching the reference load
$CMOD_{ci}^{15'}$	short-term CMOD deformation 15 minutes after the beginning of the loading process
$CMOD_{cd}^{j}$	delayed CMOD after j days in the creep test

$CMOD_{ct}{}^{j}$	total CMOD after j days in the creep test (sum of instantaneous and delayed CMOD)
$CMOD_{cts}{}^{j}$	total CMOD after j days in the creep test compensated by shrinkage
$CMOD_{cri}$	elastic CMOD recovery after unloading the creep test
$CMOD_{cris}$	elastic CMOD recovery after unloading the creep test compensated by shrinkage
$CMOD_{crd}$	delayed CMOD recovery 30 days after unloading the creep test
$CMOD_{crds}$	delayed CMOD recovery 30 days after unloading the creep test compensated by shrinkage
$\varphi_{CMOD,c}{}^{j}$	crack opening creep coefficient referring to creep stage at j days
$\varphi_{CMOD,o}{}^{j}$	crack opening creep coefficient referring to origin at j days
$COR^{j\text{-}k}$	crack opening rate between j and k days
$\varphi_{CS,c}{}^{j}$	compressive strain creep coefficient referring to creep stage at j days
$\varphi_{CS,o}{}^{j}$	compressive strain creep coefficient referring to origin at j days
$CSR^{j\text{-}k}$	compressive strain rate between j and k days
j	days of creep test
k	time lapse days of creep test
$CMOD_1$	crack mouth opening displacement of 0.5 mm
$CMOD_2$	crack mouth opening displacement of 1.5 mm
$CMOD_3$	crack mouth opening displacement of 2.5 mm
$CMOD_4$	crack mouth opening displacement of 3.5 mm
LOP	limit of proportionality
f_L	residual flexural tensile strength at the limit of proportionality (LOP)
$f_{R,1}$	residual flexural tensile strength corresponding to $CMOD_1$
$f_{R,2}$	residual flexural tensile strength corresponding to $CMOD_2$
$f_{R,3}$	residual flexural tensile strength corresponding to $CMOD_3$
$f_{R,4}$	residual flexural tensile strength corresponding to $CMOD_4$
$f_{PostCreep,R,2}$	residual flexural tensile strength corresponding to origin at $CMOD_2$
$f_{PostCreep,R,3}$	residual flexural tensile strength corresponding to origin at $CMOD_3$
$f_{PostCreep,R,4}$	residual flexural tensile strength corresponding to origin at $CMOD_4$
$f_{R,p}$	residual flexural tensile strength at $CMOD_p$
$F_{R,p}$	load corresponding to $CMOD_p$
$f_{R,c}$	stress applied during the creep stage
$F_{R,c}$	load applied to the specimen during the creep stage
F_L	load at the limit of proportionality (LOP)

F_1	load corresponding to $CMOD_1$
$F_{PostCreep,2}$	load corresponding to $CMOD_2$
$F_{PostCreep,3}$	load corresponding to $CMOD_3$
$F_{PostCreep,4}$	load corresponding to $CMOD_4$
t_{ci}	time duration of the loading process in the creep test
t_{cri}	time duration of the unloading process in the creep test
t_{crd}	time duration after unloading of the creep test in which recovery was registered (in days)
I_n	nominal creep index or stress level as a percentage of $f_{R,p}$
I_c	applied creep index or stress level as percentage of $f_{R,p}$ ($I_c = f_{R,c} / f_{R,p}$)
n_f	average number of fibres per cm^2 of fracture surface area (fibres/cm^2)
L	span between supports in flexural test
l_a	distance between support and nearest loading point in the flexural test
l_b	span between loading points in the flexural test
NA	neutral axis
NAE	neutral axis evolution
NA_{ci}	instantaneous neutral axis position when the sustained loading process ends
NA_{cd}^j	delayed neutral axis position at j days of creep test
r^2	goodness of fit
CV	coefficient of variation
LVDT	linear variable displacement transducer
UTM	universal testing machine
DAS	data acquisition system
RH	relative humidity

NOTE:

Flexure creep test procedure notations are defined only for crack mouth opening displacement (CMOD). Analogous notations may also apply to other procedures if CMOD is substituted by either crack opening displacement (COD) or deflection (δ).

Chapter 1.
Introduction

1.1. General approach

Actually, creep in the cracked state of fibre-reinforced concrete (FRC) is not considered in the design process of structural elements. The lack of knowledge about delayed deformations under sustained loading, together with the absence of a recognised standard methodology, hinder the consideration of creep in service limit state (SLS)

Although the interest of the scientific community in creep has recently increased, the large number of available methodologies (i.e., flexure, tensile, panels, structural elements…) do not provide enough knowledge or confidence to consider delayed deformations in the design codes of FRC structures. Due to such available methodologies, creep experimental results cannot be globally assessed, and conclusions cannot be stated. In addition, the long duration of the creep test and the required space in the facilities, together with the strict controlled environmental conditions required during the creep test, entail a significant outlay in terms of both space and resource expense that have reduced the research investment on this topic.

Creep testing methodology on fibre-reinforced concrete is a long and complex process involving multiple variables. On the one hand, creep testing parameters such as pre-cracking level and creep index or stress sustained level, as well as boundary and environmental conditions, can be found among other variables. It has been observed that variations on these parameters have a significant impact on the experimental results obtained among the existent methodologies. Moreover, considering the intrinsic variability of FRC due to random fibre distribution, it becomes a complex task to make any global assessment and obtain any valuable conclusion from such a maze of variable results. Hence, after an exhaustive analysis of the state-of-the-art and starting from an existent creep testing methodology, different experimental programmes were carried out to assess the effect of main creep testing parameters and the influence of creep frame construction as well as other procedure steps on the experimental results when the flexure

creep testing methodology is applied. This PhD work intends to define creep test parameters focused on characterising the effect of creep in the service limit state (SLS), as well as to unify criteria and processes of creep test, developing a procedure that can be standardised.

On the other hand, it is difficult to understand what happens within the cross-section during the flexure creep test beyond the crack opening variation. Although the direct tension creep test seems more appropriate to tensile behaviour characterisation, their experimental procedure is more complex than the flexure creep test. Nonetheless, despite being an easier procedure, flexure creep test results interpretation may be more complicated due to the combination of compressive and tensile forces. The stress redistribution within the cross-section during the flexure creep test is still uncertain. This work also aims to shed some light by studying both the evolution of the crack opening and the compressive deformations in the compressed concrete area. Experimental programmes were designed to quantify both the tensile (crack opening) and compressive (compressive strains) creep simultaneously to determine the contribution of compressive creep in the concrete area in the delayed crack opening and to assess the evolution of the neutral fibre position of the cross-section during the flexure creep test duration.

In addition, although creep behaviour is a long-term property of concrete, shrinkage deformations were not considered in the existent creep methodologies to date. Therefore, the shrinkage in flexure was registered in the experimental programmes to assess the shrinkage influence creep test results. As a result, a new procedure for shrinkage consideration in future creep test methodologies was developed and included in the proposed flexure creep methodology.

Furthermore, the wide range of fibres available in the industrial market for concrete reinforcement provides multiple and varied post-crack performances. This fact implies that creep behaviour shall be characterised for each fibre type and specific dosage hindering any global conclusion. The success of the previous creep database for reinforced concrete has been assessed. Therefore, the creation of an international flexure creep test database that could provide overall conclusions is proposed due to such parameters, variables and FRC matrix compositions.

This PhD research results from 7 years of deep study on the creep behaviour of cracked FRC. As a result, a unified flexure creep methodology is proposed to characterise the long-term behaviour of FRC in the cracked state, together with guidelines to consider both creep in compression and stress redistribution during the creep test. I hope this research contribution could significantly improve creep consideration in the following international codes for FRC structures design.

1.2. Objectives

This PhD work aims to help the scientific community better understand the complexity of the characterisation of the long-term behaviour of cracked FRC in flexure by

recommending a flexure creep methodology that could support future guidelines to consider creep in the design process of FRC structures.

The primary matter of this research work is not only to improve an existing procedure but to develop improvement towards a new creep experimental proposal for creep characterisation of fibre-reinforced concrete (FRC) in the cracked state considering all the available methodologies in the state-of-the-art. To this purpose, different experimental programmes in creep were defined and carried out to assess the most relevant variables (i.e. stress level, initial crack opening,…) and procedure variations (i.e. boundary condition, flexure configuration…).

As a result of the deep analysis done during this comprehensive experimental programme of the creep test methodologies available, significant improvements and recommendations are proposed in this PhD thesis regarding the methodological procedure, boundary conditions, creep frame construction and creep test result analysis.

In addition, significant contributions to the flexure creep knowledge were analysed for the first time. New aspects of flexure creep, like shrinkage deformations, the influence of compressive creep in the compression flexure zone and the long-term evolution of the neutral axis due to stress redistribution during the creep test, are studied.

The existence of a creep test methodology that could provide enough confidence in terms of long-term behaviour characterisation of FRC is needed. This methodology is a relevant contribution to the scientific community and the fibre industry: long-term behaviour of FRC understanding and prediction would provide valuable information to structural designers to include creep in lifetime FRC structures calculation.

1.3. Structure

This PhD thesis document is arranged into seven chapters ordered so the reader can go through the thesis evolution and understand the motivation of each specific experimental programme and its conclusions.

The present Chapter 1 defines the starting point of this work, introducing a general approach to the motivation, main objectives pursued with the experimental work and the structure of the document so that the reader can go through the scientific achievements.

The review and analysis of the state-of-the-art on FRC creep is deeply explained in Chapter 2. It focuses on the assessment of different existent creep testing methodologies. Moreover, a brief introduction of the FRC material properties and composition is given. All the methodologies available on creep (i.e., flexure, tensile, panels, structural elements…) are assessed and compared to seek and define relevant parameters of FRC long-term behaviour under sustained load.

Chapter 3 describes the current flexure creep methodology and gives the reader a starting point to understand the proposed improvements. Equipment, frame construction, and initial assumptions for the creep characterisation of FRC are presented.

The scope of Chapter 4 is to experimentally assess and define all the significant parameters for SLS creep characterisation in flexure. Parameters such as initial crack opening damage (pre-crack level) and creep index ratio defined as the applied stress during the long-term test are studied. Experimental creep test programmes destined to assess each variable are fully described, and conclusions are exposed. In addition, the influence of procedure variations, such as recovery capacity after unloading, apparatus and boundary conditions construction, procedure timing or creep test setup, are analysed towards a unified procedure and equipment proposal.

Improvements in creep characterisation from experimental results are described in Chapter 5. Guidelines are proposed to consider shrinkage and compressive creep in the experimental creep results. Moreover, it was assessed that exists a stress distribution in the cracked section during the flexure creep tests, and thus, the neutral axis position varies in time during the flexure creep tests. The creation of flexure creep in cracked state database creation is also proposed.

As a result of this PhD work, a flexure creep test methodology of FRC in the cracked state is proposed and defined in Chapter 6. Procedure guidelines and creep test parameters are defined for each stage of the proposed methodology.

Finally, general conclusions and future research proposals are addressed in Chapter 7. Most relevant findings derived from this PhD work are collected, providing valuable tips and knowledge on flexure creep characterisation. Future research proposals define the paths to follow in the research on flexure creep in the cracked state.

The document concludes with the relevant bibliographic references and the Appendixes where the experimental programmes carried out and the obtained results are presented in depth.

Chapter 2.

State of the Art: Review and analysis

This chapter deals with the deep analysis of the state-of-the-art regarding the fibre-reinforced concrete (FRC) creep testing methodologies in the cracked state found in the scientific literature. In addition, a brief introduction about the FRC material composition, characterisation and most extended industrial application is given to understand the evolution of this PhD research work.

2.1. Fibre-reinforced concrete (FRC)

FRC is a composite material characterised by a concrete matrix with discrete fibres randomly distributed in the fresh concrete matrix. Fibres provide an enhanced post-cracking tensile residual strength [1] to FRC that depends on factors such as fibre material, dosage, aspect ratio, length, or shape. The introduction of FRC material in construction has been a fact for many years [2]. FRC is commonly used for industrial slabs-on-ground pavements [3,4], suspended elevated slabs [5,6,7], or precast elements such as tunnel lining [8,9,10] or pipes [11]. FRC is also suitable for thin structural elements like shells [12] since the dispersion of fibres provides tensile strength in all directions.

FRC can be used as unique reinforcement or combined with traditional rebar reinforcement. In those cases where FRC is combined with longitudinal reinforcement, it is common to use fibres as a partial substitution of steel rebars in highly reinforced sections, crack control due to plastic shrinkage [13] and even durability enhancement [14] of the structural elements.

2.1.1. Concrete matrix composition

Fibres not only modify concrete matrix properties in the hardened state but also in the fresh state. Fibres are poured into the mixer and randomly distributed during the mixing

process. Therefore, some additional considerations should be regarded in the FRC concrete matrix design process.

The use of fibres may reduce workability depending on fibre type and length as well as fibre dosage. The use of second-generation superplasticiser is then highly extended. Superplasticiser dosage shall be done according to the fibre dosage: the more fibres added, the more superplasticiser dosage shall be considered. This fact will provide workability enough for pouring concrete. Indeed, it is common to provide self-compacting properties to FRC mixes, called fibre-reinforced shelf-compacting concrete (FR-SCC). In addition, the maximum aggregate size (MAS) shall be limited according to the fibre length to allow a proper dispersion of fibres in the concrete matrix in the fresh state. It is recommended to use aggregates sized from 1/2 to 1/3 of fibre length to improve the workability and no greater than 32 mm.

Fibre properties will also have an incidence of the FRC response. On the one hand, fibre shape (i.e., straight, hooked-end, crimped…) will directly affect the concrete matrix bond properties. Figure 1 shows typical shapes of fibres used for concrete reinforcement. On the other hand, fibre materials have significant mechanical properties that directly affect the short- and long-term performance of FRC. Although there is a wide range of materials for fibres (i.e., steel, carbon, synthetic fibres, glass, natural fibres…), so far, the most used materials for structural elements of FRC are steel and synthetic fibres such as polypropylene or polyethylene. The use of glass fibres is not as extended but increases thanks to the alkali-resistant glass fibres. Steel fibres have a high modulus of elasticity (200 GPa) and tensile strength (MPa) suitable for concrete reinforcement providing ductility to the FRC matrix. On the contrary, synthetic fibres have a low modulus of elasticity (10-15 GPa) and tensile strength of about 640 MPa. However, synthetic fibre deformation is quite influenced by temperature and climatic conditions. Mechanical properties of glass fibres range between steel and synthetic fibres, with 80 GPa of elastic modulus and 2600 MPa tensile strength. In the case of glass fibres for concrete reinforcement, alkali-resistant glass is required to reduce fibre degradation in the concrete matrix and improve the durability of FRC. The choice of fibre material for concrete reinforcement depends on the final application.
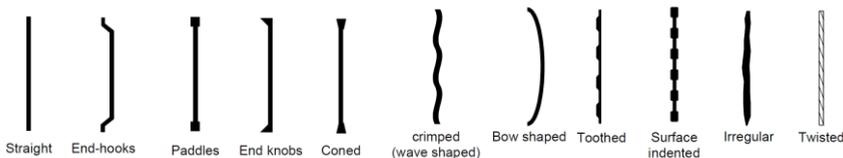
Figure 1. Typical shapes of fibres used for concrete reinforcement [15].

It is essential to highlight significant differences in the density of these materials. Whereas the density of steel is near 7800 kg/m^3, the density of propylene and glass is 900 and 2500 kg/m^3. This factor has an impact on fibre dosage since the required number of fibres may differ a lot depending on the fibre material and, consequently, concrete

workability in the fresh state. Therefore, fibre dosage is usually reported in terms of volume percentage instead of weight per cubic meter.

Fibres are classified according to their length in micro-fibres (typically from 12 to 19 mm) and macro-fibres (typically from 38 to 50 mm). Although micro-fibres provide an optimal response to the formation of plastic shrinkage cracks [13], they cannot provide any resistance to larger cracks caused by drying shrinkage and structural loads, as seen in Figure 2. However, micro-fibres are regularly specified in any type of concrete to improve cracking resistance, spalling protection, freeze-thaw durability and improve the homogeneity of concrete during the placement process. Although macro-fibres can also provide resistance to plastic shrinkage, they will provide enhanced durability to concrete matrix, toughness, and the ability to provide limited structural capacity in either flexure [16] or shear [17] when adequately designed. The dosage of either micro- or macro-fibres shall be done according to the FRC application. The use of hybrid fibre-reinforcement (both micro- and macro-fibres) is extended for ultra-high-performance fibre-reinforced concrete (UHPFRC), providing enhancement for both micro- and macro-crack propagation [18]. Nevertheless, in the case of UHPFRC with high fibre dosages, the concrete matrix requires specific improvements of the concrete matrix composition and therefore, the long-term behaviour of UHPFRC is out of the scope of this PhD thesis study.
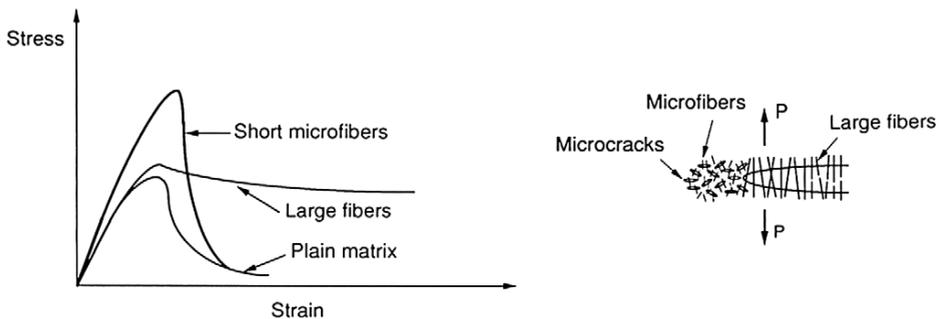
Figure 2. Performance differences among plain concrete and FRC with micro- and macro-fibres [2].

2.2. Mechanical properties

When FRC is subjected to tensile or bending stresses, the concrete matrix initially provides a reduced tensile capacity. Once the tensile strength (f_{ct}) of the concrete matrix is exceeded, concrete cracks and fibres provide a residual tensile strength ($f_{R,k}$) to FRC material using an either bond or pull-out mechanisms depending on the fibre type, material and shape.

Although FRC has been used in construction for many years, structural design codes and standards recently included this composite material in designing codes. In 2010, the Model Code 2010 [19] included the fibre contribution in the FRC mechanical

performance in Chapter 5. Hereafter, the ACI 544 committee also included FRC mechanical characterisation guidelines [20] as well as the recently published Código Estructural [21] provided guidelines for FRC characterisation and design in Spain based on Eurocode 2 [22]. Unfortunately, no international codes provide guidelines for considering FRC creep in the cracked state in the design of the structural elements.

2.2.1. Characterisation

The mechanical properties of FRC are determined by performing a flexure beam test under either the three-point bending test (3PBT) as recommended by RILEM TC162-TDF [23] or the four-point bending test (4PBT) setup as prescribed by ASTM C1609 [25]. The Model Code 2010 [19] recommends the EN 14651 [26] procedure with notched specimens under 3PBT to obtain nominal values of the material properties. This test is also prescribed by Código Estructural [21] and EC2 [22] to assess FRC mechanical properties. The use of notched specimens significantly decreases the scatter of experimental data compared to unnotched flexure tests.

The EN 14651 [26] method indirectly evaluates the tensile behaviour of FRC, considering the areas below the diagram of the applied force (F) versus the deformation. Although both midspan deflection (δ) and crack mouth opening displacement (CMOD) can be used as references for the diagram, the deformation is generally expressed in terms of CMOD measured at the bottom face of the notched specimen. A typical Load-CMOD diagram for FRC obtained is given in Figure 3 as a reference. This test method determines the limit of proportionality (LOP) and the equivalent residual flexural tensile strengths $f_{R,j}$ at different CMOD values. The most relevant residual strengths, $f_{R,1}$ and $f_{R,3}$, are obtained at $CMOD_1$ (0.5 mm) and $CMOD_3$ (2.5 mm), respectively. These CMOD values are related to the service limit state (SLS) and the ultimate limit state (ULS).
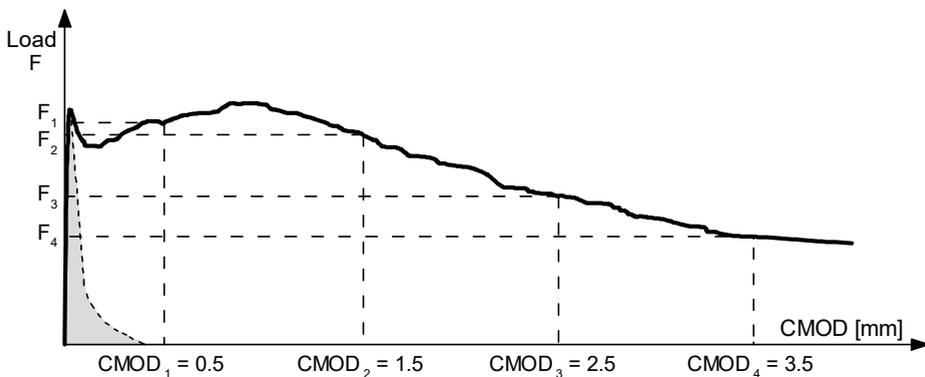
Figure 3. Typical load F–CMOD diagram for FRC compared to plain concrete [19].

In post-crack behaviour, international standards define two possibilities depending on softening or hardening behaviour. Post-crack hardening FRC behaviour is obtained

when the residual strength increases with deformation, whereas in post-crack softening behaviour, the residual strength decreases when deformation increases. The Model Code 2010 [19] defines simplified post-cracking constitutive laws considering the post-crack behaviour, as seen in Figure 4, depending on the ultimate tensile strength (f_{Ftu}) referred to the serviceability tensile strength (f_{Fts})
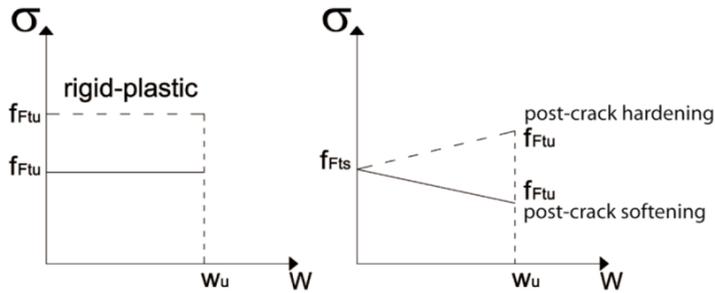
Figure 4. Model Code 2010 simplified post-cracking constitutive laws: stress-crack opening (continuous and dashed lines refer respectively to softening and hardening post-cracking behaviour) [19].

Model Code 2010 [19] classifies the residual performance of FRC according to their post-cracking residual strength, assuming a linear elastic behaviour. To this purpose, the characteristic flexure residual strength values for serviceability ($f_{R,1}$) and ultimate ($f_{R,3}$) conditions are considered. The residual performance is then classified using alphanumeric code where the first number represents the residual strength $f_{R,1}$ achieved, and the subsequent letter defines the residual strength ratio ($f_{R,3}/f_{R,1}$), providing valuable information about either the softening or hardening post-cracking behaviour. In this way, for an FRC matrix classified as 2d, the residual strength $f_{R,1}$ ranges between 2.0 and 2.5 MPa and slight hardening behaviour with $f_{R,3}/f_{R,1}$ ratio between 1.1and 1.3.

2.2.2. Long-term properties

The knowledge of the long-term response of FRC is essential to ensure long-term performance and safety. Although the short-term structural performance of FRC has been deeply studied and is widely known, the long-term behaviour of the FRC, especially in the cracked state, is still uncertain. To date, a standardised test procedure for FRC creep in the cracked state has not yet been developed. Hence, it is one of the main issues hindering the prompt FRC introduction in structural applications. In addition, although the research on creep in the cracked state has increased in recent years, there is not yet a clear consensus on how to characterise this phenomenon experimentally and consider creep in the design process.

The concrete matrix starts degradation with the curing process after casting. The volume of concrete changes during the hardening process due to the hydration of cement and the concrete drying process with the loss of water in the paste. Concrete shrinkage is defined as the change in length over time per unit length. Shrinkage deformation is

time-dependent and includes plastic shrinkage, autogenous shrinkage, and drying shrinkage, among others. Plastic shrinkage occurs in the first few hours of concrete pouring due to the evaporation from the surface of fresh concrete. It can be mitigated by sealing concrete with plastic and with a proper curing process. However, drying shrinkage occurs from 4-5 days in advance and may last for months and even years. In addition, when concrete is subjected to sustained load, creep deformation shall be considered together with shrinkage deformations, as defined in Figure 5.
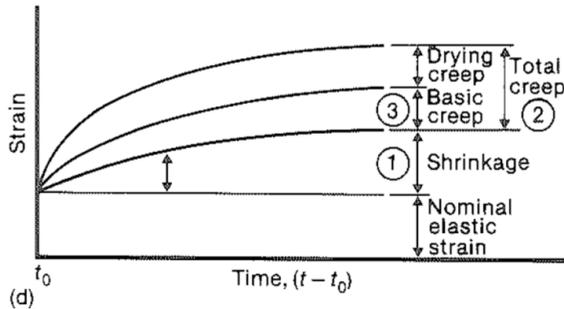
Figure 5. Long-term delayed deformations in concrete [27].

When FRC concrete is subjected to sustained stress, instantaneous deformation develops and gradually increases with time due to the creep of concrete, the creep of fibres and the debonding of the fibre-matrix interface. In the early creep stage, after the initial loading, creep develops rapidly, and the creep rate increase is slowed down with time. It is thought that about 50% of the final creep develops in the first 2–3 months, and about 90% develops after 2–3 years. ACI defines creep as the time-dependent deformation suffered by concrete under sustained load. Creep deformation shall develop in three stages before the material fails, as seen in Figure 6. In the primary creep stage, delayed deformation increases, but stabilisation in time of deformations can be observed and is expected. When the delayed deformation rate does not stabilise, the secondary creep stage starts, and the deformation rate keeps constant without stabilisation. In the tertiary creep, delayed deformations increase rapidly until specimen failure. In standard conditions and to accomplish with service limit state (SLS), the primary stage shall not be exceeded, reaching a stabilisation of deformations in time. Time-dependent deformations shall be assessed in uncracked and cracked states to ensure SLS conditions during the FRC structure lifetime.
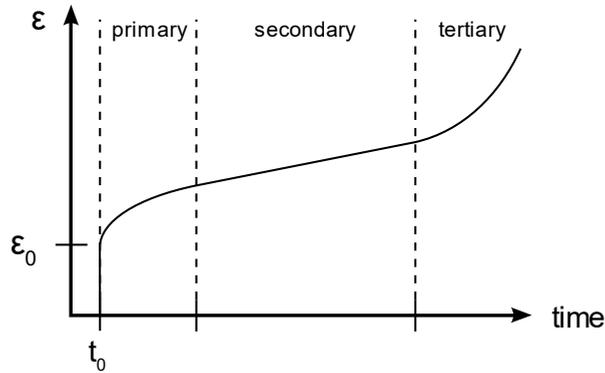
Figure 6. Creep stages in concrete before failure [27].

Compressive creep and shrinkage (uncracked state)

Compressive creep in concrete has been usually characterised by ASTM C512-02 [28] standard, as seen in Figure 7, where a compressive load is sustained in time into three specimens stacked. The applied load shall not exceed 40% of the ultimate compressive load (F_c). Together with the compressive creep test, it is recommended to measure drying shrinkage deformations of concrete by monitoring strain evolution in an unloaded specimen. Alternatively, the standard EN 12390-17:2019 [29] has been published recently, which defines a similar procedure to the ASTM standard for compressive creep and shrinkage. Although these standards were developed for plain concrete, they are also used for creep in compression characterisation in FRC specimens.
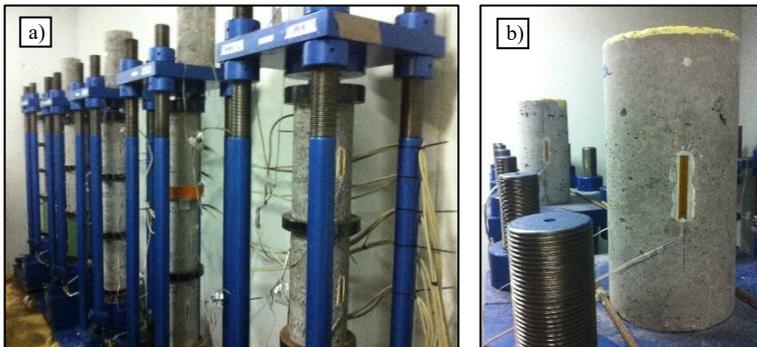
Figure 7. Creep in compression frames (a) with shrinkage specimens (b) located over the creep frame [30].

It is commonly accepted that fibres do not affect into compressive creep behaviour of FRC compared to plain concrete since the matrix is still uncracked due to the low compressive stress level. The ACI Committee 544 [20] suggests that adding less than 80 kg/m³ (1% in volume) of steel fibres in the FRC matrix does not induce any effect on

compressive creep. However, some authors [31] found on experimental tests that compressive creep and shrinkage decreased with steel fibre content. Two series of steel fibre-reinforced concrete (SFRC) with 0.38% and 0.76% of fibres were tested under sustained compressive load and compared to the plain concrete series. The stress level applied was near 20% of the ultimate load. It was noticed that after 400 days, creep deformations decreased up to 12% for those specimens reinforced with fibres compared to plain concrete specimens. Nevertheless, to date, compressive creep and shrinkage of FRC are assessed by the same testing methods as plain concrete. The effect of fibres on compressive creep and shrinkage is usually disregarded when typical fibre dosages are used and considering the expected stress level at ULS.

Ageing and embrittlement

Another aspect of the long-term properties of FRC is the concrete matrix ageing and embrittlement. It has been proved that the residual performance of FRC decreases over time. Some studies [32-35] performed short-term tests in standard and high-strength FRC prismatic specimens. Although most fibre types did not report changes in residual performance over time, some fibre types exhibited significantly lower post-crack performance at high deformations compared to characterisation tests at 28 days. Therefore, the ageing effect shall be considered in the design process since the in-service conditions of use and exposure conditions regarding potential corrosion may affect the durability of FRC structures.

The Round-Robin Test (RRT) in creep in the cracked state recently organised by the RILEM TC 261-CFF [30] included the ageing effect assessment. To this purpose, in parallel to the creep test, short-term tests were carried out at different ages (0, 180 and 360 days of creep test) to assess any variation in the residual performance. These tests revealed no significant differences at high deformations for the two FRC types reinforced with either steel or synthetic fibres. However, a substantial increase in terms of LOP was reported. Nonetheless, since all specimens subjected to creep tests were pre-cracked at 28 days, any effect of ageing was considered in the creep tests.

Long-term properties in the cracked state: tensile and flexure creep

Due to the increased interest in FRC creep in the cracked state [36], many studies have focused on the long-term FRC behaviour [37] in the cracked state. To this purpose, multiple methodologies were developed [38-43] depending on the stress applied. However, when the creep of FRC in the cracked section is analysed, several factors influence the long-term behaviour. It was reported [44] that factors such as bond, fibre creep, fibre pull-out or fibre material may affect FRC long-term response in the cracked state. In addition, in the case of flexure creep tests, it is not yet clear how compressive creep of the top zone affects the crack opening evolution. Hence, it is not easy to advance on this topic due to the influence of so many factors and the absence of any standardised methodology on creep in the cracked state.

The knowledge of long-term properties of FRC in the cracked state is still limited due to the absence of a standardised methodology that makes it really complicated to compare results between the studies published and hinders any global conclusion. Multiple methodologies for flexure and tensile load regarding creep frame construction, procedure, and creep consideration have been developed. Many studies focused on varied aspects like the influence of the type of fibre [46], the fibre-concrete bond and fibre pull-out [47] or environmental conditions [48]. In addition, some publications lead on how to consider the effect of creep on the verifications of SLS [49], whereas others focused on creep rupture in ULS [50]. Such variations in objectives and procedures add more variability to creep behaviour assessment and make it more difficult to compare experimental results. Therefore, there is no clear consensus on how to experimentally characterise the creep phenomenon and the influence of such variables. I.e., as reported in the RILEM TC 261-CCF round-robin test (RRT) [51], although participants agreed on the creep test parameters such as stress and pre-cracking levels before the RRT execution, significant differences were found among participants due to creep frame construction, creep test setup, and both boundary and environmental conditions.

It is generally accepted that the FRC creep in the cracked section shall consist of three main phases (pre-cracking, creep and post-creep phases), as depicted in Figure 8. During the pre-cracking phase, the specimen is tested to develop a defined initial crack width that serves as a reference for creep tests. Once pre-cracked, the specimen is moved to the creep rig and subjected to sustained load during the creep phase. When the creep test is finished, the specimen is tested again until failure to assess the influence of sustained load on the residual performance.
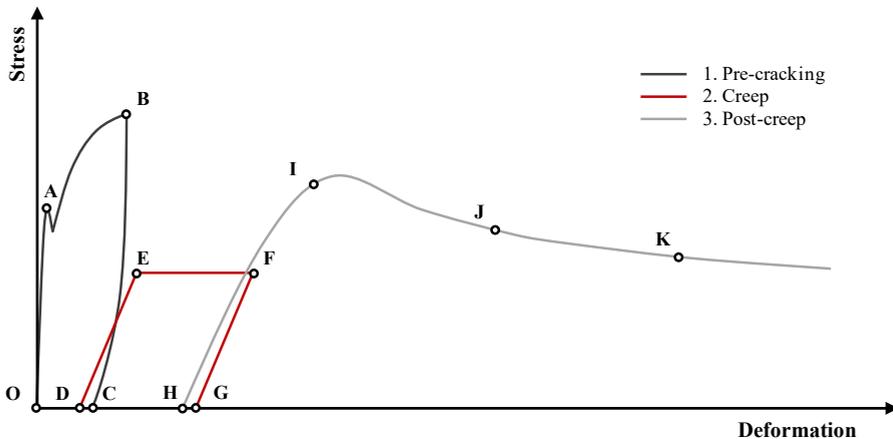
Figure 8. Creep test procedure idealised curve containing three phases.

This three-step procedure is widely extended and accepted by researchers. However, many variables remain undefined, and procedures differ a lot among them besides similar structure due to significant differences in creep frame construction, boundary and

environmental conditions, instrumentation, methodological procedures, and the creep test variables such as stress level or pre-cracking level. This PhD work assesses and compares all the existent creep testing procedures towards a standardised creep test proposal that could help FRC long-term behaviour characterisation.

2.3. Creep testing methodologies for cracked FRC review

At the beginning and regularly during the PhD experimental work duration, exhaustive research of scientific publications in the most relevant repositories (Scopus and Web of Science) was conducted to assess and compare all the available methodologies on creep in the cracked state. The obtained items were sifted, searching the relevant publications based on methodologies of FRC creep in cracked state topic and disregarding those publications out of scope. As a result, the selected publications and personal files collected within the RILEM TC 261-CCF activity were used for this bibliometric study of the FRC creep in the cracked state state-of-the-art.

It should be noted that those publications referring to uncracked creep conditions of FRC long-term properties were not considered for this bibliometric study on creep testing methodologies of FRC in the cracked state. In addition, publications exclusively related to assessing the creep of fibres or fibre pull-out tests were neither included. Only publications related to FRC creep test with an experimental programme, systematic review, or modelling make up this study.

All testing methodologies are grouped (i.e., flexure creep, tensile creep, panel creep tests…) to be analysed in depth and compared with similar procedures to assess the most significant differences individually.

2.3.1. Bibliometric study

This bibliometric study is focused on publications regarding creep in the cracked state of FRC and the multiple available methodologies developed. In recent years, the interest in the creep of FRC in the cracked state has rapidly increased, as depicted in Figure 9. A total of 151 documents were published regarding the FRC creep in the cracked state topic from 1980 to July 2022. The number of publications about FRC creep has continuously increased during the last decade, as seen in Figure 9. This fact highlights the importance of this research topic nowadays.

The published documents investigated include journal articles, conference papers, reports, and books. As seen in Figure 10, conference papers (87 publications) followed by publication in peer-reviewed scientific journals (58 publications) comprises 96% of the available publications on FRC creep in the cracked state. In addition, four reports and two books [51, 52] can be found on this topic. It is worth mentioning that multiple PhD and MSc theses (10 and 4, respectively) related to this topic have not been included in this bibliometric study.
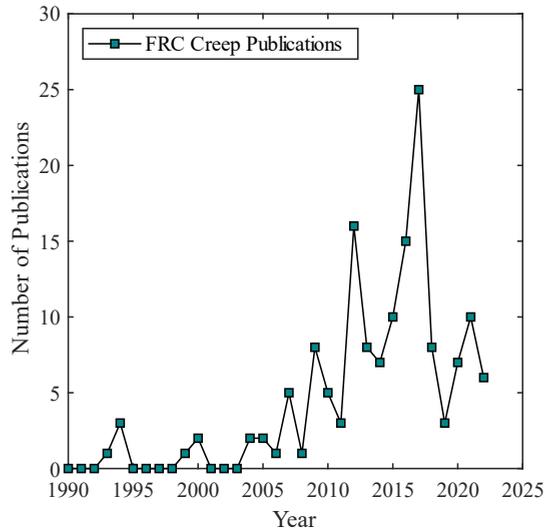
Figure 9. FRC creep in the cracked state publications from 1985 to July 2022.
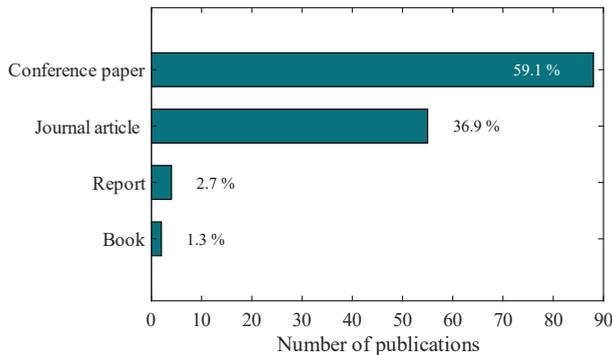
Figure 10. Types of published documents in FRC creep in cracked state topic.

The published bibliography can be arranged considering the reference test on which the methodology is based and the nature of the stress sustained in time, as shown in Figure 11. So far, most of the available publications (112) are related to long-term flexure creep tests in both prismatic specimens (68) and structural elements (44). The former aims to characterise the long-term properties of FRC material based on EN 14651 [26] standard procedure (or similar), whereas the latter seeks to assess the structural enhancement and performance of FRC elements usually combined with traditional longitudinal reinforcement. Secondly, 27 publications are reported related to tensile creep tests. Long-term tests carried out in panels are also reported, usually focused on fibre-reinforced shotcrete (FRS) properties: 12 publications comprised square panels creep tests, whereas only eight reported creep tests carried out in round panels. Some other publications (7) provide a review of either the structural effect of FRC creep [36],

15

creep methodologies [45] or factors influencing the long-term behaviour [44]. Although publications related exclusively to fibre pull-out tests were not included in this bibliometric study, some publications related to FRC creep experimental programmes also include long-term fibre pull-out tests [47]. In recent years, research on modelling the long-term behaviour of FRC has also increased, and five publications reported analytical models of creep in the cracked state.
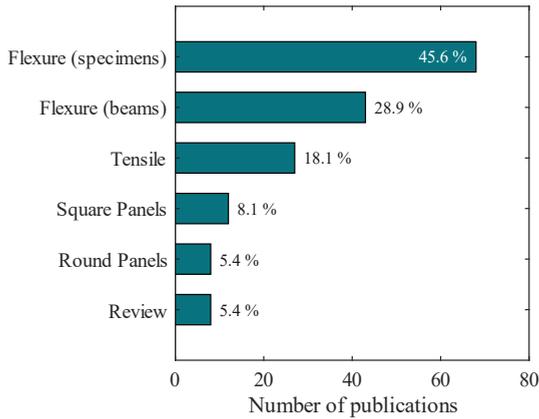
Figure 11. The number of publications arranged by methodology.

Besides the publications, the percentage of specimens tested per methodology was also obtained to assess the absolute impact of the different methodologies on the available experimental results. Thus, it was confirmed that the flexure creep test procedure on prismatic specimens is the most extended one comprising 60% of the specimens tested in cracked state creep (Figure 12). Publications related to the creep of structural elements represent only 10% of the specimens tested due to the larger size of the structural elements and more space and equipment requirements. Although the tensile
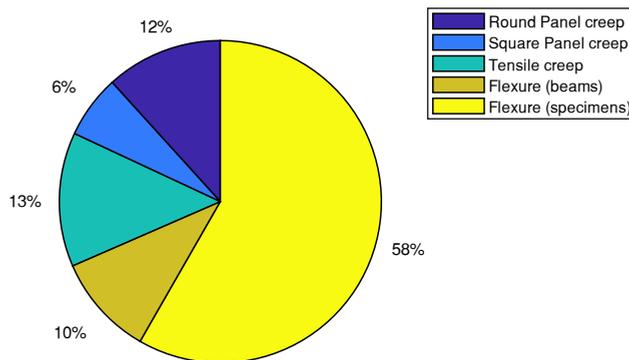
Figure 12. Percentage of FRC specimens tested in creep per methodology.

creep test comprises 16.6 % of the publications, it could be observed that, in absolute terms, it is the second methodology in tested specimens (13%). Such differences between flexure and tensile methodologies can be explained by the difficulties of the tensile creep test procedure [45]. Although the long-term performance is more suitable for FRC mechanical properties characterisation to obtain material laws, flexure methodology is easier to conduct. Finally, the specimens tested in creep using panel methodologies represent 6% and 11% for square and round panel specimens, respectively.

Standard FRC is used in most publications (78.8%) related to creep in the cracked state, as seen in Figure 13. Notwithstanding, different FRC matrices were also considered. The long-term behaviour of fibre-reinforced self-compacting concrete (FR-SCC) was assessed in 7.3% of the publications, whereas fibre-reinforced shotcrete (FRS) in 6.0%. The rest of the publications (8.7%) reported experimental programmes focused on high- or ultrahigh-performance matrix reinforced with fibres (i.e., UHPFRC, SHCC, ECC, HPFR, HSC-PFR…).
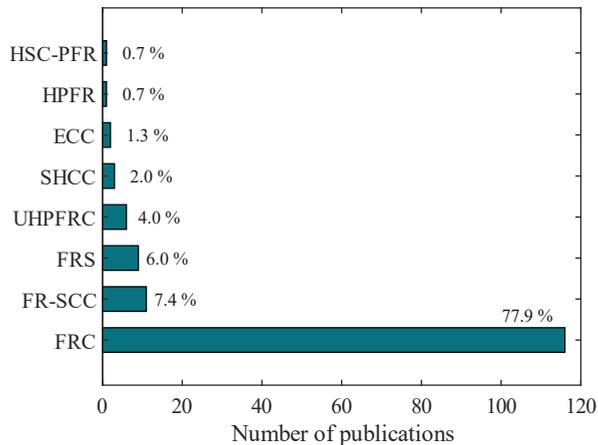
Figure 13. Tested FRC types reported in the studied literature (a); cast procedure and production of tested FRC reported in the literature (b).

Although most of the tested specimens in creep were cast (83.7%) in moulds, some studies present experimental results obtained from either sawed or cored specimens (10.2%). Some experimental programs studied the effect of fibre orientation due to matrix flow in flexure creep of prismatic specimens sawed from large FRC slabs [53]. In contrast, other studies carried out tensile creep tests in core specimens drilled from prismatic specimens used for flexure performance characterisation tests [54]. In addition, 6.1% of the specimens, usually both round and square panels, were sprayed (wet mix) into the moulds, as observed in Figure 14.
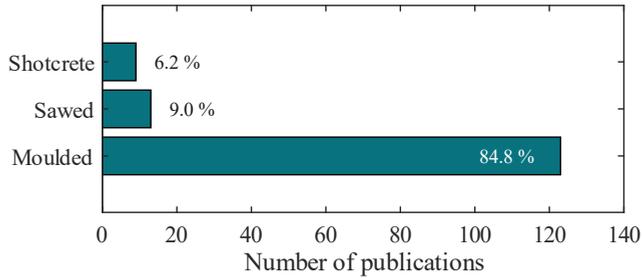
Figure 14. Fabrication method classification for FRC specimens.

A wide variety in terms of the shape and dimensions of the specimens was noticed when studying the bibliography. The classification of the specimen's shape reported in the literature is presented in Figure 15. The most tested specimen shape was prismatic, reported in 53.0% of publications, mainly related to flexure creep tests but also to tensile creep tests. A wide variety of specimen dimensions was also noticed within the prismatic specimens used for the flexure creep test. Structural FRC beams were reported in 23.2% of the publications, usually combining both fibre and traditional reinforcement but also with fibres as unique reinforcement. Some other structural element shapes, such as suspended slabs, slabs-on-ground and pipes, were also reported but represented a minor percentage of publications. Besides prismatic specimens, cylindrical cores and dog-bone specimens were used for tensile creep characterisation in 7.3% and 4.0% of publications, respectively. Publications related to creep tests in both square and round panels represent 7.9% and 5.3%, respectively.
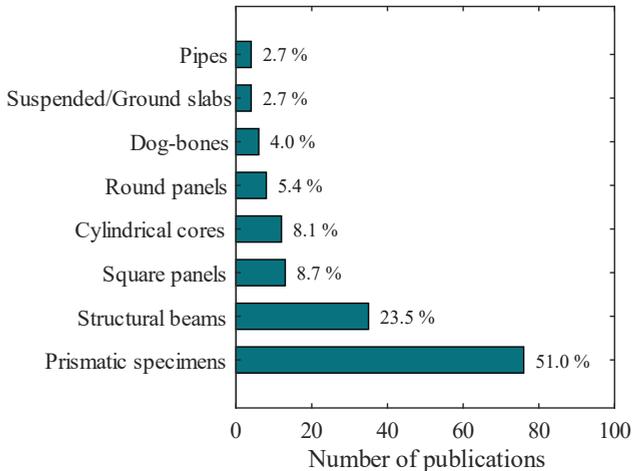
Figure 15. The shape of the specimens reported in the literature and significance in publications.

A summary of the FRC series reported and the number of specimens tested-in-creep in the cracked state is given in Table 1, arranged by methodology and fibre material. In total, 1091 FRC specimens were reported. It could be stated that the most fibre materials used for FRC creep tests were steel and macro-synthetic fibres, with 568 and 497 specimens, respectively. To date, scientific publications reported 34 specimens reinforced with glass fibres, whereas basalt fibres were used as reinforcement in only two specimens.

Table 1. Summary of publications, experimental programs bibliometric study.

Methodology	Publications	Exp. prog.	Series	Specimens				
				Total	Steel	Synthetic	Glass	Basalt
Flexure (spec.)	68	34	114	636	345	268	28	2
Structural el.	43	24	67	111	65	43	6	0
Direct tension	27	16	40	147	74	73	0	0
Square panel	12	6	19	69	36	33	0	0
Round panel	8	4	13	128	48	80	0	0
Total	–	90	253	1091	568	497	34	2

Specimens considering the fibre material and arranged by methodology are depicted in Figure 16. It can be observed that the use of most extended fibre materials (steel and synthetic fibres) is balanced for each testing methodology. However, it was noticed that the use of steel fibres is predominant in the case of structural elements. On the contrary, in the case of round panel tests, the use of macro-synthetic fibres in creep tests is predominant. Regarding glass fibres, most of the reported specimens reinforced with this material were tested in flexure using prismatic specimens and only a reduced percentage were used in structural elements. Basalt fibres represent a negligible percentage of flexure creep in prismatic specimens.
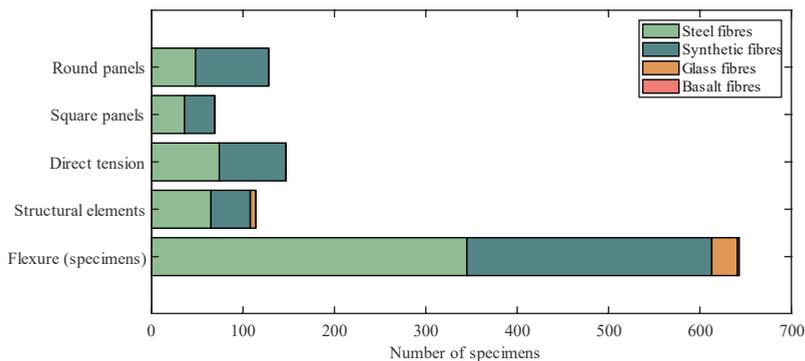
Figure 16. Fibre materials used for FRC reinforcement in specimens reported in the literature.

In conclusion, it can be stated from this bibliometric study of the available publications that many variables exist among publications on creep in the cracked state (i.e. FRC matrix composition, methodology, casting procedure, the shape of specimens, fibre materials…). In addition, the flexure creep test in prismatic specimens is revealed, so far, as the most extended procedure to characterise the long-term behaviour of FRC material. Hereafter, the available methodologies will be individually deeply assessed and compared.

2.3.2. Flexure creep

Although the flexure creep test on prismatic specimens and structural elements are both methodologies based on flexure, the nature and intention of procedures differ from material characterisation in prismatic specimens to structural characterisation in large-size specimens. This distinction implies significant differences in terms of experimental procedure and results. Therefore, these flexure methodologies are divided into short-beam tests and structural elements in this state-of-the-art analysis.

Short-beam flexure creep test: prismatic specimens

Many testing procedures were developed to characterise long-term behaviour in flexure. Flexure creep test methodology on prismatic specimens is, so far, the most developed methodology, as confirmed in Figure 11. This analysis comprises 68 scientific publications, including flexure creep test methodologies in short beams, where 35 experimental programmes were identified and carried out by 22 international laboratories. Although some procedures are pretty similar, this fact implies that exist 22 different methodologies in flexure. Table 2 resumes chronologically ordered the relevant information of reported publications grouped by experimental programmes. Certain publications (i.e. references 59, 60, 61, 62 and 63) were grouped in a sole row since these publications refer to the same experimental campaign. By this action, the number of specimens tested in creep that served as the basis for the publication and their conclusions could be approximately determined. In some cases, the grouped publications correspond to large experimental programs published in different journals or symposia, varying the assessment criteria. Alternatively, groups may appear in the case of long-duration experimental tests in which results were published at either different ages [64-67] or different programme steps, such as the RILEM Round-Robin Test [51, 110, 111]. Relevant data regarding specimen dimensions, the presence of the notch, reference deformation control, flexure setup in both pre-cracking and creep tests, frame construction, pre-cracking and stress level, environmental conditions and test duration are provided in Table 2. It is worth mentioning that only publications related to experimental tests on flexure creep were included in Table 2. Publications related to modelling flexure long-term behaviour [116, 117] without experimental tests and results were not included.

Dimensions of tested prismatic specimens vary significantly within the earliest flexure creep experimental programmes [55-58] from 1999 to 2004. However, when the

RILEM beam test EN 14651 was proposed in 2005, dimensions of specimens in flexure creep tests homogenised to 150×150 mm of cross-section, varying specimen length depending on the laboratory. In some cases, different dimensions were used due to the experimental programme requirements or equipment limitations. For instance, sawed specimens sized 60×60×200 mm were used by [53, 90-91] to study the influence of fibre orientation in creep, whereas in [96], the effect of beam width in the creep test was analysed, ranging from 50 to 150 mm. In the case of [97, 98], beams sized 75×225×700 mm due to creep frame limitations. Despite these variations in dimension, 72% of the flexure creep tests were performed in standardised 150×150 mm cross-section specimens where length ranges from 500 to 700 mm.

The use of a notch to localise a single crack at midspan is widely extended in flexure creep methodologies, where 80% of the experimental programmes reported notched specimens. It is noticed in German laboratories [67, 70, 106] the use of unnotched specimens following the DAfStb code for FRC [118] and the Austrian Society for Construction Technology ÖVBB [119] recommendations. Furthermore, some creep tests were performed without a notch when UHPFRC was used [89, 100, 105].Figure 17 resumes the most used deformations to control creep tests. Depending on the flexure test standard on which the creep test is based, it is chosen either CMOD (22 experimental programmes) or deflection δ (15 experimental programmes) as control deformation to assess the long-term behaviour of FRC. Since most flexure creep procedures are based on the EN 14651 standard, CMOD is revealed as the most used deformation to assess the long-term behaviour in flexure. In addition, some studies [77, 86, 89] reported that compressive strains and CMOD were registered simultaneously to determine the influence of compressive creep in the crack opening deformation. In some experimental programmes where a multi-specimen setup is chosen for creep tests [49, 76, 93, 96, 103], crack tip open displacement (CTOD) instead of CMOD is registered due to lack of space between specimens to locate the transducer at the bottom face of the specimen. As expected, no flexure creep procedure used crack opening displacement (COD) since this deformation is exclusively used in direct tension creep tests.
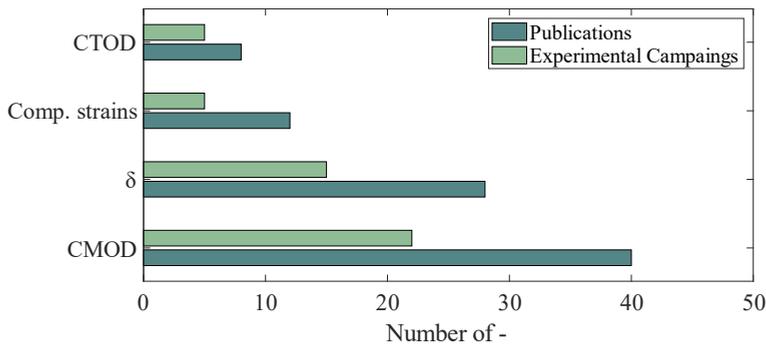
Figure 17. Deformations measured in flexure creep tests.

Table 2. Flexure creep experimental programmes in short beams.

Reference	Dimensions (mm)	Notch	Control	Pre-crack		Creep				Climate		Time
				Setup (span)	Stop (mm)	Setup	Frane	F transfer	l_c (%)	Temp. °C	HR %	(days)
[55]	150×200×700	Yes	δ	3PBT (600)	0.3; 0.6	3PBT (600)	Multi-	Hydraulic	70, 80	20	50	120, 200
[56]	150×200×700	Yes	CMOD, δ	3PBT (600)	0.3	3PBT (600)	-	-	60	-	-	360
[57]	100×100×350	No	δ	3PBT (300)	first crack	Cantilever	Single-	Lever arm	22-88	20	50	28
[58]	100×100×350	Yes	δ	4PBT (300)	first crack < 0.2	4PBT (300)	Multi-	Lever arm	20-80	NC	NC	420
[59, 60, 61, 62, 63]	150×50×500	No	δ	4PBT (450)	5	4PBT (450)	Single-	Dead load	50	-	-	4318
[38, 64, 65, 66, 67]	150×150×500	No	δ	4PBT (450)	1.75	4PBT (450)	Single-	Lever arm	50-80	NC	NC [5]	3200
[68, 69]	150×150×600	Yes	CMOD	3PBT (500)	0.2, 0.5, 0.8; 1.0, 1.5, 3.5	4PBT (450)	Multi-	Lever arm	37-105	NC	NC	630
[70, 71]	150×150×700	No	δ	4PBT (600)	0.5; 1.75	4PBT (600)	Multi-	Hydraulic	50, 60, 70	19	60	950
[72]	150×150×600	Yes	CMOD	3PBT (500)	3.5	3PBT (500)	Single-	Lever arm	13-122	-	-	254
[73, 74]	150×150×600	Yes	CMOD	3PBT (500)	0.2, 0.5, 1.5, 3.5	3PBT (500)	Single-	Lever arm	70-107	-	-	320
[75]	150×150×600	Yes	δ	4PBT (450)	0.2	4PBT (450)	Single-	Hydraulic	50	20	50	1836
[76]	150×150×550	Yes	CTOD	3PBT (500)	0.5	4PBT (500)	Multi-	Hydraulic	25-90	20	70	400
[39, 77, 78, 79, 80, 81]	150×150×600	Yes	CMOD, ε	4PBT (450)	0.5, 1.5	4PBT (450)	Multi-	Lever arm	60-95	20	50-70	90, 100, 140,300
[82, 83]	150×150×600	Yes	CMOD, ε	3PBT (500)	0.5	4PBT (450)	Multi-	Lever arm	90	20	60	90; 95
[84]	150×150×600	Yes	CMOD, δ	3PBT (500)	0.2, 0.5, 1.5, 3.5	3PBT (500)	Single-	Lever arm	22-140	NC	NC	273
[85]	150×150×600	Yes	CMOD, ε	4PBT (450)	0.5	4PBT (450)	Multi-	Lever arm	45	20	50-70	230
[86]	150×150×600	Yes	CMOD, ε	3PBT (500)	0.2, 0.5, 0.8, 1.2, 1.5, 2,0	4PBT (450)	Multi-	Lever arm	45	20	50-70	180
[87, 88, 89]	150×150×600, Yes 150×40×600, No		CMOD, ε	4PBT (450)	0.65; 50% stiffness	4PBT (450)	Multi-	Lever arm	50-86	20	50-70	270

Table 2. Flexure creep experimental programmes in short beams. (continue)

Reference	Dimensions (mm)	Notch	Control	Pre-crack Setup (span)	Stop (mm)	Creep Setup	Frame	F transfer	L_c (%)	Climate Temp. °C	HR %	Time (days)
[53, 90,91]	60×60×240	Yes	CMOD	4PBT (180)	0.3; 0.5	4PBT (180)	Multi-	Hydraulic	48-100	20	60	60
[92, 93]	100×100×700	Yes	CTOD	3PBT (500)	0.2	4PBT (450)	Multi-	Lever arm	30, 50	23	65	240
[54]	150×150×600	Yes	CMOD	3PBT (500)	0.5	4PBT (450)	Multi-	Lever arm	50	-	-	110
[94, 95]	150×150×600	Yes	CMOD, CTOD	3PBT (500)	0.2, 0.5	3PBT (500), 4PBT (450)	Multi-	Lever arm	13-109	21	NC	289
[96]	b×150×600[3]	Yes	CMOD	3PBT (500)	0.5	4PBT (450)	Multi-	Lever arm	55-74	23	NC	100
[97, 98, 99]	75×225×700	Yes	CMOD, δ	4PBT (600)	0.5, 0.7	4PBT (600)	Single-	Hydraulic	45-85	23	50	50
[100]	100×50×400	No	CMOD	4PBT (300)	1[2]	4PBT (300)	Multi-	Screwed	50, 60	20	40	28
[101]	150×150×600	Yes	CMOD	4PBT (450)	0.5	4PBT (450)	Multi-	Screwed	50	20	40	28
[102, 103]	150×150×600	Yes	CTOD	4PBT (450)	0.25, 1.5, 2.5	4PBT (450)	Multi-	Lever arm	50, 60	21-26[4]	50-70[4]	150
[104]	150×150×600	Yes	δ	3PBT (500)	0.5	3PBT (500)	Single-	Lever arm	50, 60	NC	NC	738
[105]	70×70×280	No	δ	4PBT (210)	0.6[2]	4PBT (210)	-	Lever arm	25-90	-	-	1.17
[106]	150×150×700	No	δ	4PBT (600)	0.5	4PBT (600)	Multi-	Lever arm	45-80	20	60	372
[49, 107]	150×150×600	Yes	CMOD, CTOD	3PBT (500)	0.05, 0.1, 0.2; 0.3, 0.5	4PBT (450)	Multi-	Lever arm	25, 35, 45	22	NC	180
[108, 109]	150×150×550	Yes	CMOD	3PBT (500)	0.5	4PBT (500)	Multi-	Hydraulic	30	20	50	30
[51, 110, 111]	150×150×600	Yes	CMOD, δ	3PBT (500)	0.5	3PBT, 4PBT[1]	Single-Multi-	Multiple	50	Variable	Variable	360
[112, 113]	150×150×600	Yes	CMOD	3PBT (500)	0.5	4PBT (450)	Multi-	Lever arm	50	20, 30, 40	50	300
[114]	150×150×700	Yes	δ	3PBT (500)	0.3	3PBT (500)	Single-	-	50	20	65	360
[115]	150×150×600	Yes	CTOD	3PBT (500)	0.3	4PBT (450)	Multi-	Lever arm	100	NC	NC	116

NC = not controlled; [1] five different 4PBT setups were used; [2] referred to deflection; [3] b = 50, 100 and 150 mm; [4] one series in uncontrolled conditions; [5] wrapped in aluminium foil.

A general rule of all experimental programmes on flexure creep in the cracked state is that all the specimens were pre-cracked before the long-term tests. Nonetheless, the absence of an agreed criterion for the pre-cracking process provides that the pre-cracking level differs significantly within the published experimental programmes from 0.2 to 3.5 mm crack width [69] and exceptionally up to 5 mm deflection [60]. This fact hinders any global comparison of the reported results. The histogram of pre-cracking levels used in reported experimental programmes, presented in Figure 18, reveals that the most extended pre-cracking level ranges from 0.3 to 0.5 mm, being 0.5 mm, corresponding to $f_{R,1}$. This threshold is consistent with the target of assessing the long-term behaviour of FRC in SLS. Within the large deformations, 1.5 and 3.5 mm are also commonly used as the pre-cracking levels to assess long-term behaviour in ULS.
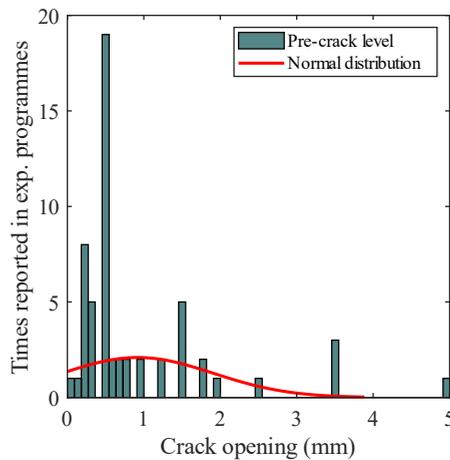
Figure 18. Pre-cracking level criteria in flexure creep experimental programmes.

The flexure setup used for the pre-cracking flexure test was either 3PBT or 4PBT. It is commonly used the 3PBT where the creep test methodology is based on EN 14651 standard. Hence, the pre-cracking 3PBT flexure setup was used in 62% of the experimental programmes, whereas 38% used the 4PBT flexure setup. Some laboratories [64, 70, 106] used 4PBT since their flexure creep methodology was based on the DAfStb code [118] instead of EN 14651. In contrast, other laboratories [85] justified the use of the 4PBT setup due to the location of strain gauges at the top face midspan of specimens to measure compressive strain evolution during creep tests.

On the contrary, regarding the long-term test under sustained load, the most reported flexure setup is 4PBT (79%), where only 21% of experimental programmes performed creep tests in 3PBT. The first studies in creep in the cracked state [55, 56] were carried out in 120×150 mm cross-section specimens using a 600 mm span 3PBT setup. However, the 3PBT setup defined by EN 14651 standard [26] in a 150×150 mm cross-section with a 500 mm support span was rapidly extended. Besides these 3PBT flexure

configuration possibilities, one laboratory [57] used a cantilever flexure setup where the specimen was clamped at one end and the load applied at the supporting point. Table 3 collects existent 3PBT flexure setups, together with the support span, the cross-section, the presence of the notch, and the reference to publications reported.

Table 3. Reported 3PBT creep flexure configurations.

The use of 4PBT setup for creep test is preferred when multi-specimen setup (85%) is reported. However, three laboratories [60, 67, 98] reported 4PBT flexure configuration in the single-specimen creep test setup. Although the 4PBT setup in the creep phase is more extended, many possibilities of 4PBT flexure setups were detected, as collected in Table 4. Variations in cross-section, notch, and both load and support span were detected among 14 different 4PBT setups.

Together with the flexure setup, it is important to notice the wide range of boundary conditions reported in the methodologies. The absence of any standardised creep test methodology implies that each laboratory developed its own support rollers and transfer plate systems. Although boundary conditions are not usually reported in publications, it could be possible to identify, thanks to provided pictures, that most of the studies (61% of experimental programmes) reported flexure creep tests with simple steel rollers as supports, as seen in Figure 19. On the contrary, the use of steel plates between specimens was only reported in 30% of the experimental programmes. However, some methodologies that reported steel plates used fixed steel rollers and supports, hindering any rotation. Only a few studies (22%) reported transfer steel plates, including constructed supports with certain degrees of freedom.

Table 4. Reported 4PBT creep flexure configurations.

Type	Creep flexural setup	Ref.	Type	Creep flexural setup	Ref.
4P-1		[58]	4P-9		[53, 90, 91]
4P-2		[59-63]	4P-10		[96]
4P-3		[38, 64-67, 51]	4P-11		[96]
4P-4		[68, 69, 39, 77-83, 85, 86, 92, 93, 96, 54, 101-103, 49, 107, 112, 113, 115, 51]	4P-12		[97, 98, 99]
4P-5		[70, 71, 106]	4P-13		[51]
4P-6		[75]	4P-14		[100]
4P-7		[76, 51]	4P-15		[105]
4P-8		[87-89]	4P-16		[108, 109]
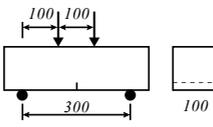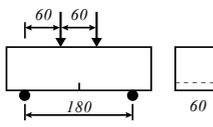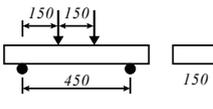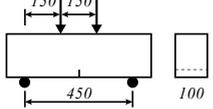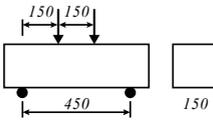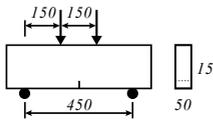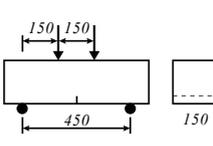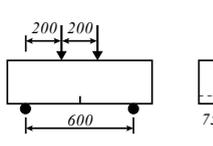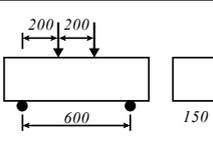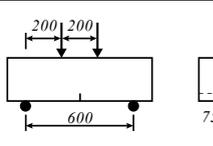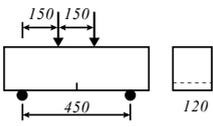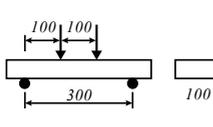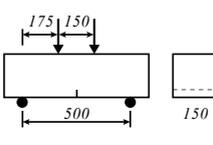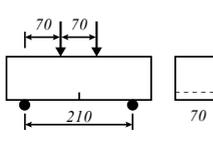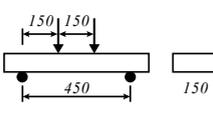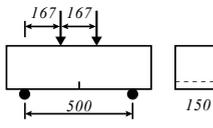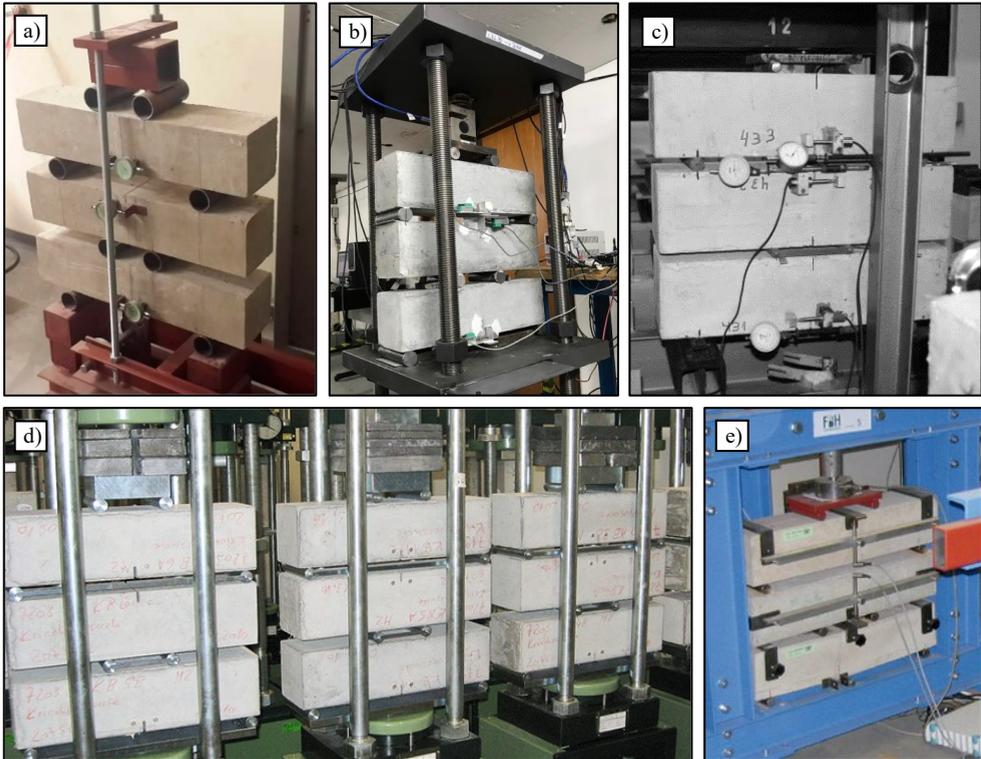
Figure 19. Simple steel rollers as support boundary conditions: a) [92], b) [108], c) [51], d) [76], e) [70].

The multi-specimen creep setup allowed to increase in the number of specimens tested simultaneously. This procedure is widely accepted since the creep test is a high-consuming resources methodology. By increasing the number of specimens tested, facilities, space and time were optimised, providing more experimental results at once. Hence, 66% of creep experimental programmes were carried out in a multi-specimen setup, and 34% of the experimental programmes were carried out in a single-specimens setup. Examples of single- and multi-specimen setups are presented in Figure 20.

The creep frame construction also noticed a wide variety of frames and load transfer systems. So far, the most extended load transfer system uses a second-degree lever arm (68%) to induce load through a multiplier factor depending on the lever arm length. Two possibilities can be found based on the lever arm position: *top lever arm* [54, 94], where compressive force is applied by laying on directly the lever arm on the top specimen or *bottom lever arm* [66, 77], where the load is transferred to the top specimen by tensile forces with steel bars. Both systems can be recognised in Figure 21. The *top lever arm* creep frame is reported in 33% of the experimental programmes that used the lever arm load transfer system, whereas the *bottom lever arm* in 67 %. The use of hydraulic jacks
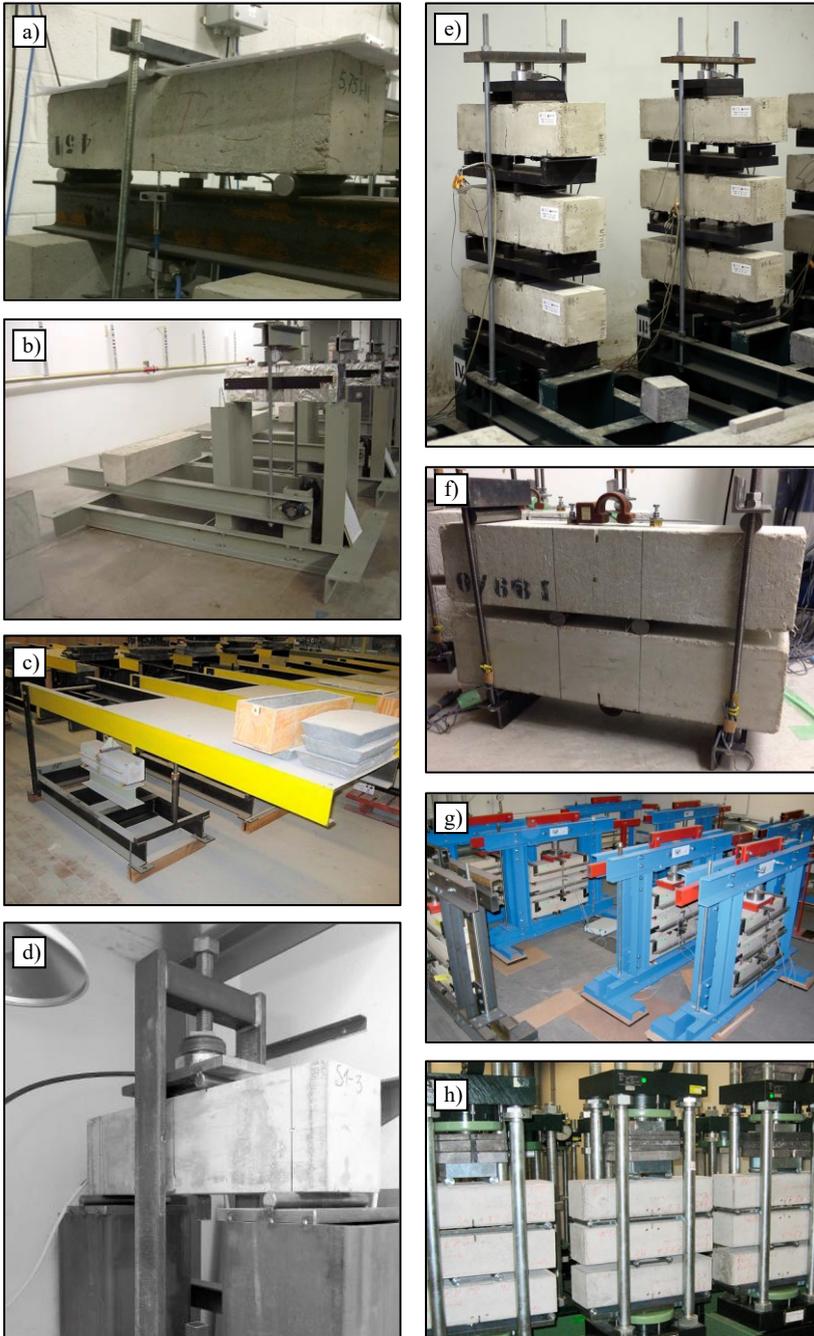
**Figure 20. Single-specimen setup: a) [51], b) [65], c) [104], d) [75].
Multi-specimen setup: e) [86], f) [51], g) [70], h) [76].**

to induce the load in creep frames [70, 76, 91, 98, 109] is the second extended load transfer system reported in 24% of the experimental programmes, followed by screwed bars [100] used to tighten one specimen against other reported in 9%. The use of dead load directly applied over the specimen [62] is only reported in one experimental programme having a negligible significance on the methodologies analysis.
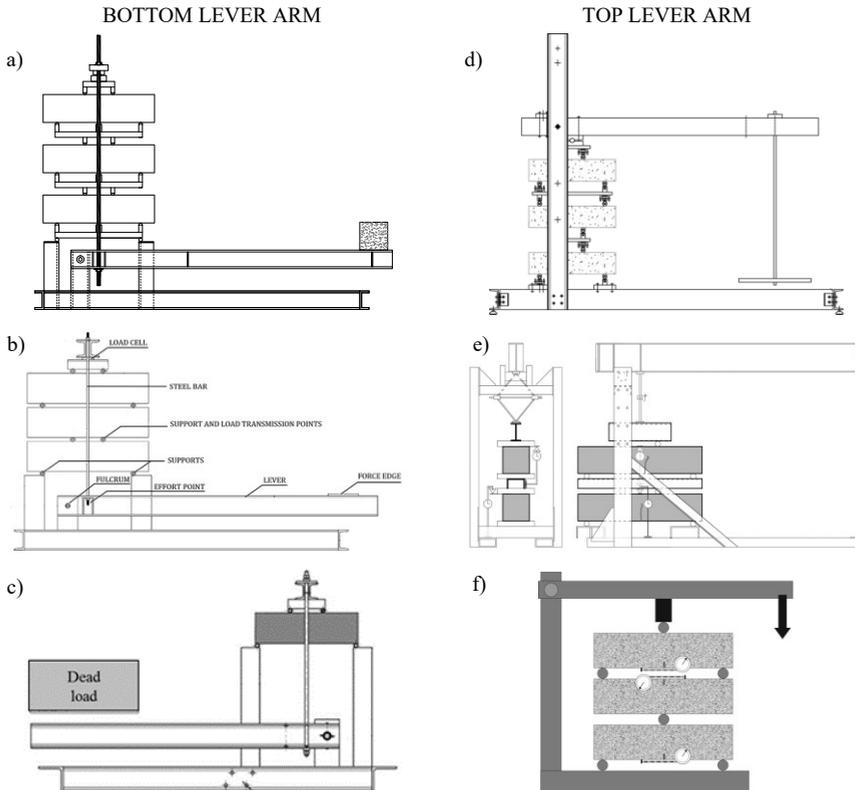
Figure 21. Bottom lever arm creep frame designs: a) [85], b) [103], c) [66]; Top lever arms frame designs: d) [112], e) [106], f) [94].

It exists a large variety in terms of creep test duration. Although Figure 22 depicts the histogram of test duration in days up to 1000 days, three experimental programmes exceeded this limit. Kanstad and Zirgulis [75] reported creep tests of 1836 days duration, Kusterle et al. [66] reported 3200 days-duration tests and Van Bergen et al. [104] 4318 days of sustained load for some series. However, the most common creep test durations are 90, 180 and 360 days corresponding to 3, 6 and 12 months-lapses. Although short-duration creep tests were also reported [105, 101, 57, 108, 53], conclusions of such short creep tests shall be carefully considered since secondary creep usually appears later.
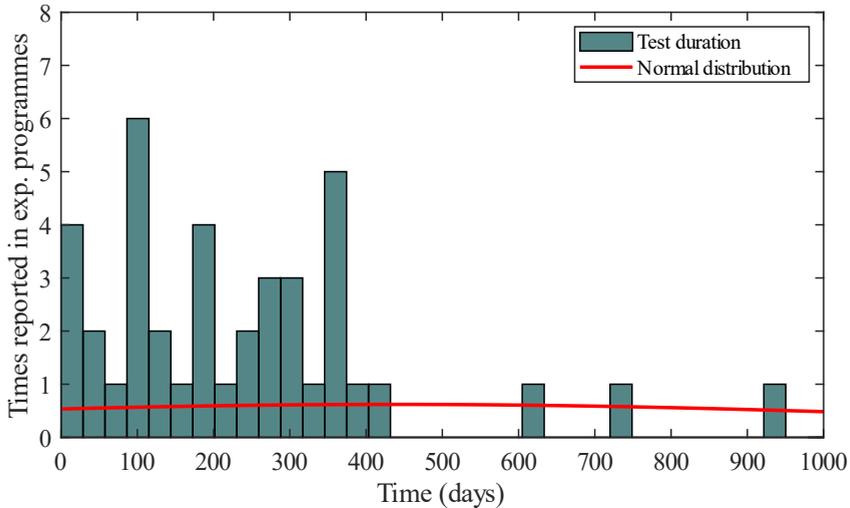
Figure 22. Duration of flexure creep test in days.

Environmental conditions during the creep test are the most controversial topic regarding creep test methodologies in the cracked state. Although it has been assessed that either temperature or relative humidity does not significantly affect the long-term behaviour of steel fibre-reinforced concrete (SFRC), they became relevant for synthetic fibre materials in that long-term performance is directly affected by temperature and humidity. However, many laboratories performed the long-term tests in uncontrolled environmental conditions: some laboratories [61, 102, 104] carried out creep test in ambient laboratory conditions, whereas others [58, 66] located creep frames in the laboratory basement to reduce temperature variation during the creep test. In addition, Kusterle et al. [66] wrapped specimens in aluminium foil to minimise the drying shrinkage of specimens during the creep test. Fortunately, near 70% of creep tests were conducted in a climate room where either temperature of RH could be controlled. Nevertheless, it is clearly stated that temperature control is easier than RH since some creep tests [79, 85, 86, 89, 103, 107] were reported in controlled temperature, but a considerable scatter in RH where it could be just restricted. Temperature is usually kept constant in values ranging from 19 to 25 ºC, being 20 ºC the most used temperature during the creep test. However, Del Prete et al. [112] varied temperature in 10 ºC steps during the creep tests to assess the influence of temperature on SyFRC long-term performance. On the contrary, RH conditions sustained in time ranges from 40 to 70 %, usually affected by the season where creep tests were conducted. Many studies reported both temperature and RH evolution with creep test results where the influence of environmental conditions can be stated if required.

Regarding the fibre materials used in flexure creep tests carried out in prismatic specimens, 28 experimental programmes included steel fibres (54.2% of prismatic specimens), whereas 22 experimental programmes included synthetic fibres (42.1%).

Glass fibres were reported as concrete reinforcement in 2 experimental programmes [85, 106] (4.4%), where basalt fibres were reported only once [75] with only two specimens.

Many variables were studied in the reported publications, as seen in Figure 23. Fibre type is the most used variable, reported in 25 experimental programmes, considering two or more different fibre types within the same experimental programme. The use of different stress levels to assess the long-term behaviour of the same concrete is reported in 21 experimental programmes [49, 70, 78, 93]. The pre-cracking level parameter was reported in 17 experimental programmes [49, 68, 84, 86, 102] that carried out pre-cracking tests up to different levels ranging from 0.05 to 3.5 mm. Some studies reported different fibre dosages instead of using different fibre types, whereas 6 experimental programmes considered different environmental conditions as creep test parameters. Finally, only one experimental programme [90] reported the fibre orientation factor as a creep test parameter.
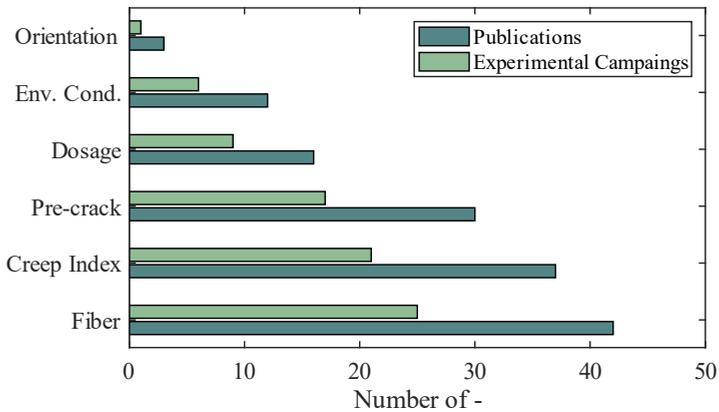
Figure 23. Variables studied in flexural creep methodologies publications.

Regarding the creep index parameter, although a wide range of stress levels was reported, the most frequent creep index ranges from 45 to 80% of the residual stress at pre-cracking, as seen in Figure 24. Within this range, 50% is the most used creep index in flexure creep tests carried out in prismatic specimens.

It can be concluded from this deep comparison of existent methodologies that exists a wide variability of experimental procedures in terms of flexure setup, long-term test setup, parameters, creep frame construction, environmental and boundary conditions, and test duration. Each experimental procedure provides conclusions that can only be compared to those specimens tested in similar conditions. Unfortunately, obtaining overall conclusions is not at all easy due to such procedure and conditions variations. It is then concluded that it is urgently required to develop an agreed procedure that could provide comparable results.
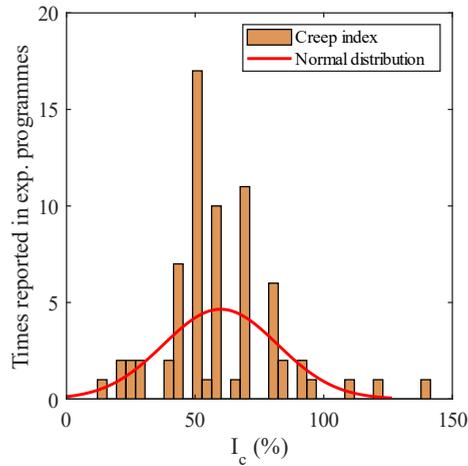
Figure 24. Variables studied in flexural creep methodologies publications.

Considering such variations among methodologies, the RILEM Technical Committee 261-CCF launched in 2015 an international Round-Robin Test [51] on creep in the cracked state to assess how comparable results were in agreed conditions. Both experimental results and methodologies [120] were deeply analysed, and it was found that the procedure of some of the participant laboratories provided comparable experimental results. On the one hand, among laboratories that performed creep tests in the 3PBT setup, it was detected that both labs provided similar long-term results due to procedure similarities. On the other hand, seven laboratories among ten participants that reported 4PBT setup in flexure creep tests were grouped into one cluster and identified as comparable procedures.

Structural elements flexure creep test

Long-term tests on structural elements are usually focused on the long-term durability of FRC structural elements. However, most studies reported experimental tests in either structural elements or beams reinforced with traditional rebars and fibres. Therefore, many studies assessed the contribution of fibres to long-term crack and durability control. Table 5 collects the reported experimental programmes in structural elements reinforced with fibres and the main parameters and variables of creep tests. As previously done in flexure tests on prismatic specimens, publications that report experimental results from the same experimental programme were grouped.

Table 5. Flexure creep experimental programmes in structural elements.

Reference	Element	Dimensions (mm)	Notch	Control	Pre-crack Setup (span)	Pre-crack Stop	Creep Setup	Span	Frame	Transfer	l_c (%)	Time (days)
[121]	Beam	100×176×2000	No	δ	4PBT (-)	-	4PBT	1920	Single-	Hydraulic	60	28
[122, 123, 124, 125]	Beam	100×125×2000	No	δ	Cracked when loaded	loaded	UDL[6]	1800	Single-	Dead Load	35, 50, 60, 65, 80	3678
[70, 71]	Slab[1]	3000×3000×150	No	δ	Central load	6.2 kN[4]	Central load	-	Single-	Hydraulic	50	780
[126]	Beam	150×250×3300	No	δ, ε	-	-	4PBT	3000	Single-	Spring	6.2 kN	280
[127, 128, 129, 130]	Beam	300×120×2000	Yes	w, δ	3PBT (800)	0.2	4PBT	1800	Single-	Dead Load	50	385
[131, 46]	Beam	300×120×2000	Yes	w, δ	3PBT (800)	0.2; 0.35	4PBT	1800	Single-	Dead Load	50	320
[132, 133]	Beam	300×120×2000	Yes	w, δ	3PBT (800)	0.5	4PBT	1800	Single-	Dead Load	50	240
[14, 134, 135, 136, 137, 138, 139]	Beam	250×250×3000	No	δ	Cracked when loaded	loaded	4PBT	2800	Multi-	Hydraulic	50	2160
[140, 141, 142]	Beam	150×280×3000	No	δ	4PBT (2800)	g+q[5]	4PBT	2800	Single-	Lever arm	39; 58	360
[143]	Slab	400×161×3700	No	δ	Cracked when loaded	loaded	UDL[6]	3500	Single-	Dead Load	30; 50	240
[144]	Beam	300×120×2000	Yes	w, δ	3PBT (800)	0.2	4PBT	1800	Single-	Dead Load	50	270
[145, 146]	Pipes	Ø600/900/1200 ×e×600/2400[3]	No	w, δ	-	first crack (~0.25 mm)	--	--	Multi-	Lever arm	65 kN/m/m	175
[48]	Beam	300×120×2000	Yes	w, δ	3PBT (800)	0.2	4PBT	1800	Single-	Dead Load	50	110
[147]	Beam	200×600×4000	No	δ	4PBT (3600)	0.1; 0.5	4PBT	3600	Single-	Hydraulic	60, 75, 90	64
[148]	Slab[2]	914×125×5000, 914×150×5000	No	w, δ	Cracked when loaded	loaded	UDL[6]	2300	Single-	Dead Load	50, 100	875
[149]	Beam	80×40×1200	No	δ	3PBT (500)	Peak	3PBT	1100	Single-	Lever arm	25; 35; 50	190
[104]	Slab	870×1500×40	No	δ	3PBT (-)	3 mm	3PBT	800	Single-	Dead Load	60	1967
[150]	Beam	150×150×2800	No	ε	-	-	UDL[6]	2600	Single-	Dead Load	30-45	210
[151]	Beam	100×200×2000	No	δ, ε	Cracked when loaded	loaded	4PBT	1800	Single-	Spring	67	300
[152, 153]	Pipes	1200×50×1200, 1500×63×1200	No	δ	Cracked when loaded	loaded	-	-	Single-	Lever arm	40, 50, 70	90
[154]	Beam	130×180×1800	No	δ	Cracked when loaded	loaded	4PBT	1500	Multi-	Lever arm	10, 40, 50, 70	469
[155]	Beam	200×260×3250	No	w, δ, ε	Cracked when loaded	loaded	4PBT	3050	Single-	-	40	90
[115]	Beam	200×250×3200	No	w, δ, ε	3PBT (3000)	0.3	4PBT	3000	Single-	Dead Load	100 (crack)	365

[1] slab-on-ground; [2] steel-deck-slab; [3] e = 76, 100, 121 and 127 mm; [4] related to SLS conditions; [5] pre-cracked at service load (g=q); [6] UDL = uniform distributed load.

33

It is worth mentioning that studies focused on modelling creep of beams [156, 157, 158] were not included in Table 5 since no experimental creep tests were reported and applied their developed model on already published studies [125, 136, 143] experimental results.

Although most of experimental programmes of structural elements (74%) were focused in FRC structural beams [121, 125, 131, 136, 141, 149, 115], experimental tests carried out on suspended slabs [143, 148] slabs-on-grade [70], and FRC pipes [145-146, 152-153] were also reported. Regarding creep tests on beams, a wide range of beam dimensions were reported from 1.2 to 4.0 m in length. The cross-section is also variable among reported experimental programmes according to beam size. Most of the studies out on beams used fibres as additional reinforcement to the traditional longitudinal rebars. Only a few studies [127-133] were conducted in FRC beams without steel reinforcement. Although the notch is usually used in prismatic specimens, the use of notched beams is rarely reported in beam creep tests. However, experimental creep tests on beams carried out in Bologna [127-133] reported a sawed notch in beams to localise crack propagation and measure delayed crack opening evolution together with deflection. Regarding slab creep tests, three experimental programmes [104, 143, 148] were carried out on suspended slabs, whereas Goosla and Rieder [70] tested in creep slabs-on-ground sized 3000×3000×150 mm with a sustained central load for 780 days. Altoubat et al. [148] tested two continuous spans of steel-deck slabs with a total length of 4.6 m and a clear span of 2.3 m, as seen in Figure 25.
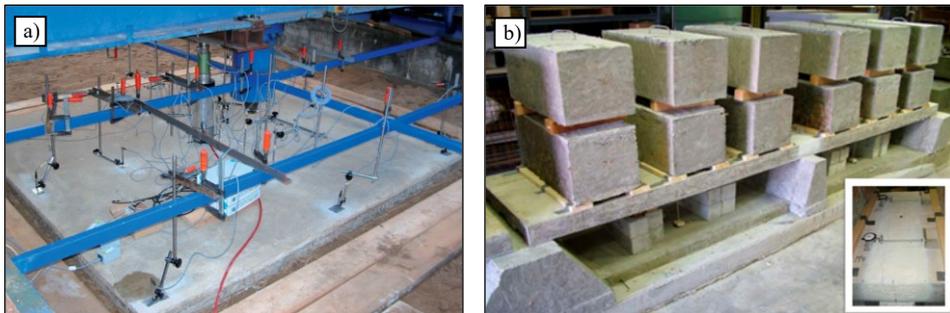
Figure 25. Creep test on slab-on-ground (a) by Goosla and Rieder [71] and steel deck slab (b) by Altoubat et al. [148].

Although the pre-cracking process of structural elements is not always reported, all tests were carried out in a cracked state since structural elements cracked during the sustained loading process [125, 134-139, 143, 148, 151-155]. Alternatively, some publications reported that specimens were loaded to the ultimate load to induce cracks and then reduced to the sustained service load [140-142]. Hence, the pre-cracking level was not controlled in terms of either crack opening or deflection but in load terms. Nevertheless, in those procedures that reported pre-cracking tests, the pre-cracking level ranged from 0.2 to 0.5 mm crack opening [127-133, 144] and 3 mm deflection [104]. In

addition, the pre-cracking test flexure setup corresponds, in most cases, to the flexure setup used in creep tests, where only a few studies [127-133, 149] reported a different flexure setup in pre-cracking tests than used in long-term tests. Due to the absence of a notch in most procedures to localise crack propagation and specific pre-cracking procedures, deflection is the most registered deformation to assess long-term performance on structural elements, as seen in Figure 26. Delayed crack opening evolution is reported in 9 experimental programmes, and either compressive or tensile strains were registered in 5 procedures.
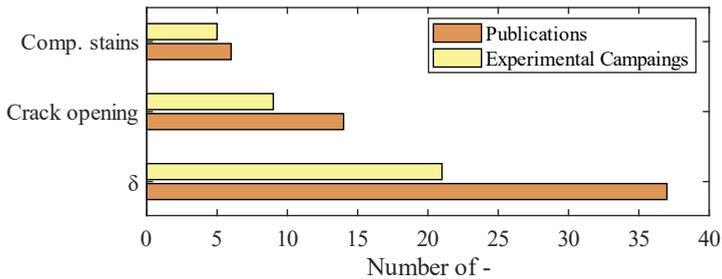
Figure 26. Deformations measured in flexure creep publications in structural elements.

The creep index is usually reported as a fraction of the ultimate load [143, 153] but is also referred to the pre-cracking load [115]. Moreover, some reported load levels in terms of service load: 6.2 kN in [126] or 65 kN/m/m [145, 146]. Although reported load levels are quite scattered, ranging from 10 to 100%, the most common load level range is 50-60%, as observed in Figure 27. Although most studies kept a constant load in time, some studies [i.e., 142, 147, 154] increased load level in steps during the creep test duration to assess the load level influence on delayed deformations.
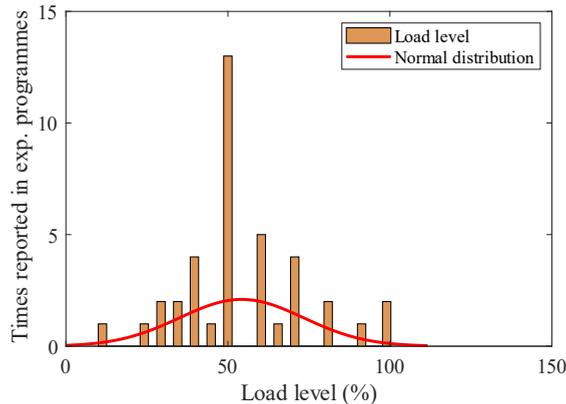
Figure 27. Histogram of load levels reported in structural elements creep experimental programmes.

Regarding the long-term test setup and creep frames, a 4PBT is widely extended in 57% of experimental programmes, followed by uniform distributed load (UDL) (17%) and 3PBT (9%). In the case of pipes, due to the singular shape of specimens, a three-edge bearing test setup [145-146, 152-153] was conducted in long-term tests. In contrast to flexure creep tests on specimens, using creep frames based on lever arm to transfer sustained load is not the most extended, only reported in 5 procedures. Figure 28 shows two creep frame samples for structural beams based on the lever arm. The most common load transfer system is concrete blocks dead load, reported inducing either 4PBT flexure setup [115, 128] or UDL [143, 148, 150] on beams and slabs 11 times. Hydraulic jacks [121, 70-71, 134-139, 147] or spring cassettes [126, 151] as sustained load transfer systems are less extended, reported 4 and 2 times, respectively, among experimental programmes.
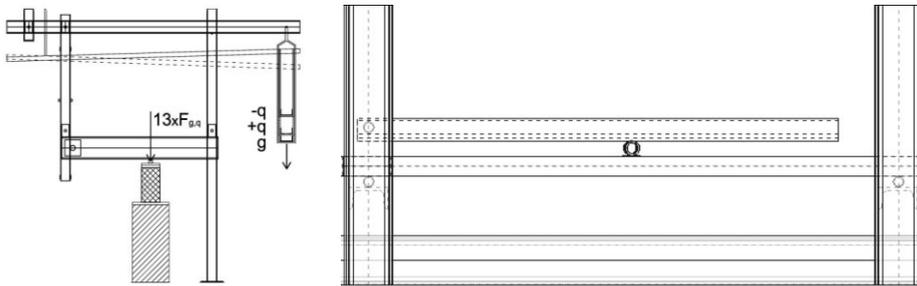
Figure 28. Lever arm frame for structural beams: [140] (left) and [149] (right).

Single-specimen setup is primarily chosen for 87% of the reported structural elements creep test programmes. Only three experimental programmes conducted multi-specimen creep tests in structural elements. Vasanelli et al. [136] reported long-term tests on five superposed beams (Figure 29 left), whereas Kassimi and Khayat [154] carried out creep tests on creep frames able to test two specimens simultaneously. Multi-specimens creep tests were also reported in pipes [146], where two pipes of 1.2 m length were tested aligned in the same creep frame (Figure 29 right).

Figure 29. Samples of multi-specimen creep test setup: 5 superposed beams (left) [135] and 2 aligned pipes (right) [146].

Although the duration of creep tests ranged from 28 days to 10 years, 48% of long-term tests usually lasted between 240 and 365 days. However, 22% of experimental programmes exceeded the average duration: Goosla [70] performed field tests on slabs-on-ground tests for 2 years; Althoubat et al. [148] carried out creep tests on steel-deck-slabs for 2.4 years, Van Bergen et al. reported test on slabs for 5.5 years; long-term tests on beams carried out by Micelli et al. [139] last 6 years and are still on-going; finally, Tan et al. [125] kept sustained load on beams during 10 years.

Many variables were studied in creep tests on structural elements. The most studied variable is the creep index, reported on 65% of the experimental programmes, as seen in Figure 30. Some studies [149] assess load level influence by loading identical beams at different load levels, whereas other publications [142, 147, 154] reported studies where the sustained load was increased in load-level steps during the creep test duration. Fibre type and pre-crack level variables, with 39% and 35%, respectively, are also quite reported.
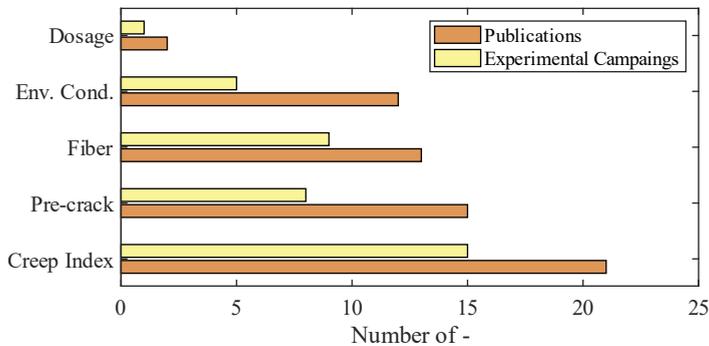
Figure 30. Variables studied in structural elements flexure creep methodologies publications.

Only a few studies of structural elements [126-133, 143, 147, 154] were reported in controlled environmental conditions, where 20-23ºC constant temperature and relative humidity 50-60% is reported. Due to the oversized shape of specimens and, consequently, the large size of creep frames, most studies were conducted in the laboratory ambient conditions instead of inside a climate-controlled chamber. In addition, field tests were reported in slabs-on-ground [70] and buried pipes [145-146] to assess in-site long-term conditions. Flexure field tests on beams [136] exposed to marine conditions were also reported to determine the long-term degradation of fibres and FRC performance.

As observed in this analysis, a wide variety of long-term methodologies are conducted on structural elements in terms of element shape, load setup and both pre-cracking and load levels. Therefore, general conclusions of long-term structural behaviour are hindered, as in creep tests on specimens. Although most studies concluded that using fibres reduced both long-term deflection and crack opening, no more useful quantitative conclusions can be stated.

2.3.3. Tensile creep

Direct tension creep tests are not as easy to perform as flexure creep tests [45]. Three main possibilities for specimen shape were detected among direct tension or tensile creep tests: dog-bones, cylindrical cores and prismatic specimens. The shape of the specimens may affect experimental results considering the corner effect in the fibre distribution during the casting process. Table 6 collects the main variables and creep test setups reported in tensile creep test publications. From 27 publications on the tensile testing procedure, five different procedures were observed in four international laboratories. Two tensile creep methodologies were developed by Boshoff et al. at Stellenbosch University: one based on SHCC dog-bones and the other based on FRC prismatic specimens. Casucci et al. developed one tensile creep methodology in TU Kaiserslautern based on dog-bones of UHPFRC. Both tensile creep methodologies developed in Leuven and Bologna tested cylindrical cores drilled from prismatic specimens to avoid the corner effect of fibre alignment.

One of the main issues is how the specimen is connected to the universal testing machine (UTM) to properly apply the tensile load without any bending effect by creating free hinges at both ends. In the case of dog-bones specimens, it is an easier task thanks to the holes in the specimens where the steel frame is connected to the specimen providing anchors to perform tensile tests. In the case of cast prismatic specimens, some authors developed a system where steel anchors were placed in moulds to provide hinges for tests. However, in the case of drilled cores, it was required to glue steel plates with hinges to both ends of the core using epoxy, which required additional tests to assess the feasibility of this system. Figure 31 collects anchor systems depending on the shape of the specimen.
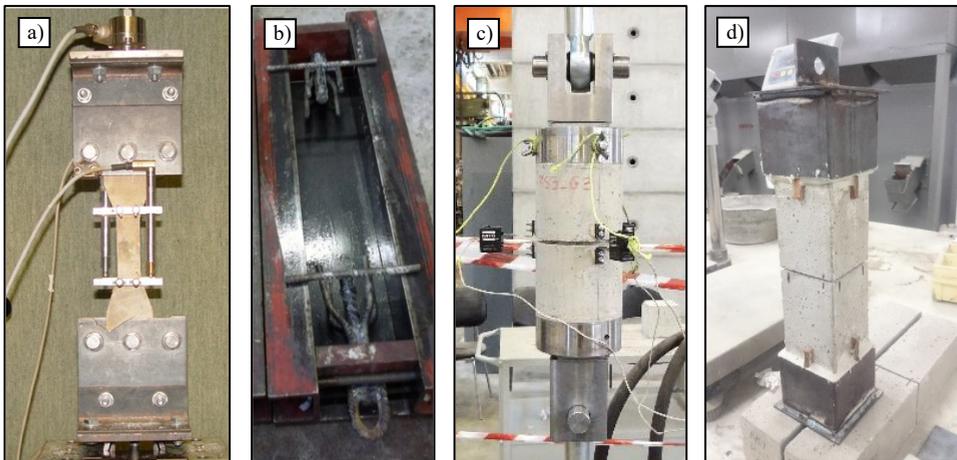
Figure 31. Systems developed to affix steel frames to specimens: a) dog-bones, b) cast anchor in prismatic specimens, c) glued steel frames with epoxy in cylindrical cores and d) glued with epoxy steel frames in prismatic specimens.

Table 6. Main variables of direct tension creep tests experimental programmes.

Reference	Specimen		Notch	Control	Pre-crack	Creep	Load transfer	I_c (%)	Climate		Time
	Shape	Dimensions (mm)			Stop (mm)	Frane			Temp. °C	HR %	(days)
[159]	Dog-bone	30×16×80	No	Strains	Uncracked	Multi-	Lever arm	50	23	65	240
[160]	Dog-bone	30×16×80	No	Strains	Uncracked	Multi-	Lever arm	50	-	-	
[47]	Dog-bone	30×16×80	No	Strains	1% strain	Multi-	Lever arm	30, 50, 70, 80	23	65	240
[161]	Prismatic	100×100×500	Yes	COD	0.5	Multi-	Lever arm	50	23	65	90
[162, 163, 164]	Core	Ø100×300	Yes	COD	0.05; 0.2	Single-	Lever arm	30	20	60	180
[165, 166]	Dog-bone	30×16×80	No	Crack width	Uncracked	Multi-	Lever arm	40, 50, 60, 80	23	65	50
[167]	Prismatic	100×100×500	Yes	COD	0.5	Multi-	Lever arm	70	23	65	46
[168, 169, 170]	Prismatic	100×100×500	Yes	COD	0.5	Multi-	Lever arm	30, 40, 50, 60, 70	23	65	240
[171]	Dog-bone	15×16×21	Yes	Crack width	Uncracked	Multi-	Lever arm	60	23	65	16
[54]	Core	Ø94×200	Yes	COD	0.2	Multi-	Lever arm	50	-	-	110
[172, 173, 174, 175, 176, 177]	Core	Ø100×300	Yes	COD	0.2	Single-	Lever arm	30, 45	20	60	270
[51, 110, 111]	Core; Prismatic	Ø94×200; 100×100×500	Yes	COD	0.2	Multi-	Lever arm	50	21; 25	55; 65	360
[178]	Prismatic	100×100×500	Yes	COD	0.53	Multi-	Lever arm	30, 50, 70, 85	23	65	240
[105]	Dog-bone	40×15×80	No	Strains	0.01% def.	Multi-	Lever arm	25, 40, 80, 90	-	-	1.17
[179]	Prismatic	100×100×500	Yes	COD	0.5	Multi-	Lever arm	30, 50, 70, 85	23	65	240
[112, 180]	Prismatic	Ø125×150	Yes	COD	0.3	Multi-	Lever arm	50	20, 30, 40	55	282

Crack control in the pre-cracking test is also tricky since specimens usually do not crack uniformly, and multiple transducers shall be located to obtain average values of crack opening. Although tensile creep test based on dog-bones measured strains as a reference of delayed deformation, methodologies on both prismatic and cylinders measured crack opening displacement (COD). In the case of prismatic specimens, an auxiliary frame is used to host two LVDTs at two opposite sides of the specimens. The average reading of both transducers provides the COD evolution in creep tests. Regarding cylindrical cores, two types of transducers are reported to measure COD during creep tests. Whereas some studies used COD clip transducers [54, 180], others used LVDTs [162-164, 172-176] crossing the notch. In both cases, three transducers are located around the specimen spaced 120º. Transducer location in different methodologies can be observed in Figure 32.
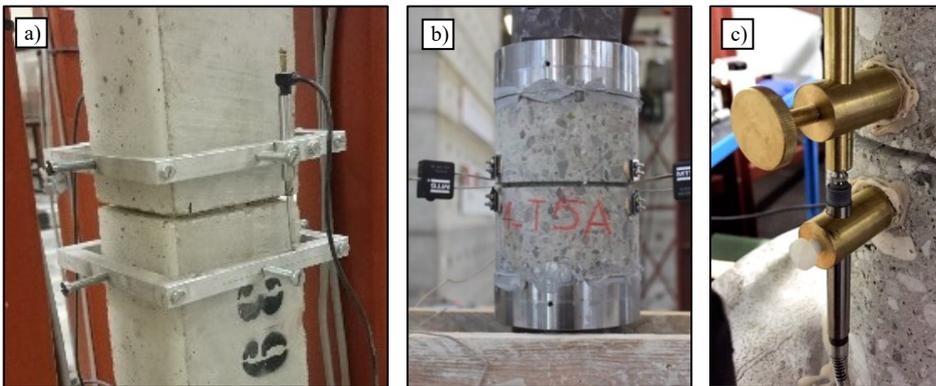
Figure 32. Transducers mounting system in tensile creep procedures: a) ancillary aluminium frames for LVDT [51], b) COD clip transducer around notched section spaced 120º [112], c) LVDT transducers glued around notched core [172].

Finally, once the specimen was pre-cracked, it became complicated to move the cracked specimen from the universal testing machine (UTM), where specimens were pre-cracked to the creep frames for long-term tests without influencing the crack opening. Although crack remains more stable in flexure specimens where the cross-section is not entirely cracked, in direct tensile pre-cracking tests, the whole cross-section of the specimens is cracked and is more sensitive to unexpected variations. Some studies [162-164, 172-176] used steel bars to fix temporary hinges to the steel frame to transport specimens to the creep frame. The same bars used for pre-cracking (noted as B in Figure 33) are tightened to fix the developed crack, ensuring a constant crack width. However, the additional weight of such steel auxiliary plates makes the specimen heavier; consequently, auxiliary lifting devices are required for transport.

Figure 33. Pre-cracking and hinge fixing system (left) and specimens placed in direct tensile creep frames (right) under sustained load [172].

First tensile creep experimental programmes reported in the literature were carried out in dog-bone specimens [159-47] using strain-hardening cementitious composites (SHCC), often referred as engineered cement-based composites (ECC). Further studies on tensile creep were also reported using dog-bone shape on SHCC [166, 171] or UHPFRC [105], always in a strain-hardening matrix with a multi-crack pattern. Although initially uncracked dog-bones were subjected to sustained load, some specimens cracked [159, 160] in the first minutes/hours of creep tests and developed more significant delayed deformations than uncracked specimens. In later experimental tests on dog-bones [171, 105], specimens were pre-cracked up to 1% strain before long-term tests. Tensile creep tests on standard FRC are only reported in either prismatic or cylindrical specimens, where control crack opening deformation (COD) is used instead of strain. Cylindrical cores are usually obtained from characterisation broken prismatic specimens. Specimens were pre-cracked to a defined COD ranging from 0.05 to 0.3 mm for cylindrical cores [162-164, 172-176, 180] and 0.5 mm in prismatic specimens [167-170, 178]. Dimensions of dog-bone specimens are collected in Figure 34.
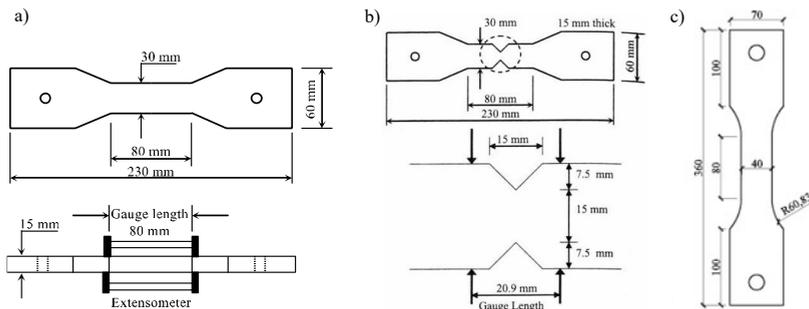
Figure 34. Dog-bones specimens in tensile creep methodologies: SHCC dog-bones [160], b) notched SHCC dog-bones [165], c) UHPFRC dog-bones [105].

Although most dog-bones were not notched, some dog-bone specimens were designed to provide a sole cross-section [171] that serves as a notch, ensuring the multi-crack location (see Figure 34.b and Figure 35.a). The use of either FRC prismatic [168] or cores [54, 163] as testing specimens is, thereafter, most extended where the notch is required to locate the single crack within the transducer measure range. In these cases, a perimetral notch is sawed at midspan around the specimen, as seen in Figure 35.
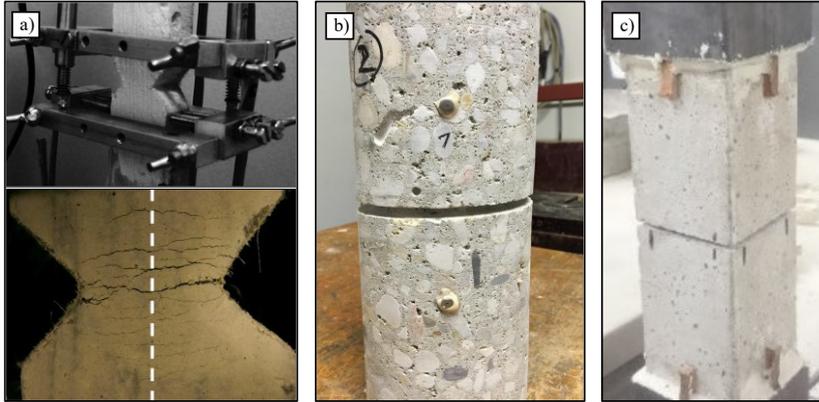
Figure 35. Notch in tensile creep methodologies: a) dog-bones [171], b) cores [172], and c) prismatic specimens [51].

Regarding the long-term test setup, most laboratories reported creep tests carried out in multi-specimen setup as done in flexure methodologies, testing either two [167-170] or three [54, 180] specimens simultaneously. However, the methodology developed in Leuven [162-164, 172-176] tested specimens individually. All creep frames were designed using a lever arm to induce the tensile load into the specimens. Figure 36 collects the creep frames used in reported methodologies.
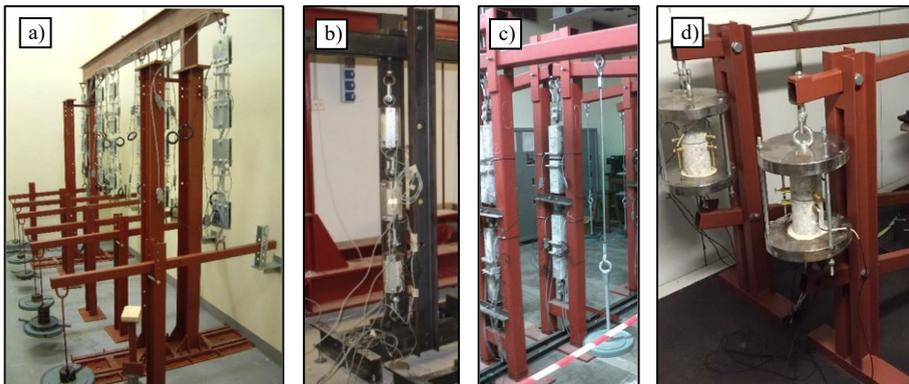
Figure 36. Developed tensile creep frames: a) multi-specimen frame (dog-bones) [159]; b) multi-specimen frame (cores) [180]; c) multi-specimen frame (prismatic specimen) [179]; d) single-specimen frame (cores) [172].

The most studied variable in tensile creep methodologies was the creep index [167-169, 178-179] reported in 11 publications, as depicted in Figure 37. Studies focused on the influence of COD pre-cracking level, environmental conditions, and fibre type and dosage were also reported but represented a low percentage.
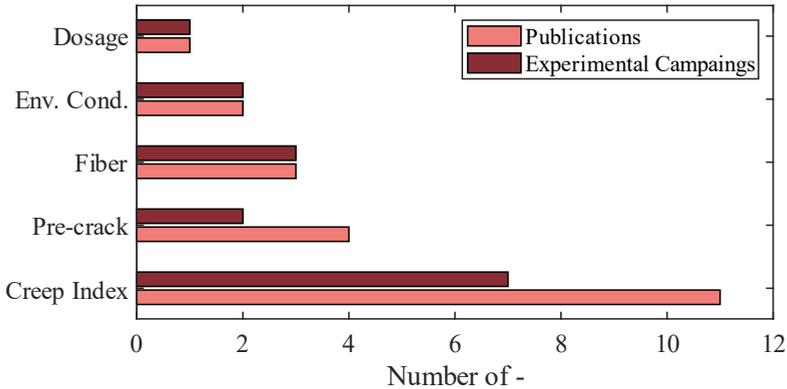
Figure 37. Variables studied in tensile creep methodologies publications.

All reported experimental tests on tensile creep were carried out in controlled environmental conditions, ensuring a constant temperature and relative humidity. Nevertheless, conclusions are rarely comparable due to such variation in specimens and testing conditions, such as pre-cracking and stress levels. Fortunately, it could be possible to assess two direct tension methodologies carried out in similar conditions by two laboratories within the RRT [120] framework. The experimental results obtained by both laboratories were similar, and it was concluded that both methodologies were comparable.

2.3.4. Flexure creep test in panels

Flexure creep tests on sprayed panels arise from the worry of civil engineers focused on tunnel design, where sprayed FRC is used in tunnel construction. Characterisation tests of spayed FRC are based on either square or round panels defined by EN 14488-5 [181] and ASTM C1550 [184], respectively. Thus, creep methodologies based on both square and round panels were developed and reported. Table 7 collects the experimental creep tests carried out in square and round panels, where publications related to the same programme were grouped.

Although these methodologies may seem similar in load application, significant differences in boundary conditions and stress redistribution exist. On the one hand, square panel tests based on EN 14488-5 [181] standard are based on 600×600×100 mm panels and define continuously supporting boundary conditions that provide hyperstaticity to flexure energy absorption test and substantial stress redistribution during both the short- and long-term test. However, some authors [182, 183] concluded

Table 7. Experimental creep tests carried out on square and round panels.

Reference	Specimen		Control	Pre-crack		Creep			Climate		Time
	Shape	Dimensions (mm)		Test setup	Stop (mm)	Frane	Transfer	I_c (%)	Temp. °C	HR %	(days)
[42, 185, 186]	Round	Ø800×75	δ	ASTM C-1550	1 to 5	Single-	Dead load	10-100	23	50	90 [2]
[187]	Square	600×600×100	δ	EN 14488-5	3	Single-	Lever arm	60	NC	NC	70
[76, 188, 189]	Square	600×600×100	δ	SIA 162/6	2	Single-	Hydraulic	50, 60	20	70	650 [3]
[50]	Round	Ø800×75	δ	ASTM C-1550	5 to 13	Single-	Dead load	60, 85	23	50	failure
[190]	Square	600×600×100	δ	EN 14488-5	2	Single-	Lever arm	40, 60, 80	NC	NC	843
[191, 192, 193]	Square	600×600×100	δ	EN 14488-5	First crack	Single-	Lever arm	120 [1]	NC	NC	360
[51, 110, 111]	Square	600×600×100		EN 14488-5	2	Single-	Lever arm	60, 120 [1]	Various	Various	360
	Square	600×600×100	δ	EN 14488-5	2	Multi-	Hydraulic	60	22	55	360
	Round	Ø800×75		ASTM C-1550	2	Single-	Dead load	60	23	50	90
[104]	Square	600×600×100	δ	EN 14488-5	3	Single-	Lever arm	40, 60, 80	NC	NC	280
[194]	Round	Ø800×75	δ	ASTM C-1550	2	Single-	Dead load	80	23	50	failure

[1] referred to matrix pick load; [2] tested at the age of one year; [3]: exposed to aggressive environments.

that friction due to hyperstaticity in square panel tests significantly influences energy flexure tests. On the other hand, ASTM C1550 [184], based on Ø800×75 mm round panels, define isostatic boundary conditions with three rotation-free supports.

In both cases, the absence of a notch makes it challenging to predict the crack location. Therefore, both short- and long-term tests are usually controlled by deflection. However, some laboratories reported studies [195] with both deflection and crack opening measurements in long-term tests, as seen in Figure 38. LVDT transducers were located below the square plate after the pre-cracking test, crossing the primary crack to assess crack opening evolution.

Figure 38. Crack opening and deflection monitorisation in square panels [195].

General procedure is similar for all panel methodologies, where specimens are pre-cracking until a defined deflection and then subjected to sustained load. However, significant differences were noticed in pre-cracking level and load level parameters. On the one hand, the pre-cracking level ranges from 2 to 3 mm deflection reported in square panels [63, 188, 190, 193, 195] and 1 to 13 mm deflection in round panels [185, 186]. This fact is explained by the target of each methodology; square panel procedures aim to characterise the long-term behaviour of FRC material in SLS, whereas round panel procedure is focused on assessing the safety factor of cracked structures when large cracks appear in ULS. On the other hand, load level is not only referred to the residual strength at the pre-cracking level, but some studies [191-193] refer load level to matrix strength or pick load obtained in panel tests carried out in plain concrete specimens following the Asquapro procedure [41]. Initially, the idea was to reach smoothly 2 mm deflection pre-cracking level inducing a sustained load of 120% of pick load in plain concrete and then reduce the load to 60% for creep tests. However, panels rarely reached the target deflection for a one-year test duration due to the short crack opening initially created. Although the reported load level referred to the residual strength ranges from 40 to 100%, the most used load level is 60%.Although in both flexure and tensile creep test, the use of the multi-specimen setup is extended, in the case of panel creep tests, the use of single-specimen setup is, so far, the most extended setup due to the challenging

stacking procedure of cracked specimens. To date, only one laboratory reported creep tests in a multi-specimen setup [195], testing two superposed specimens simultaneously. However, this setup forced them to invert upper specimens generating a more complex procedure. Figure 39 shows examples of both single- and muti-specimen creep test setups on panels.
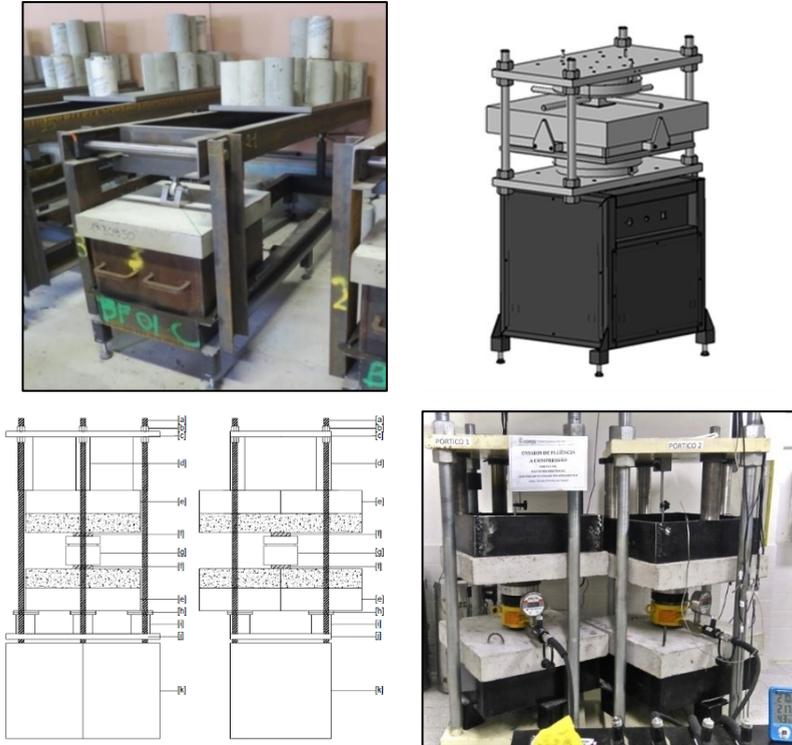
Figure 39. Square panel creep frames examples: (up-left) single-specimen lever arm frame [192]; (up-right) single-specimen hydraulic frame [188,]; (down) multi-specimen hydraulic frame [195].

Although creep tests on round panels have been reported since 2004 [42], the EFNARC organisation defined in 2012 the first approach to a square panel creep test procedure [40]. The French association Asquapro [41] coordinated international efforts to define an agreed procedure to assess FRC long-term behaviour on shotcrete square panels in 2014. To this purpose, Asquapro organised an international Round-Robin test with international laboratories and companies. Obtained results [191-193] arise that regarding the studied sustained loads, neither failure nor deflection above 3 mm (except for one sample) was observed in both steel and polymeric fibre-reinforced panels. However, additional studies of shotcrete creep on square panels carried out following the Asquapro procedure are required to assess the repeatability and reproducibility of the methodology.

Only one methodology was developed to assess FRC long-term behaviour in round panels [42, 185, 186, 194]. The round panel creep frame was designed to test individually round specimens under gravity load. The creep frame designed by Bernard is presented in Figure 40. The gravity load lays on the steel plate connected to the piston that applies the load in the centre of the round panel. One LVDT transducer is connected to the piston to measure delayed deflection during the creep test. The hydraulic lift mechanism serves to lift the load when creep test ends.
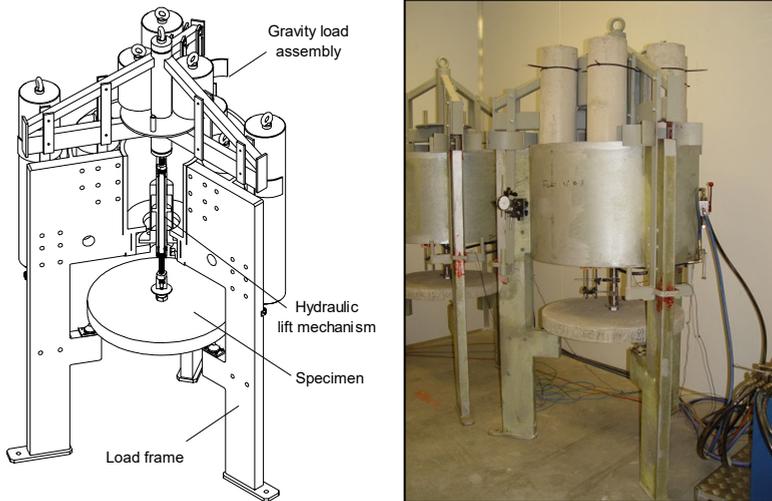
Figure 40. Round panel creep test frame developed by Bernard [194].

Among the reported variables, fibre type influence is studied in 89% of experimental programmes. Whereas most publications compare steel and synthetic fibre materials (77%), some studies reported experimental creep tests to assess the influence of fibre geometry and type [50, 188]. In addition, studies to determine the impact of the creep index and pre-crack level on long-term behaviour are also reported, as seen in Figure 41.
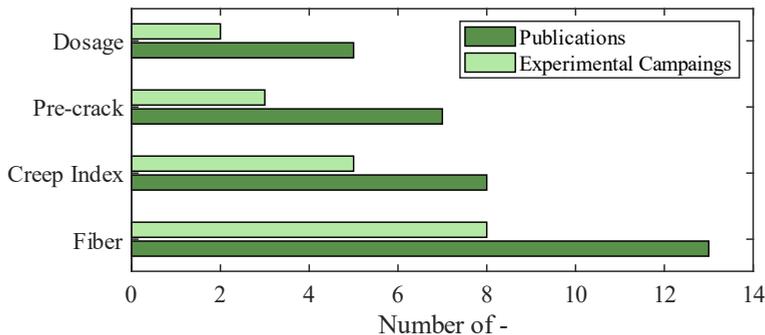
Figure 41. Variables studied in panel creep methodologies publications.

Depending on the laboratory, creep tests were conducted on controlled or uncontrolled environmental conditions. Although creep tests on square panels were usually reported in uncontrolled conditions [187, 190-193], Kaufman [188] and two participants of the RILEM Round-Robin Test [195] carried out in constant temperature and humidity. Square panel creep tests carried out in Rio de Janeiro were conducted in a climate-controlled chamber, whereas creep tests carried out by Versuchsstollen Hagerbach were conducted in the underground Hagerbach Test Gallery, as seen in Figure 42. On the contrary, every round panel creep tests reported were carried out inside a room where both temperature and RH were kept constant.

Figure 42. Creep tests on square panels carried out in an underground test gallery to keep constant environmental conditions.

Chapter 3.
Starting Methodology

For the realisation of his PhD work, creep frames available from previous research were used. Creep frames and flexure creep methodology were developed by Arango [39, 196]. This chapter describes the existing creep frame construction and the corresponding methodology procedure to understand the starting point of this PhD work providing the reader guidelines to follow the evolution of the methodology assessment and improvements proposed.

3.1. Equipment and creep frame construction

The available creep test frame consists of a second-degree lever arm with an x15 multiplier factor to induce flexure load on prismatic specimens. The creep frame basement is constructed with steel profiles, as described in Figure 43.
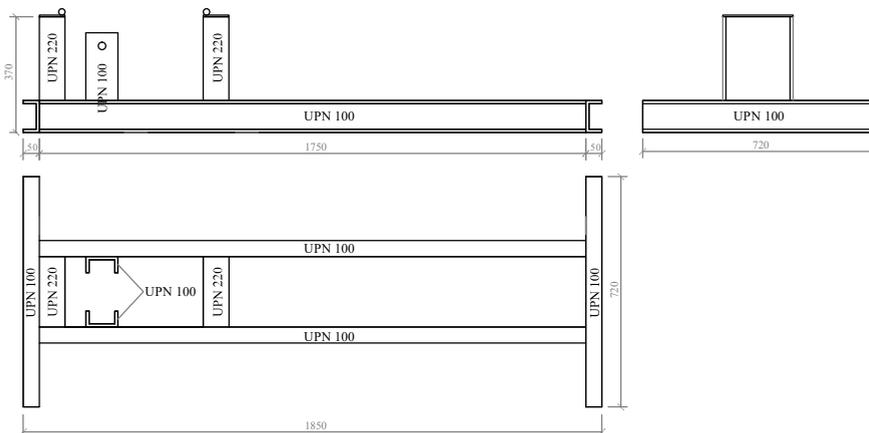
Figure 43. Starting creep frame construction.

The creep frame composing elements are identified in Figure 44. The frame basement (a) includes both specimens (c) and lever arm (d) support profiles. Lever arm (b) is connected to the basement by the fulcrum. Load is induced onto the specimens using screwed bars (i) connected by nuts from the lever arm to the top transfer plate (h). Load cell (g) is placed over the load transfer plate (f) that contains loading rollers for the top specimen. Intermediate load transfer steel plates (e) containing both supporting and loading rollers are placed between the specimens to transfer the load among the stacked specimens. Counterweight (j) is placed at the end of the lever arm to take advantage of the multiplier factor. The load can be adjusted by adding more counterweight to the lever arm or moving the counterweight along the lever arm. A general view of the creep frame and the stacked specimens is presented in Figure 45.
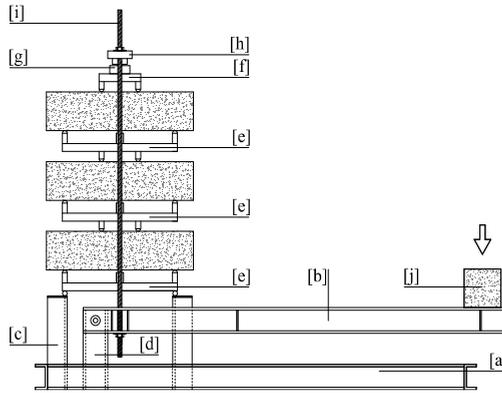
Figure 44. Creep frame elements.
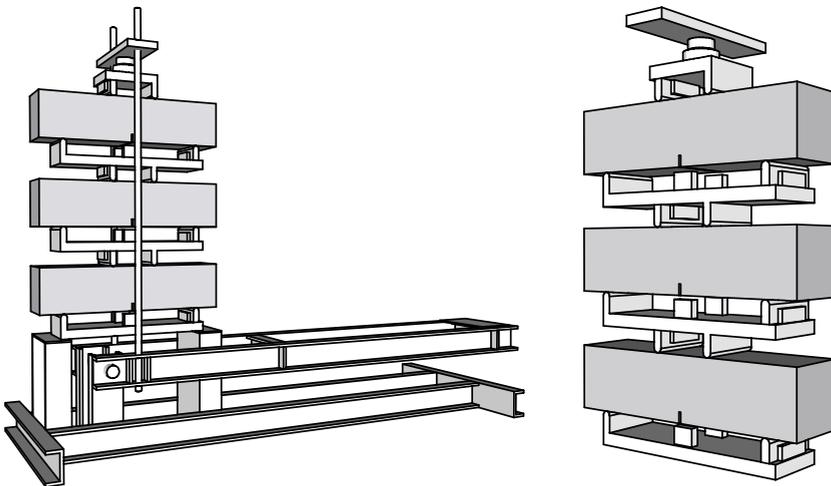
Figure 45. View of creep frame view (left) and stacked specimens view with transfer plates (right).

Creep frames allow testing simultaneously up to three stacked prismatic specimens in flexure. Although this procedure is based on EN 14651 standard [26], to improve the stability of the stacking specimens during the creep test, a four-point bending test (4PBT) flexure setup adapted from EN 14651 is adopted. Hence, both pre-cracking and creep flexure tests were carried out in a four-point bending test (4PBT) flexure setup with a 450 mm support span and 150 mm loading points span, as seen in Figure 46. The starting procedure provides instructions to measure both crack opening (*w*) and compressive strains (*ε*) simultaneously using a linear displacement transducer and strain gauges, respectively. A strain gauge is possible when a 4PBT flexure setup is used in all stages since the supporting rollers span provides enough area to place measurement devices.
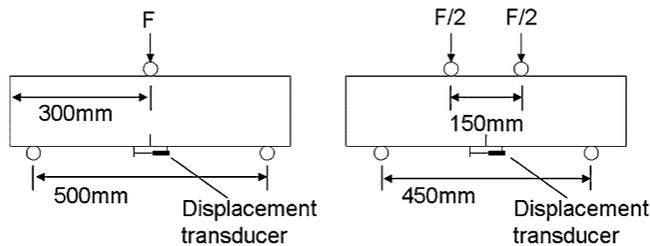
Figure 46. Flexure test scheme from EN 14651 (left) and adopted for creep methodology (right) by Arango et al. [39].

Inter-specimen load transfer steel plates include supporting and loading rollers and support flanges acting as emergency breaks in case of specimen collapse. As seen in Figure 47, one support of each allows rotation in the transversal axis of the specimen for a proper alignment during the stacking process. Unfortunately, rollers do not allow any
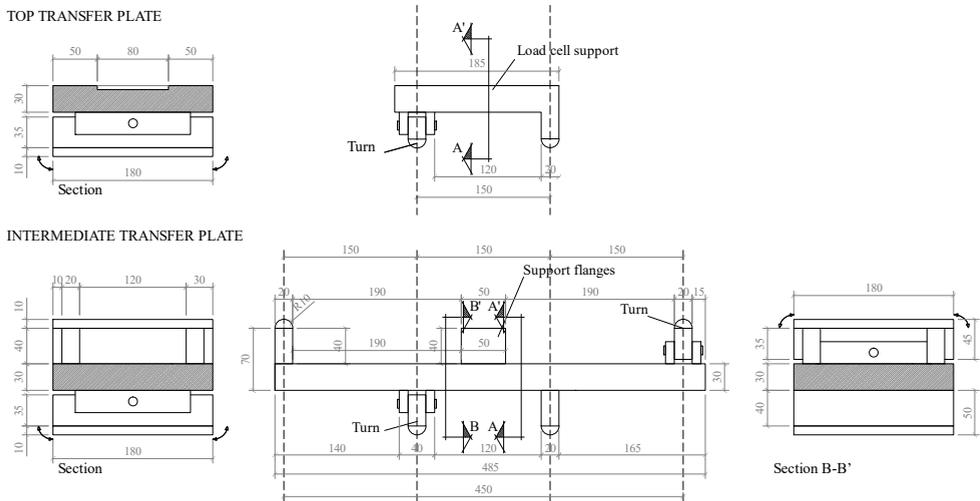
Figure 47. Transfer plate constructions, including supporting and loading rollers with transversal free rotation.

rotation in the longitudinal axis of the specimen. The top transfer plate for the top specimen only contains loading rollers and the load cell support. As done for intermediate steel plates, one support allows rotation in the transversal axis of the specimen for a proper alignment of specimens.

3.2. Creep test procedure

The starting creep test procedure developed by Arango et al. [39] defines three stages: pre-cracking (O-C), creep (CF) and post-creep (FH). A diagram of the creep test containing the three phases is presented in Figure 48. The division of creep test in these phases is widely extended and accepted, as seen in the analysis of existent methodologies carried out in Chapter 2.
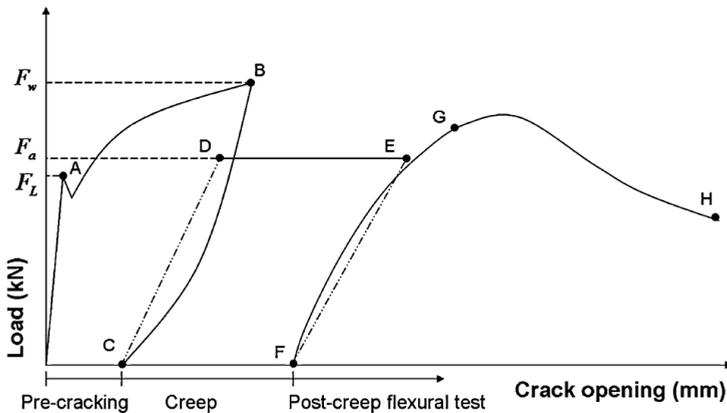
Figure 48. Starting creep test procedure phases definition [39].

Deformation measurement is related to crack opening parameter (w) instead of crack mouth opening displacement (CMOD). Specimens were pre-cracked up to multiple pre-cracking levels (w_p) and then unloaded where instantaneous crack opening recovery registered (w_{pr}). Since the pre-cracking test finished when specimens were unloaded, no delayed recovery was reported in the pre-cracking stage, as seen in Figure 49. Regarding load parameters, the load at the limit of proportionality (LOP) named F_L and load F_w at the pre-cracking level (w_p) are obtained from pre-cracking flexure tests. Pre-cracked specimens were stored in the climate room turned 180 º for two days before being tested in creep.
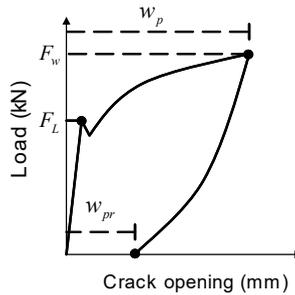
Figure 49. Starting creep test procedure pre-cracking phase definition [39].

During the creep stage, the desired load (F_a) was applied in the creep frame according to the desired load level (IF_a). The load level parameter was related to a percentage of the residual load F_w obtained at w_p. The instantaneous crack opening deformation w_{ci} was registered when load F_a was achieved. Delayed crack opening deformation (w_{cd}^j) and total deformation (w_{ct}^j) were recorded at different j ages, as seen in Figure 50.
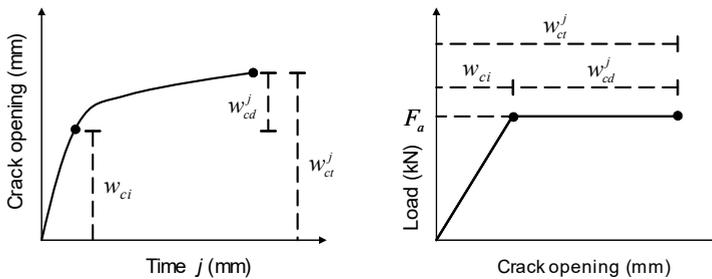
Figure 50. Starting creep test procedure creep phase definition [39].

Once the creep stage was finished, creep frames were unloaded, and both instantaneous (w_{cri}) and delayed crack opening recovery after two weeks (w_{cr}^{tt}) were recorded. Parameters related to the unloading step of the creep stage are defined in Figure 51.
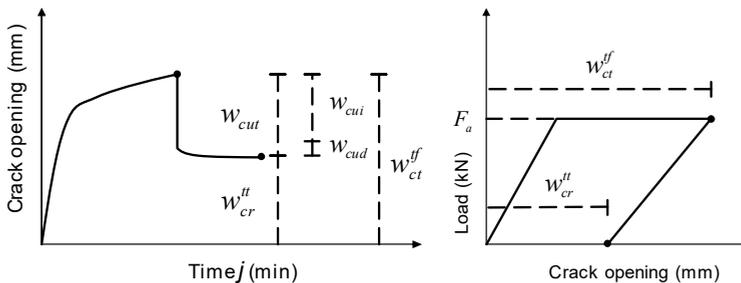
Figure 51. Unloading step after the creep phase [51].

As seen across the previous figures, the load parameter instead of stress was the reference for creep test representation. Therefore, the load level parameter used for the creep test is referred to the residual load obtained in pre-cracking tests instead of residual stress. This assumption could disappoint with the EN 14651 standard, which aims to define the residual stresses of FRC specimens. In addition, in those methodologies where both 3PBT and 4PBT are used for pre-cacking and creep phases, using the load level parameter as a reference may induce misunderstanding.

This methodology was assessed on 7 FRC series [39, 77-79] comprising 39 prismatic tested on flexure creep. Long-term experimental results obtained using the presented methodology [77-81] are included in the state-of-the-art analysis carried out in Chapter 2.

Chapter 4.
Procedure and Methodological Improvements

After the deep analysis and comparison of all the test methodologies available in the state-of-the-art concerning the creep behaviour of fibre-reinforced concrete (FRC), multiple features were detected as susceptible to improvement towards a standardised methodology. Aspects such as the glossary, environmental conditions, testing parameters, procedures or boundary conditions have been considered. The relevant information regarding the creep test experimental campaigns carried out to assess the proposed improvements is fully described in this chapter.

4.1. Glossary review

Different test methodologies have been developed for creep in the cracked state characterisation depending on the specimen shape and primary either flexure or tensile stress sustained in time, as described in Section 2.3. Depending on the methodology adopted, either deflection or crack opening evolution in time is registered. Besides the differences in deformations, the absence of a standardised methodology and corresponding glossary provides multiple terminologies available in the scientific literature (i.e. w for crack opening, δ for deflection…).

Creep tests in the cracked state of FRC are generally multiple-phase long-term tests involving many parameters and variables. In the case of delayed variables, multiple values can be registered for different time lapses (i.e. at 30, 90, 180 or 360 days), and the number of variables increases considerably. The number of variables, parameters and methodologies may be very confusing for comparative purposes of the creep test results.

Currently, the flexure creep test in short beam specimens is the most extended creep in the cracked state procedure. In the case of the flexure creep test, it is generally assessed the delayed crack opening deformation. The most extended term in either international standards or scientific papers for crack opening deformation is w. However, the crack opening concept is commonly used in conventional reinforced concrete (RC) for the

Service Limit State (SLS) control in concrete structural elements. In the case of FRC, the concept of crack opening (w) may be confusing due to significant differences in the international standards available for characterisation. On the one hand, the EN 14651 standard [26] assesses the residual performance of FRC notched specimens where both the crack mouth opening displacement (CMOD) and the crack tip opening displacement (CTOD) are defined depending on the relative position of the transducer to the notch. Alternatively, the ASTM C1609 [25] standard proposed to measure deflection (δ) to assess the FRC matrix performance in a four-point bending test (4PBT). Considering that EN 14651 standard [26] was designed to determine the flexural performance of the FRC material using the crack opening deformation, it can be assumed that similar crack opening definitions and terms could be adopted to assess the long-term properties of the FRC specimens. Therefore, it is proposed to use the CMOD instead of w for the crack opening deformation reference since the crack opening at the mouth of the notch will be measured during the creep test.

Notwithstanding, this glossary proposal not only intends to define the respective reference displacement but also define a clear structure for using subscripts and superscripts. There exist multiple glossary definition criteria in the scientific literature, and it is very convenient to unify criteria to make easier data exchange and comparison between creep test results obtained from different laboratories. Properly use of the required scripts will enable identifying the phase and type of variable along the creep test duration. This fact is crucial for the creep test report, where all the results are collected and could enable the creation of creep test international databases.

Therefore, considering CMOD as the deformation reference for the flexure creep test, it is proposed in Table 8 the following subscripts and superscripts system to identify both the creep test phase and the type of measurement.

Table 8. Subscript and superscript system for creep test CMOD variable glossary.

Type	Name	Subscript	Superscript	Description
Phase	Pre-crack	p		Refers to pre-crack
	Creep	c		Refers to creep phase
	Post-creep	post-creep		Refers to post-creep phase
	Origin	o		Absolut deformation referred to origin
Measure	Instantaneous	i		Instantaneous deformations
	Delayed	d		Delayed in time deformation
	Recovery	r		Recovery deformation after unloading
	Total	t		Includes both instantaneous and delayed
	Shrinkage	s		Refers to shrinkage specimen
Time			j	Start time lapse
			k	End time lapse

This creep test glossary proposal provides enough accuracy to identify any variable in terms of the creep test stage and type of deformation. Following the proposed variable construction, the variable $CMOD_{cd}^{360}$ represents the crack mouth opening displacement (CMOD) according to EN 14651 [26] measured in the creep (subscript c), delayed deformation (subscript d) at 360 days of creep test (superscript 360).

Moreover, some parameters are defined in the nominal and real value, such as the nominal creep index (I_n) and the applied creep index (I_c). Regarding the residual stress and load terminology, similar construction that provided in EN 14651 [26] standard is proposed to be in accordance with residual strength terms. Therefore, considering the base term f_R for residual stress and F for the corresponding load to respective residual stress, additional parameters can be defined by adding the corresponding phase subscript to the corresponding term (i.e. $f_{R,p}$ for the residual stress at $CMOD_p$ in the pre-cracking test or $f_{R,c}$ for the residual stress to be sustained during the long-term stage).

Besides the crack opening, some authors also eventually measure the compressive strains evolution in time in the flexure creep test [39, 89] using strain gauges located on the top face of the specimen. Although the compressive strains evolution assessment is crucial in flexure creep tests where both tensile and compressive forces are combined, this aspect is still uncertain. It is important to know how the creep deformation in compressive affects the crack opening evolution in time. The measurement of compressive strains is still not extended since there is no standardised procedure, and thus, the glossary is still not defined. This glossary construction proposal aims to provide guidelines for the glossary construction for either crack opening or compressive strain variables for the flexural creep test based on the EN 14651 [26] test, as stated in Table 9.

Notwithstanding, the best advantage of this glossary classification is that it may be adapted for the different available creep methodologies (i.e. flexure creep, uniaxial creep, panels…). Although creep test displacement notations are defined in this proposal for CMOD in flexure methodology, analogous notations for the rest of the methodologies can be easily obtained by substituting CMOD with the corresponding crack opening displacement (COD) or deflection (δ) terms.

The proposed terminology developed in this PhD has been successfully assessed and adopted by the RILEM Technical Committee CCF-261 for the realisation of an international Round-Robin Test (RRT) on creep from 2015 to 2019. Since laboratories that carried out all the available methodologies were involved in the RRT, it could be concluded that the proposed glossary served to simplify the parameter and variable definition for all methodologies and enabled a better understanding and data exchange among the participant laboratories.

Table 9. CMOD and CS variables glossary for flexure creep test.

Subscript position				Superscript	Flexure	Compressive area
First	Second	Third	Fourth		Tensile area	
Name					crack mouth opening displacement	compressive strains
Acronym					CMOD (microns)	CS (microstrains)
pre-crack	nominal				$CMOD_{pn}$	CS_{pn}
					$CMOD_p$	CS_p
	recovery	instantaneous			$CMOD_{pri}$	CS_{pri}
	recovery	delayed			$CMOD_{prd}$	CS_{prd}
creep	instantaneous				$CMOD_{ci}$	CS_{ci}
	instantaneous			15'	$CMOD_{ci}^{15'}$	$CS_{ci}^{15'}$
	delayed			j (day)	$CMOD_{cd}^{j}$	CS_{cd}^{j}
	total			j (day)	$CMOD_{ct}^{j}$	CS_{ct}^{j}
	total	shrinkage		j (day)	$CMOD_{cts}^{j}$	CS_{cts}^{j}
	recovery	instantaneous			$CMOD_{cri}$	CS_{cri}
	recovery	instantaneous	shrinkage		$CMOD_{cris}$	CS_{cris}
	recovery	delayed		j (day)	$CMOD_{crd}^{j}$	CS_{crd}^{j}
	recovery	delayed	shrinkage	j (day)	$CMOD_{crds}^{j}$	CS_{crds}^{j}
origin	instantaneous				$CMOD_{oi}$	CS_{oi}
	delayed			j (day)	$CMOD_{o}^{j}$	CS_{o}^{j}
				j (day)	$\varphi_{CMOD,c}^{j}$	$\varphi_{CS,c}^{j}$
				j (day)	$\varphi_{CMOD,o}^{j}$	$\varphi_{CS,o}^{j}$
				j-k	$COR^{j\text{-}k}$	$CSR^{j\text{-}k}$
				j-k	$COR^{j\text{-}k}$	$CSR^{j\text{-}k}$

4.2. Pre-cracking level (CMOD$_p$)

The study of long-term deformations is usually related to the service limit state (SLS). Concrete structural elements are generally designed to work within their SLS and not overcome the ultimate limit state (ULS) during their lifetime. The use of crack opening levels larger than those limitations in SLS for the long-term behaviour characterisation test would not be representative of the real structures working conditions. Therefore, the reference pre-crack opening level proposed for the creep test procedure should be correlated to the crack opening restrictions in SLS.

The absence of any standardised creep procedure for the long-term behaviour of cracked FRC causes a wide variety of pre-cracking levels found in the scientific literature depending on the methodology, as explained in Chapter 2. Although some studies carried out creep tests considering large crack openings to assess the long-term performance in ULS [50], it is most extended the use of low initial crack openings (i.e., 0.2, 0.5, 1.0, 1.5…) related to SLS [49].

As previously explained, specimens are pre-cracked during the first stage of the creep test procedure. Since the initial damage or pre-cracking level (CMOD$_p$) may result decisive in the corresponding creep test results, a comprehensive experimental work was developed to assess the influence of the pre-cracking level on the delayed crack opening deformation. To analyse a wide range of crack levels, the WP1 experimental programme was designed considering six different pre-cracking levels (CTOD$_p$): 0.2, 0.5, 0.8, 1.2, 1.5 and 2.0mm. These values were defined considering that Model Code 2010 [19] correlates the serviceability with the $f_{R,1}$ (residual strength obtained at CMOD = 0.5mm) and the ultimate conditions to $f_{R,3}$ (residual strength obtained at CMOD = 2.5mm). Therefore, crack opening levels larger than 2.0 mm were not considered since it was stated to use crack opening related to SLS.

To this purpose, two FRC batches with macro-synthetic and steel fibres were cast and tested in creep under flexure sustained load. The synthetic fibre-reinforced concrete (SyFRC) mix was reinforced with 9 kg/m^3 of Sikafiber 48 with 48 mm length, whereas in the case of the steel fibre-reinforced concrete (SFRC) 40 kg/m^3 of Bekaert 3D 65/35 steel fibre were used. Three specimens per mix were tested in flexure following the EN 14651 [26] standard procedure to assess the residual behaviour, and results are given in Figure 52. The residual strength ratio $f_{R,3}/f_{R,1}$ provides for the SyFRC mix a '1.5e' classification according to the Model Code 2010 [19], whereas for the SFRC mix, a '3.0d' classification was obtained. Average strength at the limit of proportionality (f_L), $f_{R,1}$ and $f_{R,3}$ obtained in characterisation tests are also provided. Full information about the WP1 experimental programme including the concrete matrix composition, flexure test setups and experimental results can be consulted in the Appendix B.
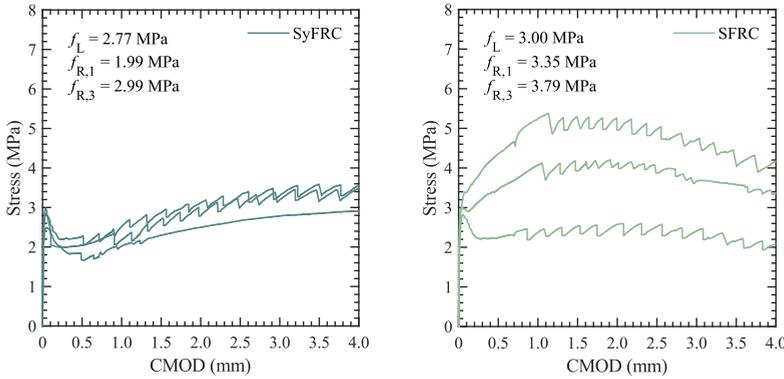
Figure 52. SyFRC and SFRC mixes flexure characterisation test.

Prior to the long-term tests, six specimens per batch were notched and pre-cracked in a three-point bending test (3PBT) in compliance with the EN 14651 procedure [26]. The crack tip opening displacement (CTOD) was used for the crack opening control. One linear variable displacement transducer (LVDT) on each side of the specimen was located at the crack tip to measure the average CTOD. Six nominal pre-cracking levels were considered in this experimental programme: 0.2, 0.5, 0.8, 1.2, 1.5 and 2.0 mm. The pre-cracking levels $CTOD_p$ for each specimen and the corresponding crack mouth opening displacement $CMOD_p$ values are provided in Table 10, where the residual strengths f_L and $f_{R,1}$ are also provided. Stress-CTOD performance obtained in pre-cracking tests can be observed in Figure 53. Note that specimen $B_{1.2}$ exceeded the desired $CTOD_p$ by 120 microns, and it should be considered in the analysis of the results.

Table 10. Pre-cracking tests and corresponding creep index of SyFRC and SFRC series.

Mix	Specimen	$CTOD_p$	$CMOD_p$	f_L	$f_{R,1}$	$f_{R,c}$	I_c
		[mm]	[mm]	[MPa]	[MPa]	[MPa]	[%]
SyFRC	$A_{0.2}$	0.209	0.255	2.94	--	1.10	--
	$A_{0.5}$	0.513	0.627	3.01	2.43	1.10	45.1
	$A_{0.8}$	0.812	0.984	2.98	2.19	1.20	55.0
	$A_{1.2}$	1.231	1.483	2.91	2.08	1.20	57.8
	$A_{1.5}$	1.552	1.856	3.14	2.06	0.99	48.0
	$A_{2.0}$	2.117	2.490	2.84	1.99	0.99	49.7
SFRC	$B_{0.2}$	0.202	0.263	3.31	--	2.01	--
	$B_{0.5}$	0.502	0.637	3.36	6.56	2.02	30.7
	$B_{0.8}$	0.806	0.964	3.44	4.76	2.12	44.5
	$B_{1.2}$	1.328	1.661	3.03	4.88	2.12	43.5
	$B_{1.5}$	1.500	1.808	2.86	2.97	1.91	64.2
	$B_{2.0}$	2.034	2.497	3.37	3.67	1.91	52.0
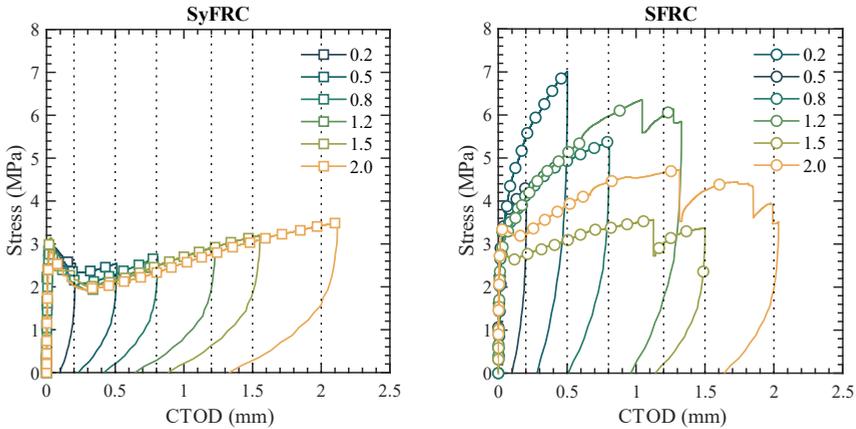
Figure 53. Pre-cracking test in both SyFRC (a) and SFRC (b) specimens at different pre-cracking levels (CTOD$_p$).

Considering the residual stresses obtained in both the characterisation and pre-cracking test, 2.1 and 4.0 MPa average $f_{R,1}$ was obtained for SyFRC and SFRC, respectively. The stress level (I_c) is usually defined as a percentage of the residual strength obtained per specimen at the desired pre-crack opening CMOD$_p$. Nevertheless, this experimental programme implies a wide range of pre-cracking levels could hinder the creep index application. Note that specimens with pre-cracking level CTOD$_p$ = 0.2 mm did not reach the CMOD enough to obtain $f_{R,1}$. Therefore, the creep index parameter was exceptionally defined for this experimental program as 45% of the average $f_{R,1}$ of each mix. It is known that the use of the average residual strength of the FRC mix instead of the specific strength of each specimen increases the scatter in terms of the applied creep index when a multi-specimen setup is adopted.

After the pre-cracking phase, the specimens were moved to the climate-controlled chamber where the creep frames were located. The sustained stress $f_{R,c}$ during the creep test was applied for 182 days, and then the specimens were unloaded. A data logger continuously registered the crack opening during the creep test duration. CMOD$_{crd}$ recovery deformations were recorded for 10 days after being unloaded. The evolution in time of the total crack opening deformation CMOD$_{ct}$ for both mixes is depicted in Figure 54, where the gradient of colours highlights the pre-cracking level of the specimens. Unfortunately, the displacement transducer of specimen B$_{1.5}$ failed 57 days after the beginning of the creep test, and no further readings could be recorded. Besides the nominal pre-cracking level CTOD$_p$, legends also include the specific creep index I$_c$ applied on each specimen to assess any influence of the creep index on CMOD$_{ct}$ deformation. In the case of the SyFRC mix, it can be observed that specimens A$_{0.8}$ and A$_{1.2}$ develop higher CMOD than the expected tendency. This unexpected behaviour can be explained due to the high I_c of 55.0 and 57.8%, respectively applied. A similar trend is found for specimens B$_{0.5}$ and B$_{1.5}$ of SFRC mix where a creep index of 30.7 and 64.2% were applied respectively. It is then confirmed that the applied creep index I$_c$ produced

relevant variability in terms of delayed crack opening deformations, which significantly influences both $CMOD_{ci}$ and $CMOD_{ct}$ variables.
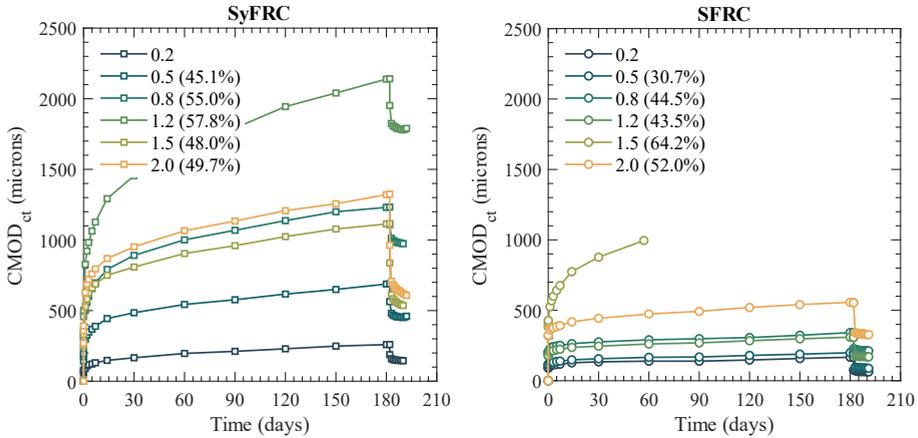
Figure 54. CMOD evolution during the creep test for SyFRC (left) and SFRC (right) mixes.

Although it can be observed that crack opening deformations of both mixes increase in time, a slight stabilisation is appreciated for the SFRC mix. Regarding the pre-cracking level $CMOD_p$, it can be easily observed that both instantaneous $CMOD_{ci}$ and delayed $CMOD_{ct}$ increase with the pre-cracking initial damage $CMOD_p$. However, delayed crack opening deformations are not proportional to the pre-cracking level. Although the pre-cracking level 2.0 mm is four times larger than 0.5 mm, the $CMOD_{ci}$ and $CMOD_{ct}^{180}$ obtained by the $A_{2.0}$ specimen were 1.8 and 1.9 times larger than specimen $A_{0.5}$ respectively. In the case of the SFRC mix, the $B_{2.0}$ to $B_{0.5}$ obtained ratios were 2.7 and 2.8 for $CMOD_{ci}$ and $CMOD_{ct}^{180}$ respectively.

Since the creep stage was carried out in a multi-specimen setup, the additional dead load of the upper specimens and transfer plates shall be considered for the creep index calculation. Thus, the creep index was obtained for each specimen, and some scattered values were obtained. Notwithstanding, in the case of SFRC, more creep index variation was found ranging from 31 to 64% due to the low fibre dosage as it occurs for the pre-cracking test. Creep index values obtained for each specimen are shown in Table 11.

To reduce the influence of such scattered creep index in the long-term behaviour assessments, delayed $CMOD_{ct}$ deformations were normalised by the applied creep index I_c using Equation 1.

$$CMOD_{ct}^* = CMOD_{ct}^j \cdot \left(\frac{I_n}{I_c}\right) \qquad \textbf{Equation 1}$$

Table 11. Applied creep index and CMOD experimental values obtained in the creep stage for SyFRC and SFRC.

Mix	Specimen	I_c (%)	$CMOD_{ci}$ (μm)	$CMOD_{ct}^7$ (μm)	$CTOD_{ct}^{14}$ (μm)	$CTOD_{ct}^{30}$ (μm)	$CTOD_{ct}^{90}$ (μm)	$CMOD_{ct}^{180}$ (μm)
SyFRC	A0.2	-	58.3	130.8	147.4	166.1	210.6	258.4
	A0.5	45.1	140.9	388.8	444.1	485.4	576.8	688.2
	A0.8	55.0	225.2	696.5	792.1	891.0	1068.4	1231.4
	A1.2	57.8	340.8	1126.9	1294.0	1456.8	1791.8	2140.0
	A1.5	48.0	244.5	688.6	751.5	808.4	959.6	1113.2
	A2.0	49.7	251.3	795.1	870.9	953.5	1134.2	1323.5
SFRC	B0.2	-	88.6	117.5	128.3	135.1	138.2	167.0
	B0.5	30.7	116.0	139.3	148.3	156.1	168.6	198.9
	B0.8	44.5	193.6	251.0	264.1	276.5	297.6	342.8
	B1.2	43.5	177.5	223.5	236.3	245.7	268.8	309.3
	B1.5	64.2	380.1	675.8	774.5	877.9	-	-
	B2.0	52.0	316.8	391.6	417.8	443.5	492.6	556.5

$CMOD_{ci}^*$ and delayed deformations $CMOD_{ct}^*$ at 7, 14, 30, 90 and 180 days were depicted in Figure 55 for each $CMOD_p$ to assess the evolution and the influence of the pre-cracking level on the long-term behaviour. Logarithmic fitting curves were obtained for each time-lapse, and the influence of the pre-cracking level was then confirmed since $CMOD_{ct}$ increases as the pre-cracking level increases for both mixes, as observed in Figure 55.
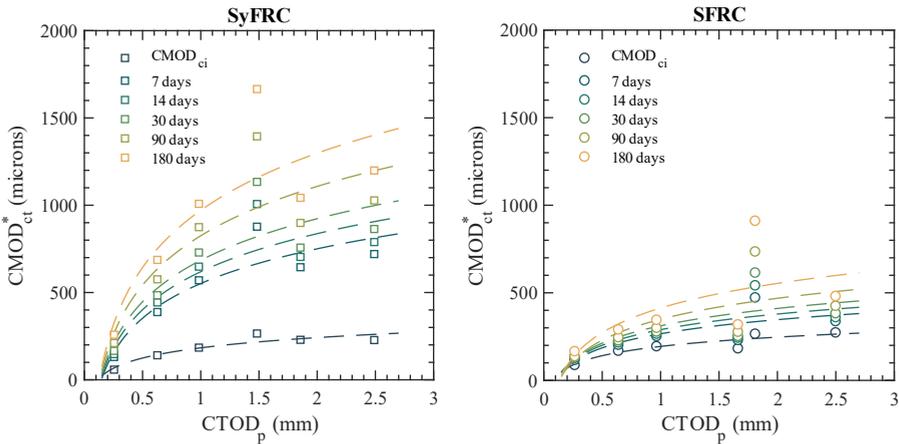
Figure 55. Influence of CMODp on the normalised CMODct evolution.

The delayed behaviour of specimens from each mix pre-cracked at the same $COMD_p$ is compared in Figure 56. Due to the extraordinary creep index sustained by specimen $B_{1.5}$, the comparison with the corresponding specimen of the SyFRC mix does not follow a similar trend to the rest of the specimens. Excluding the specimens with 1.5 mm of $CMOD_p$ due to the outlined creep index value, it is confirmed that the SyFRC mix developed on average 3.5 times more CMOD deformations than SFRC in similar pre-cracking conditions. In contrast, the instantaneous $CMOD_{ci}$ deformations seems to be larger for the SFRC mix than the SyFRC specimens. It is observed in Figure 56 that, the first marker of each specimen, corresponding to the $CMOD_{ci}$ comparison between mixes, drops in the SFRC side. This behaviour implies that, for the same pre-cracking level, SFRC specimens provide more instantaneous deformation when the loading process ends than SyFRC specimens.
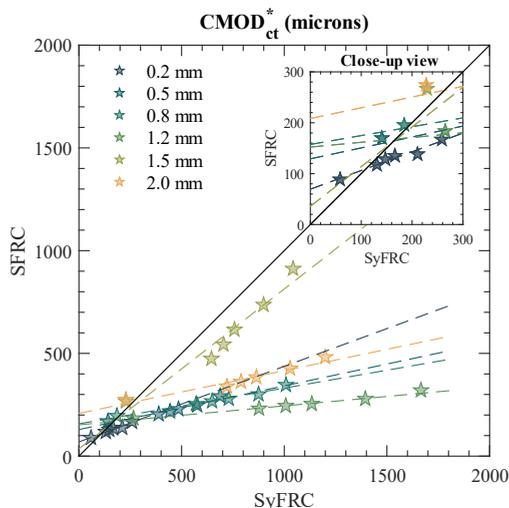
Figure 56. Comparison of normalised CMOD$_{ct}$* between SyFRC and SFRC.

Analogously, creep coefficients referred to the creep stage (φ_c) at 7, 14, 30, 90 and 180 days were analysed for both FRC mixes. The creep coefficient referred to the creep stage is defined as the ratio of the delayed crack opening deformations CMOD$_{cd}$ during the creep stage to the instantaneous crack opening deformation CMOD$_{ci}$. Creep coefficients were obtained (Equation 2) considering normalised CMOD* deformations and depicted versus the pre-cracking level for each specimen in Figure 57. In the case of the SyFRC, the trend curve of the creep coefficient considering all the pre-cracking levels CMOD$_p$ for each time-lapse is similar regardless of the time-lapse considered. Moreover, it is also appreciated that among the first three time-lapses of 7 (7 to 14 days), 16 (14 to 30 days) and 30 days (30-60 days), the distance between curves is kept relatively constant. It is explained since the long-term CMOD deformations follow a logarithmic trend and delayed deformations tend to decrease in time towards zero. This creep behaviour provokes the creep coefficient trend curves for each time-lapse to get closer in time. Regarding the SFRC mix, creep coefficients below one were obtained for all specimens except B$_{1.5}$, subjected to an extraordinary 64.2% creep index. Since creep deformations of the SFRC mix show excellent stabilisation at early ages providing straight long-term evolution, linear trend curves were obtained for each time-lapse considering all pre-cracking levels. It was concluded that creep index I_c significantly influences the creep coefficients compared to the low influence observed by the pre-cracking level CMOD$_p$. Although the creep coefficient increases with the pre-cracking level, the creep coefficient does not increase as much as expected with such a pre-cracking level variation. I.e., comparing pre-cracking levels of 0.5 and 2.0 mm, creep coefficients at 180 days (φ_c^{180}) increased from 3.9 to 4.3, respectively. Nevertheless, considering the huge increase of 400% in terms of pre-cracking level (from 0.5 to 2.0 mm), only an increase of 10.2% in the creep coefficient at 180 days was produced. Even

the influence on the creep coefficient decreases in time, being higher at early ages (i.e. variation of 14.5% from creep coefficients at 7 days of both 0.5 and 2.0 specimens).

$$\varphi_c^{\,j} = \left(CMOD_{ct}^{\,j} - CMOD_{ci}\right) / CMOD_{ci} = CMOD_{cd}^{\,j} / CMOD_{ci} \qquad \text{Equation 2}$$
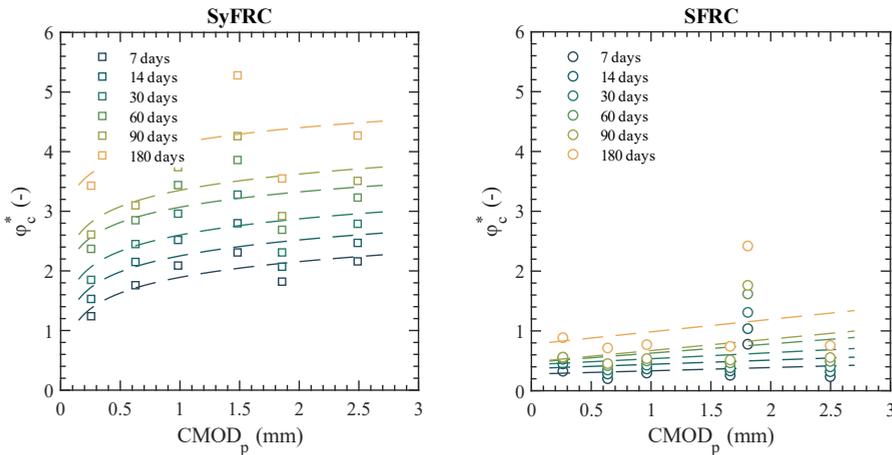
Figure 57. Influence of the CMOD$_p$ on the normalised creep coefficients φ_c^*.

The crack-opening rate (COR) parameter provides valuable information about the deformation rate in time. It allows estimation of the crack opening at further ages since it provides the crack-opening rate in µm/year. COR is obtained using Equation 3:

$$COR^{\,j-k} = \left(CMOD_{cd}^{\,k} - CMOD_{cd}^{\,j}\right) / \left((k-j)/365\right) \qquad \text{Equation 3}$$

Daily COR was obtained for each specimen, considering the normalised CMOD deformations. Since the COR parameter is quite sensitive to sudden changes, the moving average considering 30 days time-lapse was considered and depicted in Figure 58 for each specimen. Since creep index influences delayed deformation, creep index influence on the COR parameter is also observed on A$_{0.8}$ and A$_{1.2}$ specimens but especially on the B$_{1.5}$ specimen. Regarding the SyFRC mix, moving average COR at 180 days of test provide a crack opening rate of 350.1 µm/year for 0.5 pre-crack level and 554.1 µm/year for 2.0 mm pre-cracking level. These COR values predict that if the crack opening rate keeps constant, the 0.5 pre-cracked specimens shall exceed 2 mm crack opening in 5.7 years, whereas the 2.0 pre-cracked specimen in 3.6 years. Nevertheless, COR usually decreases in time, and specimens will probably exceed a 2.0 mm crack opening later.

Regarding the SFRC mix, moving average COR at 180 days provides a 48.9 µm/year crack opening rate for 0.5 pre-crack level and 125.4 µm/year for 2.0 mm pre-cracking level. The COR increased between 0.5 and 2.0 pre-cracking levels 58.3% and 156.6%

for SyFRC and SFRC mixes, respectively. Note that for the SFRC mix, such COR increase is due to the extremely high creep index sustained by specimen $B_{1.5}$. For comparative purposes, considering the COR values obtained, the 0.5 and 2.0 mm pre-cracked specimens shall exceed 2 mm crack opening in 40.9 and 15.9 years, respectively.
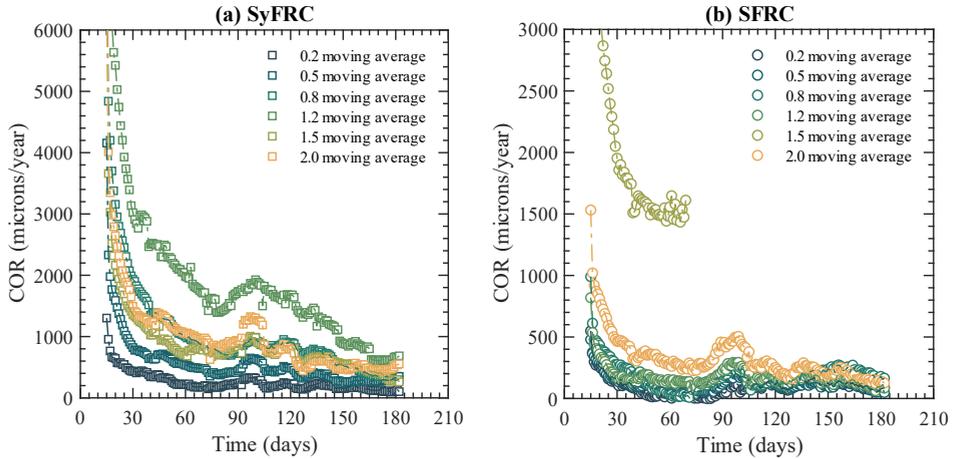
Figure 58. Influence of the pre-cracking level on the COR evolution.

In short, it can be concluded from this analysis that the pre-cracking level $CMOD_p$ has a low influence on both delayed deformations and the creep coefficient obtained in the creep test. Nevertheless, defining a reference value for the pre-cracking level parameter is important to get comparable results among laboratories. As previously stated, creep characterisation tests shall represent the real working conditions of FRC structures in service. Therefore, it is proposed 0.5 mm as the $CMOD_p$ reference value for creep characterisation due to the following statements:

- Flexure CMOD of 0.5 mm is a crack width related to SLS.

- Since the $CMOD_p$ parameter has a low influence on both delayed deformations and creep coefficient, it shall be permitted to exceed the $CMOD_p$ up to 0.02 mm in the pre-cracking test.

- In the flexure test of prisms, considering a variable crack opening along the cross-section height, a CMOD of 0.5 mm is equivalent to an average 0.2 mm crack opening, accepted in most structural codes.

- Moreover, the proposed 0.5mm for $CMOD_p$ correspond to $CMOD_1$, which is the reference crack opening for the residual stress $f_{R,1}$ and allows to assess the long-term behaviour based on the basic residual strength referred to SLS in the Model Code 2010 [19].

- It is revealed that applied creep index I_c is more significant in the long-term behaviour than the pre-cracking level $CMOD_p$. Therefore, the creep index

parameter definition for any standard procedure shall be more restrictive than the pre-cracking level parameter definition.

Note that these recommendations are given to define a creep test procedure with characterisation purposes. Notwithstanding these recommendations, pre-cracking level $CMOD_p$ acceptance thresholds may be increased or modified for research purposes.

4.3. Creep index (I_c)

The principle of the flexural creep test is to induce a certain stress level in the cracked FRC specimens and measure long-term crack-opening deformation under sustained load. Among the three stages of the creep test procedure, both 3PBT and 4PBT load configurations can be used, as highlighted in Section 3.2. Therefore, the *load level* expression, which its use is extended in the scientific literature, can be confusing since the load depends on the flexure load configuration chosen. The proposed expression stress level or creep index (I_c) is a more appropriate term than *load level* since it is related to stress instead. Therefore, the proposed creep index (I_c) term is defined as the ratio of sustained stress during the creep stage ($f_{R,c}$) to the residual strength $f_{R,p}$ at $CMOD_p$ obtained during the pre-cracking phase.

The creep index may be related to either the residual stress individually obtained by each specimen or the average stress obtained from each concrete batch or FRC mix. Depending on the chosen reference residual strength, the procedure and the results obtained could differ significantly in terms of creep index. If the stress $f_{R,p}$ obtained at $CMOD_p$ during the pre-cracking tests by each specimen is considered, the stress to be applied into each specimen shall be obtained individually for each specimen to keep the creep index constant due to the residual performance inherent variation. The sustained stress may be alternatively obtained by applying the creep index factor to the average residual strength registered by all specimens composing the concrete batch or mix. Although the latter option may be easier to perform since the same load is applied in all creep frames, this approach would lead to more scattered results in terms of creep index related to $f_{R,p}$.

The flexure test EN 14651 [26] provides relevant residual performance data to assess the structural contribution of fibre reinforcement. The residual flexure strengths $f_{R,1}$ and $f_{R,3}$ obtained according to EN 14651 are used in the structural Model Code 2010 [19] to predict either the *rigid-plastic* or *linear* tensile FRC performance model employed in the design of structures. Both models are defined by the serviceability residual strength f_{Fts} representing the post-cracking strength for serviceability crack openings and f_{Ftu} representing the ultimate residual strength. The simplified "*Rigid-plastic model*" is defined only by the reference value f_{Ftu} that corresponds to $f_{R,3}/3$ and is based on the ultimate behaviour. The "*Linear model*" is more convenient for a complete structural analysis considering the ultimate since the ultimate limit state (ULS) is analysed considering the ultimate crack opening in the service limit state (SLS). The "*linear model*" defines the serviceability residual strength $f_{Fts} = 0.45\, f_{R,1}$ being suitable when

fibres are used for crack control in service conditions. The use of the *linear model* as a reference to define the creep index on creep studies related to SLS is more frequent in the bibliography.

Considering these statements, a new experimental programme to assess the influence of the creep index on the long-term flexure behaviour of FRC and define stress levels safe enough to ensure the service conditions during the lifetime of the structures. In the previous experimental programme, it was observed that creep index variations influenced long-term results. Therefore, three creep index levels (25, 35 and 45%) were defined for this experimental creep test, as represented in Figure 59. Since creep characterisation tests in the cracked state of FRC specimens are focused on determining the long-term behaviour of FRC material in service conditions, this experimental programme will consider 0.45 $f_{R,1}$ as reference creep index as done for the serviceability crack openings by the linear model proposed in the Model Code 2010 [19]. To be in accordance with service conditions, 0.5 mm of $CMOD_p$ was chosen as reference, but lower pre-cracking levels were also considered to assess the long-term behaviour when reduced damages are applied. Consequently, the $CMOD_p$ levels 0.05, 0.1, 0.2, 0.3 and 0.5 mm were considered in the present experimental work. Full information about the WP2 experimental programme including the concrete matrix composition, flexure test setups and experimental results can be consulted in the Appendix E.
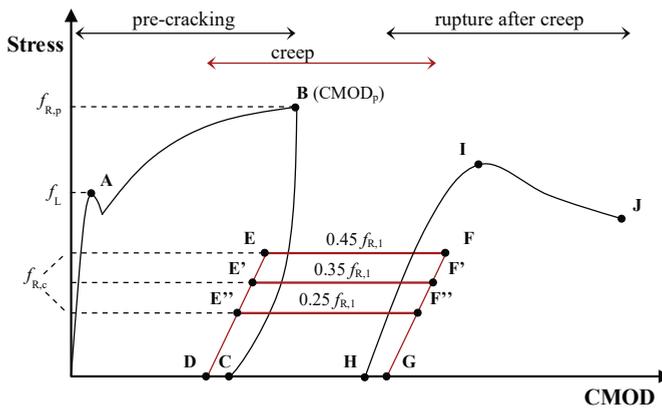
Figure 59. Creep index considered in the experimental programme [49].

To this purpose, two FRC batches were cast with the same concrete matrix reinforced with 50 kg/m³ of hooked-end steel fibres. Steel fibres were 50 mm in length and 1 mm in diameter and provided common residual performance of standard FRC used for structures. The mean compressive strength for batches A and B was 41.7 and 39.2 MPa, respectively. Besides the cylindrical specimens for compressive strength characterisation, 18 prismatic specimens sized 150×150×600 mm were cast and cured in a moist chamber. One specimen per batch was destined for a flexure characterisation test, whereas the rest were pre-cracked and tested in creep. Pre-cracking tests were

carried out according to EN 14651 standard [26] at 0.05 CMOD/min ratio. Specimens were notched at midspan, and CMOD was controlled using a clip gauge crossing the notch. Characterisation and pre-cracking flexure test results are summarised in Table 12, arranged by pre-cracking level and within the same $CMOD_p$, arranged by ascendant creep index. The CMOD-stress curves obtained for both characterisation and pre-cracking flexure test are shown in Figure 60. It can be observed that once the desired $CMOD_p$ is reached, specimens are unloaded, and the corresponding instantaneous recovery $CMOD_{pri}$ is registered. The instantaneous recovery capacity increases with the pre-cracking level deformation. Note that the pre-cracking test of specimen 0.2b-25 was unexpectedly interrupted, and the desired $CMOD_p$ was not reached. Notwithstanding, it was decided to continue the creep test considering the reached 137 microns as the damage level.

Table 12. Characterisation and pre-cracking flexure test results.

Test phase	Specimen	$CMOD_p$ (μm)	f_L (MPa)	$f_{R,p}$ (MPa)	$f_{R,1}$ (MPa)	$f_{R,3}$ (MPa)	$CMOD_{pri}$ (μm)
Pre-crack	0.05a-25	52	4.24	4.78	--	--	28
	0.05b-35	51	3.90	4.79	--	--	15
	0.05a-45	56	3.58	5.27	--	--	21
	0.1a-25	106	4.00	4.04	--	--	61
	0.1b-35	102	3.54	5.15	--	--	40
	0.1b-45	100	4.66	4.35	--	--	45
	0.2b-25	137*	3.96	4.69*	--	--	--*
	0.2b-35	205	3.88	5.02	--	--	113
	0.2a-45	205	3.72	4.39	--	--	114
	0.2b-45	195	4.16	4.96	--	--	112
	0.3a-25	300	4.20	4.94	--	--	191
	0.3b-35	306	3.25	4.25	--	--	113
	0.3b-45	308	4.27	5.75	--	--	195
	0.5a-25	501	3.99	6.44	6.44	--	347
	0.5a-35	512	4.41	4.42	4.42	--	340
	0.5b-45	503	5.35	5.85	5.85	--	341
Characterisation	3.5a	--	3.74	--	4.56	4.53	--
	3.5b	--	3.60	--	5.7	5.86	--
Average		--	4.03	--	5.39	5.20	--
CV (%)		--	11.9	--	16.2	18.1	--

* Flexure test was unexpectedly interrupted by the testing machine.
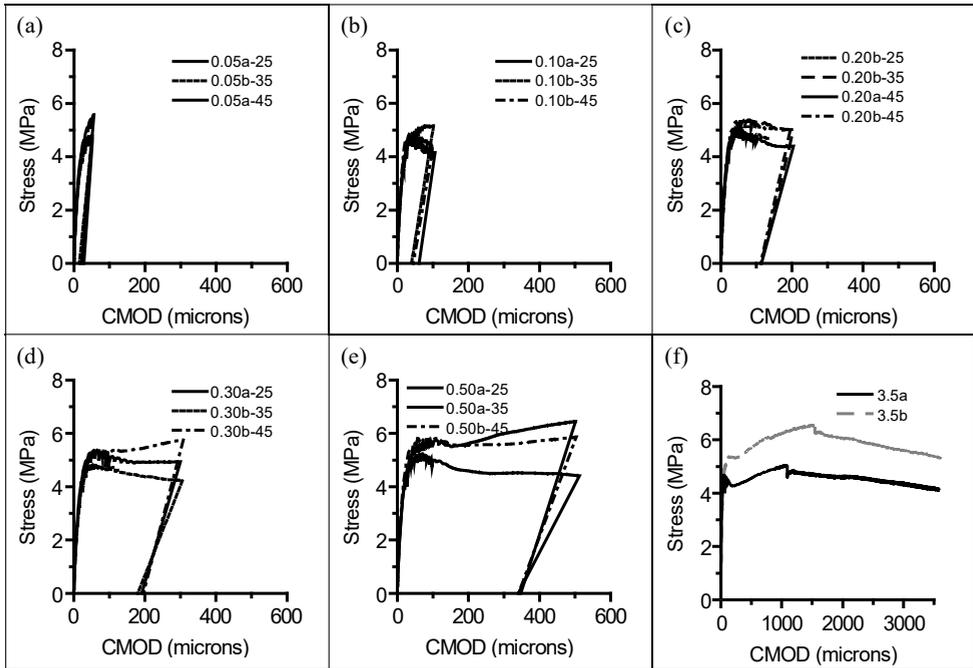
Figure 60. Flexure pre-cracking test at (a) 0.5 mm, (b) 0.1 mm, (c) 0.2 mm, (d) 0.3 mm and (e) 0.5 mm CMOD$_p$ including characterisation test (f). [49].

Considering the proposed CMOD$_p$ values, most specimens did not reach CMOD$_1$ in the pre-cracking test. Consequently, the reference residual strength $f_{R,1}$ could not be obtained for all specimens. The average residual strength $f_{R,1}$ of both specimens destined for characterisation and three specimens pre-cracked up to CMOD$_1$ was considered as reference $f_{R,1}$. To obtain the stress sustained in time ($f_{R,c}$) during the creep test, the corresponding creep index was applied to the reference average $f_{R,1}$. A multi-specimen setup was adopted, and specimens were grouped according to their residual strength at pre-cracking test $f_{R,p}$ to minimise the creep index variation.

Specimens were stacked in the creep frames, and the corresponding 4PBT load $F_{R,c}$ that shall induce the desired stress was applied on each frame. After 180 days of sustained load, the specimens were unloaded, and CMOD recovery capacity was registered. Specimens were removed from creep frames 30 days after being unloaded and tested in flexure to assess the influence of the long-term test on the post-creep residual performance.

Considering such low creep index and pre-cracking levels considered for this experimental program, shrinkage was expected to significantly impact the long-term behaviour of cracked FRC. To assess the shrinkage effect in the delayed CMOD deformations, additional series of prismatic FRC specimens were cast with the same concrete mix. Shrinkage specimens were instrumented and conserved in the same

conditions that specimens destined to creep tests but unloaded. Both creep and shrinkage tests were carried out inside a climate room under controlled temperature conditions (22 ± 3 ºC). Relative humidity inside the room was not controlled but restricted and ranged from 40% in winter to 80% in summer. The drying shrinkage deformations registered for 30-60, 60-90 and 90-180 days time-lapses were 47, 32 and 60 microstrains, respectively. Considering the distance between strains measuring points, crack opening deformations were obtained and delayed CMOD deformations compensated.

The CMOD experimental results were updated with the drying shrinkage during the creep test, and the corrected CMOD deformations evolution is shown in Figure 61, arranged by the creep index 25% (a), 35% (b) and 45% (c), respectively. Additional information regarding the recovery capacity, such as instantaneous recovery $CMOD_{cri}$ and delayed recovery $CMOD_{crd}$ at 30 days unloaded, is also given. Specimens are arranged in three groups depending on their creep index (25, 35 and 45%) and within each group arranged by $CMOD_p$.
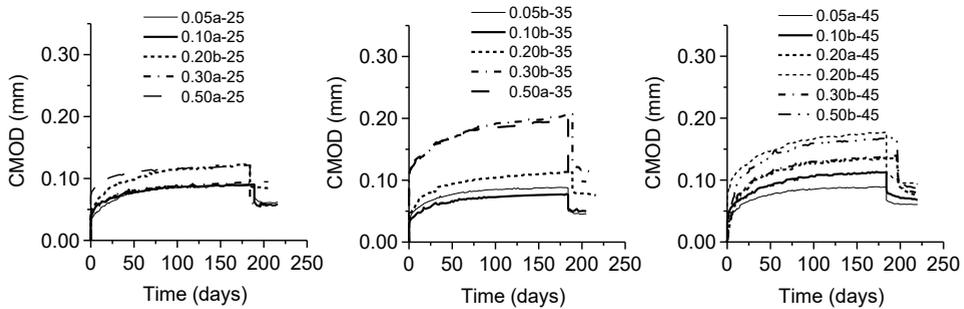
Figure 61. $CMOD_{cts}$ deformations compensated with shrinkage for creep index 25% (a), 35% (b) and 45% (c) respectively [49].

The instantaneous $CMOD_{ci}$ and total delayed $CMOD_{ct}$ at 14, 30, 90 and 180 days are collected in Table 13, that also includes valuable information regarding the applied stress and the corresponding creep index. The creep index (I_c) ratio of the applied stress $f_{R,c}$ to the average $f_{R,1}$ is exposed in Table 13. Considering such a pre-cracking level variation, the creep index referred to the individual residual strength $f_{R,p}$ at CMODp was also obtained. It was confirmed that defining the creep index to the average $f_{R,1}$ provides more creep index variation due to the intrinsic scatter behaviour of FRC. This creep index variation, due to the average $f_{R,1}$ reference value and the multi-specimen setup, explains some of the atypical delayed CMOD behaviour observed in Figure 61. Specimens 0.3b-35 and 0.5a-35 from Figure 61.b developed extraordinary deformations in instantaneous and delayed CMOD. Although both specimens were tested under 33.7 and 36.2 % of $f_{R,1}$ creep index, it is not negligible that referred to $f_{R,c}$, these specimens suffered creep index of 42.8 and 44.1 %, respectively. Similar behaviour was observed by specimen 0.2b-45 from Figure 61.c with 51.1% related to $f_{R,p}$ creep index. However, specimen 0.1b-45 did not develop such large deformations despite being tested under 53.5% $f_{R,p}$ due to the lower creep index influence in short $CMOD_p$ deformations.

Table 13. Creep index and delayed CMOD values corrected by shrinkage effect developed in the creep stage.

Specimen	$f_{R,c}$ (MPa)	I_c (%) $f_{R,c}/f_{R,1}$	$f_{R,c}/f_{R,p}$	$CMOD_{ci}$ (μm)	$CTOD_{ct}^{14}$ (μm)	$CTOD_{ct}^{30}$ (μm)	$CTOD_{ct}^{90}$ (μm)	$CMOD_{ct}^{180}$ (μm)	$CMOD_{cri}$ (μm)	$CMOD_{crd}$ (μm)
0.05a–25	1.30	24.1	27.2	21.0	52.2	62.0	79.2	81.1	59.1	49.1
0.1a–25	1.35	25.0	33.3	31.0	60.4	66.3	80.1	84.6	53.6	48.6
0.2b–25	1.31	24.3	27.7	35.0	67.5	81.2	100.9	106.2	71.7	66.7
0.3a–25	1.35	25.0	27.3	32.0	55.1	65.9	78.3	82.5	51.5	46.5
0.5a–25	1.38	25.6	21.4	32.0	89.5	97.6	105.3	107.8	42.8	39.8
0.05b–35	1.82	33.7	38.0	17.0	53.0	60.7	71.4	72.2	45.7	38.7
0.1b–35	1.89	35.0	36.7	22.0	44.1	55.9	62.3	64.9	49.5	44.5
0.2b–35	1.88	34.9	37.5	30.0	70.6	77.7	97.6	107.0	86.0	76.0
0.3b–35	1.82	33.7	42.8	98.0	135.4	155.3	183.6	199.6	123.6	90.6
0.5a–35	1.95	36.2	44.1	90.0	134.6	151.4	174.8	186.0	96.5	82.5
0.05a–45	2.27	42.1	42.7	25.0	54.9	68.4	84.7	88.4	67.4	61.4
0.1b–45	2.34	43.4	53.5	25.0	68.3	80.1	103.9	112.3	83.8	67.8
0.2a–45	2.34	43.4	53.3	49.0	74.9	98.3	125.6	135.5	95.0	78.0
0.2b–45	2.54	47.1	51.1	65.0	116.3	133.1	164.9	176.3	114.3	93.3
0.3b–45	2.34	43.4	40.7	51.0	83.6	104.9	133.2	143.2	101.7	86.7
0.5b–45	2.46	45.6	42.1	71.0	99.9	119.8	156.6	167.0	97.5	82.5

The influence of the pre-cracking level $CMOD_p$ on the creep index was analysed, and CMOD deformations were depicted versus $CMOD_p$ for each creep index in Figure 62. It was observed that the influence of the pre-cracking level on delayed deformations increased as the creep index increased. In the case of low creep index ($25\% f_{R,1}$), $CMOD_p$ has a low influence on the delayed deformations (32.9% increase in $CMOD_{ct}^{180}$ of specimens 0.05a-25 to 0.5a-25 despite such $CMOD_p$ increase. Considering the same $CMOD_p$ increase from 0.05 to 0.5mm, the influence on delayed $CMOD_{ct}^{180}$ deformation increased 72.6% and 88.9% for 35 and $45\% f_{R,1}$ respectively.
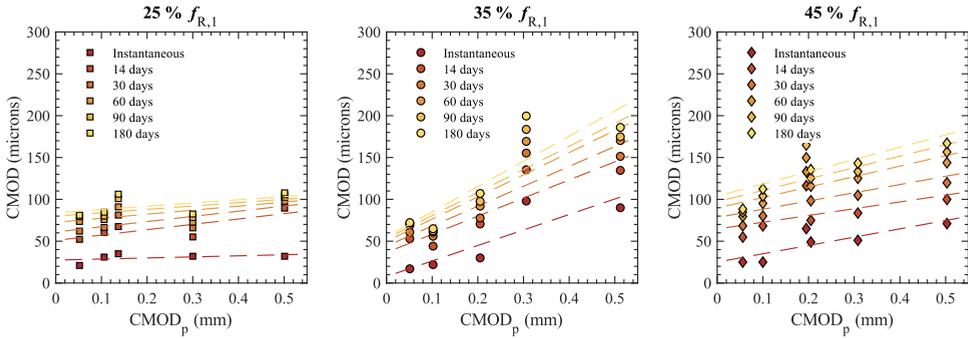
Figure 62. Influence of low pre-cracking $CMOD_p$ levels on the delayed $CMOD_{ct}$ at different creep index: (a) 25%, (b) 35% and (c) 45%.

Alternatively, the creep index influence was individually assessed for each pre-crack level in terms of delayed CMOD in Figure 63 with one chart per $CMOD_p$ pre-cracking level (0.05, 0.1, 0.2, 0.3 and 0.5 mm). It can be concluded that the creep index influence on delayed CMOD deformations at short $CMOD_p$ pre-cracks (0.05 mm) is rare and negligible. From the $CMOD_p$ = 0.1 mm (Figure 63.b) chart in advance, an ascendant trend of the influence of the creep index is observed. It is then confirmed that the creep index influence on delayed deformation increases with the pre-cracking level.
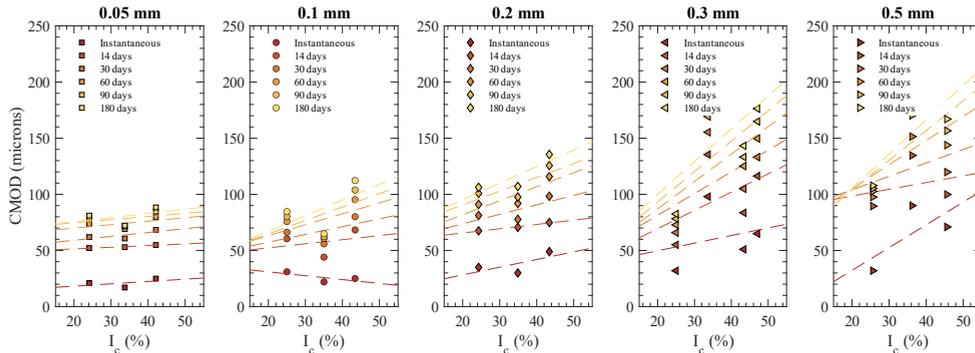
Figure 63. Creep index (I_c) influence on the delayed $CMOD_{ct}$ at different pre-cracking levels: (a) 0.05, (b) 0.1, (c) 0.2, (d) 0.3 and (e) 0.5 mm.

In addition, creep coefficients referred to the creep stage (φ_c) at 7, 14, 30, 90 and 180 days were respectively obtained. As previously explained, the creep coefficient is defined as the delayed deformation ($CMOD_{cd}$) ratio to the instantaneous deformation $CMOD_{ci}$. Creep coefficients at the defined ages versus pre-crack level $CMOD_p$ are depicted in Figure 64.a to assess the influence of the pre-cracking level on the creep coefficients. As observed, the creep coefficient at all ages tends to decrease in time following a power law: creep coefficients decrease significantly for low pre-cracking levels (0.05-0.2 mm), whereas for large pre-cracking levels (0.3-0.5 mm), the influence is reduced considerably. This behaviour may be explained since the instantaneous $CMOD_{ci}$ increases with the pre-cracking level. Similarly, the impact of the creep index on the creep coefficients is analysed in Figure 64.b. In this case, creep coefficients follow a linear descendant trend when the creep index increases. However, the descendant slope of the influence trend reduces in time when the creep coefficient at older ages is considered, producing that the influence of the creep index on the creep coefficients at 180 days (φ_c^{180}) is almost negligible. It is then concluded that creep coefficients at the creep stage reduce when either the pre-cracking level or the creep index increases. However, the pre-cracking level (power trend) has more influence than the creep index (linear trend) on the creep coefficient reduction regardless of age. Note that creep index influence at 180 days of creep test is almost negligible or trends to zero at time infinity due to the significance of the instantaneous deformation $CMOD_{ci}$, which controls the creep coefficient equation.
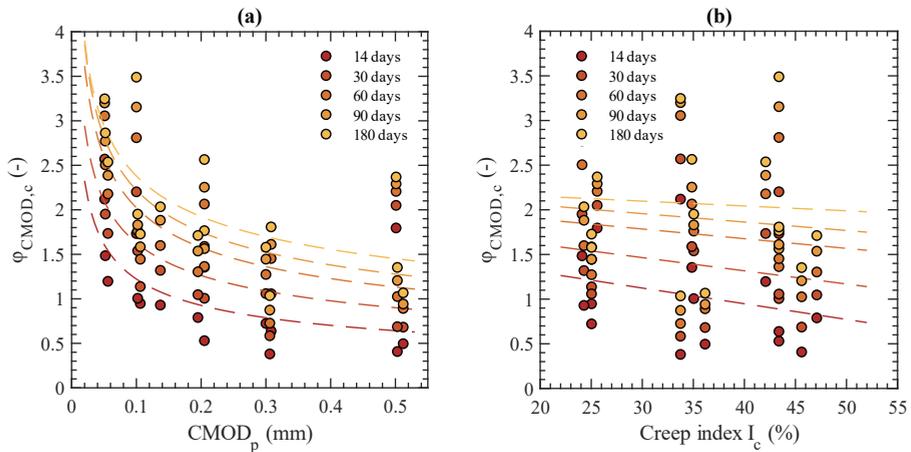
Figure 64. Influence of pre-cracking level CMOD$_p$ (a) and creep index I_c (b) on creep coefficients at different ages.

COR parameter in 30-day time lapses was also obtained for the long-term test duration and analysed in terms of both pre-cracking level $CMOD_p$ and creep index I_c in Figure 65. Regarding the pre-cracking level influence (Figure 65.a), an ascendant influence trend of the $CMOD_p$ on COR parameter at early ages was observed. In contrast,

the influence gets reduced when later time-lapse periods are considered. On the other hand, creep index influence on the COR parameter increases following an exponential law, as seen in Figure 65.b, where the highest COR values were obtained under a 45 % high creep index. The influence of the creep index on COR parameters decreases when later time-lapses are considered for COR calculation, as observed in Figure 65.a. COR values are more scattered at an early age due to the influence of instantaneous and short-term high deformations. Hence, assessing COR parameters at long-term ages is more suitable, where less variation and more confidence in the results are found.
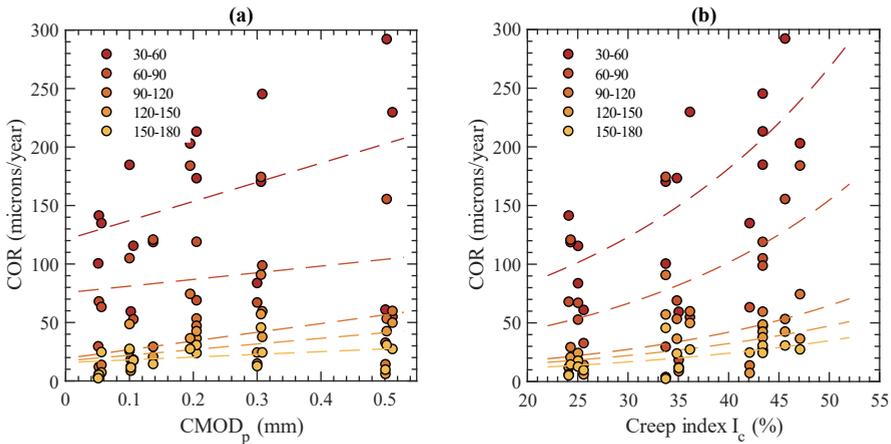
Figure 65. Influence of pre-cracking level CMOD$_p$ (a) and creep index I_c (b) on COR at different time lapses.

It is then crucial to define a reference creep index I_c or stress level value to obtain comparable results between laboratories in creep tests and a reference residual strength to apply the corresponding creep index. When the average $f_{R,p}$ obtained from one FRC batch or mix is used as the residual stress reference value, it must be expected to obtain a relevant variation in terms of creep index related to individual $f_{R,p}$. Considering the average $f_{R,p}$ to characterise the creep behaviour of one FRC batch would provide long-term curves from specimens tested under such scattered creep index related to individual $f_{R,p}$ that it could not be easy to identify the influence of either the creep index or the intrinsic variability of the FRC material in such scattered behaviour. On the contrary, if the creep index is kept constant for each specimen referring creep index to the individual $f_{R,p}$, the obtained results shall be comparable besides a certain variability since specimens were tested in similar conditions. It could be assumed that the variability obtained in creep tests considering the creep index referred to the individual residual stress at the pre-cracking test shall be explained by the intrinsic variability of FRC material since all specimens were tested in similar conditions.

Therefore, from this PhD work and analysis, it is proposed as a general procedure to use the individual stress of each specimen shown at CMOD$_p$ as the reference stress value

to apply the creep index parameter to homogenise testing conditions and results obtained by removing variables from such a complex creep test procedure. In addition, it is proposed the use of 50% of the stress $f_{R,p}$ individually obtained by each specimen at $CMOD_p$ as creep index (I_c) nominal reference value for the creep characterisation tests due to the following statements:

- It was concluded that the creep index significantly influences the CMOD long-term behaviour considering pre-cacking levels from 0.2 mm in advance. The significance of the creep index on delayed CMOD increase with the pre-cracking level.

- No specimen failures were detected at the studied creep index. The creep characterisation testing procedure assesses the long-term behaviour under sustained load. To this purpose, using the proposed creep index shall provide stable delayed deformations (primary or secondary creep) but not tertiary creep.

- It was confirmed that a low creep index (25%) does not influence the delayed deformation enough to provide comparable results blurring any long-term assessment.

- Since the proposed reference pre-cracking value $CMOD_p$ correspond to the $CMOD_1$ (0.5 mm), the creep index is then referred to $f_{R,1}$ performance, which is the reference residual strength for the post-cracking behaviour assessment.

- Moreover, as previously stated, creep characterisation tests shall be representative of the FRC structures working conditions in serviceability. This creep index proposal is related to the serviceability residual strength $f_{Fts} = 0.45$ $f_{R,1}$ of the linear model proposed in the Model Code 2010 [19] and defined as the post-cracking strength for serviceability crack openings.

- It was concluded that the creep index acceptance range shall be restrictive enough to provide confidence due to its highly significant influence on the long-term performance of FRC. Therefore, the $50 \pm 5\%$ $f_{R,p}$ creep index acceptance range is proposed for both single- and multi-specimen setups. All specimens tested out of the creep index accepted range shall be identified in the test report as tested out of limits.

- It has been detected that for low pre-cracking values ($CMOD_p < 0.5mm$), delayed deformation may be blurry or too influenced by the shrinkage deformation.

- It is proposed as a general procedure to use the individual stress $f_{R,p}$ as the reference stress value to homogenise testing conditions and results by removing variables from such a complex creep testing procedure.

Note that these proposals aim to define a creep test procedure with characterisation purposes. Notwithstanding the recommendations, creep index acceptance thresholds may be increased or modified for scientific research purposes.

4.4. Recovery capacity during the multi-phase creep test

Whereas compressive creep tests are typically carried out in uncracked specimens, flexure creep tests are usually performed in the cracked state. FRC specimens are previously pre-cracked up to a specific crack mouth opening displacement ($CMOD_p$) to simulate an SLS damage level.

As explained in Section 3.2, the current flexure creep procedure aimed to assess delayed deformations to the instantaneous deformations using the creep coefficient referred to the creep stage ($\varphi_{w,c}$). Therefore, delayed recovery deformations in both pre-cracking and creep phases were ignored, as seen in Figure 66. The pre-cracking test is finished once the desired pre-cracking level is achieved, and then the specimen is unloaded. Once unloaded, the specimens are removed from the universal testing machine (UTM) and moved to the creep test climate conditions chamber, neglecting the delayed recovery deformation.
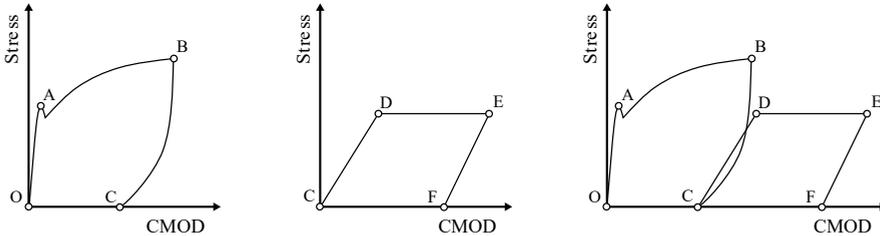
Figure 66. Creep process chart ignoring CMOD recovery deformations.

The relevance of both the post-creep residual behaviour and the creep coefficient referred to the origin of deformations ($\varphi_{w,o}$) has recently increased. Therefore, it became relevant to register the crack evolution properly during the whole process, even when short-time delayed deformations occur. The new creep testing procedure considering delayed recovery deformations of both pre-cracking and creep tests are represented in Figure 67.
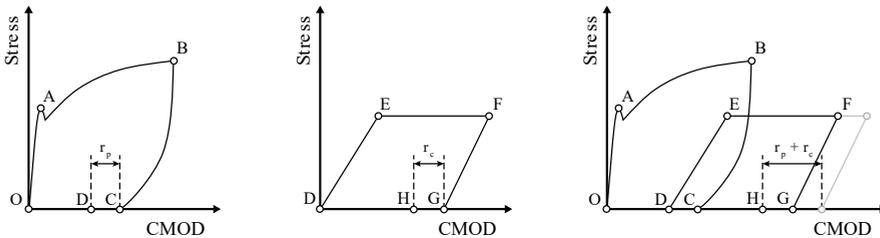
Figure 67. Creep process chart considering CMOD recovery deformations at the end of both the pre-cracking and long-term stages.

Recovery capacity becomes relevant when creep coefficients are analysed referred to the origin of deformation ($\varphi_{CMOD,o}$) instead of the creep stage only ($\varphi_{CMOD,c}$). Whereas

the former defines the ratio of delayed deformation to the origin of deformations (segment O-E in Figure 67) of the specimens, the latter defines the ratio of delayed deformation to the instantaneous deformation (segment D-E in Figure 67). Therefore, it is important to highlight that the creep coefficient referred to the origin could be underestimated when ignoring delayed recovery deformations. Regarding the post-creep residual capacity of FRC specimens after the long-term tests, delayed recovery deformations are also relevant. It is required to concatenate the Stress-CMOD deformation behaviour curves during the different phases of the creep test procedure to obtain the post-creep residual performance of FRC specimens.

During this PhD experimental program, it was noticed that neglected delayed recovery deformations represented a significant percentage of the residual deformation that could lead to underestimating the creep coefficient referred to the origin and overestimating post-creep residual performance. Therefore, a specific experimental program was designed to assess the delayed recovery deformations after the pre-cracking and the creep tests and their influence on the residual post-creep performance. The procedure and duration of delayed recovery depending on the phase of the creep test are analysed and established in this section.

4.4.1. Delayed CMOD recovery after the pre-cracking phase

Three different batches of steel, synthetic and glass fibre-reinforced concrete were designed to assess delayed recovery after the monotonic pre-cracking tests. The dosage of fibres was selected depending on the fibre material to obtain similar residual performance. Therefore, 40 kg/m^3 of steel fibres were used for the steel fibre-reinforced concrete (SFRC) batch, whereas 10 kg/m^3 of both synthetic and glass fibres for synthetic fibre-reinforced concrete (SyFRC) and glass fibre-reinforced concrete (GFRC) batches respectively. Full information about the concrete matrix composition and test setups can be consulted in the Appendix D and Appendix F.

Three 150×150×600 mm prismatic specimens were pre-cracked in flexure following the EN 14651 procedure [26] from each batch. Pre-cracking tests were carried out following the three-point bending test (3PBT) setup up to a crack mouth opening displacement (CMOD) of 0.5 mm. Specimens were loaded at 0.05 mm/min CMOD rate, and when the desired crack opening deformation was achieved, the specimens were unloaded at 0.3 mm/min rate. When the load applied was removed entirely, the instantaneous deformations $CMOD_{pri}$ were registered, and the data acquisition equipment continued recording delayed $CMOD_{pr}$ deformation for 10-15 additional minutes. The pre-cracking curves for both batches are depicted in Figure 68. As it can be observed in Figure 68, similar pick load f_{LOP} and average $f_{R,1}$ residual performance was achieved for the three mixes. Instantaneous recovery $CMOD_{pri}$ can be identified and starts when 0.5 mm CMOD is reached. Net $CMOD_{pri}$ ranges from 174.7 microns for SFRC specimens to 228.9 microns for the SyFRC batch. Results obtained for each specimen and the average of different batches are described in Table 14.
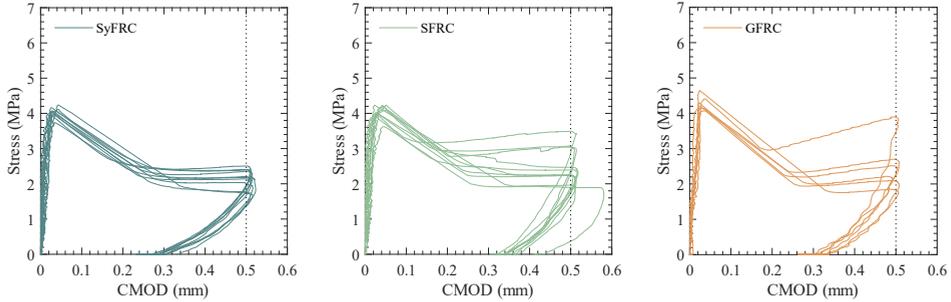
Figure 68. Pre-cacking test carried out on different batches: a) SyFRC, b) SFRC, and c) GFRC.

Table 14. Main parameter of pre-cracking tests of SyFRC, SFRC and GFRC.

Batch		f_L	$f_{R,p}$	$CMOD_p$	$CMOD_{pri}$	$CMOD_{pr}$			
					t = 0'	t = 2'	t = 5'	t = 10'	t = 15'
SyFRC	mean	4.06	2.17	513.9	298.2	262.8	256.3	250.2	--
	CV	3.3	11.9	0.8	6.2	6.7	7.1	6.5	--
FRC	mean	4.07	2.50	519.5	358.5	341.9	339.0	338.2	--
	CV	4.7	20.8	4.2	8.8	8.7	9.0	9.3	--
GFRC	mean	4.31	2.55	510.1	323.0	305.0	300.6	295.8	290.3
	CV	5.0	28.6	1.3	4.8	5.9	6.2	6.2	6.3

Delayed recovery deformations cannot be easily identified in Figure 68 since they are represented by a straight line in the horizontal axis and may induce to ignore this recovery capacity. Therefore, delayed CMOD net recovery deformation ($CMOD_{pri} -$ $CMOD_{pr}$) is represented in Figure 69 versus time considering time zero when the specimen is entirely unloaded (point C in Figure 66). By this action, it can be observed in Figure 69 how CMOD recovery deformation increases in time for different batches after performing pre-cracking tests.
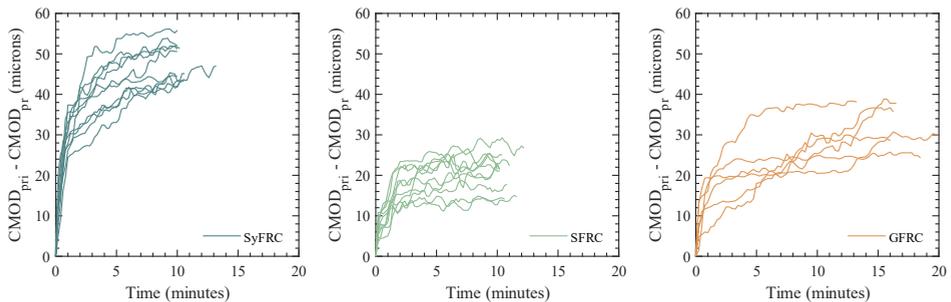
Figure 69. Delayed CMOD net recovery evolution after the pre-cacking test: a) SyFRC, b) FRC, and c) SFRC specimens.

The recovery capacity differs from batches depending on the material of the fibres, as observed in Figure 70. Recovery capacity is higher for SyFRC than SFRC due to the elasticity of the propylene material. Average delayed CMOD net recovery 10 minutes after the pre-cracking test range from 20.3 µm in the case of SFRC mix to 48.0 µm in the case of SyFRC.
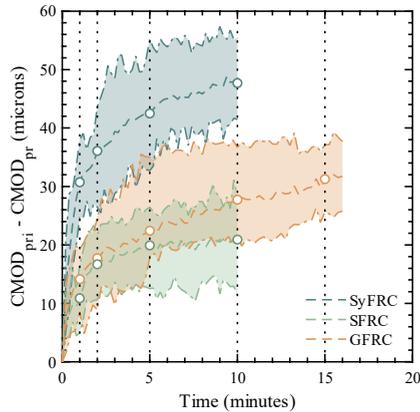
Figure 70. Minimum, maximum and average delayed CMOD recovery after the pre-cacking test carried out in GFRC, SyFRC and SFRC specimens.

Table 15 summarises the significant ratios of delayed deformation compared to both instantaneous and residual deformation. Delayed recovery registered 10 minutes after the pre-cracking tests represents 22.3, 12.6 and 14.6% of the instantaneous net recovery recorded for each SyFRC, SFRC and GFRC mix, respectively. In terms of residual deformation, the delayed recovery 10 minutes after unloading represents 16.1, 5.7 and 8.4 % of the residual deformation after the instantaneous recovery $CMOD_{pri}$ of each mix, respectively.

Table 15. Significant ratios of delayed recovery deformation for SyFRC, SFRC and GFRC.

Batch	$CMOD_p$	$CMOD_{pri}$	$CMOD_{pr}^{10'}$	$\dfrac{CMOD_{pri} - CMOD_{pr}^{10}}{CMOD_p - CMOD_{pri}}$	$\dfrac{CMOD_{pri} - CMOD_{pr}^{10}}{CMOD_{pri}}$
SyFRC	513.9	298.2	250.2	22.3 %	16.1 %
FRC	519.5	358.5	338.2	12.6 %	5.7 %
GFRC	510.1	323.0	295.8	14.6 %	8.4 %

4.4.2. Delayed CMOD recovery after the creep phase

Analogously to the proposed procedure for delayed recovery after the pre-cracking test, it was considered that a similar procedure was required after the creep phase unloading for a certain lapse of time to register delayed recovery deformations.

In the monotonic pre-cracking test, the specimens are loaded for a while and then unloaded. In contrast, the load is applied to the specimen for long periods of 90, 180, 360 days or even more in the long-term creep tests. Considering the difference in load application duration between both phases, it is easy to assume that the specimen will require more time to recover elastic delayed deformations. Since the long-term test duration is usually measured monthly (30-day lapses), a delayed unloading recovery duration of 30 days was first established. This proposed procedure was applied again for the same three SyFRC, FRC and GFRC batches after their respective creep tests. Delayed deformation under sustained stress curves obtained during the creep phase are shown in Figure 71 for the batches where the unloading recovery deformations are marked in red.
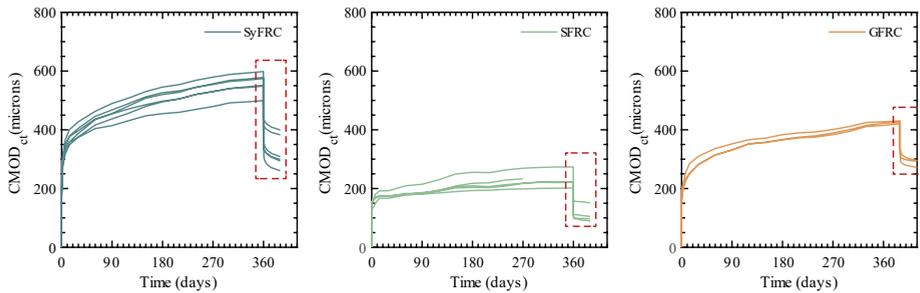
Figure 71. Delayed deformations during the creep phase of the creep test for SyFRC (a), SFRC (b) and GFRC (c) specimens.

The instantaneous and delayed residual CMOD deformation after unloading, $CMOD_{cri}$ and $CMOD_{crd}$, were registered for all specimens. Average recovery net values were obtained to assess the recovery capacity after the creep test of different FRC mixes and collected in Table 16. Regarding the $CMOD_{cri}$, similar average instantaneous net recovery ($CMOD_{ct} - CMOD_{cri}$) was obtained for SyFRC, SFRC, and GFRC mixes, 109.9, 102.5 and 97.3 µm, respectively. In contrast, significant differences were found in the $CMOD_{crd}$ capacity of FRC mixes depending on their fibre material. The average delayed CMOD net recovery ($CMOD_{cri} - CMOD_{crd}$) obtained after 30 days for SyFRC, SFRC, and GFRC mixes was 124.6, 16.8 and 41.4 µm, respectively. Figure 72 plots delayed CMOD net recovery deformation evolution for each specimen and FRC mix.
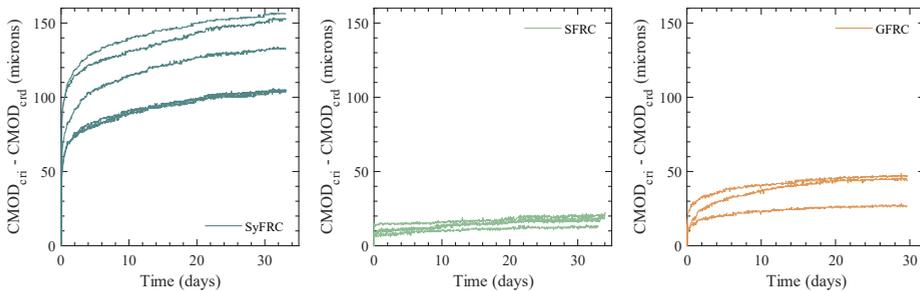
Figure 72. Delayed CMOD net recovery deformation after 30 days unloaded.

Table 16. Instantaneous and delayed net average CMOD recovery in microns after the creep tests of SyFRC, SFRC and GFRC mixes.

Batch		$CMOD_{ct} - CMOD_{cri}$	$CMOD_{cri} - CMOD_{crd}^{j}$							Ratio (%)
		0 days	1 day	2 days	3 days	5 days	7 days	14	30 days	
SyFRC	Average	109.9	84.5	91.1	95.7	100.8	104.5	114.0	124.6	113.3
	CV (%)	18.6	22.4	22.9	22.1	21.9	21.9	20.3	19.6	
SFRC	Average	102.5	11.3	11.3	11.3	11.9	12.0	13.8	16.8	16.4
	CV (%)	9.2	25.7	25.7	21.7	21.0	19.3	18.4	21.3	
GFRC	Average	97.3	21.3	24.7	26.2	28.8	31.4	36.1	41.4	42.5
	CV (%)	8.7	34.6	31.3	29.5	29.8	27.6	26.6	27.4	

Delayed net recovery registered 30 days after the creep test, represents 113.3, 16.4 and 42.5% of the instantaneous net recovery recorded for each SyFRC, SFRC and GFRC mix, respectively. It is important to highlight that, in the case of SyFRC mix, the delayed recovery deformation of SyFRC mix is 1.3 times larger than the instantaneous recovery. Therefore, if delayed recovery deformations are neglected, the post-creep performance assessment shall be underestimated.

Considering such different behaviour regarding delayed deformation, the average long-term behaviour of each mix in the creep phase has been analysed. Average CMOD values were obtained for each experimental creep test and compared in Figure 73. Note that all batches were subjected to similar stress $f_{R,c}$ during the creep phase since a similar residual performance was obtained in the pre-cracking tests, as seen in Figure 68.
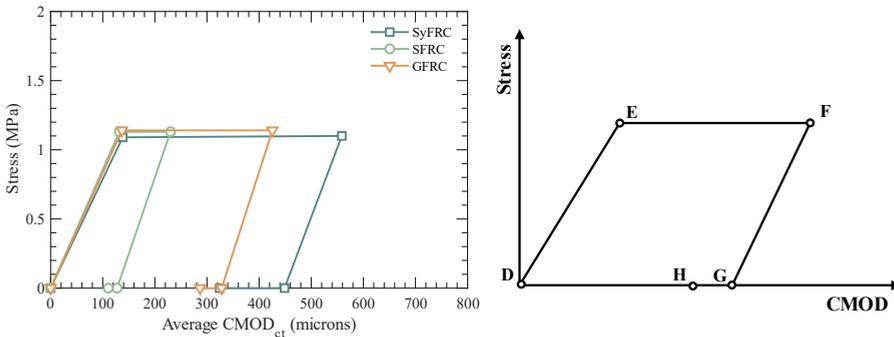
Figure 73. Simplified average creep behaviour obtained by SyFRC, SFRC and GFRC batches after 360 days of creep test.

It can be observed that all mixes present similar behaviour in terms of instantaneous $CMOD_{ci}$ after loading (segment D-E) and $CMOD_{cri}$ instantaneous recovery after unloading (segment F-G), regardless of the FRC mix. On the contrary, significant differences can be observed in terms of delayed deformations $CMOD_{ct}$ (segment E-F) and $CMOD_{crd}$ (segment G-H), depending on the material of the fibres. Therefore, it can be concluded that FRC mixes behave similarly in instantaneous deformations regardless of the fibre material, but material leads the delayed FRC behaviour providing different responses.

Furthermore, to assess not only FRC mixes with similar residual performance but also with different fibre dosages and residual capacity, one GFRC additional series was cast with the same concrete matrix and different fibre dosage. Therefore, two GFRC series with 10 and 20 kg/m^3 of glass fibre were tested in similar creep conditions. Since both series share the same concrete matrix, all pre-cracked specimens show a similar limit of proportionality (LOP) (4.31 and 4.25 MPa for 10 and 20 kg series, respectively), as seen in Figure 74.a. On the contrary, as expected, the residual strength $f_{R,p}$ is clearly influenced by the high fibre dosage. The average residual strength $f_{R,p}$ ranges from 2.28 MPa for the 10 kg/m^3 series to 5.85 MPa for the 20 kg/m^3 series. After the pre-cracking

tests, three specimens of each series were selected for the creep phase. All specimens were subjected to the same creep index (I_c) of 50% of their respective $f_{R,p}$ of each selected specimen, obtaining average sustained stress $f_{R,c}$ of 1.14 and 2.82 MPa, respectively, for each series. Three specimens of each series were tested in creep for 390 days and then kept unloaded for 30 days to measure recovery deformations (Figure 74.b). Delayed CMOD net recovery deformations of both series are compared in Figure 74.c.
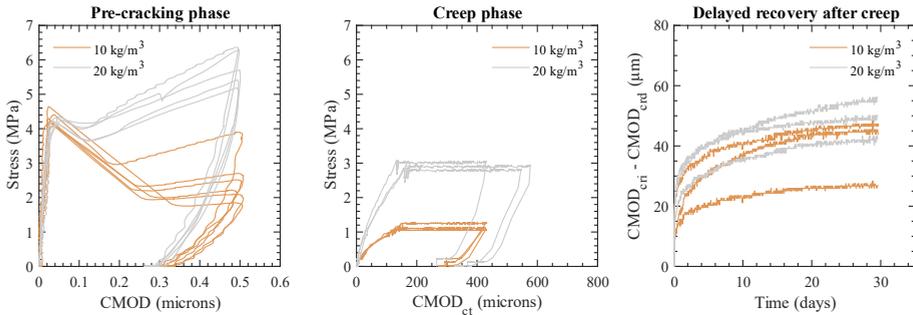
Figure 74. Comparison between delayed recovery capacity of two GFRC mixes with 10 and 20 kg/m³ after 390 days under sustained load.

Interesting conclusions can be deducted from this comparison regarding the dosage of fibres in the concrete matrix. In terms of mechanical performance, the residual strength increases more than 2.5 times if the fibre dosage is doubled from 10 to 20 kg/m³, as could be expected. However, no delayed deformation reduction is achieved by increasing the fibre dosage. The average CMOD of the reference parameters obtained in pre-cracking and creep phases for both mixes are shown in Table 17. It can be confirmed that CMOD net deformations and recoveries are both higher for the 20 kg/m³ series in all steps. In the pre-cracking phase, the net recovery is around 8 % higher on average (instantaneous and delayed) for the 20 kg/m³ series than 10 kg/m³. In the creep phase, the instantaneous deformation $CMOD_{ci}$ and delayed deformation $CMOD_{ct}$ at 390 days are 20.7% on average larger for 20 kg/m³ series than 10 kg/m³. Significant differences were found regarding the instantaneous net recovery after the creep test, where the 20 kg/m³ series experimented a recovery 51.2% larger than the 10 kg/m³ series.

Table 17. Delayed recovery capacity of GFRC series in pre-cracking and creep phases.

Phase	Pre-cracking	10 kg/m³	20 kg/m³	Ratio 10/20	$\Delta_{20\text{-}10}$ / 100
Pre-cracking	$CMOD_p - CMOD_{pri}$	181.4	196.8	0.92	8.5 %
	$CMOD_{pri} - CMOD_{pr}^{10'}$	27.2	29.1	0.93	7.0 %
Creep	$CMOD_{ci}$	136.7	164.0	0.83	20.0 %
	$CMOD_{ct}^{390}$	425.5	517.0	0.82	21.5 %
	$CMOD_{ct} - CMOD_{cri}$	97.3	147.1	0.66	51.2 %
	$CMOD_{cri} - CMOD_{crd}^{30}$	41.4	48.3	0.86	16.7 %

These results conclude that increasing the fibre dosage does not reduce the long-term CMOD deformations when the FRC mixes are tested at the same creep index since the residual performance improved, and thus, specimens are subjected to 2.5 more stress. Delayed deformations obtained in the creep test by 20 kg series only increased by 20% compared to 10 kg/m^3 despite the substantial increase of applied stress. However, delayed deformation reduction could be expected when the fibre dosage is increased and the sustained stress $f_{R,c}$ kept constant (1.14 MPa) since the creep index is considerably reduced to 20% of $f_{R,p}$ obtained for the 20 kg/m^3 series.

4.5. Flexure boundary conditions and flexure load configuration

Due to the absence of a standardised creep test methodology, each laboratory developed its own procedure and designed its creep frame, support rollers and transfer plates. This fact implies a wide range of support boundary conditions and creep testing frames, as previously described. Support boundary conditions are highly correlated to residual performance on flexure tests and may influence the long-term performance of FRC specimens. Since both support and loading rollers are not directly reported in publications, it is not easy to classify publications in terms of boundary conditions. However, it could be possible to identify some of them thanks to the pictures of the creep frame and equipment provided. Classification in terms of degrees of freedom is proposed in Figure 75 to assess the used boundary conditions. Three degrees of freedom are analysed and classified by creating a three-letter code where (O) and (X) represent the free and restricted degrees of freedom, respectively. By this action, boundary conditions variations can be compared to assess any correlation among laboratories.

| Rotation in X | Rotation in Z | Translation in X |
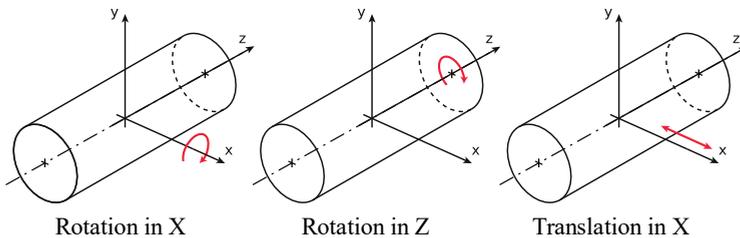
Figure 75. Boundary conditions classification depending on degrees of freedom.

Five different boundary conditions typologies were observed depending on the freedom or restriction on each axis. Some samples of each boundary condition typology detected in the literature are classified in Table 18 in terms of the proposed degrees of freedom code. The type OOO is usually made of simple steel cylinders fixed or welded to steel plates hindering neither rotation nor translation. Although simple steel rollers placed between specimens for multi-specimen setup seem to allow free rotation, they were also included in type OOO. This decision is explained by the fact that the roller cannot definitively rotate free if the symmetric specimens force the roller to turn in the opposite sense. The second typology XOX allows free rotation in the longitudinal axis

Table 18. Reported boundary conditions classified by proposed degrees of freedom code.

Code	Description	Roller construction	References
XXX			[75, 90, 92, 67]
XOX			[86, 51, 112]
OXX			[97, 86, 90]
OOX			[112, 51]
OXO			[51, 104, 67]
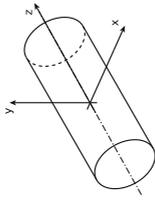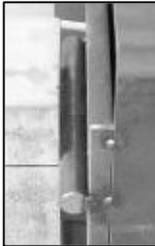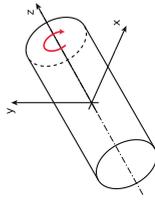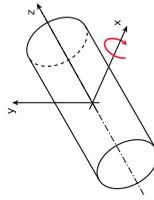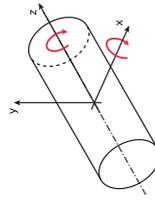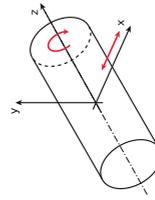
of the roller but restrains both translation and rotation in the transversal axis, whereas the third typology OXX enables the roller to swivel in its transversal axis but restrains any other movement. If the second and third typologies are combined, it is obtained typology OOX, where rotation in both longitudinal and transversal axis of rollers are free. The last support typology OXO is a simple steel roller commonly used in simple-specimen setups as supports. Although it may seem similar to OOO typology due to similar construction, rotation is not restricted by any symmetrically located specimen.

After the boundary conditions analysis, the first conclusion is that most methodologies used simple rollers between specimens instead of mechanical supports in steel plates as flexure boundary conditions. Although this roller construction is easier, faster, and cheaper, it is not definitively appropriate to perform flexure creep tests. On the one hand, the deformation of each specimen depends on the deformation of the rest of the specimens. On the other hand, if the creep test flexure setup is based on EN 14651 [26], it should be guaranteed the same boundary conditions as recommended by the standard. The proposed boundary conditions for either 3PBT or 4PBT are described in Figure 76.

	Position	Support A	Support B
	Top:	OOX	--
	Bottom:	OOX	XOX
	Top:	XOX	OOX
	Bottom:	OOX	XOX
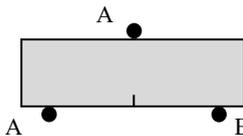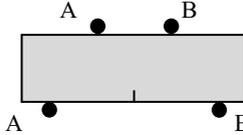
Figure 76. Recommended boundary conditions for either 3PBT or 4PBT flexure creep test setup.

Typologies XOX, OXX and OOX construction require a steel plate to fix both support and loading rollers. Therefore, these boundary conditions allow specimens to develop deformations independently of each other. In conclusion, the use of steel plates between the specimens is highly recommended to ensure proper boundary conditions.

4.5.1. Supporting rollers design improvements

Both supporting and loading rollers used in this PhD experimental programme were upgraded to be in accordance with previous conclusions. The actual steel plates of the creep frame define XXX and XOX boundary conditions for each pair of loading and supporting rollers. Hence, the most restrained support (XXX) was redesigned and upgraded from XXX to XOX, as shown in Figure 77. Firstly, a solid steel roller was used to allow rotation instead of a half roller fixed in the supports. Moreover, two bearings were included at each roller end to ensure deformation despite the loading condition. By

this action, it was expected to reduce horizontal restrictions due to the rollers construction and obtain higher creep deformations. It is worth mentioning that during the creep test, crack opening increase microns over days. Any restriction shall be avoided since it may highly influence delayed deformations and, consequently the long-term performance and characterisation of FRC.
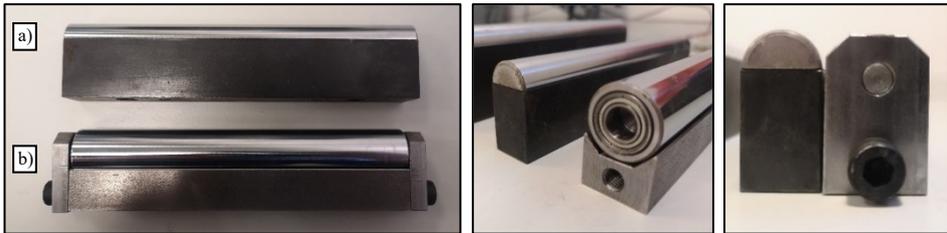
Figure 77. Supporting rollers construction improvements: old rollers (a) versus improved rollers (b).

Upgraded rollers were used in the creep test from 2018 in advance. To assess if the upgraded rollers work correctly, two marks were drawn with a black marker at starting position and checked along the creep test duration. Although no specific experimental programme was carried out to compare both old and upgraded rollers, it was noticed that rollers freely rotate during creep tests.

4.6. Creep phase loading process duration (t_{ci})

No guidelines are usually given regarding the loading rate in creep test standards. In the case of the creep in compression test ASTM C512-02 [28] standard, any recommendation is given about the loading ratio besides the load range since tests are carried out on uncracked specimens following the elastic load-deformation trend, and the loading ratio does not influence the material response. Compressive strains are expected to increase following the elastic modulus slope of the material despite the loading process duration. Recently, the EN 12390-17:2018 [29] standard proposed the following recommendation to "increase the load as quickly as possible, but no longer than 30 s without interruptions or delays", providing some instructions and restrictions about the loading time.

Currently, in the case of flexure creep tests, there are neither standardised procedures nor recommendations to define the loading steps. Due to the absence of standardised procedure, a wide range of t_{ci} may arise, as observed in the recent international Round-Robin Test carried out by the RILEM Technical Committee 261-CCF (Figure 78). The influence of the frame design and testing procedure on the loading process duration was then proved.
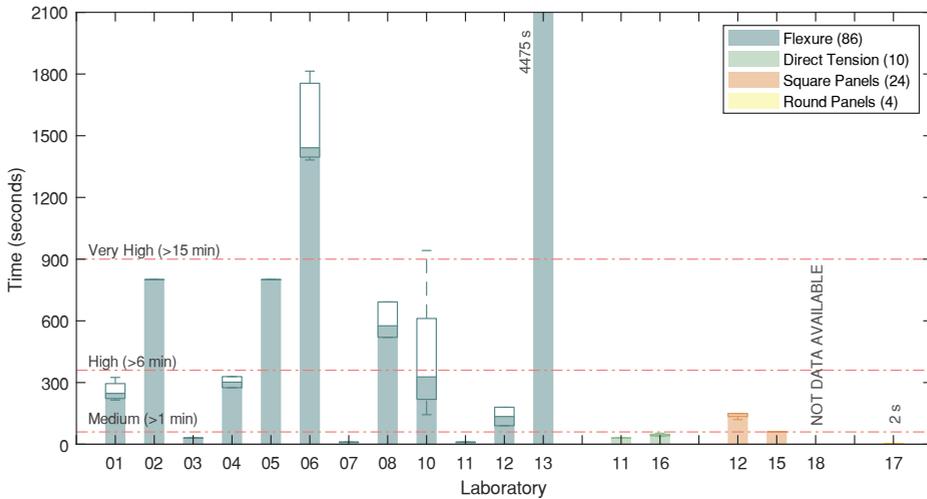
Figure 78. Variability in t_{ci} observed among the 17 participant laboratories in the international Round-Robin Tests in creep tests developed within the RILEM Technical Committee 261-CCF activities [120].

The creep phase is carried out on cracked FRC specimens where the sustained stress $f_{R,c}$ during the creep phase is usually a reduced percentage of the achieved stress during pre-cracking tests $f_{R,p}$. In other words, during the loading stage in the creep phase, $CMOD_{ci}$ crack opening deformation shall not reach the uncracked concrete matrix. This fact implies that $CMOD_{ci}$ deformation will directly depend on the fibre deformation depending on the elastic modulus of the material of the fibres. Thus, the influence of the t_{ci} may differ from FRC mixes reinforced with different fibre materials.

Considering these statements, it can be expected that the creep frame loading time duration affects the instantaneous deformation following the proposed pattern in Figure 79: the more time t_{ci} considered, the larger $CMOD_{ci}$ obtained. Considering that the instantaneous $CMOD_{ci}$ parameter belongs to the equation of creep coefficient [Equation 2], it can be assumed that the loading process differences (i.e., frame construction, load application system…) and the time t_{ci} have a certain influence on the creep coefficients. If this influence is confirmed, it could be concluded that creep coefficients obtained from two laboratories with significant differences in terms of t_{ci} could not be compared. Therefore, it is essential to assess how t_{ci} influences the instantaneous deformation and whether the loading procedure or the way the load is induced is also relevant for the instantaneous deformation.

Due to the significance of the $CMOD_{ci}$ and the wide variability in terms of loading procedures, creep frames designs and creep setups, it is crucial to assess the influence of this procedure step on the creep test and define the loading time guidelines for the creep phase to obtain comparable results and avoid unexpected scatter in the creep coefficients calculation.
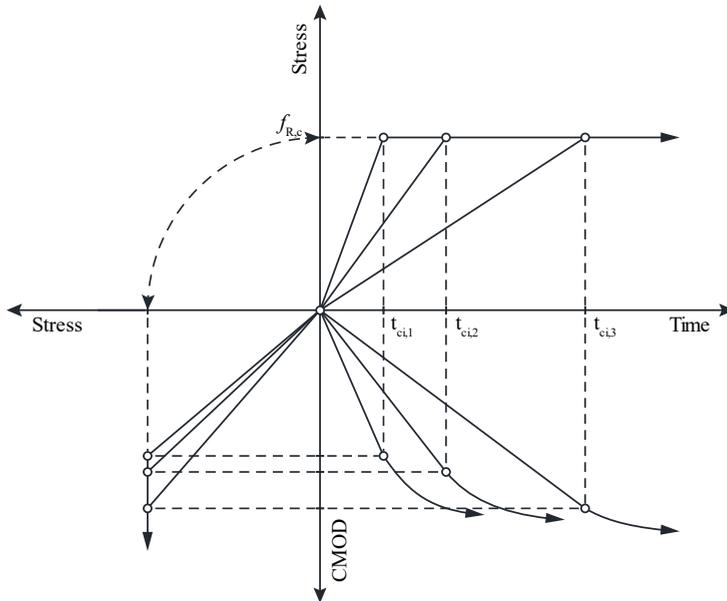
Figure 79. Influence of the time t_{ci} required to reach $f_{R,c}$ on the instantaneous deformation $CMOD_{ci}$.

4.6.1. Influence of the loading ratio on the instantaneous deformation

An experimental program containing three specimens of each SyFRC and SyFRC mix was developed to assess the influence of the loading process duration (t_{ci}) on the instantaneous deformation $CMOD_{ci}$ at the beginning of the creep stage. Full information about the concrete matrix composition and experimental results can be consulted in the Appendix G.

Most laboratories induced the load in less than 15 minutes, but some atypical t_{ci} values between 20 to 75 minutes were also found, as later presented in Figure 94. Although the loading process rarely exceeds 15 minutes, considering the wide range of t_{ci} observed, large t_{ci} times were also proposed as a reference. The t_{ci} times below are proposed to induce the load in the selected specimens:

- 10, 15, 30 and 60 seconds
- 5, 10, 15, 30, 45, 60 minutes.

Following the recommendations proposed in this thesis for the creep testing in flexure, all specimens were notched and pre-cracked in 3PBT flexure until 0.5 mm of $CMOD_p$ and then unloaded. The residual stresses obtained from the pre-cracking test are collected in Table 19. Moreover, valuable information is provided regarding the average sustained stress ($f_{R,c}$) reached during the loading ratio tests and the load and the corresponding creep index (I_c) achieved. To simulate creep test conditions, 50% of $f_{R,p}$ creep index was considered to obtain sustained stress $f_{R,c}$.

Table 19. Pre-cracking test parameters.

Mix	Specimen	f_L (MPa)	$f_{R,p}$ (MPa)	$f_{R,c}$ (MPa)	Load (4PBT) (kN)	I_c (%)
SFRC	S-01	3.29	4.59	1.06	5.54	23.2
	S-02	3.88	4.69	2.36	12.30	50.4
	S-06	3.95	4.71	2.46	12.84	52.3
SyFRC	MS-02	3.89	2.94	1.57	8.17	53.3
	MS-03	3.67	3.15	1.49	7.78	47.4
	MS-06	4.18	4.57	2.13	11.11	46.7

The loading tests were conducted individually for each specimen in a servo-controlled universal testing machine (UTM) instead of in the creep frames to reproduce optimal loading conditions. Specimens were tested in 4PBT flexure configuration as done in multi-specimen setups. The corresponding CMOD/min ratio was programmed to reach the desired $f_{R,p}$ in the defined lapses. Once the desired stress was reached, the load was sustained for 60 additional seconds reproducing the long-term stage and then unloaded at 0.3 CMOD/min ratio. Global behaviour among the SFRC and SyFRC specimens for the different t_{ci} considered can be compared in Figure 80.
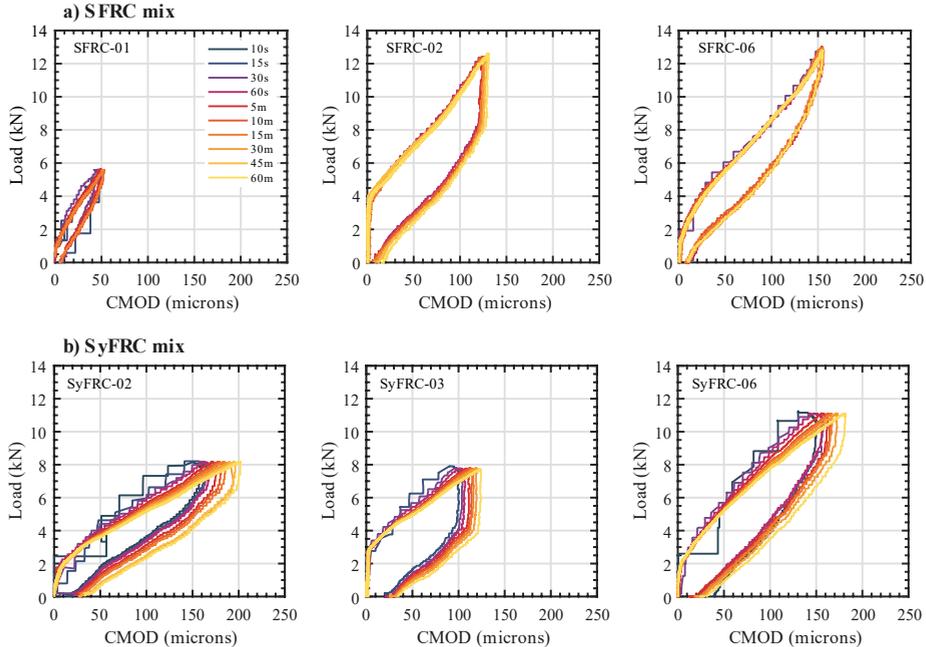
Figure 80. Stress-CMOD curves obtained by (a) SFRC and (b) SyFRC specimens depending on the time t_{ci} required to reach $f_{R,c}$.

SFRC specimens (Figure 80.a) show a quite stable Stress-CMOD behaviour despite the t_{ci} considered with a CMOD increase of up to 9 microns for 60 minutes t_{ci}. Regarding the SyFRC specimens corresponding to Figure 80.b, a gradual CMOD increase can be observed as the time t_{ci} considered increases. Unfortunately, due to some mechanical issues in the UTM, the specimen SFRC-01 did not reach the desired load and could only complete four loading steps at 1, 5, 10 and 15 minutes. Notwithstanding, it was considered important to keep the results in the global comparison since the same behaviour as for the rest of the SFRC specimens was found despite the low stress achieved. The instantaneous $CMOD_{ci}$ values obtained for each specimen at the tested t_{ci} loading times in the flexure test are provided in Table 20.

Table 20. Instantaneous CMOD$_{ci}$ results in μm from flexure loading test considering different time lapses of the t_{ci} parameter.

t_{ci}	Specimen					
	SFRC-01	SFRC-02	SFRC-06	SyFRC-02	SyFRC-03	SyFRC-06
T1-10s	-	-	-	151.3	-	141.2
T2-15s	46.2	-	-	156.8	95.1	-
T3-30s	45.8	-	147.5	160.7	98.7	143.3
T4-60s	47.4	121.6	152.5	163.0	100.6	151.9
T5-5m	48.1	122.2	152.9	171.0	108.8	155.1
T6-10m	52.0	124.9	153.6	177.7	112.1	162.7
T7-15m	52.0	124.7	154.0	183.9	113.7	165.7
T8-30m	-	125.0	154.6	189.4	118.8	172.0
T9-45m	-	128.0	-	195.6	-	-
T10-60m	-	130.4	154.8	201.0	122.8	180.6

If both Load-Time and CMOD-Time curves are deeply analysed, the instantaneous residual performance produced by the different loading times on each specimen can be easily compared. Monotonic flexure test results for each t_{ci} considered of specimen SFRC-02 are depicted in Figure 81. It can be observed that whereas the load reached (Figure 81.a) is constant for all times considered, the instantaneous CMOD (Figure 81.b) deformation slightly increased from 121.6 to 130.4 μm for 1 and 60 minutes, respectively. It was then concluded that the t_{ci} has a minor influence on the instantaneous CMOD deformation for the SFRC mix.
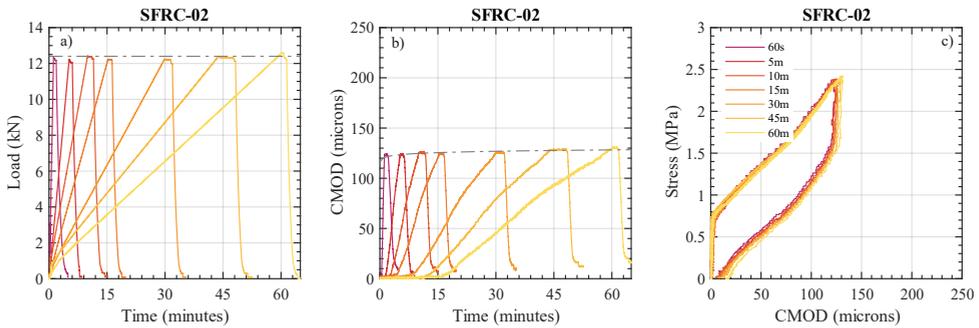
**Figure 81. Stress-CMOD (a), CMOD-Time(b) and Load-Time (c) curve obtained
in monotonic test by SFRC specimen at different lapses.**

On the contrary, a relevant influence of the t_{ci} on instantaneous CMOD deformation was found for the SyFRC mix specimens. Detailed charts obtained for SyFRC-02 specimens are depicted in Figure 82. It was observed that if the specimens reached the target load at different timings (Figure 82.a), instantaneous CMOD increased from 151.3 to 201 µm with the t_{ci} considered (Figure 82.b). If all the $CMOD_{ci}$ values obtained for all t_{ci} considered were connected (Figure 82.b), a theoretical envelope of $CMOD_{ci}$ deformation is created. This envelope provides the $CMOD_{ci}$ performance at any t_{ci} considered, including a basic $CMOD_{ci}$ value for $t_{ci} = 0$ seconds, representing the minimum instantaneous deformation for the specimen at instantaneous loading.
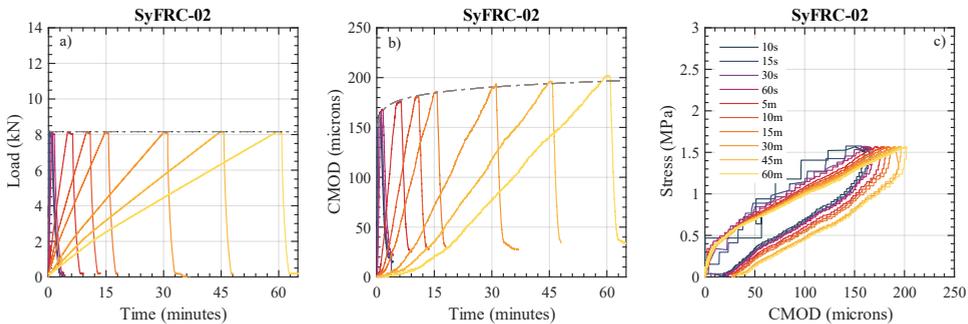
**Figure 82. Stress-CMOD (a), CMOD-Time(b) and Load-Time (c) curves
obtained in monotonic test by SyFRC specimen at all lapses.**

It was confirmed that the loading process duration significantly influences pre-cracked SyFRC specimens obtaining a CMOD increase of 40% if the load is applied in 1 hour instead of 1 minute. The net CMOD increase (Δ_{CMOD}) in time can be obtained if the first available CMOD reference for each specimen is deducted from the $CMOD_{ci}$ deformations of the latter t_{ci}. It can be observed in Figure 83 that Δ_{CMOD} increased on average for 60 minutes of t_{ci} 38.9 and 8.0 microns for SyFRC and SFRC mixes, respectively. This behaviour implies a 29.9 and 6.1% CMOD increase referred to the

first available reading for SyFRC and SFRC, respectively, when t_{ci} is increased by 60 minutes.
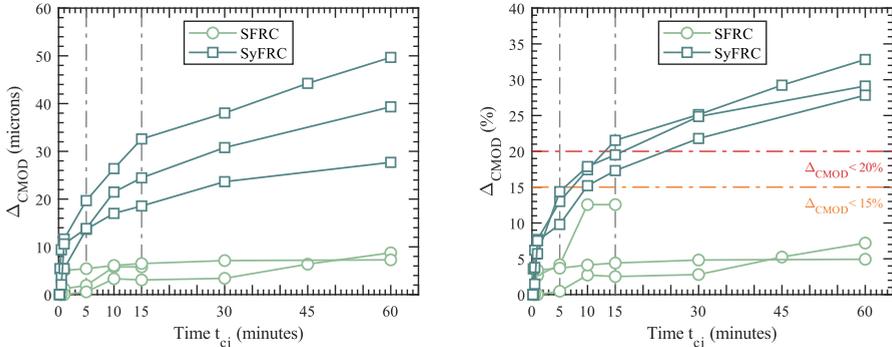
Figure 83. CMOD increase in both net microns and percentage considering as reference the first t_{ci} available for each specimen and at least T4 at 60 seconds.

Relevant conclusions were obtained from this experimental programme, where the significant influence of the t_{ci} parameter on the instantaneous deformation of SyFRC mixes and minor effects in the case of SFRC mixes could be confirmed. Therefore, the new t_{ci} parameter shall be defined and considered in the future flexure creep testing methodology proposal.

Due to the procedure and the "instantaneous" essence of the loading process, it has no sense to spend 60 minutes to induce the load in the creep frames. Short time variations at early t_{ci} times produced larger Δ_{CMOD} than more considerable time variations at later ages, as observed in Figure 83. In the case of the SyFRC mix, a 5.4% increase was noticed in only 4 minutes difference at early times ($1 < t_{ci} < 5$ minutes), whereas in 30 minutes difference in later times ($30 < t_{ci} < 60$ minutes), similar increase of 6.0% was observed. This variation indicates that t_{ci} shall be as short as possible to reduce the instantaneous deformation increase at early ages. Since the most relevant deformation occurs at the early creep stage, different loading procedures may lead to scattered $CMOD_{ci}$ and creep coefficients. Therefore, it is proposed that the loading process shall not exceed 5 minutes to keep the CMOD increase caused by the t_{ci} below the 15% threshold suggested in Figure 83.b.

In conclusion, a new t_{ci} parameter is proposed to limit the loading process duration and reduce scatter in terms of instantaneous deformations among laboratories. The load shall be gradually applied in the creep frame for at least 30 seconds but no more than 5 minutes ($30\ s < t_{ci} < 5\ min$). Furthermore, the load shall not be suddenly but gradually applied to avoid a hit or impact effect of the load. The creep methodology and the load application system shall be simple enough to gradually reach sustained stress in a few minutes. The use of gravity lever arm creep frames is highly recommended for this purpose.

4.7. Short-term deformation definition (CMOD$_{ci}$$^{15'}$)

Structural codes usually use creep coefficient as the reference parameter to assess the long-term behaviour in the design of the traditional structures. In the case of cracked FRC structures it is not yet clear how to consider this delayed behaviour in the design process. The interest of the scientific community on creep behaviour of cracked FRC has increased in last few years. Unfortunately, the absence of a standardised creep methodology does not allow a global assessment of long-term behaviour since research groups designed their own creep frames and developed their creep methodology, providing scattered performances.

The previous section confirmed how different are the existing creep methodologies in terms of the procedure to apply the load in the creep frame and t_{ci} parameter. Such differences imply a not negligible influence on the instantaneous deformation and, consequently, on the creep coefficient. The instantaneous deformation CMOD$_{ci}$ is a crucial parameter since it is in the denominator of Equation 2 and therefore is a dominant variable for the creep coefficient calculation.

Considering that the most relevant deformation occurs during the early creep stage and different loading procedures may lead into different CMOD$_{ci}$, a new parameter defined as short-term deformation is proposed to reduce the influence of such scattered t_{ci}. The short-term deformation describes the related deformation at a specific reference time after the loading process starts. This new parameter aims to homogenise the instantaneous deformation to obtain comparable creep coefficients from experimental test results.

To assess the influence of the short-term parameter on the creep coefficients, a first attempt of the short-term parameter definition was proposed to the participants of the recently developed RRT [197]. Two different references were considered at 10 and 30 minutes after the sustained stress $f_{R,c}$ is reached, as described in Figure 84. The proposed short-terms CMOD$_{ci}$$^{10'}$ and CMOD$_{ci}$$^{30'}$ were applied in the creep coefficients equation of 86 prismatic specimens of SyFRC and SFRC mixes tested in flexure creep for one year.

Figure 84. Short-term deformation proposal for RRT at 10 and 30 minutes after the load is applied [197].

Besides the RRT coordination, I contributed to the RRT from my PhD research with six prismatic specimens of each FRC mix tested in four creep frames in a multi-specimen creep test setup. Creep coefficients were obtained according to Equation 2 considering both instantaneous ($CMOD_{ci}$) and short-term ($CMOD_{ci}^{10'}$ and $CMOD_{ci}^{30'}$) deformations. Figure 85 depicts the evolution in time of the creep coefficients during the creep test duration for each deformation.

Figure 85. Creep coefficient evolution considering (a) $CMOD_{ci}$, (b) $CMOD_{ci}^{10'}$ and (c) $CMOD_{ci}^{30'}$ deformations of 6 specimens from each mix tested for the RRT participation.

It is then confirmed that using short-term deformations reduces the creep coefficient scatter within the same laboratory results and long-term deformations are homogenised. Nevertheless, this effect is more relevant for SyFRC than SFRC due to fibre properties. Considering the regular instantaneous deformation $CMOD_{ci}$, median creep coefficients referred to creep stage at 360 days of 3.46 and 0.71 were obtained for SyFRC and SFRC mixes, respectively. In the case of SyFRC, when short-term deformations are considered, the creep coefficient decreases to 2.52 and 2.13, representing a percentage decrease of 19.8 and 32.3%. Creep coefficients of SFRC specimens decreased to 0.59 and 0.55, respectively, for the short-term considered (8.0 and 13.5% referred to the instantaneous deformation). Moreover, it is also appreciated in the box a whiskers plot that the size of the boxes decreases when larger short-term deformations are considered. This quartile range reduction confirms that short-term deformation homogenises the obtained creep coefficients.

To assess the influence of the short-term deformation on the inter-laboratory results, the available creep coefficients of the flexure participants were analysed in Figure 86. Whereas the median creep coefficient of the SyFRC mix decreased by 15.6 and 23.9 % with 10 and 30 minutes short-term, respectively, 6.4 and 12.4 % reductions were observed for the SFRC mix.

Figure 86. Inter-laboratory creep coefficient scatter reduction comparing short-term deformations CMOD$_{ci}^{10'}$ and CMOD$_{ci}^{30'}$ to instantaneous CMOD$_{ci}$ for SyFRC and SFRC specimens.

Although the inter-laboratory creep coefficient variation and the corresponding median decreased, a better homogenisation effect was expected. It is important to highlight that the t_{ci} parameter was not defined for the RRT, and some participants reported t_{ci} values near 30 minutes, providing extra-large shot-term CMOD$_{ci}^{30'}$ of one hour. It was then concluded that a wide range of t_{ci} among participants interfered with the creep coefficient homogenisation. The amplitude of the loading process duration t_{ci}, which ranges from 10 to 1800 seconds, exceeds the time-lapses considered for short-term deformations. Consequently, some laboratories reported instantaneous CMOD$_{ci}$ deformations after 30 minutes loading process concurrent with the reported short-term deformations at 30 minutes by other participants. This fact blurred the homogenisation effect in the creep coefficients. Therefore, to avoid the influence of the t_{ci} on the short-term parameter, it was decided to include the t_{ci} within the time considered for the short-term deformation. Regarding the proposed guidelines in this PhD work for both the loading procedure and the t_{ci} acceptance range reduced to 5 minutes, a significant homogenisation is expected in terms of instantaneous deformation.

Regarding the time lapse to considered, as observed in Figure 85 and Figure 86, the more time considered as short-term deformation, the more is reduced the creep coefficients due to most deformation occurs during the early creep age. If short-term deformation at 30 minutes is used, FRC creep coefficient may be undervalued due to such reduction. Short-term at 10 minutes seems to be enough in terms of homogenisation effect since no significant scatter improvements were found for 30 minutes. Furthermore, short-term deformation 10 after inducing the load seems more representative of instantaneous deformation, keeping the homogenisation properties.

Therefore, the short-term deformation proposal shall consider the 5 minutes maximum range to induce the load and 10 additional minutes. The short-term deformation (CMOD$_{ci}^{15'}$) is finally defined as the deformation at 15 minutes from the beginning of the loading process, as described in Figure 87. Indeed, this proposal is in accordance with the $\Delta_{CMOD} < 15$ % proposed limit in Figure 83.b.

Figure 87. Definition of the short-term deformation CMOD$_{ci}$$^{15'}$ proposed for creep testing procedure analysis [43].
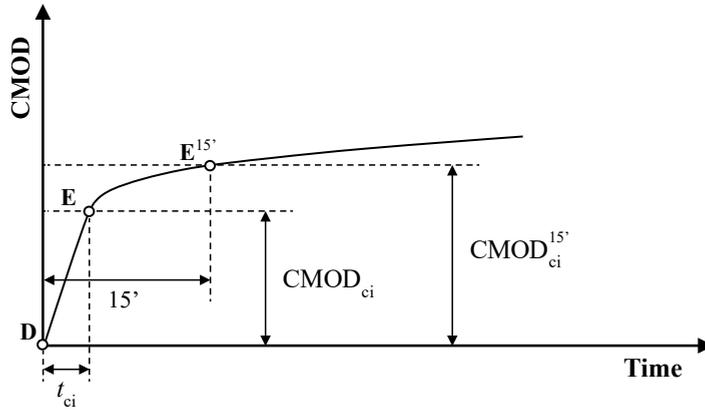
4.8. Multi-specimen setup

Creep tests are usually long-term (more than three months) occupying a significant space in the laboratories. Therefore, it became crucial to develop and establish a multi-specimen procedure reliable and safe enough to optimize both time and laboratory facilities.

The use of multi-specimen setup for creep test is highly extended, as stated in Chapter 2. The creep in compression standard ASTM C512 [28] allows to test 3 specimens simultaneously in compressive creep frames since the specimens are tested in uncracked conditions. This implies that each specimen's deformation does not significantly influence the rest of the specimen's behaviour. Therefore, it can be affirmed that multi-specimen testing is accepted when delayed deformations of each specimen may be registered without any interaction with the deformation of the rest of the specimens. This principle must also be respected in the case of the flexure creep test when a multi-specimen setup is carried out, even if FRC specimens are in their cracked state. The main advantages of the use of the multi-specimen setup can be described as follows:

- Save space in the laboratory facilities.

- Increase of the number of tested specimens in similar conditions.

- Reduce time to obtain a significant number of specimens tested in creep.

Nevertheless, using a multi-specimen setup also presents several disadvantages to consider before the experimental program design and execution. The following disadvantages should be considered before the single- or multi-specimens setup decision:

- Instability of stacked FRC cracked specimens in 3PBT. Therefore, a flexure configuration change to 4PBT is recommended.

- Creep index (I_c) may result more scattered since all the specimens in the frame will be subjected to the same applied load. Notwithstanding, this thesis develops a procedure proposal to solve this issue by pre-cracking more specimens than strictly required and proper selecting according to their residual performance.

- Boundary conditions are crucial since roller frictions or different degrees of freedom may induce horizontal restraints in the force system.

- More complex procedure for stacking the specimens and inducing the load

- Additional time required for stacking the specimens

- The upper specimens induce a certain dead load over the lower specimens to be considered in the creep applied load calculation. Once again, this PhD develops a procedure proposal to solve this issue in Section 4.8.2.

- The sudden failure of one of the stacked specimens may compromise the continuity of the creep test of the rest of the specimens

Despite the described disadvantages, the multi-specimen test setup can be successfully carried out if the following procedure recommendations and improvements are considered.

4.8.1. Flexure configuration

The first item to consider defining a multi-specimen creep test setup is that the stability of the specimens must be guaranteed during the whole process of the long-term test procedure. Therefore, whereas a standard 3PBT is recommended for single specimens (Figure 88.a), in the case of the multi-specimen creep test setup, a 4PBT flexure load configuration (Figure 88.b) is usually adopted and recommended to improve the stability of the column of specimens.
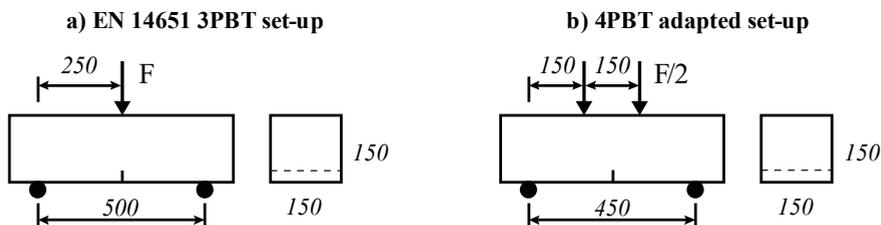
Figure 88. Recommended flexure load configurations: a) EN 14651 3PBT flexural setup and b) 4PBT adapted set-up.

Note that the objective of the creep test is to induce a specific flexure stress to each specimen. This flexure setup change implies a numerical conversion due to the bending moment variation between both setups. Using the right equation, it is possible to obtain the required load that induces the desired sustained stress $f_{R,c}$.

Considering that pre-cracking tests are carried out in a 3PBT bending setup following the EN 14651 standard [26], the residual stress performance $f_{R,p}$ can be obtained using Equation 4.

$$f_{R,j} = \frac{6M_j}{bh_{sp}^2} = \frac{6}{bh_{sp}^2}\frac{F_j l}{4} = \frac{3F_j L}{2bh_{sp}^2}$$

Equation 4

On the contrary, when the 4PBT bending setup depicted in Figure 88.b is used for the long-term phase, the residual stress shall be obtained using Equation 5:

$$f_{R,j} = \frac{6M_j}{bh_{sp}^2} = \frac{6}{bh_{sp}^2}\frac{F_j l}{6} = \frac{F_j L}{bh_{sp}^2}$$

Equation 5

It is important to highlight that creep index I_c must be applied to the $f_{R,p}$ stress achieved in the 3PBT pre-cracking test but creep tests can be carried out in either 3PBT or 4PBT for single- or multi-specimen setups, respectively. Therefore, given the target $f_{R,c}$ sustained stress, the corresponding load $F_{R,c}$ to apply in the creep frame can be determined using Equation 6 according to the 3PBT bending setup for single-specimens creep test:

$$F_{R,c} = \frac{f_{R,c}\, 2\, b\, h_{sp}^2}{3\, L}$$

Equation 6

Analogously, the corresponding load $F_{R,c}$ to apply in the multi-specimen creep frame according to the 4PBT bending setup can be obtained by Equation 7.

$$F_{R,c} = \frac{f_{R,c}\, b\, h_{sp}^2}{L}$$

Equation 7

Using the right equation in each step of the creep procedure is quite relevant for the success of the creep test methodology. Otherwise, the desired creep index could be exceeded.

4.8.2. Specimen selection

FRC is a material with a relative scatter in the residual performance. This property must be considered for the success of the creep testing methodology. Compared to those tests carried out individually, when a multi-specimen creep test setup is applied, the load induced to the creep frame obtained in Equation 7 will affect two or three FRC specimens with different residual strengths. Therefore, specimens destined to creep tests must be selected according to their residual performance obtained in the pre-cracking tests. Otherwise, the residual performance scatter may lead to a scattered creep index (I_c) when the multi-specimen setup is adopted.

In the case of a single specimen creep test, additional specimens are not required since it is easier to achieve the desired creep index I_c during the creep test. Considering the scattered residual performance of FRC, in the case of either two or three multi-specimen setups, it is highly recommended to cast more specimens than strictly required for the long-term tests, as shown in Table 21.

Table 21. Minimum number of specimens recommended for the specimen selection.

Specimens per frame	Specimens to be pre-cracked
1	1
2	4
3	5

If these minimum requirements are followed, it is easy to ensure enough residual performance variety for a proper specimen selection. The more pre-cracked specimens available, the more possibilities to obtain a combination of specimens that accomplish the targeted creep index.

It is important to advise that, due to the absence of a standardised creep test methodology, creep index I_c may be quite scattered among research laboratories. The international Round-Robin Test organised by the RILEM Technical Committee 261-CCF in creep in the cracked state [51, 120] is a clear example of how the creep index may vary depending on the procedure adopted by the laboratory. Figure 89 shows the creep index box and whiskers plot for the tested methodologies: flexure, direct tension, square panels, and round panel.

Figure 89. Creep index scatter obtained by each participant laboratory in the international Round-Robin Test organised by the RILEM Technical Committee 261-CCF.

Laboratories that carried out flexure creep tests are highlighted in red dashed square (1 to 13). It can be observed how the creep index scattered may range from 42.4 to 68.8 % between laboratories. Such variability is due to slight differences in the creep test procedure, methodological aspects, and equipment between laboratories since no standardised methodology exists. It can be assumed that results obtained in such variable conditions cannot be easily compared. To develop a standardised and comparable methodology, it is required to establish acceptance thresholds for some parameters.

Figure 90 plots the creep index values grouped by laboratory obtained for 86 specimens tested in flexure creep. The methodology directly influences the creep index variability obtained by each laboratory. Laboratories 3, 5 and 7 carried out a single-specimen creep test setup and achieved the best fit to the targeted creep index. Regarding the laboratories that adopted multi-specimen creep test setup, significant scatter in terms of creep index can be observed. On the one hand, the procedure adopted by five participants (laboratories 1, 2, 4, 5 and 11) could fit most of the specimens within the 5% creep index acceptance threshold. On the other hand, four participants (laboratories 6,8,12 and 13) could not successfully reach the desired creep index in most of their specimens. Therefore, it can be concluded that the adopted procedure significantly influenced the creep index accuracy when the multi-specimen setup is adopted. Note that it is marked if single- (S) or multi-specimens (M) setups were used to assess that the single-specimen procedure provides more accurate creep index values.

Figure 90. Application of the creep index acceptable ranges to the specimens tested in creep in the RRT.

Two different creep index acceptance thresholds (5% and 10%) are compared in Figure 90: the former is closer and provides more creep index accuracy; the latter is wider, and the creep index may result too scattered. Considering the 50% agreed target creep index, it can be deduced that 23.2% of the specimens could not accomplish the 5% threshold, but only 12.8% of the specimens would be considered out-of-bounds if the

threshold is widened to 10%. Considering the high impact of the creep index on the delayed deformations, it is proposed the use of the 5% creep index acceptance threshold.

The selection process flowchart presented in Figure 91 is proposed for a proper specimen selection in multi-specimen setup. It provides guidelines to reach the best creep index fit considering the residual performance, relative position of the specimens in the creep frame, and the dead load of load transmission elements.
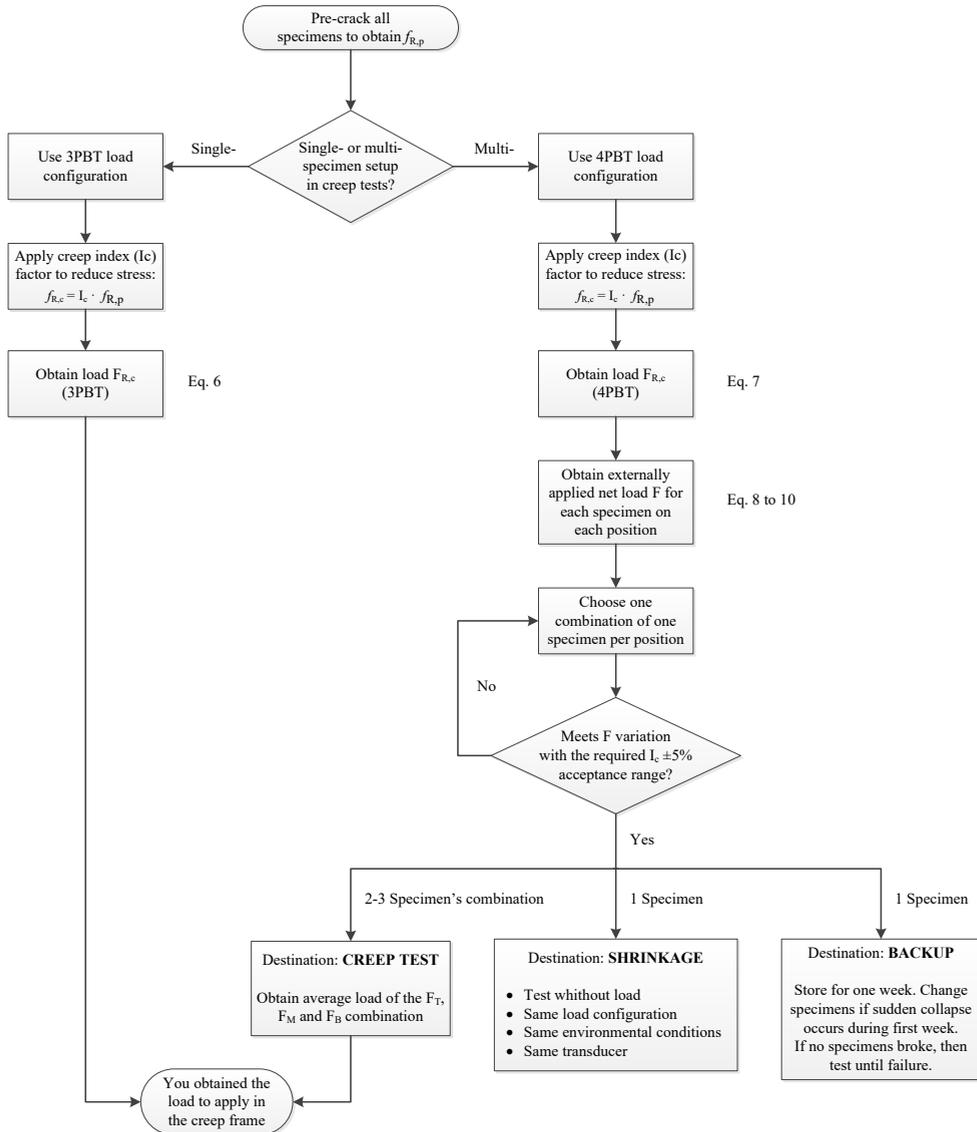
Figure 91. Specimen selection process flowchart for multi-specimen setup.

It is observed in the flowchart how simply the procedure is when the single-specimen creep test setup is adopted since the load to be applied that accomplishes the creep index acceptance threshold is individually obtained for each specimen. Nevertheless, it is feasible to perform a multi-specimen setup accomplishing the proposed restrictions to get comparable results if the proposed procedure is followed.

Transmission elements dead load to consider

In the case of multi-specimen creep test configuration, both the upper specimens and the load transfer plates weight induce an additional dead load over the lower specimens. This extra load must be adequately considered, as explained in Figure 91, for the creep applied load $f_{R,c}$ and creep index I_c calculation. Figure 92 shows the elements that shall be considered as additional dead load depending on the relative position of the specimen.
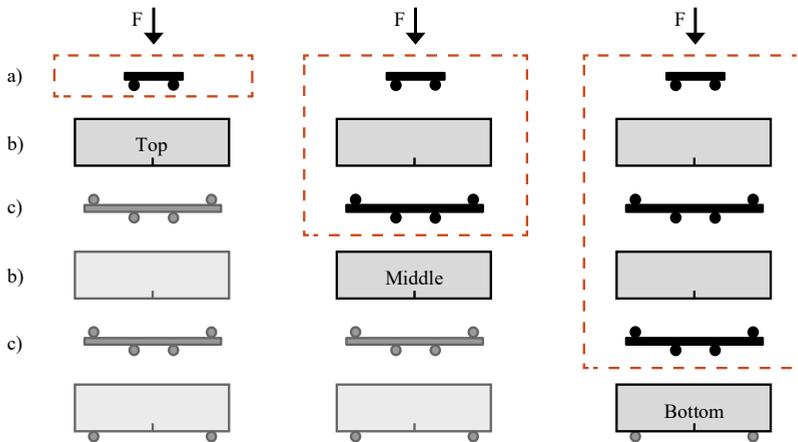
Figure 92. Dead load of the additional elements to consider for the load calculation during the selection process.

Considering the elements required to mount the specimens in flexure, the dead load of three different elements must be considered for the load calculation:

- a) top transfer plate: the load is directly applied over this steel plate, and transfer the load to the top specimen
- b) FRC specimen dead load
- c) intermediate transfer plate: this steel plate contains both supporting and loading rollers to transfer load between two specimens and is usually bigger and heavier than plate a).

The dead load of these transfer plates depends on their construction and materials. Therefore, each laboratory shall weigh its own equipment to know the dead load to consider in the calculation. Table 22 provides the information relative to the weight and load of the equipment used in this PhD experimental program. The dead load applied in

the corresponding specimens depending on their relative position is also provided. Note that the dead load ranges from 0.1 kN from the top specimen to 1.25 kN applied to the bottom specimen: the lower position of the specimen, the more dead load is applied.

Table 22. Analysis of the best combinations selection process.

Element	Weight (kg)	Load (kN)	Dead load over specimens (kN)		
			Top	Middle	Bottom
a	10.26	0.10	0.10	0.10	0.10
b	32.00	0.31	-	0.31	0.31
c	26.58	0.26	-	0.26	0.26
b	32.00	0.31	-	-	0.31
c	26.58	0.26	-	-	0.26
TOTAL			0.10	0.67	1.25

Specimen location

Not only the residual performance of the specimens but the location of each specimen within the specimen columns is also relevant to achieve the target creep index. Due to the natural scatter of FRC specimens, different location of a group of three specimens provides different creep index scatter within the column.

Following the flowchart described in Figure 91, three specimens that accomplish the creep index acceptance range must be selected to be mounted in one column for the creep test. Note that in the multi-specimen setup, the same load F applied in the creep frame affects all the specimens simultaneously. Therefore, the required loads of each specimen, excluding upper elements dead load, shall be as equal as possible.

Considering Table 21 proposal, five FRC specimens from the same batch were pre-cracked. To compare the theoretical applied loads (excluding upper elements dead load) of all the specimens on each position, the loads F_{TOP}, F_{MID} and F_{BOT} were obtained for each specimen following equations:

$$F_{TOP} = F_{R,c} - (a) \hspace{3cm} \textbf{Equation 8}$$

$$F_{MID} = F_{R,c} - (a + b + c) \hspace{2cm} \textbf{Equation 9}$$

$$F_{BOT} = F_{R,c} - (a + b + c + b + c) = F_{R,c} - (a + 2b + 2c) \hspace{1cm} \textbf{Equation 10}$$

As previously concluded, the lower position of the specimen, the more dead load is applied into the specimen. Therefore, it can be concluded that specimens with higher $F_{R,p}$ shall be placed at the lowest position. Table 23 provides de results obtained in the pre-cracking tests, the required load to be applied in creep to each specimen ($F_{R,c}$) to reach the target creep index, and the theoretical loads (F_{TOP}, F_{MID} and F_{BOT}) applied for each possible location. Note that specimens are ordered in ascendant $F_{R,p}$ to make the comparison easier.

Table 23. Residual performance and theoretical loads comparison to select specimens.

Specimen	f_L (MPa)	$f_{R,p}$ (MPa)	$F_{R,p}$ (kN)	$F_{R,c}$ (kN)	F_{TOP}	F_{MID}	F_{BOT}
S3	3.75	2.19	11.55	5.77	**5.67**	5.10	4.53
S1	4.19	2.36	12.58	6.29	6.19	**5.62**	5.05
S5	4.13	2.39	12.91	6.45	6.35	5.78	5.21
S4	3.98	2.40	12.95	6.47	6.37	5.80	5.23
S2	3.98	2.51	13.58	6.79	6.69	6.12	**5.55**

At first sight, it can conclude that specimen S2, with the highest $F_{R,c}$ 6.79 MPa, shall be located at the bottom position with F_{BOT} of 5.55 MPa. Additionally, specimen S3, with the lowest $F_{R,c}$ 5.77 MPa, could be located at the top position with an F_{TOP} of 5.67 MPa. It is confirmed that both F_{BOT} and F_{TOP} are pretty equal, as required. Finally, specimen S1 is revealed as the best option for the middle position car its 5.62 MPa of F_{MID} are within the F_{BOT} and F_{TOP} bounds. Finally, specimens S3, S1 and S2 were chosen for the multi-specimen creep test setup with $F_{R,c}$ 5.77, 6.29 and 6.79 MPa, respectively.

Notwithstanding, to assess the influence of the specimen location in the creep index variation, all the possible combinations were compared. Six different combinations are given depending on the specimen location of the selected specimens S1, S2 and S3. Table 24 analyses and compares the combinations in load and creep index.

Table 24. Analysis of the best combinations selection process.

Parameter		Combination					
		C1	C2	C3	C4	C5	C6
		(1-2-3)	(1-3-2)	(2-1-3)	(2-3-1)	(3-1-2)	(3-2-1)
Load	F_{TOP}	6.19	6.19	6.69	6.69	5.67	5.67
	F_{MID}	6.12	5.10	5.62	5.10	5.62	6.12
	F_{BOT}	4.53	5.55	4.53	5.05	5.55	5.05
	Mean F (kN)	5.61	5.61	5.61	5.61	5.61	5.61
	Mean $F_{R,c}$ (kN)	6.28	6.28	6.28	6.28	6.28	6.28
Creep index	Min. I_c	45.42	45.42	42.08	42.08	49.47	46.27
	Median I_c	46.27	50.47	49.95	54.41	49.95	49.47
	Max. I_c	59.34	54.41	59.34	54.48	50.47	54.48
	Mean I_c	50.35	50.10	50.46	50.32	49.96	50.08
	CV (%)	15.5	9.0	17.1	14.2	1.0	8.3

It can be observed in Table 24 that all the combinations provide the same mean load F to be applied in the creep frame (5.61 kN). Moreover, when the additional load of the top transfer plates and specimens are considered, the same average creep load $F_{R,c}$ for all

the combinations (6.28 kN) is obtained. However, it is important to highlight that the average creep index shall not be considered as the sole indicator for both the combination and position selection. Although all the combinations provide excellent accuracy in terms of mean creep index I_c, the median creep index is quite scattered among the combinations, as observed in both Table 24 and Figure 93. The median creep index shall be as close as possible to 50% to ensure that all specimens simultaneously accomplish the acceptable range of creep index variation.
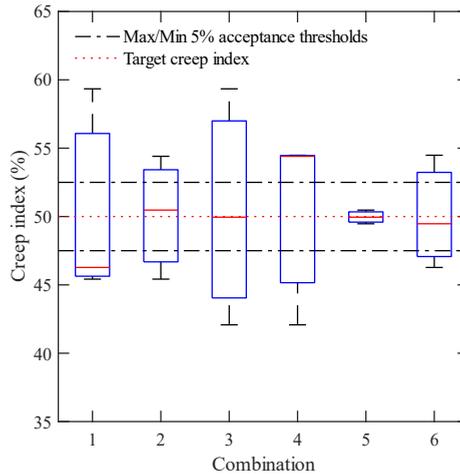
Figure 93. Box and whiskers plot of the creep index obtained for each combination.

As well as the mean load F to be applied, all the combinations provide enough accuracy in terms of mean creep index (I_c) but unsatisfactory values when median creep index values are assessed. If either minimum or maximum creep index values are observed, many outlier values are found for most combinations. These significant differences are confirmed thanks to the creep index CV that ranges from 1.0 to 17.1% obtained by combinations C5 and C3, respectively. Therefore, despite the similar mean load and creep index obtained by all combinations, it is clearly observed in Figure 93 that only combination C5 accomplished the creep index requirements in terms of mean value and acceptance variation range. It is confirmed that the selection of the specimens S3, S1 and S2 located in the top, middle and bottom positions, respectively, provide the best combination with an average applied load F of 5.61 kN and CV of 1.0%. Hence, it can be concluded that the proposed procedure improvements make it possible to achieve great accuracy in terms of creep index when a multi-specimen setup is adopted.

Specimen destination

Following the proposed procedure, three specimens have been selected to be tested in creep in a multi-specimen setup. Considering that the FRC batch was composed of five

specimens, two specimens were discarded for the creep test. To take advantage of the discarded specimens, it is proposed in the selection process flowchart (Figure 91) to use one of the discarded pre-cracked specimens for the long-term shrinkage test. The shrinkage test procedure proposal is widely explained in the incoming section 5.1. The last specimen shall be stored for one week as specimen backup. If any specimen fails during the first week of the creep test, either by a sudden collapse or any procedure issue during the loading process, the broken specimen could be restored by the backup specimens, and the long-term test restarted. Note that in this case, the relative position of the new specimen within the specimen stack shall be reconsidered and analysed to ensure the required creep index.

4.8.3. Loading and unloading procedures

Many factors influence the loading and unloading procedure and, consequently, the loading process duration. The use of single- or multi-specimen setup, the use of lever arm or hydraulic jack to induce the load,

It is easy to understand that using the single-specimen test setup provides easier and more confident loading and unloading procedures. Notwithstanding, although the multi-specimen setup procedure includes several additional steps to be considered, it is also possible to proceed with confidence. To understand the stacking and loading procedure of multiple specimens in the CMOD-time and Load-time curves of the loading process of one creep frame are provided in Figure 94. As previously explained, a bottom-lever arm (tensile force) creep frame was used on these creep tests. Note that tensile lever arm creep frames (bottom position) imply screwed bars to transfer the load to the loading plate by tensile forces, and the loading procedure duration may increase.
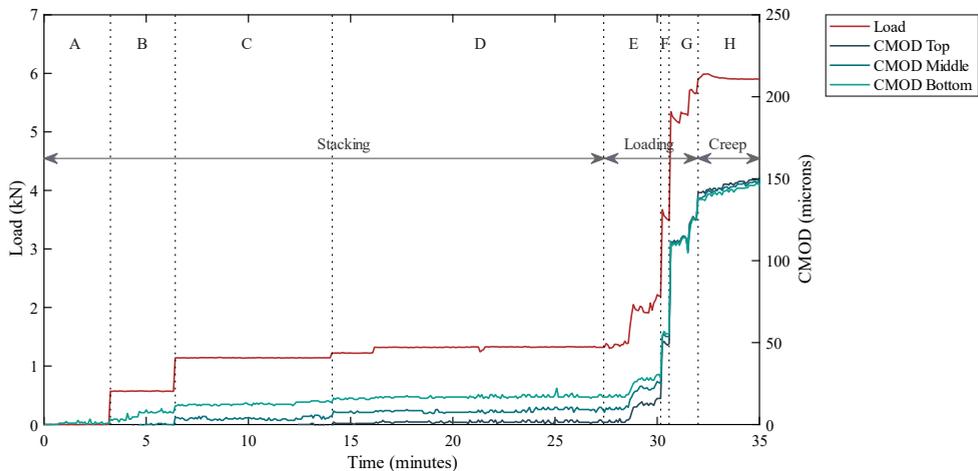
Figure 94. Multi-specimen setup stacking and loading procedure.

Figure 94 is divided into time lapses named with a letter to explain what happens on each step. During the first area, called "A", the bottom specimen is located, and the corresponding transducer is connected. As expected, both the load and the CMOD are 0 kN and 0 µm, respectively. In the next time-lapse, "B", the load transfer plate and the middle specimen are located over the bottom specimen. At this point, any load is applied over the load cell. Therefore, the corresponding load to the dead load of the transfer plate and the specimen was manually weighted and included. The CMOD of the bottom specimen starts to increase due to the dead load. The following transfer plate and the top specimen are mounted in the "C" time-lapse, and their corresponding dead load over the bottom and middle specimens are manually included again. Consequently, CMOD deformation of both bottom and middle specimens increases again. Over the top specimen, the loading transfer plate and the load cell are finally located in the time-lapse "D", which implies a reduced load but must also be considered. For this frame, around 27 minutes were required to complete the specimen stacking process (A to D). Note that the bottom specimen supports a 1.34 kN load at this time, which means 22.3% of the total $F_{R,c}$ during the creep test. Due to the residual dead load caused by the weight of upper elements, the specimens developed at 27.6 minutes 18.2 µm crack opening., representing 12.9% of the final instantaneous $CMOD_{ci}$ deformation. In conclusion, the residual dead load during stacking time represents a relatively low percentage of the deformation. Therefore, it is proposed to disregard the stacking time of the specimens for the t_{ci} parameter consideration.

At this point, the specimens are stacked and ready to be loaded. The loading process duration t_{ci} considered by this proposal is comprised from E to G G). Due to the mechanical procedure in this creep frame, the loading procedure is divided into three steps: e) prestress by tightened nuts, f) dead load of the lever arm, g) dead load of counterweights. Although the lever arm dead load application seems instantaneous (time-lapse "F" in Figure 94), the lever arm shall gradually descend in at least 15 seconds to avoid a sudden deformation. The required loading t_{ci} to reach the 5.9 kN of the target $F_{R,c}$ was 270 seconds.

The unloading process shall also be gradually done in at least 30 seconds to avoid any unexpected collapse due to balance loss. The loading t_{ci} and unloading t_{cri} times of an experimental campaign comprising four creep frames are compared in Figure 95 in a close-up view. The loading time t_{ci} of creep frames, neglecting the stacking time, ranges from 190 to 315 seconds. The three loading steps previously described can be identified for each frame. On the contrary, the unloading procedure is faster than the loading procedure. Although most of the load was removed in 15-20 seconds when lifting the lever arm, it still remains a residual load of the tightened nuts that were untightened in the later seconds.
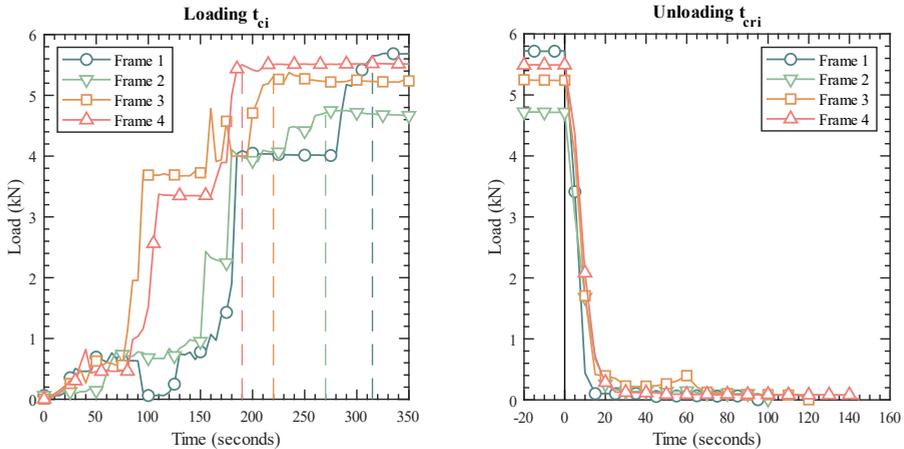
Figure 95. Loading (t_{ci}) and unloading (t_{cri}) times of four creep frames of the same experimental campaign.

4.8.4. Upper elements dead load influence

As explained in the previous section, in the case of multi-specimen creep test setup, both the upper specimens and the load transfer plates induce an additional dead load over the lower specimens. This additional load must be adequately considered in the creep applied load $f_{R,c}$ and creep index I_c calculation during the long-term phase as previously explained. Notwithstanding, there are two steps in the proposed methodology that stacked specimens are supposed to be unloaded, but the residual load of the upper elements still remains being applied: before loading and after unloading. Therefore, it is important to assess the significance of the residual dead load due to the load transmission elements on the creep index while specimens were stacked but unloaded.

During the specimens mounting stage, the different specimens and load transmission elements are in order positioned from the bottom specimen to the top transfer plate where the load cell is located. Once all the elements are correctly stacked and aligned, and before being loaded, the specimens usually remain mounted but unloaded for a short time-lapse. Considering the short duration of this procedure step, CMOD deformations caused by this dead load may be regarded as low and negligible. Notwithstanding, these residual deformations are registered and included in the instantaneous deformations since LVDT transducers were connected and started recording when each specimen was located without any load.

In addition, as explained in Section 4.4.2, once the long-term phase ends and the specimens are unloaded, it is recommended to register the delayed recovery deformation $CMOD_{cr}$ for 30 days. Then, stacked specimens shall not be removed from the column when measuring the delayed recovery deformations to avoid any sudden deformation and ensure a proper evolution of delayed recovery. In the case of a single-specimen creep test setup, there is no dead load to consider since the load is completely removed when

specimens are unloaded. On the contrary, in the case of the multi-specimen setup, specimens remain stacked but unloaded for 30 days. Hence, the residual dead load of the upper elements shall be considered and restricted when specimens are stacked.

Depending on the residual performance of the stacked specimens, the dead load caused by the upper specimens and load transmission elements represents certain stress percentage of the target sustained stress to be applied $f_{R,c}$. The residual load due to the dead load of the upper specimens and transfer plates has been assessed for three different experimental programs involving a total of 11 creep frames with multi-specimen setup. The experimental data related to creep test carried out in 33 FRC specimens in the cracked state was analysed. Results have been arranged in Table 25 by the relative position in the creep frame for a better comparison and includes the $F_{R,c}$ and the residual load due to the upper elements. The experimental programmes contained many FRC mixes with different fibre materials, dosages, and variable residual performance. Therefore, data related to mix and residual performance obtained in pre-cracking test was also included. Regarding the creep index, most of the specimens were tested at similar target creep index I_c (45% or 50% depending on the experimental programme). Only one creep frame (3 specimens) was subjected to creep index of 75% $f_{R,p}$ as marked in red in Figure 96. due to the experimental programme requirements. Exceptionally, specimen B-S3 exceeded the target creep index and reached 70.6% due to the low fibre dosage and, consequently, high residual performance scatter. This analysis intends to assess and seek a residual dead load ratio that could be sustained during both the loading and unloading recovery process steps affecting as minimum as possible the CMOD evolution. In other words, define which threshold could be established to ensure the proper development of the multi-specimen creep test procedure.

It is observed how the significance of the residual dead load due to the stack increases significantly depending on the relative position of the specimen. In the case of the top position, the significance is irrelevant since no residual dead load is applied because the top transfer plate shall be removed. Top position results are only published for comparative purposes with the rest of the positions, and the residual dead load ratio ranges from 0.68 to 2.26 % of the sustained load. Regarding the middle position, the dead load ratio ranges from 3.79 to 13.14%, whereas the bottom position ranges from 6.79 to 21.83%. If the residual load to $f_{R,c}$ ratio is compared to the sustained stress during creep tests, it can be observed in Figure 96 that the ratio increases when the $f_{R,c}$ decreases for all relative positions. It is also observed that the higher the applied creep index, the less significant the residual load became, as observed for the creep frames tested at a creep index of 75%. Obviously, it is confirmed that the bottom position is the most affected in terms of residual dead load ratio, where residual dead load due to upper elements may represent 22% of the creep index. Such a percentage of residual load sustained for 30 days where delayed recovery deformations are measured may significantly reduce the recovery capacity after the creep test. Therefore, it is proposed to establish a residual load to $f_{R,c}$ ratio threshold of 15% of the applied creep index. Considering this limitation, seven specimens of the bottom position exceed the proposed threshold, as seen in Figure 96.

Table 25. Influence and significance ratio of the residual dead load compared to the sustained load during the creep test obtained in 33 specimens.

Position	Name	FRC type	$f_{R,c}$ (MPa)	I_c (%)	$F_{R,c}$ (kN)	Dead load (kN)	Ratio
Up	MB1-052	SyFRC	1.09	50.03	5.78	0.10	1.78
	MB2-160		0.90	50.65	4.82		2.13
	SB1-273	SFRC	0.99	50.38	5.35		1.92
	SB2-366		1.05	46.79	5.60		1.84
	B3-F3	GFRC	1.06	50.42	5.62		1.83
	C4-F2		2.81	51.63	15.16		0.68
	G-S1		2.04	46.14	10.65		0.97
	C-S2		3.29	77.08*	17.16		0.60
	G-S4		1.26	49.49	6.55		1.57
	B-S5		0.87	45.58	4.55		2.26
Middle	MB1-053	SyFRC	1.18	49.02	6.35	0.67	10.59
	MB2-162		0.99	48.58	5.39		12.48
	SB1-274	SFRC	1.10	48.94	5.92		11.36
	SB2-363		1.16	51.42	6.17		10.90
	C-S3		2.38	51.65	12.40		5.43
	B1-F3	GFRC	1.11	49.98	6.19		10.87
	C3-F3		2.92	51.07	15.73		4.28
	F-S1		2.15	44.43	11.22		6.00
	B-S2		3.40	76.23*	17.73		3.79
	D-S4		1.37	44.51	7.12		9.45
	C-S5		0.98	44.14	5.12		13.14
Bottom	MB1-051	SyFRC	1.28	50.95	6.92	1.24	17.95
	MB2-159		1.11	50.45	5.96		20.84
	SB1-272	SFRC	1.21	50.44	6.49		19.14
	SB2-364		1.27	51.29	6.74		18.43
	D-S3		2.49	40.00	12.97		9.59
	B2-F2	GFRC	1.25	49.67	6.76		18.39
	C2-F2		3.04	47.64	16.30		7.62
	A-S1		2.26	44.55	11.79		10.55
	H-S1		3.51	74.02*	18.30		6.79
	C-S4		1.48	42.10	7.69		16.16
	A-S5		1.09	44.40	5.69		21.83

* Specimens under high creep index (75% $f_{R,p}$)
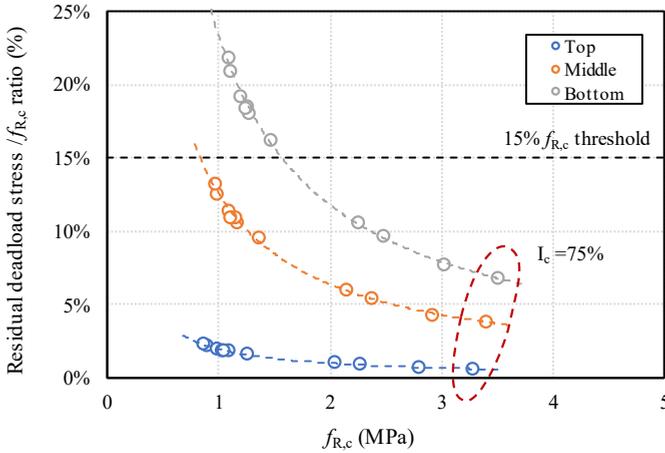
Figure 96. Residual dead load to $f_{R,c}$ ratio influence depending on the relative position in the frame compared to applied stress.

Alternatively, the residual dead load to $f_{R,p}$ residual strength ratio can also be obtained and depicted versus $f_{R,p}$ residual strength in Figure 97. It is appreciated that the residual dead load represents a reduced percentage of the residual strength $f_{R,p}$ at $CMOD_p$ obtained in the pre-cracking test. Alternatively, it could be proposed that the residual dead load to $f_{R,p}$ ratio threshold of 10% of the residual strength $CMOD_p$.
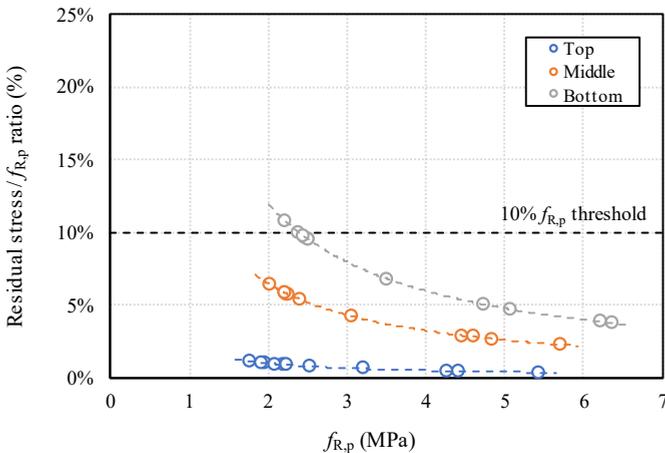
Figure 97. Residual dead load to $f_{R,p}$ ratio influence depending on the relative position in the frame compared residual stress obtained in pre-cracking tests.

Both 15% $f_{R,c}$ and 10% $f_{R,p}$ proposed thresholds are compared in Figure 98, where it is confirmed that the 15% $f_{R,c}$ threshold is more restrictive, with seven specimens rejected versus only two specimens dismissed by the 10% $f_{R,p}$ threshold.
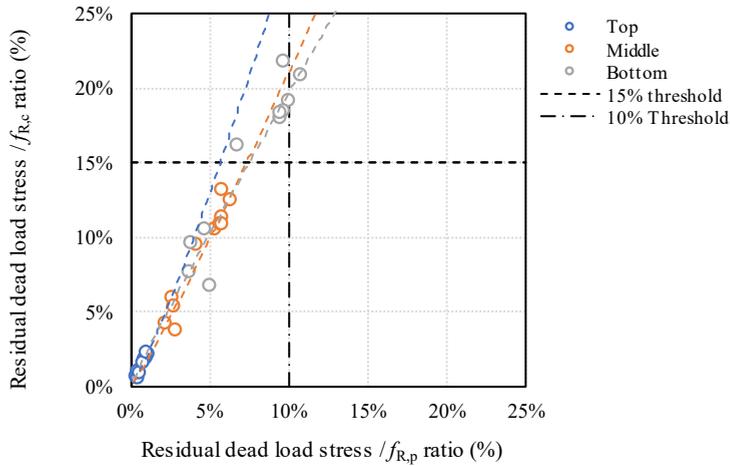
Figure 98. Comparison of 15% $f_{R,c}$ and 10% $f_{R,p}$ proposed thresholds.

It is concluded that the bottom specimen of a multi-specimen setup may be subjected to a dead load around 6 to 22% of the creep index, depending on their residual performance, where specimens remain stacked during the delayed recovery process. This residual dead load shall be reduced as much as possible to prevent any influence on the recovery capacity of the specimens after unloading. It is then proposed to limit the residual dead load over the stacked specimens to 15% of the applied creep index I_c. and consider this threshold during the specimen selection step. Therefore, if it is expected that the specimen selected to be placed at the bottom of the stack will exceed the proposed dead load threshold, it is then proposed the following solutions:

- Test simultaneously two specimens instead of three specimens in that frame,
- If there is enough space, lift the top specimen and place it near the creep frame keeping the support span and the transducer measurement on.

It is important to highlight that the transfer plates construction also influence the residual dead load meanwhile specimens are stacked: the lighter transfer plates, the less residual dead load over the bottom specimen. The construction of light transfer plates will improve the multi-specimen creep test procedure since the residual dead load on specimens is reduced, and the specimen mounting process becomes easier with lighter elements.

All laboratories shall know the weight of the different elements (i.e. transfer plates, supporting rollers, specimens…) composing their creep frame to proceed with the creep test procedure. For the realisation of this PhD programme, the creep frames available at the *Instituto de Ciencia y Tecnología del Hormigón* (ICITECH) at the *Universitat Politècnica de València* (UPV) facilities and presented in Chapter 3 were used and improved. The different elements composing the frames were weighted and used for the previously explained assessment. Considering the creep frames and weights of the transfer plates available in our facilities, the 15% residual dead load threshold can be

assured if the load applied in the creep frame $F_{R,p}$ is below 7.05 kN. This reference value implies that if the bottom specimen provides $f_{R,p}$ lower than 2.3 MPa in the pre-cracking test, any of the two proposed solutions shall be considered for the multi-specimen setup to not exceed the 15% creep index percentage: the top specimen shall be removed after unloading.

Chapter 5.
Creep Characterisation Improvements

Besides the proposed procedure improvements, different aspects regarding the long-term performance of FRC were also studied to improve the knowledge and comprehension of the obtained experimental results. Specific experimental programmes were carried out to evaluate the influence of shrinkage on delayed crack opening, the compressive creep contribution to delayed crack opening in flexure tests, the cross-section stress redistribution during the creep test and the creation of an international open-access creep database. Relevant data from experimental programmes and main conclusions are presented in this chapter.

5.1. Shrinkage flexure test

The use of unloaded specimens to assess shrinkage deformation in time is already extended and described in creep standards such as the creep in compression methodology ASTM C512M-15 [28] or EN 12390-17:2019 [29]. The creep in compression standards define procedures where one additional specimen to those subjected to load is located unloaded near the creep to ensure that both creep and shrinkage specimens are tested in similar environmental conditions, as seen in Figure 99. It was required that shrinkage specimens were identically instrumented with strain gauges (Figure 99.b) as done for the loaded specimens. By this action, the shrinkage deformations of the concrete matrix can be assessed and subtracted from the delayed deformation of loaded specimens.
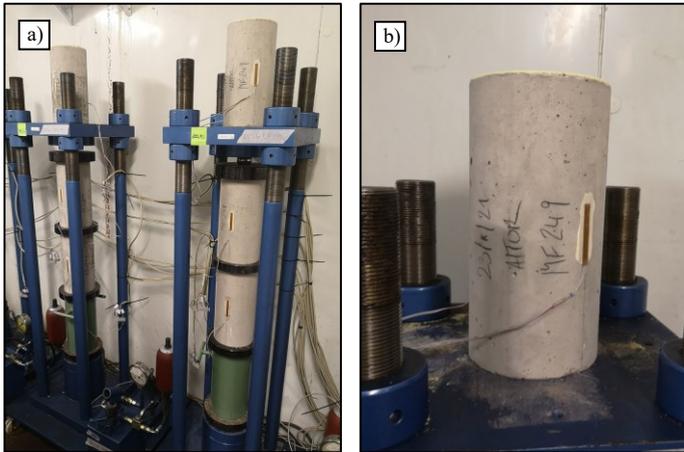
Figure 99. Creep in compression frames (a) with shrinkage specimens (b) located over the creep frame.

To this PhD programme start, no references were found in the FRC flexure creep in cracked state scientific literature about shrinkage flexure test to assess how the concrete matrix shrinkage could influence the crack opening evolution in time. Since shrinkage deformations are usually relevant in long-term tests, it was considered to determine the crack opening evolution in time of the FRC cracked specimens without any additional load besides their dead load. To this purpose, it is then proposed in the PhD flexure creep test experimental programme to carry out a similar procedure than previously described for ASTM C512M-15 [28]. Hence, close to each flexure creep frame, one FRC specimen was located in the flexure position but without any load except its dead load. This specimen, hereafter called shrinkage specimen, was pre-cracked until CMOD$_p$ following the same procedure as those that were subjected to sustained load. In addition, the same transducer type was mounted in the bottom face of the shrinkage specimen. This experimental research aimed to determine the CMOD variation in time when prismatic specimens were only subjected to self-weight compared to those tested under sustained load. Full information of these experimental programmes is provided in Appendix F, Appendix G and Appendix H.

It was expected to obtain two different long-term shrinkage behaviours depending on delayed CMOD, either increasing or decreasing in time. The former could reveal that self-weight could be enough to induce delayed crack opening deformations in the specimen. The latter could state that shrinkage deformation shall reduce the crack opening. However, the first possibility may be unlikely due to the slight load level applied by self-weight compared to creep tests; hence, it was expected to observe a crack opening reduction in the shrinkage specimen. If crack reduction finally occurs in shrinkage flexure specimens, it shall be considered crucial to measure the shrinkage flexure deformation together with creep tests to quantify how the delayed deformations measured in the creep test were influenced and reduced by shrinkage. For this purpose,

the following experimental programmes were conducted to assess shrinkage flexure influence.

5.1.1. Specimen location: environmental and boundary conditions

Due to the nature of shrinkage deformation, environmental conditions are essential to understand the behaviour of both crack opening and compressive strain evolution. Slight variations in relative humidity (RH) may significantly influence concrete shrinkage. Therefore, it is always recommended to proceed with creep tests in climate rooms with controlled environmental conditions such as temperature and humidity. Environmental conditions evolution shall be registered during the creep test duration, from the loading process start to 30 days of delayed unloading recovery. Since climate conditions shall be reported in the test report, it will help to identify how either temperature or RH influences shrinkage and delayed deformations.

As proposed in the ASTM C1550 standard, the specimen destined for shrinkage test must be tested in similar environmental conditions that specimens subjected to flexure creep tests. Therefore, flexure shrinkage specimens shall be located close to the flexural creep frame where the specimens from the same batch are being tested in creep, as seen in Figure 100. CMOD deformation due to drying shrinkage was monitored in the same way that delayed CMOD deformations in creep tests: one displacement transducer was mounted centred in the bottom face crossing the cross-section. In addition, to measure compressive strain evolution due to shrinkage, a strain gauge 50 mm in length was located centred at the midspan on the top face of the specimen, as seen in Figure 100 (right).
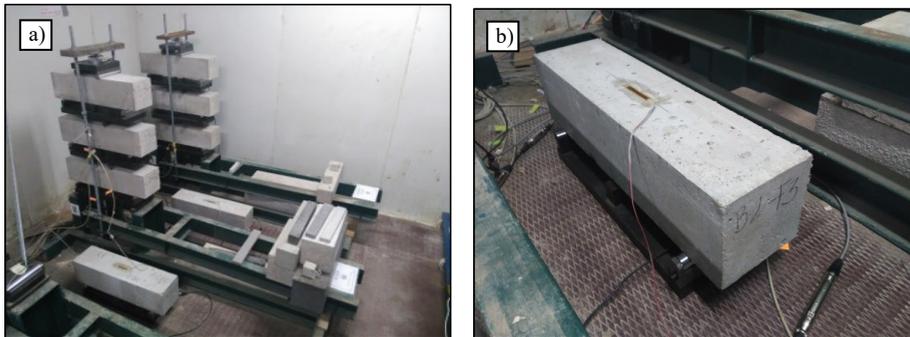
Figure 100. Shrinkage flexure specimens located between the creep frames (a). Close-up view of boundary conditions and transducers (b).

Besides the suitable location to ensure similar environmental conditions, it is also relevant to provide similar boundary conditions to the shrinkage specimen. This implies supporting rollers that can spin in their longitudinal axis to avoid horizontal restrictions that may influence the free development of shrinkage deformations. Transversal rotation of supporting rollers is not required due to the absence of loading rollers.

5.1.2. Shrinkage consideration

Since creep and shrinkage are phenomena that never occur separately, creep is usually calculated as the difference between the total time-dependent strain of a loaded specimen and the shrinkage registered on the unloaded specimen. However, in the case of flexure creep specimens, shrinkage deformations and sustained load effect provide the opposite effect. Whereas sustained load increases in time crack opening deformations, shrinkage tends to reduce crack opening due to the concrete volume reduction, as seen in Figure 101. This crack opening reduction due to shrinkage ($CMOD_{cs}^{j}$) is hindered in the standard flexure creep test if no shrinkage specimen is used, providing experimental values in terms of crack opening. Thanks to the flexure shrinkage test of FRC specimens in the cracked state, it will be possible to assess the influence of volume reduction into either the crack opening (CMOD) or compressive strains evolution in time.
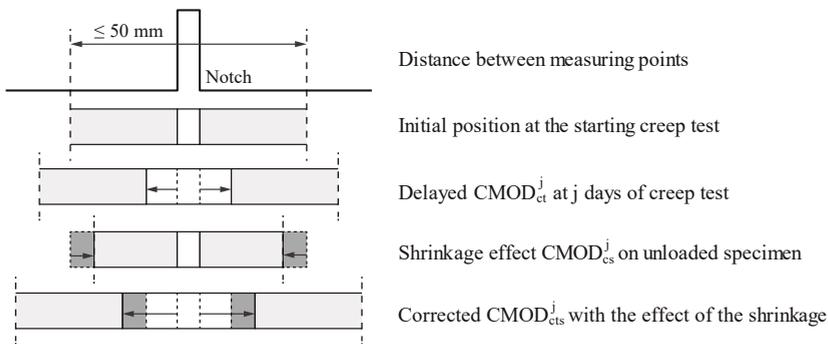
Figure 101. Shrinkage effect consideration in the delayed crack opening.

The shrinkage effect on the crack opening evolution directly depends on the distance between the measuring points. When clip crack opening displacement (COD) gauges are used, the distance between measuring points is reduced to the crack width. On the contrary, when linear variable displacement transducers (LVDT) are used, the distance between measuring points may range from 50 to 150 mm. The more distance between measuring points implies more influence of shrinkage on the crack opening readings. Although 100 mm were initially used for this shrinkage study, the distance between measuring points is recommended not to exceed 50 mm to reduce the shrinkage influence.

It is worth mentioning that it is also possible to measure the evolution of the strain in the compressive zone of the specimen destined to shrinkage if a strain gauge is centred in the top face of the specimen and aligned with its longitudinal axis.

5.1.3. Shrinkage experimental results

To assess the shrinkage effect on the long-term creep tests, shrinkage flexure specimens were included in four flexure creep experimental programmes. Table 26 summarises the most relevant information of the experimental creep programmes where the shrinkage

flexure deformation was assessed. Shrinkage flexure specimens were first used to determine the crack opening evolution due to concrete matrix shrinkage in a flexure creep test experimental campaign on glass fibre-reinforced concrete (GFRC). It was observed that the crack closed -49.3 µm CMOD after 360 days of test, and thus, one shrinkage specimen per FRC series was included in the later experimental campaigns. Due to the long duration of the creep tests, only six shrinkage specimens could be tested in 5 years of creep tests. Two specimens of GFRC, SyFRC and SFRC were tested, providing shrinkage behaviour of three main fibre materials used in the literature.

Table 26. FRC matrix properties of programmes with shrinkage flexure specimens.

Programme	Duration	Mix	Dosage (kg/m^3)	f_{ck} (MPa)	f_L (MPa)	$f_{R,1}$ (MPa)	$f_{R,3}$ (MPa)
OC2	360	GFRC	10	60.6	4.76	3.13	1.62
		GFRC	20	61.2	4.54	7.11	4.02
NAE-2	540	SyFRC	10	54.5	4.02	2.96	4.75
		SFRC	30	50.7	3.81	4.77	5.67
NAE-3	270	SyFRC	10	42.6	3.48	2.20	3.35
		SFRC	30	43.9	3.84	3.84	4.01

Regardless of the fibre material, the crack closed in time due to concrete volume reduction, as seen in Figure 102. Average $CMOD_{cs}$ values of 35.4 and 48.5 µm were obtained at 180 and 360 days, respectively, considering all mixes. Compressive strains (right) were also monitored in the top face of concrete specimens by 50 mm length strain gauges, and it was also assessed that compressive strains increased in time due to concrete shrinkage. However, compressive strains seem to be more sensitive to humidity, and sudden strains decrease were observed when humidity raised.
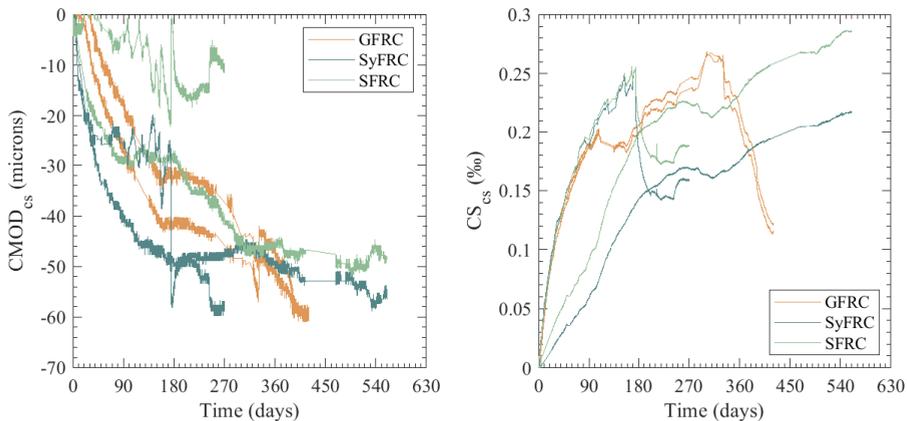
Figure 102. Shrinkage test experimental results considering delayed crack opening (left) and compressive strains (right).

The significance of delayed CMOD due to drying shrinkage can be determined if the shrinkage $CMOD_{cs}$ deformation of each mix is compared to the average total $CMOD_{ct}$ obtained by specimens from the same mix under sustained load. Table 27 presents the shrinkage specimens experimental results at 180 and 360 days for each mix together with the average total $CMOD_{ct}$ of three specimens tested simultaneously on each frame. The $CMOD_{cs}/CMOD_{ct}$ significance ratio at 360 days ranges from 9.1 to 20.5 % depending on the mix: 9.3 % for SyFRC, 10.8 % for GFRC and 20.5 % for SFRC.

Table 27. Shrinkage experimental results compared to delayed results of creep test.

Programme	Mix	Shrinkage		Creep		Ratio (%)	
		$CMOD_{cs}^{180}$	$CMOD_{cs}^{360}$	$CMOD_{ct}^{180}$	$CMOD_{ct}^{360}$	180	360
OC2	GFRC	-41.05	-52.22	371.95	421.38	11.0	12.4
	GFRC*	-31.32	-46.48	437.20	509.96	7.2	9.1
NAE-2	SyFRC	-48.40	-49.80	498.60	536.53	9.7	9.3
	SFRC	-29.50	-45.50	208.67	221.60	14.1	20.5
NAE-3	SyFRC	-53.80	-	613.13	-	8.8	-
	SFRC	-8.77	-	212.35	-	4.1	-

* Note that this GFRC series has 20 kg/m3 fibres compared to the previous series of 10 kg/m³.

It has been confirmed that during the creep test, the crack closes due to the drying shrinkage effect. It is then concluded that this effect was hindered by delayed CMOD and neglected to date in the creep test results since no shrinkage assessment was previously reported.

5.2. Influence of compressive creep in long-term flexure performance

It is well known that the flexure test results from a combination of both tensile and compressive stresses. This combination of stress is one of the main issues of flexure creep methodology. To date, it is unclear how to apply creep models in the FRC structures design considering compressive strains creep since most flexure methodologies only assess the crack opening evolution. To this purpose, the compressive creep was evaluated in one experimental test to assess compressive strain evolution and quantify the impact of compressive creep on tensile creep. The compressive strain was monitored in both SFRC and SyFRC mixes by 50 mm length strain gauges located centred at the top face of concrete specimens and aligned to its longitudinal. Table 28 provides information on the FRC mixes where compressive creep was assessed. Furthermore, full information of the experimental programmes where the compressive creep was assessed is provided in Appendix B, Appendix G and Appendix H.

Table 28. Experimental programmes to assess compressive creep impact.

Programme	Duration	Mix	Dosage (kg/m³)	f_{ck} (MPa)	f_L (MPa)	$f_{R,1}$ (MPa)	$f_{R,3}$ (MPa)
WP1	180	SyFRC	9	45.3	2.77	1.99	2.99
		SFRC	40	44.4	3.00	3.35	3.79
NAE-2	540	SyFRC	10	54.5	4.02	2.96	4.75
		SFRC	30	50.7	3.81	4.77	5.67
NAE-3	270	SyFRC	10	42.6	3.48	2.20	3.35
		SFRC	30	43.9	3.84	3.84	4.01

Experimental results of both CMOD and compressive strain evolution are provided in Figure 103. Whereas the tensile area evolution is assessed by LVDTs in terms of crack opening, compressive area behaviour is monitored by strain gauges in terms of compressive strains. By convention, compressive total creep tests exhibited positive strain variations, and tensile crack opening exhibited negative CMOD variations. By this action, they can be easily differentiated since compressive strains occur in the top face, whereas CMOD occurs in the bottom face of the specimen.
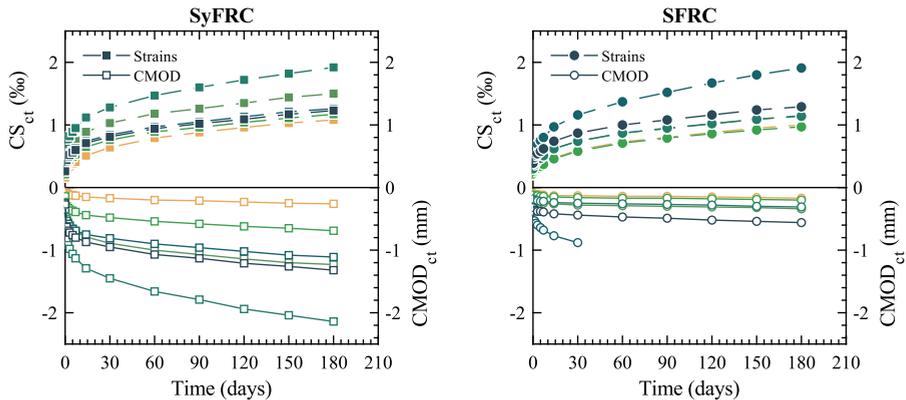
Figure 103. Delayed CMOD and compressive strains deformations arranged by mix: SyFRC (left) and SFRC (right).

It is important to remind that specimens have different $CMOD_p$ ranging from 0.2 to 2.0 mm. Figure 104 shows that delayed compressive strains seem to be more influenced by creep index, where SyFRC specimens pre-cracked up to 0.8 and 1.2 mm exhibit larger compressive strains due to the higher creep index of 55.0 and 57.8%, respectively. In addition, the SFRC specimen with 1.5mm $CMOD_p$ also developed larger delayed compressive strains due to a 64.2% creep index. Then, it can be concluded that pre-crack level $CMOD_p$ has more impact on the CMOD delayed deformations than the delayed

compressive strains. However, the creep index impact is confirmed for both CMOD and compressive strains delayed deformations.
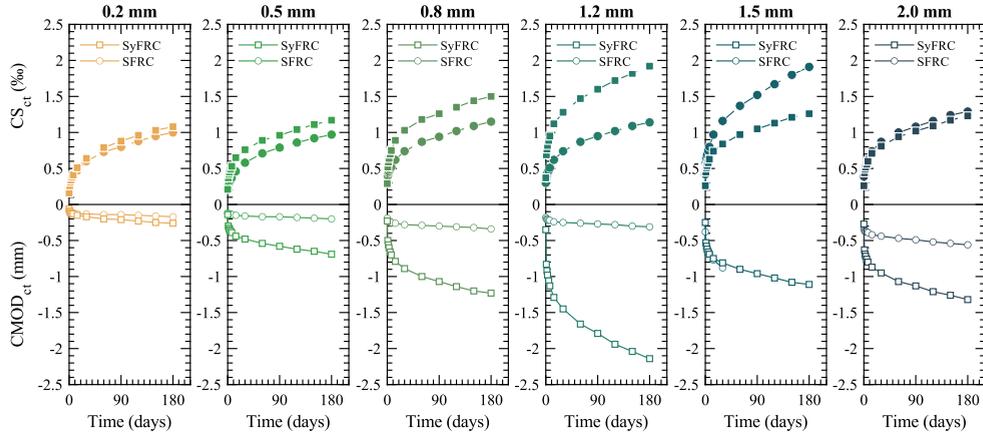
Figure 104. Delayed CMOD and compressive strains deformations arranged by the initial CMOD$_p$.

Crack opening and compressive strains cannot be directly compared since they are registered in different units (‰ and mm, respectively). However, both tensile and compressive long-term behaviour can be compared in terms of creep coefficient since creep coefficient is a dimensionless parameter.

5.2.1. Creep coefficient assessment

CMOD and compressive strain creep coefficient were obtained from experimental results to be compared. Whereas crack opening creep coefficients were obtained using Equation 2, compressive strains creep coefficients were obtained following the similar formulation presented in Equation 11.

$$\varphi_{\varepsilon,c}^{\,j} = \left(CS_{ct}^{\,j} - CS_{ci}\right) / CS_{ci} = CS_{cd}^{\,j} / CS_{ci} \qquad \textbf{Equation 11}$$

Both creep coefficients are depicted and compared in Figure 105. Following the same sign convention, compressive strains creep coefficients represent positive evolution, whereas CMOD creep coefficients show negative evolution. It can be observed that delayed compressive strains provide larger creep coefficients compared to CMOD evolution for the SFRC mix (right). This fact implies that compressive strains increase more than CMOD and confirms that compressive strains do not exhibit stabilisation within the duration of the carried-out creep test. However, in the case of the SyFRC mix, similar creep coefficients are obtained for CMOD and compressive strains delayed deformations.
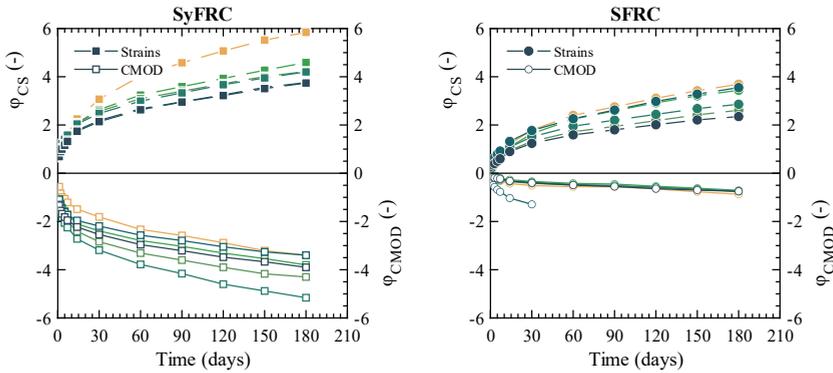
Figure 105. Comparison between CMOD and compressive strain creep coefficients for both SyFRC (left) and SFRC (right) mixes.

If the CMOD to compressive strains creep coefficient ratio is obtained, it can be assessed the significance of delayed CMOD compared to delayed compressive strains. Figure 106 depicts the evolution of φ_{cmod} / φ_{cs} ratio in time, where the significance of crack opening creep can be observed compared to compressive creep during the creep test. At first sight, it was noted that the significance among tensile and compressive creep in flexure setup is not constant and varied in time. The significance of the φ_{cmod} / φ_{cs} ratio is higher during the early creep stage (1.46 and 0.63 for SyFRC and SFRC, respectively, at one day), where most of the crack opening deformations occur. However, after 30-60 first days of decrease trend, the average φ_{cmod} / φ_{cs} ratio stabilised at 0.93 and 0.26 and remained virtually constant for the rest of the test. This variation in time of the significance ratio between crack opening and compressive strains can explain a stress redistribution that occurs during the creep test.
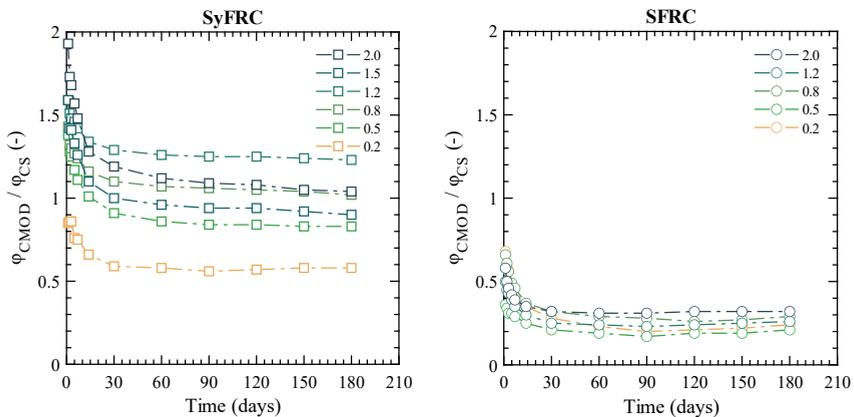
Figure 106. CMOD to compressive strains creep coefficient ratio for SyFRC (left) and SFRC (right) mixes.

A similar analysis procedure was applied to the results of the neutral axis evolution (NAE) experimental programmes to validate these conclusions and the comparison of the experimental delayed CMOD and compressive strains is shown in Figure 107.
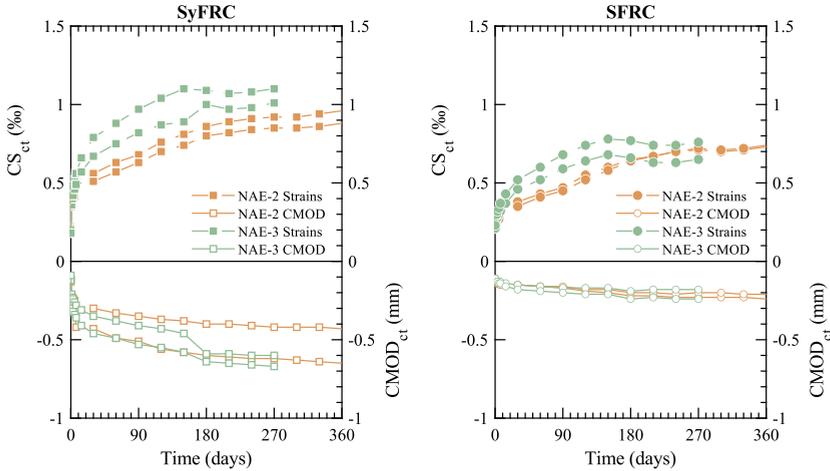
Figure 107. Comparison between CMOD and compressive strain delayed deformations obtained in NAE experimental programmes.

Creep coefficients for both deformations were obtained and compared. The CMOD to compressive strains creep coefficient ratio ($\varphi_{cmod} / \varphi_{cs}$) is evaluated, and the evolution of the ratio shown in Figure 108. It was confirmed that the significance trends of the creep coefficients ratio were similar to those previously obtained in Figure 106 for both mixes. Average crack opening to compressive creep ratios of 1.34 and 0.63 were obtained at the beginning of the creep test. The ratio decreased significantly during the early creep stage and then stabilised up to 0.99 and 0.39 at 180 days.
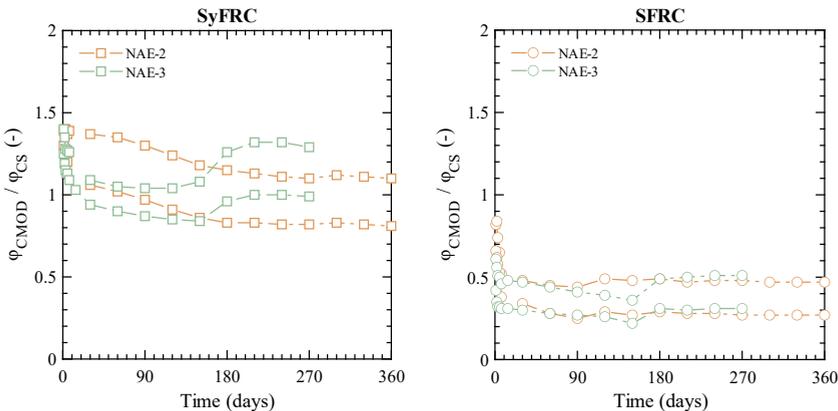
Figure 108. CMOD to strains creep coefficient ratio for SyFRC (left) and SFRC (right) mixes in NAE experimental programmes.

From this assessment, it can be concluded that the significance of compressive creep to tensile creep depends on the fibre material. The compressive creep has more impact than CMOD creep in flexure creep tests for SFRC mixes due to the reduced modulus of elasticity of synthetic fibres. On the one hand, compressive strains creep 3.8 times more than the crack opening for SFRC specimens. On the contrary, compressive strain creep coefficients are comparable to those obtained by crack opening deformations in SyFRC mixes. Moreover, the significance ratio between crack opening and compressive creep decreases over time. By this fact, it can be concluded that a stress redistribution occurs during the creep test. Hence, compressive creep shall be evaluated together with tensile crack opening long-term behaviour since both aspects act simultaneously.

5.3. Neutral axis

As concluded in the compressive strains assessment, a stress redistribution may occur during the creep test, and consequently, the neutral axis (NA) depth may vary along the creep test. Hence, a new experimental programme was designed to assess the NA location during creep tests and confirm the stress redistribution.

Although NA is defined as the section location where the stresses are equal to zero, it can be assumed that the location of zero stresses and zero deformations coincides in linear materials. Therefore, the NA location can be determined if the location of zero deformation of the cross-section is obtained using side-mounted displacement transducers. However, linear fitting shall accomplish the hypothesis of Navier that plane strain sections remain plane. The Navier assumption can be assessed if crack opening deformations measured over the height of the cross-section by side-mounted transducers are collinear or not. To this purpose, a linear fit is obtained through three crack opening (*w*) deformations measured at different heights for every experimental data point. The r^2 goodness is obtained for each linear fit to assess that deformations are collinear, and the Navier assumption is accomplished. Similar procedure was successfully used to assess the NA in monotonic characterisation flexure tests [199-200] and it was concluded that the linear fit model goodness is accurate enough.

The first approach, hereafter named the *3w model*, considers crack opening deformations over three different heights of the cross-section, as seen in Figure 109. The linear fit of *3w model* provides de equation of the deformation plane for every set of data. The NA position can be directly determined by extrapolation obtaining line *y* value at *x* = 0. The *3w model* flowchart is defined in Figure 110. The fit line equation and the fit goodness are saved for each row of data to assess the goodness of fit of both approach models.
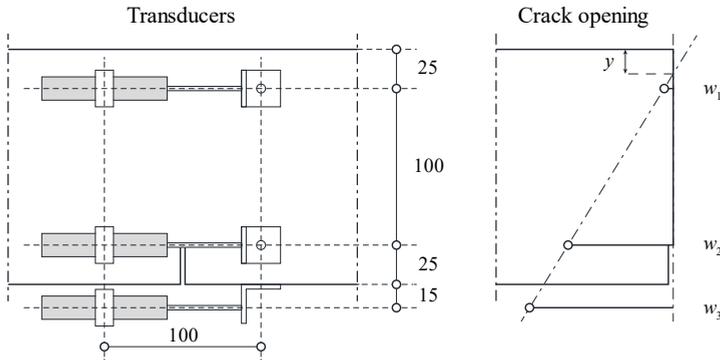
Figure 109. Deformation plane approach with three crack opening deformations.
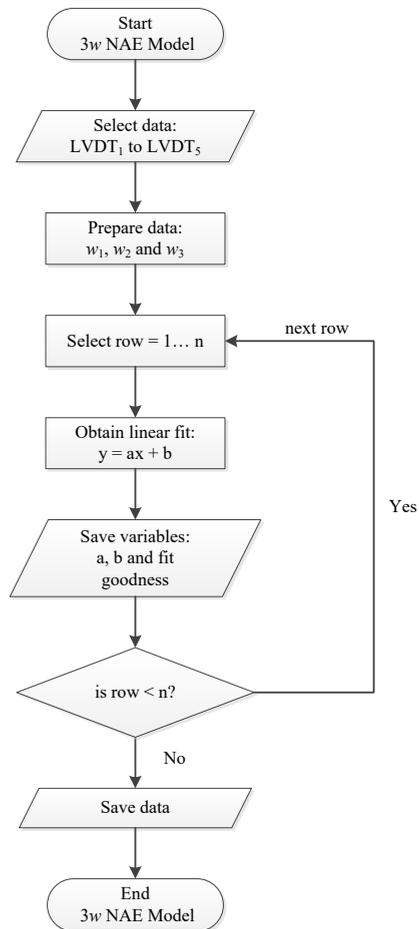
Figure 110. Flowchart of the 3w model approach.

Alternatively, considering that strain gauges were glued in the top face of specimens, it is possible to obtain the deformation plane considering a different approach. Instead of using only crack opening deformations (w_1, w_2 and w_3), the deformation plane can be obtained by linear fitting of both crack opening (w_1, w_2, w_3) and compressive strains deformations (ε). However, w deformations have different units than ε strains and cannot be directly fitted. The Model Code 2010 [19] states the strain deformation can be assumed equal to:

$$\varepsilon = w / l_{cs}$$

Equation 12

The characteristic length (l_{cs}) may be evaluated using Equation 13 in sections without traditional reinforcement under bending stress, where s_{rm} is the mean distance between cracks and $y = h$ is assumed. Considering that specimens are notched, the height of the cross-section h_{sp} was considered (125 mm) for the characteristic length calculation.

$$l_{cs} = \min \{s_{rm}, y\}$$

Equation 13

Hence, a new approach, hereafter named the l_{cs} *model*, is defined to obtain the NA location by using the characteristic length parameter and both crack opening and compressive strains deformation, as presented in Figure 111. The l_{cs} *model* checks for the defined characteristic length threshold, the minimum l_{cs} value that accomplishes the fit requirement by following the flowchart defined in Figure 112. As a result of the l_{cs} model application, the l_{cs} and the NA location are obtained for every data set. In addition, the r^2 goodness is obtained for each linear fit to assess that deformations are collinear, and the Navier assumption is accomplished.
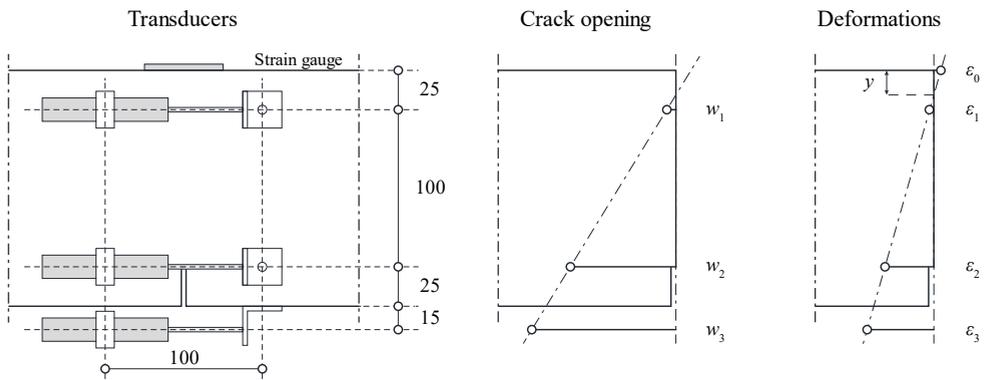
Figure 111. Deformation plane approach with both crack opening and strains.
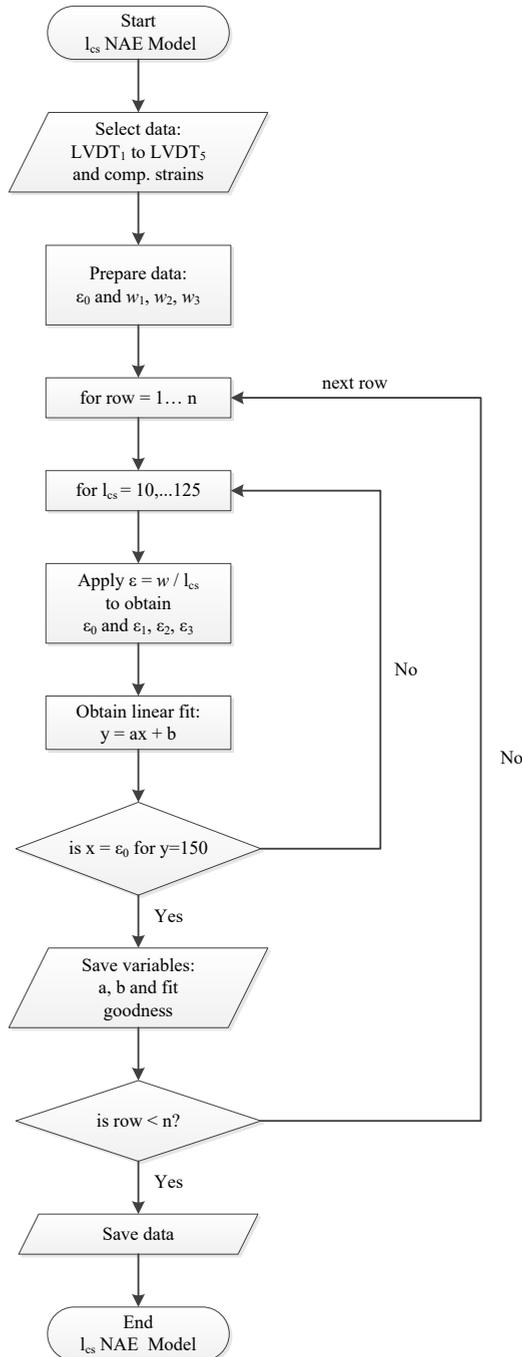
Figure 112. Flowchart of the l$_{cs}$ model approach.

5.3.1. Experimental program

To assess the NA position during the creep test, five LVDTs were mounted on each specimen, as described in Figure 113. Besides the required transducer mounted at the bottom face to measure crack mouth opening displacement (CMOD), four additional side-mounted transducers were used. Two transducers were located at both sides at 125- and 25- mm height to obtain average crack openings w_1 and w_2. Both w_1 and w_2 measures result as the crack opening average of transducers 1-2 and 3-4, respectively, located at opposite sides of the specimen. The average w_2 deformation coincides with crack tip opening displacement (CTOD) defined in EN 14651 [26].
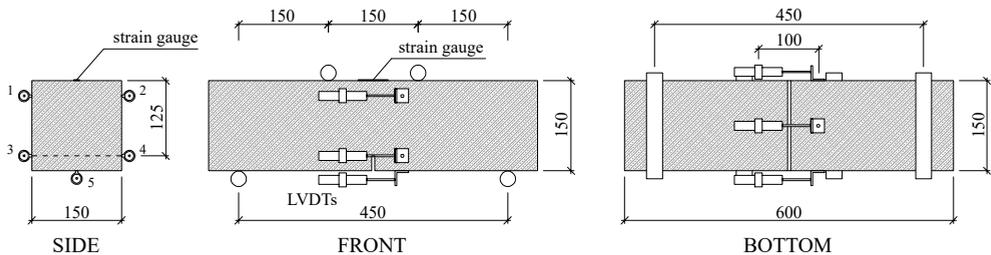
Figure 113. LVDTs and strain gauge location to assess NA position.

Note that five linear transducers and one strain gauge are mounted on each creep specimen, whereas only the CMOD transducer and strain gauge are mounted in both shrinkage specimens. Therefore, due to data acquisition system (DAS) channels limitation, only four specimens under sustained load together with two shrinkage flexure specimens, one of SyFRC and SFRC mixes, respectively, can be tested simultaneously. Thus, a single-specimen creep setup was adopted.

Due to the low number of specimens tested on each experimental programme, it was considered required to make at least two complete experimental tests to have a significant number of specimens tested for the experimental data analysis. The duration of experimental programmes destined to assess long-term NA evolution (NAE), as well as fibre and mixes information, are provided in Table 29. Note that the experimental creep test duration ranges from 6 to 18 months. The last experimental programme, named NAE-3, is still ongoing, and data is only available for this assessment for up to 270 days.

Table 29. Experimental programmes designed for long-term NA assessment.

Programme	CMOD$_P$	Ic (%)	Mix	Specimens	Dosage	Duration
NAE-1	0.5	50	SFRC	1	40	180
NAE-2	0.5	50	SFRC	2	40	540
			SyFRC	2	9	
NAE-3	0.5	50	SFRC	2	40	270
			SyFRC	2	9	

Together with specimens under sustained load, one flexure shrinkage specimen of each FRC mix was located between frames to assess shrinkage deformations. Side-mounted transducers were not used in shrinkage specimens due to channels limitation. Therefore, only delayed compressive strain and crack opening deformation at w_3 were obtained (see Figure 102). Considering that it was not possible to obtain shrinkage deformation at w_1 and w_2, delayed deformations were not compensated with shrinkage before the model application. Otherwise, the NA model results could be distorted if w_3 was compensated with shrinkage, but w_1 and w_2 were not compensated. Moreover, crack opening deformations obtained from shrinkage specimens were so low that applying the NA model to shrinkage specimens could not be conclusive.

5.3.2. Monotonic flexure test

Prior to the creep test, specimens were pre-cracked in flexure up to 0.5 mm $CMOD_p$ following the previously presented creep test procedure. To assess the NAE model in the monotonic pre-cracking flexure tests, side-mounted transducers were used, as defined in Figure 113. Note that strain gauges were located at the top face of specimens to measure simultaneously crack opening and compressive strains. Due to the strain gauge location, it was not possible to perform pre-cracking bending tests in 3PBT. Therefore, the 4PBT setup was adopted to pre-crack specimens. Flexure test results of arbitrarily chosen prismatic specimens are given in Figure 114. Average crack opening deformations w_1 and w_2 together with w_3 are plotted versus crack opening. Note that pre-cracking tests were stopped when 0.5 mm $CMOD_p$ was achieved and w_3 exceeded 0.5 mm. CMOD was obtained as the ratio between the distance of transducer w_3 to the top face and the height of specimen ($h / (h + y)$) according to EN 14651 guidelines. It can be observed in Figure 114 (left) that deformation w_1 measured by transducers located at 125 mm from the bottom of the specimen is negative due to compressive flexure forces. However, deformations turn to an increase trend when the crack occurs, getting positive values when NA exceed the transducer position.
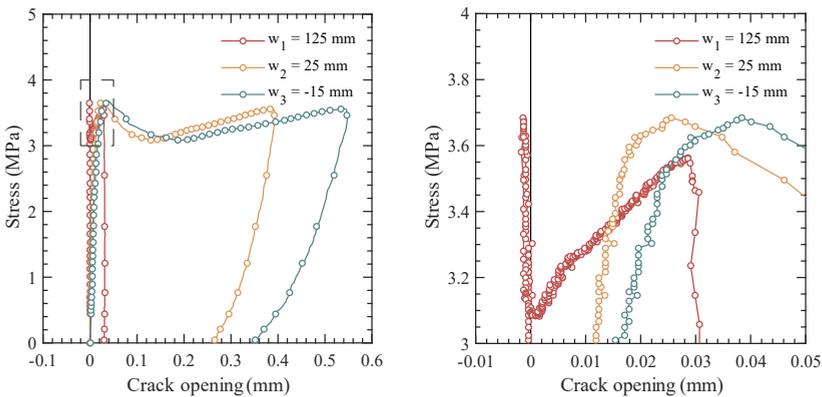
Figure 114. Pre-cracking test performed on specimen with 5 linear transducers and close-up view of cracking moment at 0.05 mm crack opening.

The previously defined 3w and l_{cs} approach models were applied to the monotonic pre-cracking flexure experimental test results. Figure 115 represents the result of the l_{cs} model application on one random specimen over more than 20,000 rows of data. As observed in the figure, during the loading phase of flexure test where specimens are not still cracked (first 10,000 rows), the crack opening deformation plane is blurred since crack opening transducer deformations are pretty low. However, when crack occurs and the crack opening increases, the deformation plane definition improves, and it is observed how the NA position rises together with the crack opening. It must be highlighted that at the end of the pre-cracking test at 0.5 mm $CMOD_p$ ($w_3 = 0.64$ mm), the NA position was 132 mm from the bottom of the specimen. Hence, most of the height of the specimen (88-92% depending on the specimen) is cracked at low crack openings.
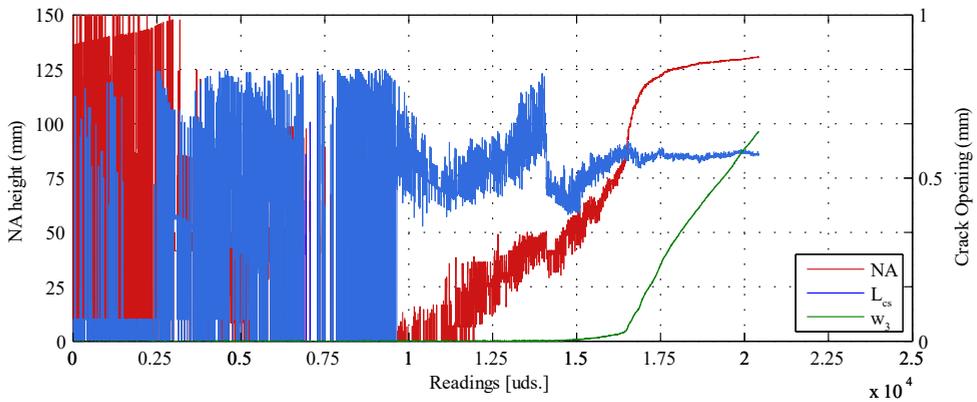
Figure 115. Pre-cracking flexure test data assessment: NA, characteristic length and w_3 evolution among experimental readings.

The deformation planes were obtained for every set of data in pre-cracking tests. Figure 116 (left) shows the deformation planes of an arbitrary chosen SFRC specimen at CMOD values in 0.05 mm steps. Deformations w_1, w_2 and w_3, are given together with the linear fit obtained by the 3w model. The NA position for each CMOD is obtained by extrapolating the fit line until the cross-section of the specimen ($x = 0$). It was observed that the slope of the deformation planes decreases with CMOD but the NA position increases. A close-up view of the cracked section is given in Figure 116 (right), where the NA position is marked with coloured flat dots. The growing evolution of the NA position during the monotonic pre-cracking test can be appreciated from 120.0 to 132.6 mm.
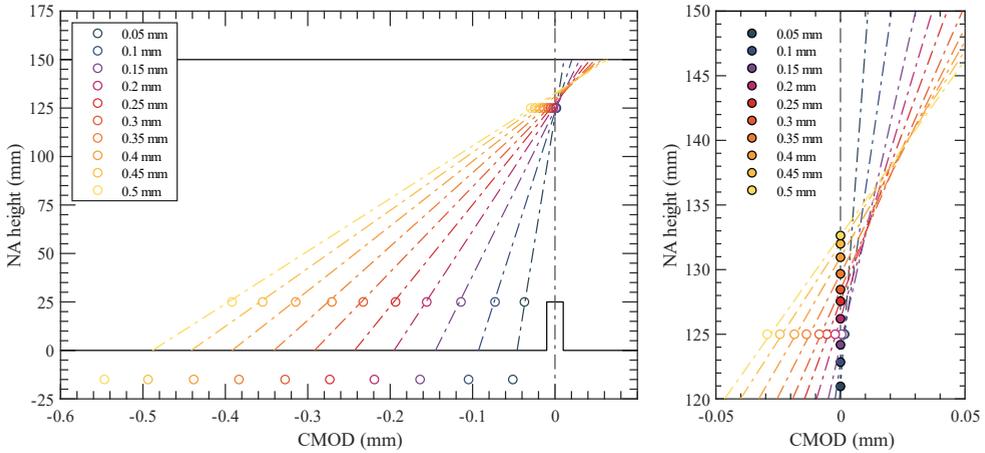
Figure 116. Deformation planes obtained in the monotonic pre-cracking test.

According to the applied model, the NA evolution can be represented compared to CMOD during the pre-cracking test. Figure 117 shows the NA position obtained by the model applied to experimental results from monotonic pre-cracking tests of both SyFRC and SFRC. It can be observed that the NA position is not accurately defined when the section is still plane. However, when CMOD exceeds the limit of proportionality (LOP) and crack occurs, the model finds the NA position rapidly. The average NA reaches 135.2 and 132.7 mm height at the end of the pre-cracking test at 0.5 mm $CMOD_p$ for the SyFRC and SFRC matrix, respectively.
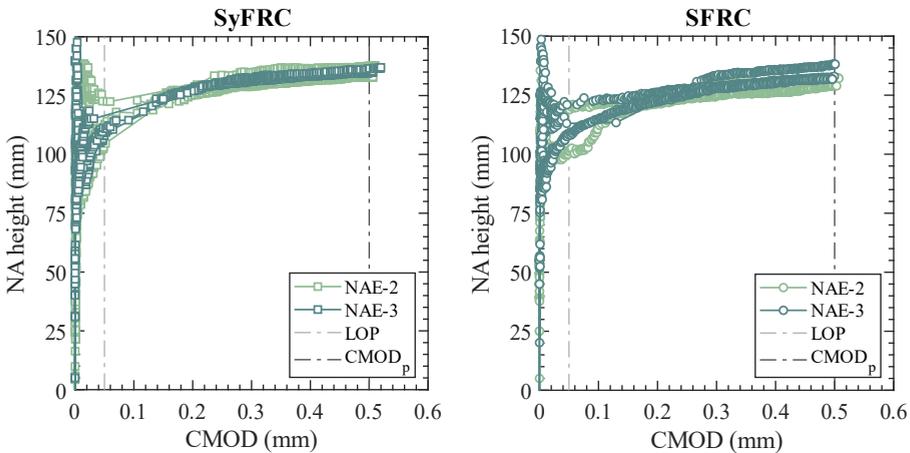
Figure 117. NA evolution obtained in the monotonic pre-cracking test.

From this NA position assessment, it can be concluded that the NA position can be determined in the monotonic flexure test by the defined models. Then they will be applied in the long-term experimental results to assess the neutral axis evolution (NAE).

5.3.3. Long-term flexure test

The first attempt to assess the NAE was carried out in one backup specimen since the standard creep experimental programme defined to use four creep frames, leaving one creep frame free. Then, side transducers were mounted, and one backup SFRC with 40 kg/m^3 of steel fibres, previously pre-cracked up to 0.5 mm CMOD$_p$, was loaded to 50% of the $f_{R,p}$ stress at pre-cracking test, as defined in the proposed methodology. The creep test setup used for this first NAE attempt is provided in Figure 118.

Figure 118. Creep test setup of the first attempt to assess NA evolution during the creep test.

The specimen was unloaded after 180 days of creep test and delayed recovery deformations were recorded for 10 days. Both the crack opening (left) and compressive strain (right) experimental results obtained are provided in Figure 119. It was confirmed that both w_2 (LVDT 3 and LVDT 4) and w_3 (LVDT 5) increased in time as expected, and tensile crack opening increased in time due to sustained load. However, top crack opening deformation (LVDT 1 and LVDT 2) started the creep test in positive values but the w_1 crack opening deformation became negative at around 30 days of creep test, which implies that the crack closed. This behaviour of top transducers can only be explained if a stress redistribution occurs within the cross-section and the neutral axis decreases in time during the creep test.
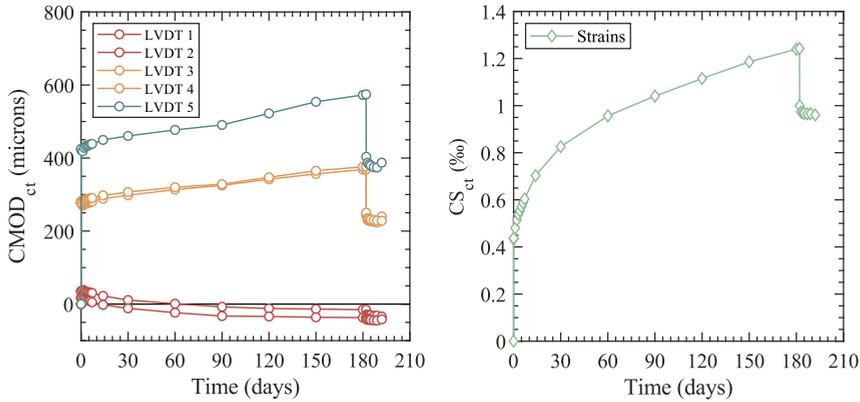
Figure 119. Experimental results of the first attempt of NA evolution assessment.

The NAE model approaches were applied to long-term experimental results, and the obtained NA position evolution is presented in Figure 120. It can be observed that the NA position moved from 131.40 to 117.2 mm within 180 days of creep test. Although constant bending moment is sustained during the creep test duration, it is confirmed that a stress redistribution occurs in the cross-section. This fact implies that the height of the compressive block increased by 76.3%. Considering that the compressed area increased, it could be expected relaxation in terms of compressive strains. However, it was observed in Figure 119 (left) that compressive strains did not decrease in time. Indeed, compressive strains increased, and no stabilisation trend was observed despite the compressive block size increase.
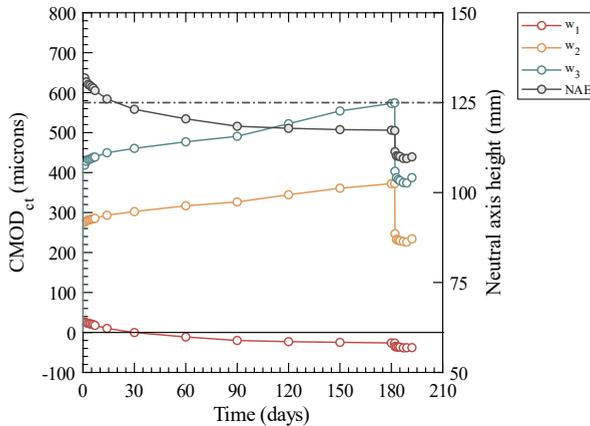
Figure 120. Obtained NA evolution during the creep test.

Figure 121 shows a close-up view of the loading and unloading process of the creep test. Figure 121 (left) shows that the NA model does not get the NA position when specimen is unloaded. On the contrary, when the loading process starts, the model gets

the NA location at 89.2 mm and increases up to 131.4 mm when the sustained load is fully applied. In contrast to monotonic tests, the NA height does not start at the bottom of the specimen since specimens are already pre-cracked. In the unloading process (right), the neutral axis position decreases when the load is removed, and even during the delayed recovery process, the NA follows the descendant trend.
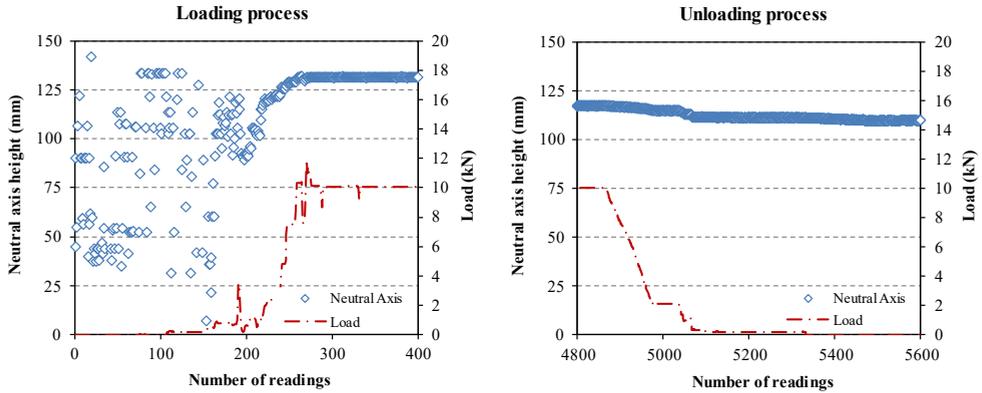
Figure 121. Experimental results of NA evolution first attempt.

Considering the conclusions obtained in this first NAE attempt, the NAE-2 and NAE-3 creep experimental programmes were launched to confirm the NA long-term evolution due to stress redistribution. As previously justified, creep tests were carried out in a single-specimen creep setup. The creep frames of the NAE-3 experimental creep test are shown in Figure 122.

Figure 122. Creep frames of the long-term NAE-3 experimental programme.

The NAE model approaches were applied to long-term experimental results after more than two years of creep tests. The NAE obtained from the model application to experimental results of NAE-2 and NAE-3 is presented in Figure 123. The general descendant trend for the NA can be observed from the experimental results. However, it is important to highlight that during the NAE-3 programme, the air conditioning equipment failed on day 95. Consequently, the temperature gradually increased to 30.1ºC pick value at 151 days of test. Although the temperature increase provoked a sudden NA decrease, the natural descendant trend of NAE was redirected when the equipment was repaired, and the 20ºC temperature was restored. Full information on the experimental results obtained in NA programmes is provided in Appendix G and Appendix H.
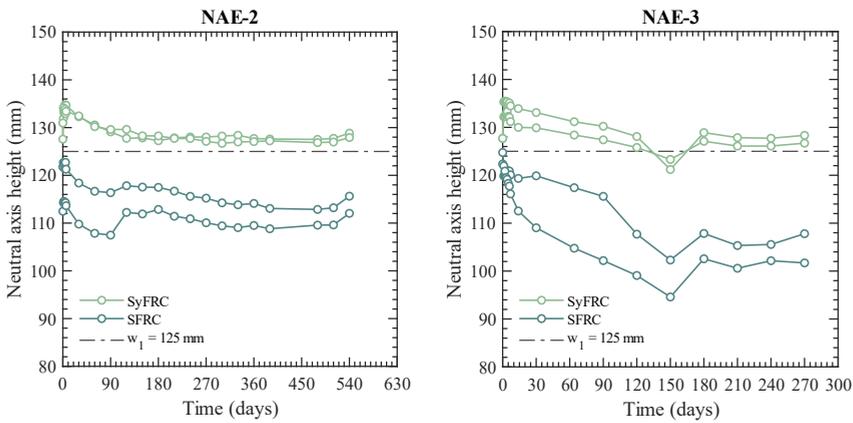
Figure 123. NA evolution of NAE-2 and NAE-3 experimental programmes.

Table 30. Experimental programmes designed the for long-term NA assessment.

	Mix	Specimen	NA	height	(mm)			
			0 days	Max. [1]	90	180	270	360
NAE-1	SFRC	NAE1-S4	131.4	132.1	118.4	117.3	-	-
NAE-2	SyFRC	NAE2-PP2	127.6	134.8	129.1	127.2	128.0	127.7
		NAE2-PP3	129.5	134.2	129.3	128.5	127.3	127.2
	SFRC	NAE2-S2	112.5	115.3	107.9	112.7	110.2	109.2
		NAE2-S6	121.1	123.5	116.1	117.5	114.9	113.8
NAE-3	SyFRC	NAE3-PP4	126.6	133.7	127.0	126.8	125.4	-
		NAE3-PP5	126.5	136.5	130.2	128.9	128.3	-
	SFRC	NAE3-S5	122.4	122.6	115.6	107.9	107.8	-
		NAE3-S6	124.8	126.3	102.2	102.6	101.7	-

[1] Maximum value obtained during the early creep stage (5 days).

However, it was observed in some specimens that during the early creep stage, the NA rises when the loading process ends, and after a few hours/days, the NA gets the maximum position and then, the trend turns into descending evolution. Figure 124 shows the NA position obtained by SyFRC specimens in the early creep stage. It can be observed that instantaneous NA_{ci} at the end of the loading process reached 126.6 and 126.5 mm, respectively, for PP4 and PP5 specimens. However, during the early creep stage, the NA raised to 133.7 and 136.5 mm at 3.7 and 1.3 days, respectively and then, NA started decreasing trend. This fact implies that a simple comparison between NA_{ci} to NA_{cd}^{j} may underestimate the absolute NA variation when NA increases during the early creep stage.
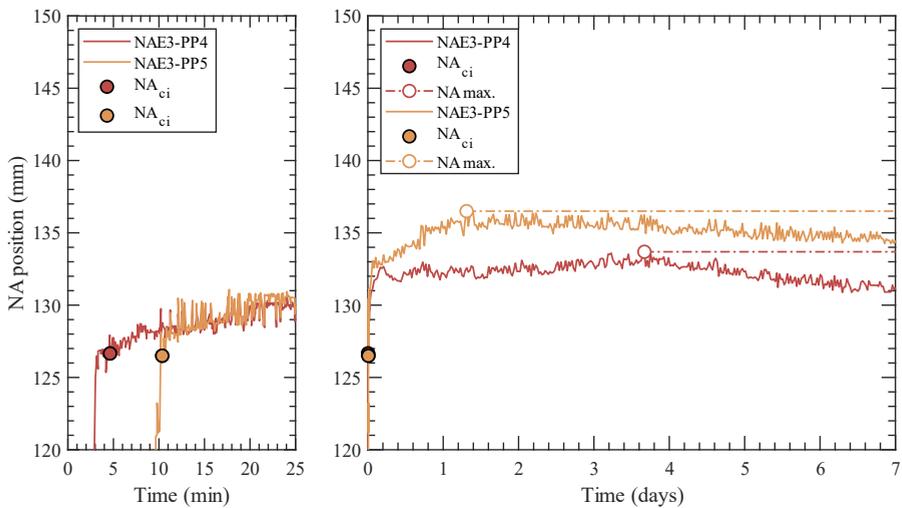
Figure 124. Early creep stage NA position of NAE3 SyFRC specimen.

Both approaches can be compared in terms of goodness and NA position to assess which approach fits better the deformation plane. The r^2 goodness obtained by both models applied to creep tests experimental results are compared in Figure 125 (left). Although the characteristic length approach (l_{cs} model) gets better goodness of fit than the *3w model*, it can be concluded that both models find the NA location with reasonable accuracy. The NA position obtained by the models were compared in Figure 125 (right) to confirm that both models predict the same NA position. Then, considering that the l_{cs} approach model consumes significantly more time (around 40 times more), the simplified 3w approach is preferred.
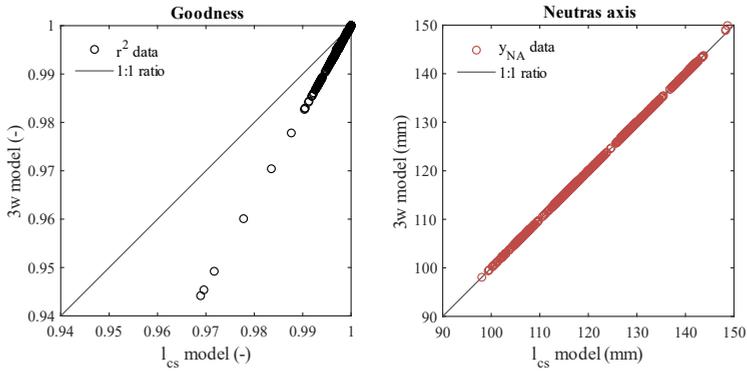
Figure 125. Comparison between 3w and l_{cs} fit models applied to creep test experimental results.

However, the l_{cs} approach allows assessing the characteristic length value along the creep tests. Due to the model approach, the characteristic length is chosen for each data set as the minimum value of the defined l_{cs} threshold that allows linear fit coinciding with compressive strains at ε_0. Figure 126 presents the obtained l_{cs} during the creep test through the model application. It was observed that l_{cs} values vary in time for some specimens. However, it was confirmed that characteristic length estimation is valid since l_{cs} remains within the threshold proposed by MC 2010.
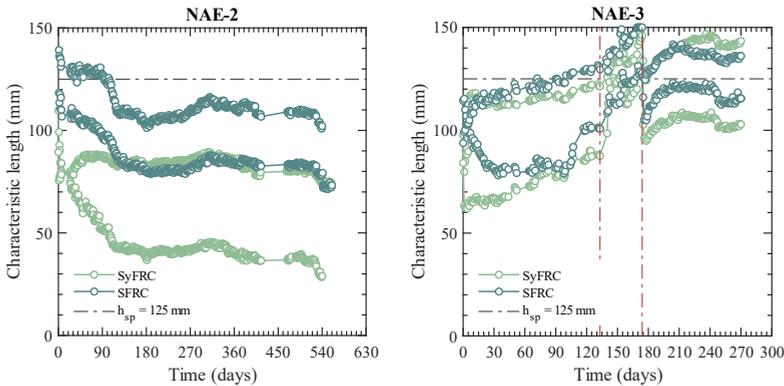
Figure 126. Characteristic length (l_{cs}) variation.

This NA assessment confirms that NA position changes in time when the sustained constant bending moment is applied. This conclusion is relevant to assess the long-term behaviour of cracked FRC material in flexure where both compressive and tensile stresses are combined. The stress redistribution developed during the creep test may influence creep test results when only the crack opening is assessed. However, further studies on this topic are required to determine the influence of the NA evolution on the experimental results in flexure creep.

5.4. Flexural creep database

Meantime the methodology improvements, a database on creep test compiled on FRC specimens was created to globally assess the long-term behaviour among different laboratories. The first database proposal was published [85] in 2014 compiling data of the starting methodology creep test experimental results to assess the global influence of certain test parameters on the long-term experimental behaviour. As a part of my PhD research, I joined the RILEM TC 261-CCF in creep in 2015, where an international Round-Robin Test (RRT) on creep was launched in 2016. The developed database was adapted for multiple methodologies and improved to be used as the basis for the data collection sheet to simplify data exchange among participants. As a result of this datasheet, the RRT database was created and published in 2021 [198]. This PhD thesis defines and proposes the data that shall be included in the international creep test database based on the flexure creep test. The evolution of the database creation and some overall conclusions are deeply explained in this section.

5.4.1. Starting methodology database first proposal

The first creep database proposal [85] was created with specimens tested with the starting methodology [51] containing experimental data of 80 FRC specimens tested in creep in 6 creep experimental campaigns. Data were organised depending on the nature of the data to collect the most significant parameters and variables related to the creep test procedure and experimental results.

An overall statistical analysis of the database was then carried out to assess variables and parameters relations to identify those creep test parameters that have statistical significance on experimental variables and coefficients. A Multiple Linear Regression (MLR) analysis was done focused on the load level (I_{Fa}), concrete matrix compressive strength (f_{ck}) and the fibre content significance. Some conclusions obtained in the statistical analysis can be observed in Figure 127, where it is concluded that the fibre content related to fibre dosage is highly significant to the creep coefficient referred to the creep stage at 90 days.
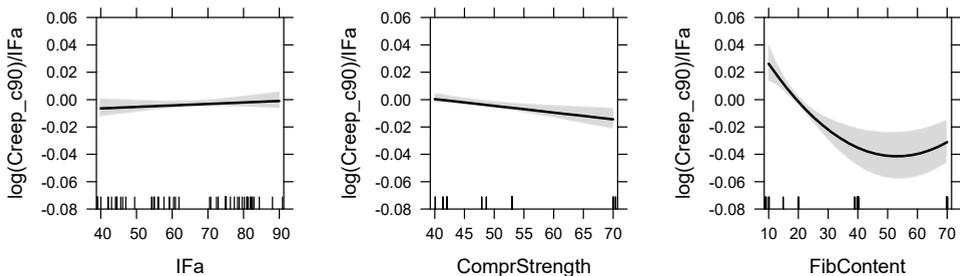
Figure 127. Creep index, compressive strength and fibre content parameter assessment on creep coefficient referred to creep stage at 90 days using Multiple Linear Regression applied to the first database proposal.

On the contrary, load level showed more significance on the creep coefficient referred to the origin, where the pre-crack recovery crack opening deformation is included, as presented in Figure 128. It was confirmed that the database became a valuable tool for assessing long-term behaviour by comparing multiple experimental tests carried out in similar conditions.
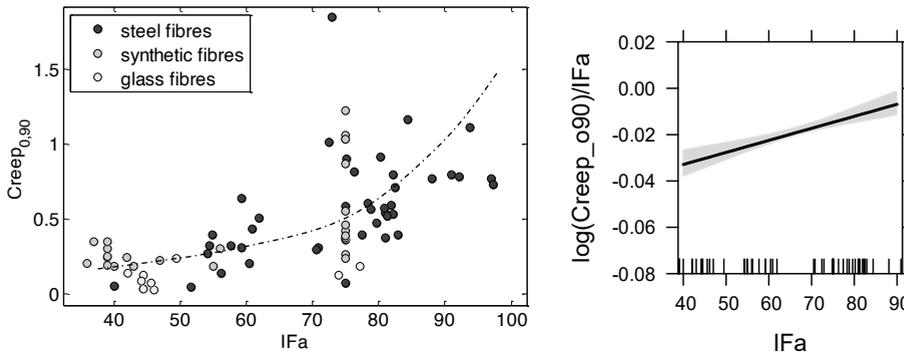
Figure 128. Creep index assessment on creep coefficient referred to the origin of deformations at 90 days by means of Multiple Linear Regression applied to the first database proposal.

5.4.2. Round-Robin Test results exchange datasheet

As previously explained, the ICITECH research group launched in 2016 the international RRT involving 19 international laboratories within the RILEM Technical Committee 261-CCF activity. Four main creep methodologies were carried out: flexure creep in prismatic specimens, square panels, and round panels and direct tension creep test. I assumed the RRT coordinator role and managed the production of 451 FRC specimens, shipment of samples to participant laboratories, testing in creep, and experimental results and methodologies analysis.

Due to the number of participant laboratories and methodologies, it was required to create an agreed datasheet to transfer and share data among different participant laboratories. Otherwise, it could be quite confusing for the ulterior analysis. Therefore, the previously presented database was proposed as starting point of the datasheet. Note that some procedure improvements developed in this PhD work were already proposed for the RRT realisation and approved by TC active members. This fact caused that some significant variables not considered by the starting methodology were included in the updated datasheet version.

The database was divided in three main sections considering: data related to creep test setup and experimental results, analysis parameters and complementary data for analysis. The datasheet structure is presented by sections and data groups in Table 31 and included 120 data for 124 specimens tested in creep in four methodologies.

Table 31. Section 1 of data related to test setup and experimental results.

Section	Group	Description
1		Global Data Obtained for each Specimen until Failure
	A	Identity data
	B	Environmental conditions during the creep test
	C	Concrete matrix characterisation
	D	Fibres
	E	Specimen dimensions
	F	Pre-cracking test output data - Stage 1
	G	Creep test parameters
	H	Creep test output data - Stage 2
	I	Unloading stage of creep test output data
	J	Post-creep residual behaviour after creep
2		Data for the Analysis from Creep Test experimental data
	K	Creep coefficients referred to creep stage
	L	Creep coefficients referred to the origin
	M	Crack opening rate
3		Complementary Data for Analysis
	C	Concrete matrix characteristics (mean value of the serie)
	E	Specimen dimensions
	N	Values of delayed displacement origin
	O	Fibre Counting

It was agreed that the RRT datasheet based on the database became a valuable tool for data exchange. Moreover, since the data was well organised, the ulterior experimental result analysis was easier. The datasheet analysis allowed to identify among 13 different flexure methodologies similar long-term behaviour and comparable results obtained by those methodologies with multiple similarities. A creep test methodology that could be improved to be standardised was then identified.

Additional information about the RRT experience and obtained conclusions [51] were published to be consulted by researchers interested in this topic. Moreover, the creep database created from creep the test carried out in the RRT programme is accessible to the scientific community for comparative and research purposes [198].

5.4.3. International flexure creep test database proposal

To reduce the number of data and simplify the data exchange, the proposed database compiles only the first section related to the data related to creep test setup and experimental results, as presented in Table 31. Guidelines for either creep coefficients

(φ) or crack opening rate (COR) calculation are given so that each researcher may obtain analysis data when required.

The first group of data (Group A) is presented in Table 32. It compiles identification data of fibre-reinforced concrete (FRC) series, the name of each specimen, the reference and the laboratory where the creep test was carried out.

Table 32. Group A parameters of creep test database: Identity data.

Nº	Data	Description	Units
A.1.	Series	Batch of the specimen	--
A.2.	Name / Specimen	Name / Specimen	--
A.3.	Reference	Reference number (Series + Name/Number)	--
A.4.	Laboratory	Reference number of the Laboratory	--

The Group B of data, presented in Table 33, compiles the relevant data of the environmental conditions during creep tests. Average, minimum and maximum temperature and RH values are collected.

Table 33. Group B parameters of creep test database: Environmental conditions during the creep test.

Nº	Data	Description	Units
B.1.	T	Average temperature	°C
B.2.	T_{min}	Minimum temperature during the creep test	°C
B.3.	T_{max}	Maximum temperature during the creep test	°C
B.4.	HR	Average relative humidity	%
B.5.	HR_{min}	Minimum relative humidity during the creep test	%
B.6.	HR_{max}	Maximum relative humidity during the creep test	%

The Group C of data compiles in Table 34 concrete matrix relevant data such as maximum aggregate size and compressive strength.

Table 34. Group C parameters of creep test database: Concrete matrix characterisation.

Nº	Data	Description	Units
C.1.	D_{max}	Aggregate maximum size diameter	mm
C.2.	f_{ck} / f_{ck}	Targeted strength / Concrete Class	MPa
C.3.	$f_{c,7}$	Compressive strength (Ø150×300mm) at 7 days	MPa
C.4.	$f_{c,28}$	Compressive strength (Ø150×300mm) at 28 days	MPa

Data related to fibres is compiled in Group D, as presented in Table 35. Fibre properties shall be obtained from the material datasheet provided by manufacturers. Note that dosage is given both related to weight (kg/m³) and volume (% of volume) since variations in the density of materials provides huge differences in fibre content.

Table 35. Group D parameters of creep test database: Fibres properties.

Nº	Data	Description	Units
D.1.	Material	Material	--
D.2.	Brand	Brand / Commercial reference	--
D.3.	Length	Length	mm
D.4.	Diameter	Diameter	mm
D.5.	Slenderness	Slenderness	--
D.6.	E	Young modulus	GPa
D.7.	σ_y	Yield strength	MPa
D.8.	σ_u	Ultimate Tensile strength	MPa
D.9.	Dosage in weight	Dosage in weight	kg/m³
D.10.	Dosage in volume	Dosage in volume	% vol.

Group E compiles data related to specimens' dimensions, as presented in Table 36. Information of cross-section and notch dimensions are used for stress calculation.

Table 36. Group E parameters of creep test database: Specimens dimensions.

Nº	Data	Description	Units
E.1.	Shape	Prismatic, cylindrical, square panel, round panel	-
E.2.	b	Average cross-section width measured by calliper	mm
E.3.	h_{sp}	Average cross-section height measured by calliper	mm
E.4.	b_{notch}	Notch width	mm
E.5.	h_{notch}	Notch height	mm

Table 37 compiles Group F with pre-cracking test output data, including both flexure setup and experimental variables and parameters related to the first creep test procedure phase.

Table 37. Group F parameters of database: Pre-cracking tests output data (Stage 1).

Nº	Data	Description	Units
F.1.	Flexure setup	Flexural Beams - Specify if 3PBT or 4PBT was adopted	-
F.2.	L	Flexural Beams - Support span	mm
F.3.	l_a	Flexural Beams - Distance between support and nearest loading point	mm
F.4.	l_b	Flexural Beams - Distance between loading points (only for 4PBT)	mm
F.5.	f_L	Residual strength at LOP	MPa
F.6.	$f_{R,p}$	Residual strength at $CMOD_p$	MPa
F.7.	F_L	Load at LOP	kN
F.8.	$F_{R,p}$	Load at $CMOD_p$	kN
F.9.	CMOD / δ	Reference displacement registered during the tests	--
F.10.	$CMOD_{pn}$	Nominal pre-cracking level expected	μm
F.11.	$CMOD_p$	Maximum CMOD reached in the pre-cracking	μm
F.12.	$CMOD_{pri}$	Elastic CMOD recovery when the unloading process ends	μm
F.13.	$CMOD_{prd}$	Residual CMOD 10' after the unloading process	μm

Data related to creep test setup and parameters (second creep test procedure phase) are grouped in Group G and presented in Table 38. The adopted flexure setup, creep index, applied stress and time spent during the loading stage are some of the included data. In addition, information regarding the multi-specimen setup and relative position (top, middle or bottom) of the specimen in the stacked set are included.

Table 38. Group G parameters of creep test database: Creep test parameters.

Nº	Data	Description	Units
G.1.	Flexure setup	Specify if 3PBT or 4PBT was adopted	-
G.2.	L	Support span	mm
G.3.	l_a	Distance between support and nearest loading point	mm
G.4.	l_b	Distance between loading points (if 4PBT is used)	mm
G.5.	I_n	Nominal Creep index [% of $f_{R,p}$]	%
G.6.	$F_{R,c}$	Load applied in creep test	kN
G.7.	$f_{R,c}$	Stress applied in creep test	MPa
G.8.	I_c	Creep index [$I_c = f_{R,c} / f_{R,p}$]	%
G.9.	t_{ci}	Loading process duration	seconds
G.10.	t_f, t_{max}	Total time that load was sustained in the creep test	days
G.11.	Specimens / frame	Single- or Multi-specimens creep test setup	-
G.12.	Position	Relative position in creep frame (top, middle or bottom)	-

The Group H of data, presented in Table 39, compiles CMOD total deformations obtained during the creep phase. Although delayed CMOD are usually reported in either mm or µm units, considering that it is expected to have short-delayed deformations, microns were chosen for data exchange unit to avoid too many decimals.

Table 39. Group H parameters of creep test database: Creep tests output data (Stage 2).

Nº	Data	Description	Units
H.1.	$CMOD_{ci}$	Instantaneous CMOD immediately after reaching $f_{R,c}$	µm
H.2.	$CMOD_{ci}^{15'}$	Short-term CMOD 15' from the loading process beginning	µm
H.4.	$CMOD_{cts}^{1}$	Total CMOD displacement at 1 day [*]	µm
H.5.	$CMOD_{cts}^{2}$	Total CMOD displacement at day 2 [*]	µm
H.6.	$CMOD_{cts}^{3}$	Total CMOD displacement at day 3 [*]	µm
H.7.	$CMOD_{cts}^{5}$	Total CMOD displacement at day 5 [*]	µm
H.8.	$CMOD_{cts}^{7}$	Total CMOD displacement at day 7 [*]	µm
H.9.	$CMOD_{cts}^{14}$	Total CMOD displacement at day 14 [*]	µm
H.10.	$CMOD_{cts}^{30}$	Total CMOD displacement at day 30 [*]	µm
H.11.	$CMOD_{cts}^{60}$	Total CMOD displacement at 60 days [*]	µm
H.12.	$CMOD_{cts}^{90}$	Total CMOD displacement at 90 days [*]	µm
H.13.	$CMOD_{cts}^{120}$	Total CMOD displacement at 120 days [*]	µm
H.14.	$CMOD_{cts}^{150}$	Total CMOD displacement at 150 days [*]	µm
H.15.	$CMOD_{cts}^{180}$	Total CMOD displacement at 180 days [*]	µm
H.16.	$CMOD_{cts}^{210}$	Total CMOD displacement at 210 days [*]	µm
H.17.	$CMOD_{cts}^{240}$	Total CMOD displacement at 240 days [*]	µm
H.18.	$CMOD_{cts}^{270}$	Total CMOD displacement at 270 days [*]	µm
H.19.	$CMOD_{cts}^{300}$	Total CMOD displacement at 300 days [*]	µm
H.20.	$CMOD_{cts}^{330}$	Total CMOD displacement at 330 days [*]	µm
H.21.	$CMOD_{cts}^{360}$	Total CMOD displacement at 360 days [*]	µm
	$CMOD_{cts}^{j}$	Total CMOD displacement at j days [*]	µm

[*] Note that delayed $CMOD_{cts}^{j}$ deformations shall be compensated with shrinkage

The Group I of data, presented in Table 40, collects the output data from the unloading process after creep test including the unloading process duration, instantaneous recovery ($CMOD_{cris}$) and delayed recovery ($CMOD_{crds}^{j}$) at different lapses of time. It is important to highlight that these values shall be compensated with shrinkage deformations.

Table 40. Group I parameters of creep test database: Creep test unloading process of output data.

Nº	Data	Description	Units
I.1.	t_{cri}	Time duration of the unloading process in the creep test	seconds
I.2.	$CMOD_{cris}$	Total CMOD immediately after unloading [*]	µm
I.3.	$CMOD_{crds}^1$	Total CMOD at 1 days after unloading [*]	µm
I.4	$CMOD_{crds}^7$	Total CMOD at 7 days after unloading [*]	µm
I.5.	$CMOD_{crds}^{14}$	Total CMOD at 14 days after unloading [*]	µm
I.6.	$CMOD_{crds}^{30}$	Total CMOD 30 days after unloading [*]	µm
I.7.	t_{crd}	Delayed recovery assessment duration after the creep test	days

[*] Note that $CMOD_{cris}$ and $CMOD_{crds}^j$ shall be compensated with shrinkage

Finally, data related to the post-creep performance of FRC specimens are collected in the Group J of data, as presented in Table 41.

Table 41. Group J parameters of creep test database: post-creep residual performance.

Nº	Data	Description	Units
J.1.	$f_{PostCreep,R,2}$	Residual strength after the creep test at $CMOD_2$	MPa
J.2.	$f_{PostCreep,R,3}$	Residual strength after the creep test at $CMOD_3$	MPa
J.3.	$f_{PostCreep,R,4}$	Residual strength after the creep test at $CMOD_4$	MPa
J.4.	$f_{PostCreep,R,3} / f_{R,1}$	Post-creep residual behaviour	-
J.5.	$F_{PostCreep,R,2}$	Load at $CMOD_2$ after the creep test	kN
J.6.	$F_{PostCreep,R,3}$	Load at $CMOD_3$ after the creep test	kN
J.7.	$F_{PostCreep,R,4}$	Load at $CMOD_4$ after the creep test	kN

As it can be observed, most of the data proposed to share in the international creep database shall be reported in the flexure creep test report proposed in Section 6.2. Hence, share data to the international database became an easy task for future experimental research.

Chapter 6.

Proposed Methodology

As a result of the deep analysis carried out during this comprehensive experimental programme of the creep test methodologies available, significant improvements and recommendations are proposed in this PhD thesis in terms of methodological procedure, boundary conditions, creep frame construction and creep test result analysis. This chapter presents a new methodology proposal considering the previously described improvements assessed in their corresponding experimental campaigns.

The main target of this PhD work is not only to improve the starting methodology but, considering the available methodologies in the state-of-the-art and analysing the variations and influence of different procedures, to propose and define a creep test procedure and parameters that could be standardised to characterise the long-term properties of cracked FRC among all laboratories.

Most of the following creep steps definitions, significant parameters, and procedure improvements were proposed in the RILEM Technical Committee (TC) 261-CCF and agreed by the active members. Then, most of these improvements were assessed in the international Round-Robin Test carried out within the TC activity.

This recommendation is applicable to standard FRC specimens that reveal a single crack when tested in flexure. Multiple cracking concrete matrices (i.e., ECC, UHPFRC…) are also considered if all cracks start from the tip of the notch. If one single crack occurs out of the tip of the notch or out of the measuring range, the FRC specimens are out of this recommendation.

6.1. Creep test procedure

The flexure creep testing procedure of fibre-reinforced concrete (FRC) in the cracked state is divided into three phases: pre-cracking, creep, and post-creep. Figure 129 presents an idealised curve of the whole process of the creep test where each phase can be identified. During the pre-cracking phase (OD), the specimen is pre-cracked in

controlled conditions up to a previously defined crack opening (B), inducing a certain damage and then unloaded (B-D). In the creep phase, specimens are kept under sustained stress where instantaneous and delayed deformations are registered (D-F) and then unloaded (F-H). The final post-creep phase (H-K) assesses any influence of the long-term test on the residual performance by flexure testing up to 4 mm crack opening.
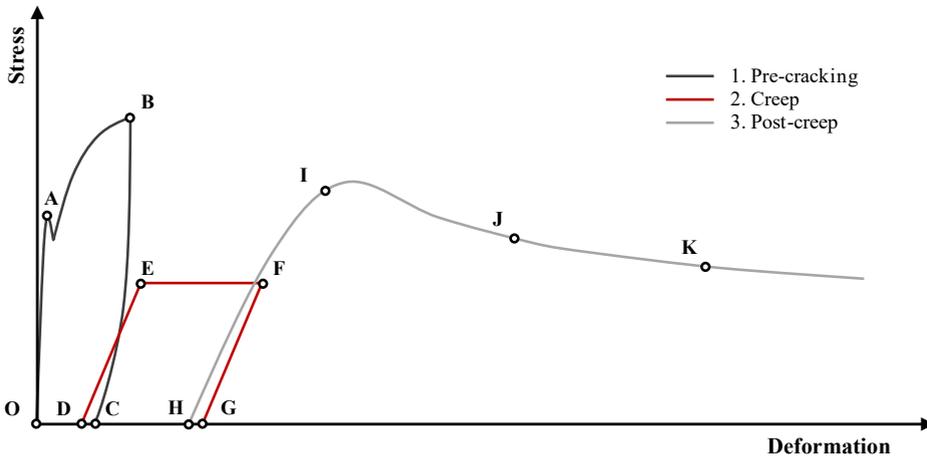
Figure 129. Creep test procedure idealised curve containing three phases.

Since creep this creep testing proposal is based on EN 14651 [26], standard prismatic specimens with 150 × 150 mm nominal cross-section shall be used. The length of specimens (L) may range from 550 mm to 700 mm. Test specimens shall be cast and cured in a moist chamber according to the standard guidelines. In addition, before the pre-cracking test, specimens shall be notched at midspan at 25 days and then stored again for at least three days in the moist chamber to keep curing conditions.

The success of the creep test depends on the proper procedure in these phases. Therefore, the proposed procedure for each phase is deeply defined and described in the following sections.

6.1.1. Pre-cracking phase procedure

According to EN 14651, specimens shall be pre-cracked at 28 days. Specimens shall be prepared for the flexure test and taken out of the moist chamber no more than 3 hours before the pre-cracking test.

The displacement transducer shall be mounted on the specimen to measure either crack mouth opening displacement (CMOD) or deflection (δ). In the case of CMOD reference, the use of both crack opening displacement (COD) clip transducer and linear variable displacement transducer (LVDT) is allowed. Nonetheless, the COD clip transducer is preferable if possible since it provides a more accurate crack opening measurement. Figure 130 provides guidelines and restrictions for transducer setup

depending on the transducer used for the long-term test. On the one hand, COD clip gauges shall be mounted under the specimens across the notch mouth, centred over the specimen width and parallel to the longitudinal axis of the specimen. The distance y between the bottom surface of the specimen and the line of measurement shall not exceed 5 mm. On the other hand, LVDT transducers shall also be mounted parallel to the longitudinal axis, centred along the specimen width, and the distance y to the measurement line shall not exceed 20 mm. The maximum distance between the two measuring points of 50 mm shall be respected to ensure the measurement of crack opening in the non-linear hinge.
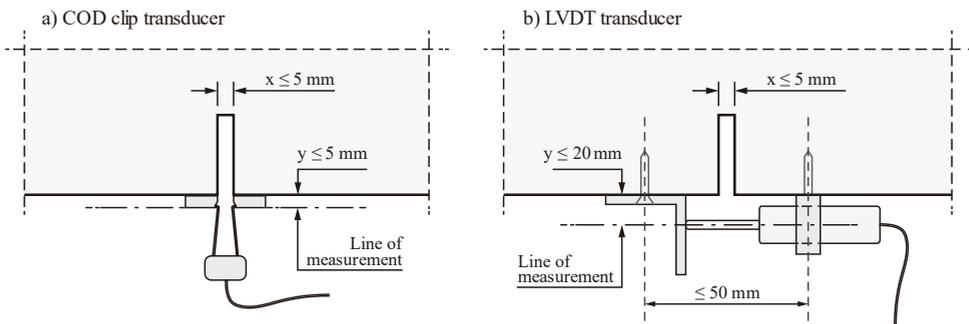
Figure 130. LVDT transducer location proposal for CMOD measurement.

Since the flexure creep test procedure is based on the EN 14651 standard [26], it is recommended to use the three-point bending test (3PBT) configuration with a 500 mm length support span for the pre-cracking test. According to the previously presented classification of degrees of freedom (Section 4.5), supporting rollers shall allow for OOX and XOX displacements, whereas the loading roller shall allow for OOX rotations. Alternatively, in those cases of creep tests based on ASTM C1609 [25] standard on unnotched specimens, specimens shall be pre-cracked in a four-point bending test (4PBT) configuration according to ASTM C1609 [25], and both supporting and loading rollers shall allow for OOX and XOX displacements. In addition, only LVDT transducers shall be mounted to measure deflection (δ) since specimens have no notch, as defined in ASTM C1609.

Considering that pre-cracking tests are short-term monotonic tests, no singular environmental conditions are required.

The idealised curve of the pre-cracking test for both hardening and softening behaviour is presented in Figure 131, where the main variables to record during the pre-cracking phase are defined. It can be observed that all CMOD parameters includes the subscript "p" related to the pre-cracking phase according to the glossary definition proposed in Section 4.1.
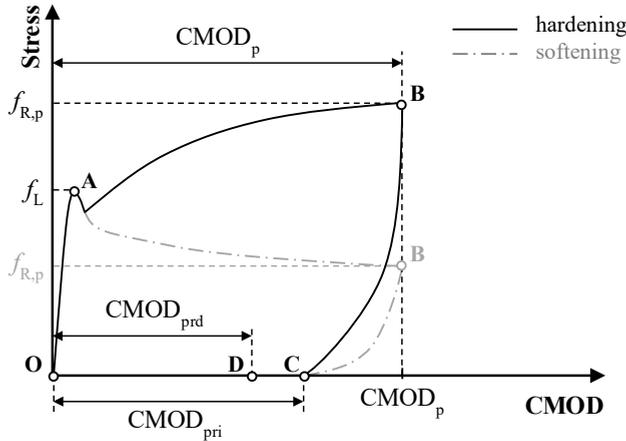
Figure 131. Pre-cracking phase parameters.

Pre-cracking tests shall be carried out in a servo-controlled universal testing machine (UTM) at a constant 0.05 mm/min CMOD rate until the target $CMOD_p$ is achieved. The initial CMOD deformation rate is 0.05 mm/min. Once the limit of proportionality (LOP) is reached (point A in Figure 131), the residual stress at LOP f_L is registered, and the CMOD rate shall be increased up to 0.2 mm/min until the nominal pre-cracking level $CMOD_{pn}$ is achieved (point B in Figure 131). To ensure proper pre-cracking conditions, the pre-cracking deformation before unloading ($CMOD_p$) shall reach $CMOD_{pn}$ and should not exceed $CMOD_{pn}$ + 0.02 mm. The proposed reference nominal pre-cracking value is $CMOD_{pn}$ = 0.5 mm, corresponding to $f_{R,1}$ residual stress. In the case of deflection-controlled flexure test, the corresponding proposal for nominal pre-cracking value is δ_{pn} = 0.47 mm, and δ_p shall not exceed δ_{pn} + 0.03 mm. When any specimen exceeds the defined $CMOD_p$, it shall not be considered for creep test or considered as tested out-of-range. If any specimen is tested out of the specified ranges, testing conditions shall be reported in the creep test report.

Once the nominal target $CMOD_{pn}$ is reached, the specimen shall be immediately unloaded at 0.2 mm/min CMOD rate, and the load shall be removed at 0.3 mm/min CMOD rate. During the unloading step, both instantaneous ($CMOD_{pri}$) and delayed ($CMOD_{prd}$) recovery deformations (points C and D respectively) after unloading shall be recorded for 10 minutes.

After the pre-cracking test, specimens shall be stored for seven days in the climate room where the creep test will be conducted. Thereby, the specimens had time enough to acclimate to the environmental test conditions to minimise interfering with the instantaneous and short-term readings. Pre-cracked specimens shall be stored supported on their side (turned 90 º) to avoid any crack opening deformation due to their dead load.

Note that depending on either single- or multi-specimen setup adopted, it is proposed to cast and pre-crack more specimens than strictly required (see Table 21). Therefore, in the case of a single-specimen creep test setup, one specimen per frame, including the

shrinkage specimen, shall be pre-cracked. In the case of a multi-specimen creep test setup with 2 or 3 specimens per frame, 4 or 5 specimens shall be respectively pre-cracked per frame/mix to provide residual performance variety enough to reduce the I_c scatter.

6.1.2. Creep phase procedure

The creep phase procedure varies depending on whether a single- or multi-specimen setup is chosen and the creep frame design. As previously explained, although the single-specimen setup is preferred, the multi-specimen setup has multiple advantages in terms of laboratory space savings and the number of specimens tested simultaneously. Therefore, it is important to adapt both the creep frame and the creep test procedure to the chosen single- or multi-specimen setup.

Creep frame design and construction

The creep frame construction shall adhere to the following specifications regarding materials, configuration, and boundary conditions to ensure rigidity enough to keep verticality, constant load and flexure conditions in time, avoiding as much as possible frictions between the different mobile elements of the creep frame.

The most extended frame construction to perform flexure creep tests on cracked fibre-reinforced concrete (FRC) specimens is based on a second-degree lever arm, as concluded from the literature assessment. Considering the previously described advantages and compared to other creep frame construction (spring- or hydraulic-loaded frames, screwed tightened bars…), the use of a lever arm creep frame is recommended. The load can be induced to the specimens in either a compressive or tensile way, depending on the relative position of the lever arm. Both frame types can be adapted to either single- or multi-specimen setups if required, as seen in Figure 132.

a) Top lever arm (compressive)   b) Bottom lever arm (tensile bar)
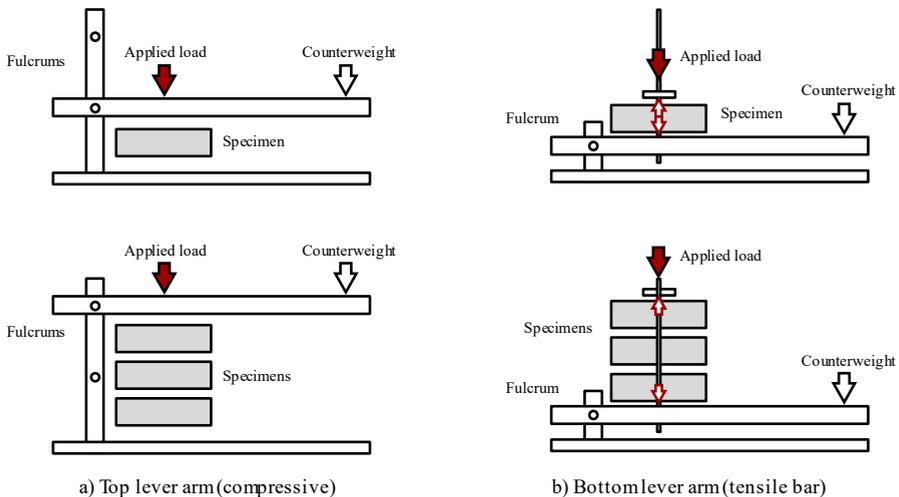
Figure 132. Types of lever arm creep frames design.

In the top lever arm creep frames, the lever arm lays directly over the top specimen and provides a constant compressive load during the creep test. The load depends only on the weight of the lever arm, the counterweights, and the lever arm multiplier factor. This creep frame construction provides high-confidence performance and a more stable load in time since the lever arm is free of friction thanks to the fulcrum. If the top lever arm creep frame has two fulcrums, the creep frame can be adapted from a single- to multi-specimen setup by changing the fulcrum position.

On the contrary, in the bottom lever arm creep frames, the lever arm is usually below the specimens, and screwed steel tensile bars are required to carry the load over the top specimen. Although this type of creep frame also provides high-confidence performance, slight load loss in time has been observed due to internal friction between the lever arm and the specimen's support profiles. Therefore, it is important to focus special attention on this friction area in the design and construction phase. This creep frame requires only one fulcrum to host either single- or multi-specimen setups since screwed bars provide enough flexibility to set the load transfer plate at any desired height. Notwithstanding, additional load transfer elements (i.e., screwed bars, nuts…) are required to carry the load to the top specimen, and more preparation time is required. Moreover, slight differences in nuts torque may influence the required stress over time. Regardless of the type of creep frame, the lever arm shall be placed at the beginning of the creep test as horizontal as possible to minimise the effect of horizontal loads.

Creep test setup and boundary conditions

In the case of a single-specimen setup on notched specimens, the same flexure configuration used for the pre-cracking test (3PBT configuration with 500 mm length support span) is recommended (Figure 133.a) in compliance with EN 14651 standard [26]. Therefore, supporting rollers shall allow for OOX and XOX displacements, whereas the loading roller shall allow for OOX rotations according to the boundary conditions classification. Alternatively, the use of single-specimen creep tests based on ASTM C1609 [25] standard on unnotched specimens (Figure 134.d) is also accepted. In this case, the use of a four-point bending test (4PBT) configuration is recommended, and both supporting and loading rollers shall allow for OOX and XOX displacements.

In the case of the multi-specimen configuration during the creep test, to improve the stability of the specimens during the long-term test, the use of 4PBT is recommended (Figure 133.b), and both supporting and loading rollers shall allow for OOX and XOX displacements. The use of 4PBT in the creep test required the use of the corresponding Equation 5 to obtain the load to apply on each frame. The relative position (top, middle or bottom) of each specimen in the column shall be decided by their mechanical performance and considering the corresponding dead load of the upper specimens and load transfer elements as proposed in the following sections. As previously explained, specimens with higher residual strengths are usually located at the bottom of the column to achieve a similar *creep index* for all the specimens of each frame.

a) EN 14651 3PBT set-up

b) 4PBT adapted set-up
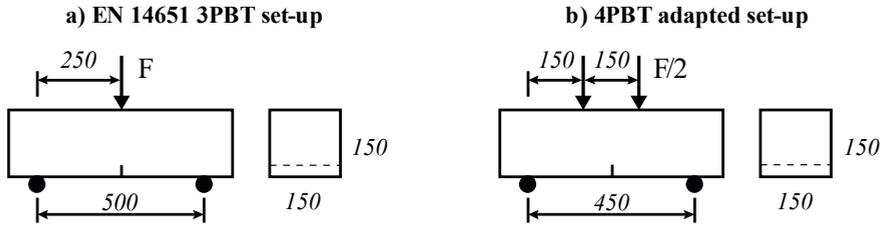
Figure 133. Recommended flexure load configurations: a) EN 14651 3PBT flexural setup and b) 4PBT adapted set-up.

The recommended creep test setups, including the corresponding flexure configuration for either single- or multi-specimen setups, are presented in Figure 134. Multi-specimen creep frames shall ensure that either the individual delayed deformation or the sudden collapse of the specimens does not compromise both the continuity of the long-term test and the stability of the stacked specimens. Therefore, to avoid any influence between specimens and ensure the required boundary conditions, steel transfer plates containing both the supporting and loading rollers shall be located between the specimens. In addition, transfer plates shall include emergency brakes device such as steel blocks to stop any broken specimen before the collapse. Otherwise, the counterweight or the stacked specimens may fall, causing severe damage to the equipment. Indeed, the load due to transfer plates, rollers, brakes, and upper specimens shall be considered as additional load onto the specimens below.

RECOMMENDED SETUPS

ACCEPTED VARIATIONS

a) 3PBT Single setup b) 4PBT Multi (3) setup c) 4PBT Multi (2) setup d) ASTM C1609
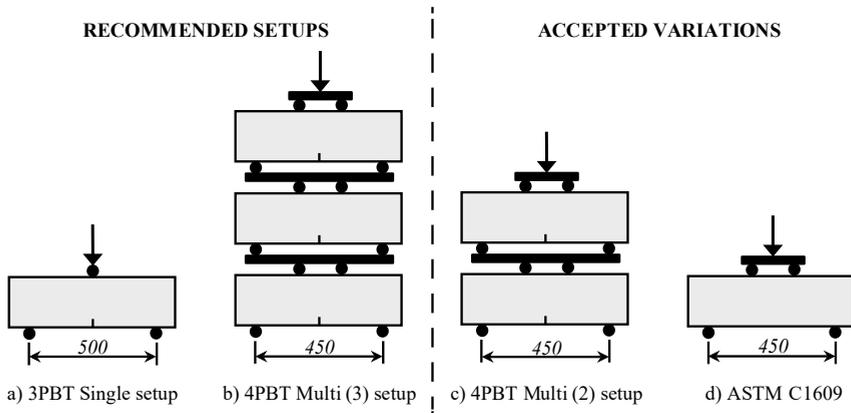
Figure 134. Recommended and accepted single- and multi-specimen creep test setups.

In all recommended creep setups, specimens shall be placed face down with the notch at the bottom face according to the flexure setups (Figure 133). The use of inverted specimens is usually observed related to the absence of transfer plates to simplify the

multi-specimen 4PBT setup with simple steel rollers. Since the use of steel transfer plates together with well-constructed support and loading rollers has been recommended, inverted specimens became unnecessary. Moreover, inverted specimens (Figure 135) may influence the recovery capacity of the specimen for 30 days when unloaded even if inverted specimens are placed with transfer plates and the corresponding recommended boundary conditions (Figure 135.a) if the crack is blocked by any aggregate spalled during the cracking process. The use of multi-specimen setups that do not include transfer plates such as setups a) and b) in Figure 135 are not accepted since boundary conditions cannot be assured.

UNRECOMMENDED SETUPS
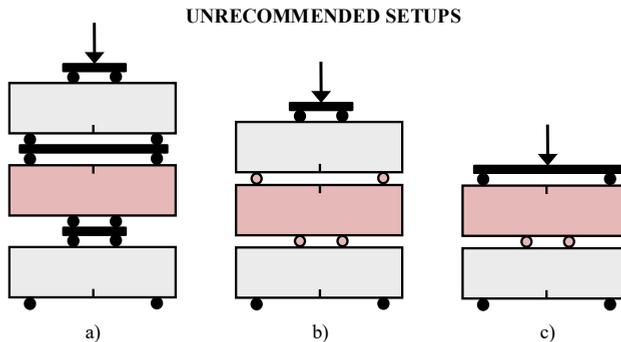
Figure 135. Not recommended creep test setups.

Environmental conditions

Environmental conditions such as temperature and relative humidity has significant influence on the long-term properties (creep and shrinkage) of some FRC mixes. Therefore, to reduce external influence on the test results, both temperature and relative humidity shall be controlled during the creep test duration. Creep frames shall be located inside a climate-controlled room equipped with hygrometric and temperature control systems to ensure the desired environmental conditions. Neither laboratory environment nor isolated rooms without hygrometric are recommended for creep tests location since climatic conditions are not controlled at all during the test duration. Note that a creep test may last for more than one year, comprising huge climatic conditions variations.

The proposed temperature range for the creep test is $20 \pm 2^{\circ}$ C. It is proposed to fix a target relative humidity between 50 and 70% and keep the humidity stable within the $\pm$ 5% acceptance range (i.e. humidity range from 45 to 55% for a 50% target value). These environmental restrictions will significantly reduce the influence of environmental conditions on the creep test results.

Any sudden variation of either the temperature or relative humidity out of the acceptance range shall be stated in the test report. Moreover, if the environmental conditions of the climate room exceed for more than ten days in a row the acceptance range, the corresponding specimens shall be reported as tested out of the recommended

range. Any specimen tested out of the recommended conditions shall be disregarded from the analysis and the database.

To monitor and record the evolution of the climate conditions along the creep test, temperature and relative humidity measurement devices connected to DAS for continuous recording are required inside the climate-controlled room. The environmental conditions recommended recording rate is one reading each 1800 seconds (30 minutes). This recording rate is helpful to assess any atypical climatic conditions variation during the creep test. Notwithstanding, the evolution of the environmental conditions in time shall be reported in one figure with two readings per day (day and night values) during the entire duration of the long-term phase. An example figure of the environmental conditions report is presented in Figure 136, including the target value and acceptable ranges for both temperature and relative humidity.
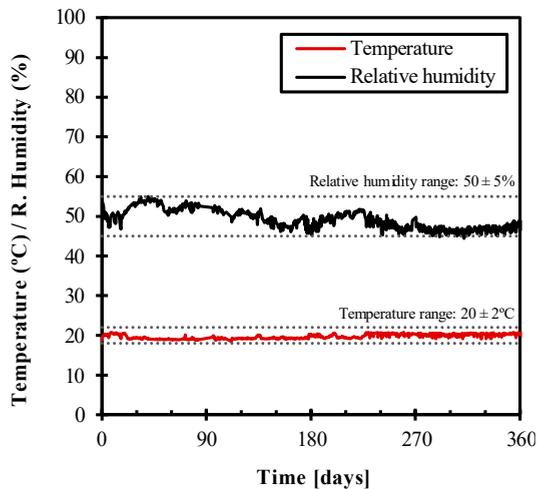
Figure 136. Example of environmental conditions report.

Specimen selection

In the case of a multi-specimen setup, pre-cracked specimens shall be selected depending on their residual performance to accomplish the requirements in terms of creep index variation and residual dead load on the specimens. To this purpose, a specimen selection flowchart was defined (Figure 91) for both single- and multi-specimen creep test setups. The proposed selection process considers aspects such as the steel transfer plates dead load, dead load due to upper specimens, and relative position combinations to reduce the scatter of creep index among the stacked specimens. The creep index requirements are usually accomplished if specimens with better residual performance are usually at the bottom position of the column.

Pre-cracked specimens not destined for the creep test shall be stored supported on their side turned 90º for one week inside the climate-controlled room as backup

specimens if any specimen suddenly fails during either the loading procedure or the first week of the creep test.

Specimens stacking procedure (for multi-specimen setup)

Before the stacking procedure, the data acquisition system (DAS) shall be switched on and start recording at a 1 Hz (one reading per second) recording rate to obtain an adequately defined CMOD evolution of the loading procedure. This recording rate provides enough data to assess any unexpected deformation during the loading procedure, and how fast and steady the load is applied in creep frames.

The stacking of the specimens shall be done in a step-by-step procedure and shall not last more than 30 minutes. The bottom specimen shall be placed in the bottom of the frame, and the corresponding transducer (COD clip or LCDT) connected to the DAS prior to registering the CMOD deformation without load. Over the bottom specimen, both the transfer plate and the middle specimen shall be located and aligned. The CMOD transducer of the middle specimen shall be connected to the DAS and register the initial unloaded deformation. Since DAS continuously records data, any deformation caused on the bottom specimen by the dead load of the transfer plate and middle specimens is recorded. The following transfer plate and the top specimens shall be placed over the middle specimen and the displacement transducer connected to DAS. The top transfer plate is finally placed over the top specimens together with the load cell, and the load transfer plate device is connected to the screwed bar with loose nuts.

It is important to highlight that during both the stacking procedure and the later unloading recovery process, the stress induced by the residual dead load of upper specimens onto the bottom specimen shall never exceed 15% of the target $f_{R,c}$ sustained stress during the creep test. Otherwise, only a multi-specimen setup with two specimens is recommended.

Load calibration and loading procedure

The applied load shall be controlled during the creep test duration. Therefore, placing one load cell over the top specimen is strongly recommended to assess the applied load frequently. By this action, the load individually applied on each frame can be monitored by DAS and allows to adjust the load if any deviation is noticed during the long-term test. The sustained load $F_{R,c}$ shall be checked weekly during the creep test duration.

Considering that both 3PBT and 4PBT can be used in different phases of the creep test procedure, the use of load level term may be confusing. Since the target of the flexure creep test procedure is to sustain a specific stress in time, either *stress level* or *creep index* (I_c) terminology is recommended. The creep index is defined as the ratio of sustained stress during the creep phase ($f_{R,c}$) to the residual stress obtained in pre-cracking tests ($f_{R,p}$) at defined 0.5 mm $CMOD_p$, usually related to SLS.

The recommended nominal creep index (I_c) for characterisation and comparison purposes of long-term flexure properties of FRC following the proposed procedure is 50% of the $f_{R,p}$, equivalent to 0.5 $f_{R,1}$. The creep index shall not exceed the $\pm$ 5%

acceptance range. Otherwise, specimens shall be reported as out-of-range. Notwithstanding, if the goal of the creep test is not flexure creep characterisation, but scientific research, different than recommended creep index value can be adopted.

Before the loading process, it is important to check that DAS is set up to 1 Hz recording rate and that the lever arm is lifted and free of load. In the case of the bottom lever arm creep frame, the loading process starts by tightening the nuts to the transfer plate connected to the screwed bar. Nuts shall be gradually and equally tightened up to 1 kN preload registered by the load cell. The next load step corresponds to the lever arm dead load. The lifted lever arm shall be gradually lowered and released of support so that the lever arm dead load amplified by the multiplier factor increases the recorded load by the load cell. Finally, the rest of the required load up to $F_{R,c}$ shall be induced using counterweights placed on the lever arm assisted by load cell readings to ensure the required sustained load. It is preferable that most of the load was due to counterweight action since counterweight mass helps the lever arm stabilisation against hits and unexpected movements. In the case of top lever arm creep frames, any torque load is required and therefore, sustained load shall be calibrated before the creep test over a dummy specimen when possible.

Regardless of the creep frame type, the loading process shall take at least 30 seconds and no more than 5 minutes (30 s < t_{ci} < 5 min). The load shall be gradually applied, avoiding sudden increases in load, hits, and overloads. The specimen stacking process duration shall not be considered for the t_{ci} parameter calculation. When the sustained stress $f_{R,c}$ is achieved, the instantaneous $CMOD_{ci}$ deformation shall be immediately registered. In addition, the short-term deformation 15 minutes after beginning the loading process ($CMOD_{ci}^{15'}$) shall be recorded. Considering that the short-term deformation parameter provides more homogeneous creep coefficients, this PhD proposal assumes the short-term deformation $CMOD_{ci}^{15'}$ for the calculation of the creep coefficient. The creep frame loading process parameters are displayed in Figure 137.
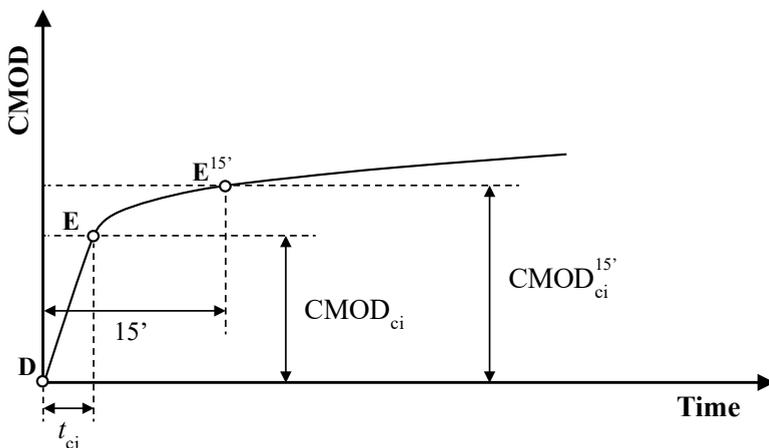
Figure 137. Creep phase loading process parameters.

Long-term stage

Considering the nature of long-term deformations, it is recommended a minimum creep test duration of one year (360 days of sustained load).

Besides the instantaneous and short-term deformation, during the long-term stage of the creep phase, both delayed ($CMOD_{cd}{}^j$) and total ($CMOD_{ct}{}^j$) CMOD deformations can be obtained, as shown in Figure 138. It is recommended to report total CMOD deformations ($CMOD_{ct}{}^j$) at 6 and 12 hours, and 1, 2, 3, 5, 7, 14 and 30 days for the first month of the test and hereafter in 30-day-lapses (60, 90, 120 days…).
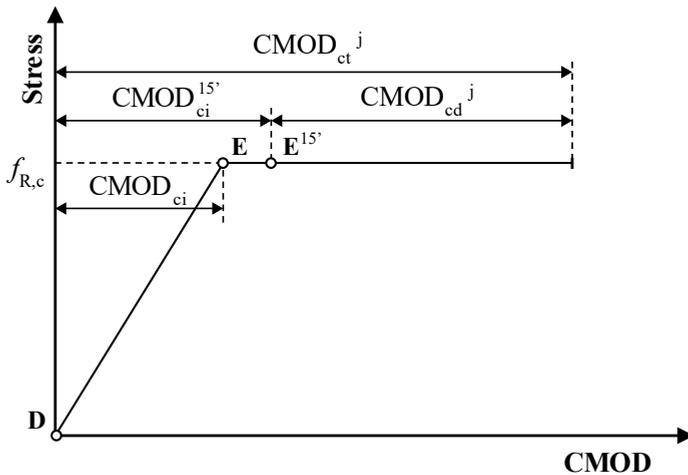
Figure 138. Creep phase parameters.

As well as recommended for the environmental conditions, the recommended recording rate for the long-term phase is one reading each 1800 seconds (30 minutes). Thus, CMOD deformations will be related to environmental conditions along the creep test.

Shrinkage control specimen

One shrinkage control specimen of each series shall be placed in a flexure position to assess the influence of shrinkage on the CMOD deformation between measuring points. Shrinkage specimens shall be located close to the creep frame inside the climate chamber in similar environmental conditions to flexure creep tests.

Shrinkage specimens shall be pre-cracked at the same $CMOD_{pn}$ that specimens destined to creep test but unloaded except their own dead load. The same boundary conditions used in specimens located in the creep frame shall be used for the shrinkage specimen. This implies supporting rollers that can spin in their longitudinal axis to avoid horizontal restrictions that may influence the free development of shrinkage deformations. The same measurement device used for creep frame specimens shall be

mounted on shrinkage specimen, and CMOD variations recorded at the same reporting ages as loaded specimens.

Shrinkage CMOD deformations ($CMOD_{cs}{}^j$) shall be considered in the total CMOD deformation following Equation 14. Thus, in the case of crack opening reduction due to shrinkage, the total CMOD deformation considering shrinkage ($CMOD_{cts}{}^j$) should increase, as depicted in Figure 139. Total deformations ($CMOD_{cts}{}^j$) corrected by shrinkage shall be reported in the creep test report.

$$CMOD_{cts}^j \; = \; CMOD_{ct}^j \; - \; CMOD_{cs}^j \hspace{3cm} \textbf{Equation 14}$$
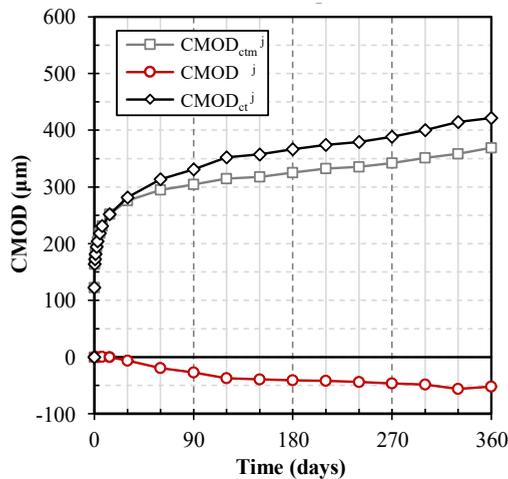
Figure 139. Evolution in time of shrinkage CMOD deformation ($CMOD_{cs}{}^j$), total CMOD deformation ($CMOD_{ct}{}^j$) and corrected total deformation ($CMOD_{cts}{}^j$).

Unloading procedure

When the target creep test duration is achieved, and the long-term phase ends, specimens shall be unloaded but not removed from creep frames. Specimens shall remain unloaded in the creep frame for 30 additional days to measure delayed recovery capacity after the creep test.

Note again that during the unloading recovery process, the stress induced by the residual dead load onto the bottom specimen shall never exceed 15% of the target $f_{R,c}$ sustained stress during the creep test. Otherwise, only a multi-specimen setup with two specimens is recommended.

Before starting the unloading process, the data acquisition system (DAS) shall be switched again to a 1 Hz (one reading per second) recording rate to obtain accurate enough CMOD data from the unloading procedure. The specimen unloading shall be

gradually done in at least 30 seconds to avoid any unexpected collapse due to balance loss. The lever arm shall be gradually lifted, the nuts of the screwed bars untightened, and the counterweights removed from the lever. When the load is completely removed, instantaneous recovery ($CMOD_{cri}$) shall be registered, and hereafter, delayed ($CMOD_{crd}$) CMOD recovery deformation for 30 days shall be registered, as defined in Figure 140. The residual delayed recovery $CMOD_{crd}$ deformation shall be reported at 1, 7, 14 and 30 days.
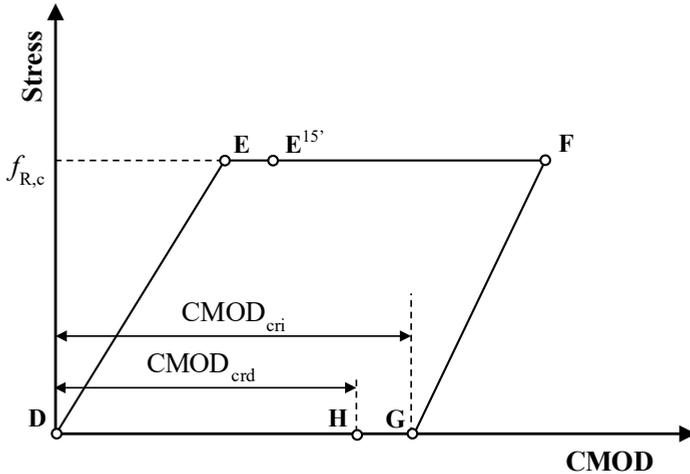
Figure 140. Creep phase loading process parameters.

After the 30-day delayed recovery period, the stacked specimens shall be removed from the creep frame and stored supported on their side turned 90º before the last post-creep flexure test.

6.1.3. Post-creep phase procedure

The recommended flexure load configuration for the post-creep flexure test is 3PBT, as proposed in the pre-cracking test. Since specimens are already pre-cracked, the post-creep flexure test shall be carried out at 0.2 mm/min constant CMOD rate up to 4 mm CMOD, and no recovery capacity is registered when the test finishes. After the flexure post-creep test, specimens shall be split into two halves to confirm the homogeneous fibre distribution in the cross-section. Fibres crossing the cracked section can be counted to correlate the residual long-term performance to the number of fibres.

To assess the residual performance of specimens after the creep test, the experimental curves of the creep test procedure stages (pre-cracking, creep and post-creep stage) shall be assembled, and post-creep residual parameters obtained, as defined in Figure 141. Notwithstanding, if the crack opening deformation corresponding to $CMOD_2$, $CMOD_3$ or $CMOD_4$ is achieved (as occurs in Point I in Figure 141) during the

creep test or the ascendant reloading process, the corresponding residual strength shall not be considered in the creep test report.
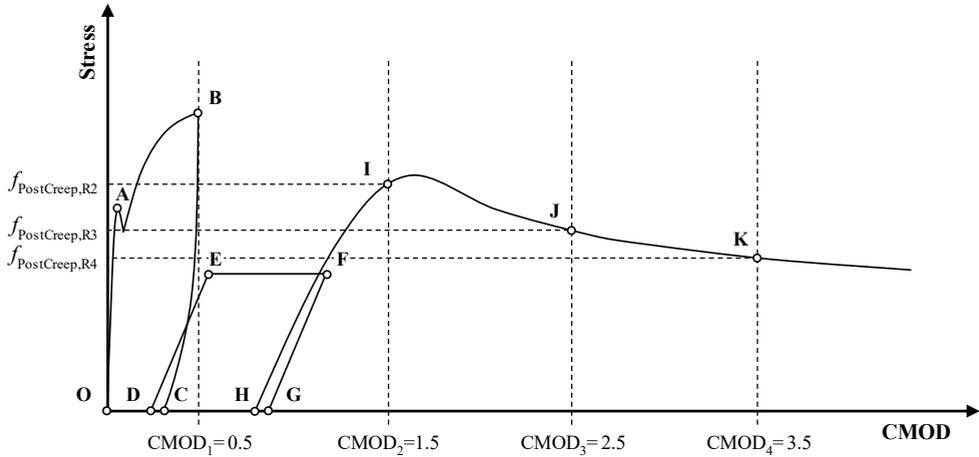
Figure 141. Post-creep phase parameters.

6.2. Creep test report

Once the creep test procedure is finished, all processed data shall be provided for each specimen in the creep test report. All the testing details that deviate from this recommendation shall also be reported. The test report shall include at least the following information:

- Reference name of the test specimen and FRC mix
- Test date
- Concrete mix properties:
  - cement type
  - w/c ratio
  - sand and aggregates (size…)
  - air content
  - admixtures used
- Fibres brand, geometrical and mechanical properties:
  - material
  - length
  - diameter
  - aspect ratio
  - tensile strength
  - Young's modulus

- Environmental conditions:
  - climate conditions control: *Controlled*, *Restricted* or *Uncontrolled*
  - mean, minimum and maximum temperature value in ºC
  - mean, minimum and maximum relative humidity value in %
  - figure with temperature and relative humidity evolution in time during the creep test duration (2 readings/day)
- Specimen properties:
  - specimen dimensions b, h, h_{sp} and l in mm
  - notch dimensions (height and width in mm)
  - specimen age at notching (in days)
  - specimen age at pre-cracking test (in days)
  - specimen age at the beginning of creep test (in days)
- Pre-cracking phase data:
  - pre-cracking test load configuration: 3PBT or 4PBT
  - dimensions related to the load configuration (support span l, l_a and l_b)
  - residual flexural tensile strength at LOP (f_L)
  - load at LOP (F_L)
  - residual flexural tensile strength at $CMOD_p$ ($f_{R,p}$)
  - load at $CMOD_p$ ($F_{R,p}$)
  - reference displacement registered during the test: CMOD or deflection (δ)
  - target nominal CMOD in the pre-cracking stage ($CMOD_{pn}$)
  - maximum CMOD reached in the pre-cracking stage ($CMOD_p$)
  - instantaneous CMOD recovery after unloading in the pre-cracking stage ($CMOD_{pri}$)
  - residual CMOD 10 minutes after the pre-cracking test unloading ($CMOD_{prd}$)
  - number of cracks that starts from the tip of the notch
- Creep phase data and parameters:
  - creep test load configuration: 3PBT or 4PBT
  - dimensions related to the load configuration (support span l, l_a and l_b)
  - number of specimens per creep frame
  - relative position of the specimen in the creep frame
  - duration of creep tests (in days)
  - nominal creep index (I_n)
  - stress applied during the creep stage ($f_{R,c}$)
  - load applied during the creep stage ($F_{R,c}$)
  - real creep index applied (I_c)
  - creep test loading process duration (t_{ci})
  - instantaneous CMOD immediately after reaching the reference load ($CMOD_{ci}$)
  - short-term CMOD deformation at 15 minutes from the beginning of the loading process ($CMOD_{ci}^{15'}$)

- total $CMOD_{cts}^{j}$ in µm at the previously defined reporting ages j compensated by shrinkage
- time duration of creep test unloading process (t_{cri})
- instantaneous CMOD recovery after unloading the creep test ($CMOD_{cris}$)
- residual $CMOD_{crds}^{j}$ recovery after unloading the creep test at the previously defined reporting ages j
- time duration of delayed recovery assessment after the creep test unloading process (t_{crd})
- CMOD-Time plot during the creep stage.

- Post-creep phase data:
  - post-creep residual flexural tensile strength ($f_{PostCreep,R,2}$) at $CMOD_2$
  - post-creep residual flexural tensile strength ($f_{PostCreep,R,3}$) at $CMOD_3$
  - post-creep residual flexural tensile strength ($f_{PostCreep,R,4}$) at $CMOD_4$
  - Stress-CMOD figure whith residual performance during the three stages of the creep test procedure.
- Creep coefficients at proposed reporting ages.
- Additional information: all incidents or unexpected events that occurred during the test duration shall be included in this section to provide valuable information about the long-term test procedure.

All information given in the creep test report can also be spread through the scientific community through the Creep Test Database proposed in Section 5.4.3. Thus, a global comparison among FRC series could be done.

Chapter 7.
Conclusions and Future Research

7.1. Conclusions

According to the flexure creep test methodology in the cracked state proposed in Chapter 6, it can be stated that the main objective of this PhD thesis, which was to develop improvement towards a new creep experimental proposal susceptible to become an international standard that enables the characterisation of long-term behaviour in the cracked state required for FRC classification and the design of FRC structures, has been successfully fulfilled. In addition, it was intended to consider for this methodology and parameters proposal the available methodologies in the state-of-the-art also fulfilled by a deep analysis of variations and influence of existent procedures.

Although many conclusions were drawn throughout the document, this chapter summarises the most significant findings to facilitate the reader to get an overall view of this PhD document. Hence, conclusions have been arranged into four sections: the large number of available FRC creep methodologies, significant improvements in flexure creep test procedure, contributions to flexure long-term behaviour assessment and proposed flexure methodology. While the first section describes the main conclusions reached from the deep analysis of the current state-of-the-art of creep in the cracked state, the rest of the sections show the most relevant findings of the conducted experimental work.

7.1.1. The large number of available FRC creep methodologies

Significant effort was made during the PhD duration to search and collect all available publications related to FRC creep in the cracked state. Consequently, the following conclusions can be noted from the state-of-the-art analysis:

- From the bibliometric study of creep in cracked state publications, it was concluded that the flexure creep test procedure in prismatic specimens is, so far, the most extended procedure to characterise the long-term behaviour of FRC

material: 58% of specimens were tested in flexure. Tensile and round panel creep tests are the second and third methodologies, with 13 and 12%, respectively. Creep tests on structural elements made with FRC represent 10% of the specimens tested in creep, whereas square panels only represent 6% of the specimens.

- It was confirmed that many variables such as FRC matrix composition, casting procedure, the shape of specimens, fibre materials, test setup and methodology were detected among publications on creep in the cracked state.

- Unfortunately, overall conclusions about FRC long-term behaviour cannot be obtained due to such procedure and conditions variations. It is then concluded that it is urgently required to develop an agreed procedure that could provide comparable results towards a knowledge enough that could allow the inclusion of creep of FRC in the design standards.

7.1.2. Significant improvements in flexure creep test procedure

Considering the variability in terms of glossary found among the available methodologies and publications, a new glossary classification has been proposed to facilitate experimental results comparison and data exchange among laboratories. These conclusions arise from the glossary assessment and corresponding proposal:

- Most of the flexure creep tests are based on EN 14651 standard; therefore, it is proposed the use of CMOD instead of *w* to refer to crack opening deformations.

- A classification of subscripts and superscripts is proposed to identify the phase of the creep test, type measurement and the time lapse in which deformation was registered. This glossary proposal for creep in cracked state methodologies provides accuracy enough to identify any variable in terms of creep test stage and type of deformation

- Moreover, the proposed glossary can be adapted from flexure creep tests, usually referred to CMOD, to both tensile and panel creep tests, referred to COD and δ, respectively. In addition, a glossary for compressive strains is also proposed if compressive strain assessment is later included in the standardised procedure.

Considering the variation in pre-cracking level ($CMOD_p$) observed in the literature, defining a reference value for flexure creep methodology was required to obtain comparable results between laboratories. From the experimental work carried out, the following statements were concluded:

- It was concluded that pre-cracking level $CMOD_p$ has a low influence on both delayed deformations and creep coefficient obtained in the creep test

- In the flexure tests conducted in prismatic specimens, a CMOD of 0.5 mm, considering a variable crack opening along the cross-section height, is equivalent to 0.2 mm average crack width accepted in most structural codes.

Moreover, the proposed 0.5 mm for $CMOD_p$ corresponds to $CMOD_1$, which is the reference crack opening for the residual stress $f_{R,1}$ and allows assessment of the long-term behaviour based on the basic residual strength referred to SLS in the Model Code 2010 [19].

- The proposed reference nominal pre-cracking value $CMOD_{pn}$ is 0.5 mm, corresponding to $f_{R,1}$ residual stress. To ensure proper pre-cracking conditions, the pre-cracking deformation before unloading ($CMOD_p$) shall reach $CMOD_{pn}$ and should not exceed $CMOD_{pn}$ + 0.02 mm.

From the experimental programme carried out to assess the creep index (I_c) parameter influence on the long-term behaviour of FRC, it was concluded that:

- creep index significantly influences the CMOD long-term behaviour from 0.2 mm pre-cacking level $CMOD_p$ in advance. Moreover, the creep index significance increases with the pre-cracking level.

- low creep index values ($\leq$ 25%) do not influence the delayed deformation enough to provide comparable results blurring any long-term assessment.

- it is proposed to use 50% of the stress $f_{R,p}$ individually obtained by each specimen at $CMOD_p$ as creep index (I_c) nominal reference value for characterisation purposes. Due to the creep index significance on the experimental result, the creep index shall not exceed the ± 5% acceptance range. Otherwise, specimens shall be reported as out-of-range. All specimens tested out of the creep index accepted range shall be identified in the test report as tested out of limits

- the use of the individual stress $f_{R,p}$ of each specimen at $CMOD_p$ instead of the average stress of the batch as the reference stress value to apply the creep index parameter was proposed to reduce creep index scatter and homogenise testing conditions.

To date, the recovery capacity of cracked FRC specimens registered on creep procedures was limited to instantaneous recovery. However, an experimental program to assess delayed recovery capacity during the multi-phase creep test was carried out, and the following conclusions were obtained:

- Delayed recovery capacity 10 minutes after the pre-cracking test unloading process represents 12-22% of the instantaneous recovery when the specimen is unloaded. Considering the creep phase, a delayed to instantaneous recovery capacity ratio of 16.4, 42.5 and 113% was obtained 30 days after the creep test unloading process for SFRC, GFRC and SyFRC, respectively.

- It was observed that the studied FRC mixes behave similarly in loading and unloading elastic deformations regardless of the fibre material. However, fibre material leads the FRC behaviour in plastic deformations providing different responses. Although in terms of mechanical performance, the residual strength increased more than 2.5 times when glass fibre dosage was doubled, in terms of

deformation, any delayed CMOD reduction was observed when fibre dosage increased.

- A new unloading procedure was proposed for both pre-cracking and creep tests. Delayed recovery deformations shall be registered for at least 10 minutes after the pre-cracking unloading process. In contrast, delayed recovery deformations shall be recorded for at least 30 days for the creep phase. When the long-term sustained load is applied, delayed CMOD recovery capacity shall be registered for longer.

As it is well known, support boundary conditions are highly correlated to residual performance on flexure tests, which may influence the long-term performance of FRC specimens. Therefore, deep research and assessment of boundary conditions reported in the scientific literature were carried out, providing the following conclusions:

- A classification of supporting rollers is proposed in terms of degrees of freedom of rotation of both longitudinal and transversal roller axis and transversal axis translation. Existent boundary conditions reported in publications were classified and analysed. Five boundary conditions were identified: XXX, XOX, OXX, OOX and OXO. It was noticed that most authors did not give relevance enough to boundary conditions and used simple steel rollers between stacked specimens.

- It was concluded that using steel transfer plates with well-constructed supports between specimens in multi-specimen creep setup is mandatory to ensure proper boundary conditions. In addition, transfer plates shall include emergency brakes device such as steel blocks to stop any broken specimen before the collapse.

- Specific boundary conditions were proposed for both 3PBT and 4PBT flexure creep setups combining supports classified OOX and XOX.

- Since both 3PBT and 4PBT can be used in either pre-cracking or creep phases, it was proposed the use of *creep index* (I_c) term defined as the sustained stress ratio to the residual stress $f_{R,p}$ at $CMOD_p$ instead of *load level* to avoid any misunderstanding between residual load obtained load in pre-racking test (3PBT) and the sustained load in creep phase (4PBT).

The loading procedure of existing methodologies was analysed, and a wide scatter was observed in terms of loading process duration ranging from 2 seconds to 75 minutes. Hence, an experimental programme was defined to assess the influence of loading process duration on the instantaneous deformation concluding that:

- Instantaneous deformation of SyFRC specimens increased with loading process duration up to 35% when the loading process lasted 60 minutes, whereas, for SFRC specimens, the instantaneous deformation increased by 8%. This fact reveals that the loading process duration has a relevant influence on the instantaneous deformation of SyFRC mixes and a minor effect in the case of SFRC mixes.

- A new t_{ci} parameter was proposed to reduce scatter in terms of loading process duration among laboratories. By defining this parameter, it is expected to reduce scatter in terms of instantaneous deformations, which do not have a despicable impact on creep coefficients.

- It is proposed that the loading process shall not exceed 5 minutes to keep the CMOD increase caused by the t_{ci} below 15%. Moreover, it is recommended that the load shall not be suddenly applied to avoid a hit or impact effect of the load.

- Therefore, it was proposed that sustained load shall be gradually applied in the creep frame where the loading process duration shall be at least 30 seconds but no more than 5 minutes (30 s < t_{ci} < 5 min).

Considering that most relevant deformation occurs during the early creep stage and the impact of loading process duration on $CMOD_{ci}$, the influence of both short-term deformations at the early creep stage loading process on creep coefficient was assessed, and the following conclusions were obtained:

- in the case of the SyFRC mix, a creep coefficient reduction of 20 and 32%, was observed at 10 and 30 minutes, respectively, after the loading process ended. On the other hand, the SFRC mix was reduced by 8 and 13%, respectively. A significant creep coefficient reduction was observed when $CMOD_{ci}^{30'}$ was used. However, the reduction observed for 10 minutes may be acceptable in favour of the homogenisation of the results.

- a new parameter named short-term deformation at 15 minutes from the beginning of the loading process ($CMOD_{ci}^{15'}$) was proposed to reduce variability among laboratories and homogenise creep coefficients. This parameter includes the loading process duration t_{ci} (5 min) plus 10 additional minutes.

The use of a multi-specimen setup is widely extended to increase the number of specimens tested in creep simultaneously. However, the multi-specimen creep setup implies some relevant matters to consider for the success of the creep test. The following conclusions were obtained from the multi-specimen creep setup assessment:

- Considering the typical scattered residual performance of FRC, in the case of two or three multi-specimen setups, it is proposed to cast and pre-crack more specimens than strictly required for the long-term tests to ensure residual performance variety enough for a proper specimen selection.

- The specimen selection procedure significantly impacts creep index accuracy when a multi-specimen setup is adopted. Therefore, a multi-specimen procedure flowchart is proposed to accomplish the proposed creep index acceptance threshold. The relative position (top, middle or bottom) of each specimen in the column shall be decided according to their mechanical performance.

- Procedures for loading and unloading stacked specimens were defined. The stacking of the specimens shall be done in a step-by-step procedure and shall

not last more than 30 minutes. The specimen stacking process duration shall not be considered for the t_{ci} parameter calculation.

- During both the stacking procedure and the later unloading recovery process, the stress induced by the residual dead load of upper specimens onto the bottom specimen shall never exceed 15% of the target $f_{R,c}$ sustained stress during the creep test. Otherwise, only a multi-specimen setup with two specimens is recommended

- It was concluded that the proposed procedure guidelines and flowchart make it possible to achieve great accuracy in terms of creep index when a multi-specimen setup is adopted.

7.1.3. Contributions to flexure long-term behaviour assessment

Although the use of unloaded specimens to assess shrinkage deformation in time is extended in creep in compression standards, the effect of shrinkage on flexure creep in cracked state tests has been neglected to date. However, a flexure creep experimental programme was defined to assess the shrinkage effect on experimental results, and the following conclusions were obtained:

- It has been confirmed that during the creep test, the crack closes due to the drying shrinkage effect. It is then concluded that this effect was, to date, hindered by delayed CMOD and neglected in the creep test results since no shrinkage assessment was previously reported.

- Formulation to consider shrinkage effect on creep test experimental results were given. The creep test results shall include delayed CMOD deformations due to sustained load plus the CMOD reduction due to the shrinkage effect.

- For the first time, the shrinkage flexure specimen of each series is proposed to be a part of the creep methodology to assess the influence of shrinkage on the delayed CMOD deformations. The shrinkage flexure specimen shall be tested in the same bending setup, pre-crack level and boundary conditions.

Although the flexure test results from a combination of both tensile and compressive forces, only tensile behaviour is usually assessed in terms of delayed crack opening. This fact may lead to neglecting the influence of compressive forces behaviour on the flexure creep experimental results. The significance of compressive creep in the creep test was then assessed, and the following conclusions arose:

- It was concluded that pre-crack level $CMOD_p$ had a negligible impact on delayed compressive strain deformations compared to CMOD. However, creep index impact was confirmed for both CMOD and compressive strains delayed deformations.

- Compressive strain creep provided different significance on crack opening deformations depending on the fibre material. Whereas for SyFRC mixes, compressive strain creep coefficients are comparable to those obtained by crack

opening deformations, in the case of SFRC mixes, compressive creep coefficients are around four times larger than crack opening ones.

- it was concluded that a stress redistribution occurs during the creep test since stabilisation was not observed by delayed compressive strains as occurs with crack opening deformations.

Therefore, a new experimental programme was designed to assess the neutral axis (NA) location during the creep tests and confirm the stress redistribution previously observed, and the following findings were obtained:

- Two NA approach models based on crack opening and compressive strain deformation were defined to assess the NA position in monotonic and long-term flexure tests. The goodness of both models was compared to validate their accuracy on NA position obtention.

- NAE models were firstly assessed in monotonic flexure tests, where it was concluded that NA reaches 135 and 132 mm at 0.5 mm CMOD for the SyFRC and SFRC studied mixes, respectively.

- After the model validation in monotonic tests, both models were applied to flexure creep experimental results, and it was confirmed that NA kept not constant but decreased over time. It was then concluded that stress redistribution occurs in the cross-section despite the constant bending moment applied during the creep test.

- Although the NA decrease implies an increase in time of the height of the compressive block, it was observed that compressive strains did not decrease but continued increasing without stabilisation, contrarily to the expected relaxation.

Due to the number of laboratories and methodologies involved in this topic, it was required to create an agreed datasheet to share comparable data among laboratories. The first open-access database on creep in the cracked state was created considering most of the proposed improvements and giving the following conclusions:

- Database became a useful tool to assess long-term behaviour, comparing multiple experimental tests carried out in similar conditions.

- Fully described guidelines for data arrangement, units and variable description for the database creation are given. Although both microns (µm) and mm are usually reported in the literature, the use of µm units is proposed for CMOD deformations since delayed deformations are generally quite small.

- Most data included in the database shall also be reported in the creep test report. Therefore, it is easy to adapt experimental data from the test report to be shared in the database.

7.1.4. Proposed flexure methodology

As a result of this PhD, an improved flexure creep test in cracked state methodology proposal was defined. As a summary of the proposed methodology, the following improvements to previous methodologies and new recommendations can be highlighted:

- Creep glossary was unified, extended and improved towards better data exchange and avoid misunderstandings among laboratories.

- Boundary conditions for both supporting and loading rollers were defined for the creep phase in either 3PBT or 4PBT flexure setups.

- Guidelines and restrictions for transducer mounting were given. Aspects such as distance between measuring points or maximum separation between specimen and line of measurements were defined.

- It was defined as a flexure creep methodology requirement that environmental conditions were controlled during the creep test duration. Temperature and relative humidity acceptance range were determined.

- The acclimatisation time for pre-cracked specimens was increased to 7 days before creep testing.

- Reference values for pre-cracking level ($CMOD_p$) and creep index (I_c) parameters were defined in the proposed flexure creep test methodology for characterisation purposes in SLS.

- Both loading and unloading procedures were defined and restricted with the loading process duration (t_{ci}) parameter

- Guidelines and recommendations for the creep frame construction were given. The use of creep frames based on either top or bottom second-degree lever arm was recommended

- Recommended creep setups and accepted variations were provided for single- and multi-specimen configurations. Furthermore, not recommended creep setups (i.e. inverted specimens) were also justified.

- Stacking procedure and dead load restrictions for multi-specimen setup were defined to ensure that the creep index is not exceeded.

- The new parameter short-term deformation ($CMOD_{ci}^{15'}$) was defined 15 minutes after the loading process started.

- Delayed recovery deformations have been included in the pre-cracking and creep phases procedure after the unloading process.

- Guidelines related to creep test duration (360 days) and recommended reporting ages and recording rates were given.

- The shrinkage assessment has been stated as a creep methodology requirement for each FRC mix. Formulation and guidelines to consider flexure shrinkage deformation in experimental creep test results are given

- The creep test report was improved and updated to new parameters and creep methodology requirements.

This methodology was defined for characterisation purposes in the service limit state (SLS) of the long-term behaviour of FRC prismatic specimens. If any specimen exceeds the specified ranges, it shall be considered as tested out-of-range and not considered for the mix characterisation. However, the proposed parameter ranges can be exceeded for research purposes.

This procedure applies to standard FRC specimens that reveal a single crack when tested in flexure. However, if a single crack occurs out of the tip of the notch or out of the measuring range, the specimens shall be considered out of the procedure scope. Multiple cracking concrete matrices (i.e., ECC, UHPFRC…) are also considered if all cracks start from the tip of the notch.

7.2. Future research

The proposed flexure creep methodology provides an improved experimental framework for the long-term behaviour characterisation of cracked FRC. However, some aspects are still uncertain, and further investigation is required in the near future. Therefore, some future works are proposed and described below:

- Since most of the creep tests reported in literature last between 90 to 270 days, a minimum creep test duration of one year (360 days) is proposed to cover the four seasons' complete range. However, creep tests with longer-term (>5 years) are required to assess that results obtained in one-year creep tests can accurately predict long-term behaviour.

- Due to the long-time consumption of the flexure creep methodology, most of the presented improvements and findings could only be assessed in SyFRC and SFRC mixes. Unfortunately, other fibre-reinforced mixes, such as GFRC, could not be considered, and studies of both compressive creep and neutral axis assessment on GFRC mixes are required.

- Regarding the shrinkage assessment in flexure, only experimental tests on specimens with a linear transducer mounted at the bottom face of the specimen were carried out. LVDTs require a larger distance between measuring points (50-100mm) than COD clip transducers (3-5 mm), and most of the measuring range is the uncracked concrete section where drying shrinkage undergoes. Therefore, studies on flexure shrinkage tests with clip transducers are required to assess if reducing the distance between measuring points to notch width reduces the shrinkage effect on delayed CMOD deformations.

- Although a stress redistribution in the cross-section during creep tests was confirmed, there is still some uncertainty about compressive creep in flexure tests. Although the height of the compression block increased in time due to the NA decrease, any relaxation on the compressive strain creep was observed.

Therefore, further sectional analysis on the cross-section during the creep test is required to sort and quantify separately both compressive and tensile creep simultaneously combined in flexure.

- The presented experimental programme considered the NA position assessment in FRC matrices with similar residual performance. However, the NA position shall be assessed for FRC matrices with strain-hardening and -softening behaviour to confirm if NA long-term variation depends on the residual performance more for softening than hardening FRCs. In addition, the NA model shall be applied in further specimens tested in flexure creep to assess the impact of parameters such as creep index and pre-cracking level on the NA delayed behaviour.

- Although the first open-access international creep in cracked state database was created, additional effort is required to coordinate and manage the future success of the database. Moreover, the support and help of the scientific researchers interested in this topic are needed to share their experimental results and enlarge the database as much as possible to make it useful to obtain overall conclusions of the long-term behaviour of FRC material.

Bibliography

1. Di Prisco, M.; Plizzari, G.; Vandewalle, L. Fibre reinforced concrete: New design perspectives. Mater. Struct. 2009, 42, 1261–1281. DOI: 10.1617/s11527-009-9529-4

2. Brandt, A.M. Fibre reinforced cement-based (FRC) composites after over 40 years of development in building and civil engineering. Compos. Struct. 2008, 86, 3–9.

3. Roesler, J.R.; Altoubat, S.A.; Lange, D.A.; Rieder, K.A.; Ulreich, G.R. Effect of synthetic fibers on structural behavior of concrete slabs-on-ground. ACI Mater. J. 2006, 103, 3–10. DOI: 10.14359/15121

4. Alani, A.M.; Beckett, D. Mechanical properties of a large scale synthetic fibre reinforced concrete ground slab. Constr. Build. Mater. 2013, 41, 335–344. DOI: 10.1016/j.conbuildmat.2012.11.043

5. Destrée, X.; Mandl, J. Steel fibre only reinforced concrete in free suspended elevated slabs: Case studies, design assisted by testing route, comparison to the latest SFRC standard documents. In: Proceedings of the International FIB Symposium 2008 - Tailor Made Concrete Structures: New Solutions for our Society. The Netherlands, Amsterdam, 2008, 437–443. ISBN 978-0-415-47535-8

6. De La Fuente, A.; Casanovas-Rubio, M.D.M.; Pons, O.; Armengou, J. Sustainability of Column-Supported RC Slabs: Fiber Reinforcement as an Alternative. J. Constr. Eng. Manag. 2019, 145, 04019042. DOI: 10.1061/(ASCE)CO.1943-7862.0001667

7. Parmentier, B.; Van Itterbeeck, P.; Skowron, A. The Behaviour of SFRC Flat Slabs: The Limelette Full-Scale Experiments to Support Design Model Codes. ACI Special Publication, American Concrete Institute: Farmington Hills, MI, USA, 2014.

8. Plizzari, G.A.; Tiberti, G. Steel fibers as reinforcement for precast tunnel segments. Tunn. Undergr. Space Technol. 2006, 21, 438–439. DOI: 10.1016/j.tust.2005.12.079

9. Caratelli, A.; Meda, A.; Rinaldi, Z.; Romualdi, P. Structural behaviour of precast tunnel segments in fiber reinforced concrete. Tunn. Undergr. Space Technol. 2011, 26, 284–291. DOI: 10.1016/j.tust.2010.10.003

10. De la Fuente, A.; Pujadas, P.; Blanco, A.; Aguado, A. Experiences in Barcelona with the use of fibres in segmental linings. Tunn. Undergr. Space Technol. 2012, 27, 60–71. DOI: 10.1016/j.tust.2011.07.001

11. De La Fuente, A.; Escariz, R.C.; De Figueiredo, A.D.; Molins, C.; Aguado, A. A new design method for steel fibre reinforced concrete pipes. Constr. Build. Mater. 2012, 30, 547–555. DOI: 10.1016/j.conbuildmat.2011.12.015

12. Domingo Cabo, A.; Lázaro, C; Serna Ros, P. Construcción de la JCHYPAR, una lámina delgada de hormigón reforzado con fibras de acero, en el oceanográfico de Valencia. Hormigón y acero. 2003, 54(228-229), 177-186.

13. Banthia, N.; Gupta, R. Influence of polypropylene fiber geometry on plastic shrinkage cracking in concrete. Cem. Concr. Res. 2006, 36, 1263–1267. DOI: 10.1016/j.cemconres.2006.01.010

14. Vasanelli, E.; Micelli, F.; Aiello, M.A.; Plizzari, G.; Molfetta M. Creep and Durability Aspects of Ordinary Reinforced FRC Beams. 2nd Workshop 'The New Boundaries of Structural Concrete'. Università Politecnica delle Marche, Ancona, 2011, 143-149.

15. Löfgren, I. Fibre-reinforced Concrete for Industrial Construction – a fracture mechanics approach to material testing and structural analysis. PhD thesis, 2005.

16. Conforti, A.; Zerbino, R.; Plizzari, G.A. Influence of steel, glass and polymer fibers on the cracking behavior of reinforced concrete beams under flexure. Struc. Conc. 2019, 20, 133–143. DOI: 10.1002/suco.201800079

17. Visser, D.; Boshoff, W.P. Shear behaviour of concrete V-shaped beams with and without steel fibres. Mater. Struct. 2021, 54, 28. DOI: 10.1617/s11527-020-01589-3

18. Foster, S.J.; Htut, T.; NG, T.S. High performance fibre reinforced concrete: fundamental behaviour and modelling. In: Proceedings of the 8th International Conference on Fracture Mechanics of Concrete and Concrete Structures FraMCoS-8, Toledo, Spain: IA-FRAMCOS, 2013, pp. 69-78.

19. fib Model Code for Concrete Structures 2010. (2013), Ernst & Sohn, Wiley. Berlin, Germany, 2013, 74-150. DOI: 10.1002/9783433604090

20. ACI Committee 544. Report on Fiber Reinforced Concrete; ACI: Farmington Hills, MI, USA, 2002.

21. Código Estructural. Real Decreto 470/2021 de 29 de junio. BOE-A-2021-13681. Permalink ELI: https://www.boe.es/eli/es/rd/2021/06/29/470

22. Eurocode 2: Design of Concrete Structures—Part 1-1: General Rules and Rules for Buildings; EN 1992-1-1; CEN: Brussels, Belgium, 2004. ISBN 978 0 580 62664 7.

23. RILEM TC 162-TDF. Recommendations of RILEM TC 162-TDF: Test and design methods for steel fibre reinforced concrete: bending test. Mat. Struct. 2000, 33, 3–5. DOI: 10.1007/BF02481689

24. di Prisco, M.; Ferrara, L.; Lamperti, M.G.L. Double edge wedge splitting (DEWS): an indirect tension test to identify post-cracking behaviour of fibre reinforced cementitious composites. Mater. Struct. 2013, 46, 1893-1918.

25. ASTM International C1609/C1609M-19a Standard Test Method for Flexural Performance of Fiber-Reinforced Concrete (Using Beam With Third-Point Loading). West Conshohocken, PA; ASTM International, 2019. DOI: 10.1520/C1609_C1609M-19A

26. EN 14651:2005+A1:2007. Test Method for Metallic Fibre Concrete - Measuring the Flexural tensile Strength (Limit of Proportionality (LOP), Residual), CEN - European Committee for Standardization, Brussels (2005).

27. Neville, A.M.; Dilger, W.H.; Brooks, J.J. Creep of plain and structural concrete. Construction Press, London and New York, 1983.

28. ASTM C512 / C512M-15, Standard Test Method for Creep of Concrete in Compression, ASTM International, West Conshohocken, PA, 2015, DOI: 10.1520/C0512_C0512M-15

29. EN 12390-17:2019, Testing hardened concrete - Part 17: Determination of creep of concrete in compression, CEN - European Committee for Standardization, Brussels (2019).

30. Llano-Torre, A.; Serna, P. Fibre Reinforced Concrete Characterization. In: Llano-Torre, A., Serna, P. (eds) Round-Robin Test on Creep Behaviour in Cracked Sections of FRC: Experimental Program, Results and Database Analysis. RILEM State-of-the-Art Reports, vol 34. Springer, 2021. DOI: 10.1007/978-3-030-72736-9_3

31. Nakov, D.; Markovski, G.; Arangjelovski, T.; Mark, P. Experimental and Analytical Analysis of Creep of Steel Fibre Reinforced Concrete, Periodica Polytechnica Civil Engineering. 2018, 62(1), 226–231. DOI: 10.3311/PPci.11184

32. Bernard, E.S. Age-dependent Changes in Post-crack Performance of Fibre Reinforced Shotcrete Linings. Tunn. Undergr. Space Technol. 2015, 49, 241-248.

33. Teixeira Buttignol, T.E.; Colombo, M.; di Prisco, M. Long-term aging effects on tensile characterization of steel fibre reinforced concrete. Struct. Concr. 2016, 17, 1082–1093. DOI: 10.1002/suco.201500149

34. Bernard, E.S. Changes in long-term performance of fibre reinforced shotcrete due to corrosion and embrittlement. Tunn. Undergr. Space Technol. 2020, 98, 103335. DOI: 10.1016/j.tust.2020.103335

35. Bernard, E.S. Long-term post-crack performance of high-strength fiber-reinforced concrete for structural applications. Struct. Concr. 2022, 1–18. DOI: 10.1002/suco.202100740

36. Plizzari, G.; Serna, P. Structural effects of FRC creep. Mater. Struct. 2018, 51(6), 167. DOI: 10.1617/s11527-018-1290-0s

37. Tošić, N.; Aidarov, S.; de la Fuente, A. Systematic Review on the Creep of Fiber-Reinforced Concrete. Materials. 2020, 13(22), 5098. DOI: 10.3390/ma13225098

38. Kusterle, W. Viscous Material Behaviour of Solids- Creep of Polymer Fibre Reinforced Concrete. In: Proceedings of the 5th Central European Congress on Concrete Engineering. Baden, 2009, 95-100.

39. Arango, S.; Serna, P.; Martí-Vargas, J.R.; García-Taengua, E. A Test Method to Characterize Flexural Creep Behaviour of Pre-cracked FRC Specimens. Exp. Mech. 2012, 52, 1067-1078. DOI: 10.1007/s11340-011-9556-2

40. EFNARC, Testing Sprayed Concrete – Creep Test on Square Panel, June 2012.

41. ASQUAPRO Technical Committee, "Programme expérimental sur l'apport des fibres à court et moyen termes pour le renforcement des bétons projetés par voie mouillée", ASQUAPRO - Association pour la Qualité de la Projection des Bétons, 2013.

42. Bernard, E.S. Creep of cracked fibre reinforced shotcrete panels', in 'Shotcrete: More Engineering Developments. In: Proceedings of the Second International Conference on Engineering in Shotcrete, Taylor & Francis Group. Cairns, Australia, 2004, 47-57.

43. Llano-Torre, A.; Serna, P. Recommendation of RILEM TC 261-CCF: test method to determine the flexural creep of fibre reinforced concrete in the cracked state. Mater. Struct. 2021, 54, 124. DOI: 10.1617/s11527-021-01675-0

44. Gettu R.; Zerbino R.; Jose S. Factors Influencing Creep of Cracked Fibre Reinforced Concrete: What We Think We Know & What We Do Not Know. In: Serna P., Llano-Torre A., Cavalaro S. (eds) Creep Behaviour in Cracked Sections of Fibre Reinforced Concrete: Proceedings of the International RILEM Workshop

FRC-CREEP 2016. RILEM Bookseries, vol 14. Springer, Dordrecht, 2017. DOI: 10.1007/978-94-024-1001-3_1

45. Buratti N.; Mazzotti C. Creep Testing Methodologies and Results Interpretation. In: Serna P., Llano-Torre A., Cavalaro S. (eds) Creep Behaviour in Cracked Sections of Fibre Reinforced Concrete: Proceedings of the International RILEM Workshop FRC-CREEP 2016. RILEM Bookseries, vol 14. Springer, Dordrecht, 2017. DOI: 10.1007/978-94-024-1001-3_2

46. Buratti, N.; Mazzotti, C. Effects of different types and dosages of fibres on the long-term behaviour of fibre-reinforced self-compacting concrete. In: Proc. 8th RILEM Int. Symp. on Fibre Reinforced Concrete: challenges and opportunities. Guimaraes, Portugal, 2012, 715-725.

47. Boshoff, W. P.; Mechtcherine, V.; van Zijl, G. P. A. G. Characterising the time-dependant behaviour on the single fibre level of SHCC: Part 1: Mechanism of fibre pull-out creep. Cem. Concr. Res. 2009, 39, 779–786. DOI: 10.1016/j.cemconres.2009.06.007

48. Buratti, N.; Mazzotti, C. Experimental tests on the effect of temperature on the long-term behaviour of macrosynthetic Fibre Reinforced Concretes. Constr. Build. Mater. 2015, 95, 133-142. DOI: 10.1016/j.conbuildmat.2015.07.073

49. Monetti, D.H.; Llano-Torre, A.; Torrijos, M.C.; Giaccio, G.; Zerbino, R.; Martí-Vargas, J.R.; Serna, P. Long-term behavior of cracked fiber reinforced concrete under service conditions. Constr. Build. Mater. 2019, 196, 649–658. DOI: 10.1016/j.conbuildmat.2018.10.230

50. Bernard, E.S. Creep Rupture of Steel Fibre Reinforced Shotcrete Loaded in Flexure. In: Seventh International Symposium on Sprayed Concrete, Modern Use of Wet Mix Sprayed Concrete for Underground Support. Sandefjord, Norway, 2014.

51. Llano-Torre A.; Serna P. (eds) Round-Robin test on creep behaviour in cracked sections of FRC: experimental program, results and database analysis. RILEM State-of-the-Art Reports. Springer. DOI: 10.1007/978-3-030-72736-9

52. Serna, P.; Llano-Torre, A.; Cavalaro, S.H.P. (Eds). Creep behaviour in cracked sections of fibre reinforced concrete: Proceedings of the International RILEM Workshop FRC-CREEP 2016. RILEM bookseries 14, Dordrecht: Springer, 2017. DOI: 10.1007/978-94-024-1001-3

53. Abrishambaf, A.; Barros, J.A.O.; Cunha, V.M.C.F. Time-dependent flexural behaviour of cracked steel fibre reinforced self-compacting concrete panels. Cem. Concr. Res. 2015, 72, 21–36.

54. Buratti, N.; Mazzotti, C. Experimental tests on the long-term behaviour of SFRC and MSFRC in bending and direct tension. In: Proceedings of the BEFIB 2016,

9th RILEM International Symposium on Fiber Reinforced Concrete. Vancouver, Canada, 2016, 163–174.

55. Chanvillard G.; Roque O. Behaviour of fibre reinforced concrete cracked section under sustained load. In: High Performance Fiber Reinforced Cement Composites (HPFRCC 3), RILEM PRO 06. Mainz, Germany, 1999, 239 – 250.

56. Granju, J.-L.; Rossi, P.; Rivillon, P.; Chanvillard, G.; Mesureur, B.; Turatsinze, A.; Farhat, H.; Boulay, C.; Serrano, J.-J.; Fakhri, P.; Roque, O. Delayed Behaviour of cracked SFRC beams. In: Proceedings of the Fifth International RILEM Symposium (BEFIB 2000) on Fibre Reinforced Concretes (FRC), Lyon, 2000, 511-520.

57. Kurtz, S.; Balaguru, P. Post crack creep of polymeric fibre-reinforced concrete in flexure. Cem. Concr. Res. 2000, 30(2), 183–190.

58. Mackay, J.; Trottier, J. F. Post-crack behavior of steel and synthetic FRC under flexural creep. In: Shotcrete, Proceedings of the 2nd International Conference on Engineering. Cairns, Australia, 2004, 183–192.

59. Lambrechts, A. The technical performance of steel and polymer based fibre concrete. The Institute of Concrete Technology Annual Technical Symposium, Concrete for a New World, 2005.

60. Ratcliffe, R. Steel versus Synthetic fiber reinforcement un shotcrete. 10th International Conference on Shotcrete for Underground Support. Whistler, Canada, 2006, 215-227.

61. Ratcliffe, R. Fibre reinforcement steel versus macro (structural) synthetic. Concr. Eng. Int. 2007, 14–16. ISSN: 1460-5856.

62. Ratcliffe R., "Fibre Reinforcement – Steel vs. Macro (Structural) Synthetic", Concrete Beton 2007, Volume 115, 16–20.

63. BEKAERT. Creep Test: Polypropylene fibres tend to creep 10-30 times more than steel fibres. BEKAERT Technical Report, 2009.

64. Bast, T.; Eder, A.; Kusterle, W.: Kriechversuche an Kunststoffmakrofaserbetonen. Untersuchungen zum Langzeitverhalten von Faserbetonen unter Biegezugbeanspruchung – ein Zwischenbericht. 11. Vilser Baustofftag, Reutte, Zement + Beton Handels- und Werbeges. m. b. H., Vienna, 2007.

65. Kusterle, W. Creep of Fibre Reinforced Concrete – Flexural Test on Beams. In: Proceedings of Fibre Concrete. Prague, 2015.

66. Kusterle, W. Flexural creep tests on unnotched beams - 9 years of experience with synthetic macro fibers. In: Proceedings of the BEFIB 2016, 9th RILEM International Symposium on Fiber Reinforced Concrete. Vancouver, Canada, 2016, 153–162.

67. Kusterle W. Flexural Creep Tests on Beams—8 Years of Experience with Steel and Synthetic Fibres. In: Serna P., Llano-Torre A., Cavalaro S. (eds) Creep Behaviour in Cracked Sections of Fibre Reinforced Concrete: Proceedings of the International RILEM Workshop FRC-CREEP 2016. RILEM Bookseries, vol 14. Springer, Dordrecht, 2017. DOI: 10.1007/978-94-024-1001-3_3

68. Barragán, B.E.; Zerbino, R.L. Creep behaviour of cracked steel fibre reinforced concrete beams. In: Proceedings of the 7th International RILEM Symposium on Fibre Reinforced Concrete: Design and Applications (BEFIB 2008). Chennai, India, 2008, 577-586.

69. Zerbino R.; Barragán B. Long-term behavior of cracked steel fiber reinforced concrete beams under sustained loading. ACI Mater. J. 2012, 109 (2), 215-224.

70. Goosla, U.; Rieder K.-A. Time Dependent Behaviour of Fibre Reinforced Concrete - Fundamentals and Applications. In: Proceedings of the 5th Central European Congress on Concrete Engineering. Baden, 2009, 109-114.

71. Goosla, U.; Rieder, K.-A., Zeitabhängiges Verhalten von Makrokunststofffaserbeton und dessen Einfluss auf die Bemessung von Industriefußböden. Beton- und Stahlbetonbau. 2009, 104, 76-87- DOI: 10.1002/best.200900660

72. Monetti, D.H.; Giaccio, G.; Zerbino, R. Comportamiento post fisuración de vigas de hormigones reforzados con fibras sometidas a cargas de flexión. In; IV Congreso Internacional de Tecnología del Hormigón; 18 Reunión Técnica AATH. Mar del Plata, Argentina, 2010, 121-128. ISBN 978-978-21660-4-5. (in Spanish).

73. Giaccio, G.; Monetti, D.; Torrijos, M.C.; Zerbino, R. Estudio de las propiedades mecánicas y de transporte en hormigones con fibras en estado fisurado. Revista Hormigón. 2012, 51, 5-17. ISSN 0325-8947. (in Spanish)

74. Zerbino, R.; Monetti, D.H.; Giaccio, G. Efecto de eventos de carga y descarga en la respuesta de elementos fisurados de hormigón reforzado con fibras. In: V Congreso Internacional; 19 Reunión Técnica AATH. Bahía Blanca, Argentina, 2012, 295-302. ISBN 978-987-21660-6-9. (in Spanish).

75. Kanstad, T.; Žirgulis, G. Long-time creep testing of pre-cracked fibre reinforced concrete beams. In: RILEM PRO88, Proceedings of the 8th RILEM international symposium on fibre reinforced concrete: Challenges and Opportunities (BEFIB 2012). Guimarães, Portugal, 2012, 835-847.

76. Kaufmann, J.; Bader, R.; Manser, M. Untersuchungen zum Biege-Kriechverhalten von Faserbeton mit makro-synthetischen bikomponentenfasern. In: Conference Proccedings of Spritzbeton-Tagung. Alpbach, Tirol, 2012. (in German).

77. Arango S.; Taengua E.G.; Martí Vargas J.R.; Serna Ros, P. A comprehensive study on the effect of fibers and loading on flexural creep of SFRC. In: RILEM PRO88,

Proceedings of the 8th RILEM international symposium on fibre reinforced concrete: Challenges and Opportunities (BEFIB 2012). Guimarães, Portugal, 2012, 704-715.

78. García-Taengua, E.; Arango, S.; Martí-Vargas, J.R.; Serna, P. Flexural creep of steel fiber reinforced concrete in the cracked state. Constr. Build. Mater. 2014, 65, 321-329.

79. Garcia-Taengua, E.; Llano-Torre, A.; Marti-Vargas, J.R.; Serna, P. Effect of Residual Strength Parameters on FRC Flexural Creep: Multivariate Analysis. In: Serna, P., Llano-Torre, A., Cavalaro, S. (eds) Creep Behaviour in Cracked Sections of Fibre Reinforced Concrete: Proceedings of the International RILEM Workshop FRC-CREEP 2016. RILEM Bookseries, vol 14. Springer, Dordrecht, 2017. DOI: 10.1007/978-94-024-1001-3_12

80. Llano-Torre A.; Arango, S.E.; García-Taengua, E.; Martí-Vargas, J.R.; Serna, P. Influence of Fibre Reinforcement on the Long-Term Behaviour of Cracked Concrete. In: Serna P., Llano-Torre A., Cavalaro S. (eds) Creep Behaviour in Cracked Sections of Fibre Reinforced Concrete: Proceedings of the International RILEM Workshop FRC-CREEP 2016. RILEM Bookseries, vol 14. Springer, Dordrecht, 2017. DOI: 10.1007/978-94-024-1001-3_16

81. Serna, P.; Llano-Torre, A.; Garcia-Taengua, E.; Marti-Vargas, J.R. Database on the Long-Term Behaviour of FRC: A Useful Tool to Achieve Overall Conclusions. In: Proceedings of the 10th International Conference on Mechanics and Physics of Creep, Shrinkage, and Durability of Concrete and Concrete Structures, Vienna, 2015, 1544-1553.

82. Serna Ros, P.; Bossio, M.E.; Zerbino, R.; Martí Vargas, J.R. Fluencia y propiedades residuales de hormigones autocompactantes con fibras expuestos en estado fisurado a diferentes condiciones ambientales. 3º Congreso Iberoamericano sobre hormigón autocompactante. Madrid, 2012, 221-230. (in Spanish)

83. Serna, P.; Martí-Vargas, J.R.; Bossio, M.E.; Zerbino, R. Creep and residual properties of cracked macro-synthetic fibre reinforced concretes. Mag. Concre. Res. 2016, 68(4), 197-207.

84. Monetti, D.H.; Giaccio, G.; Zerbino, R. Fluencia en estado fisurado en hormigón reforzado con macrofibras sintéticas. In: VI Congreso Internacional, 20ª Reunión Técnica AATH. Concordia, Argentina, 2014, 135-142. (in Spanish)

85. Llano-Torre, A.; Garcia-Taengua, E.; Marti-Vargas, J.R.; Serna, P. Compilation and study of a database of tests and results on flexural creep behaviour of fibre reinforced concrete specimens. Proceedings of the FIB Symposium Concrete Innovation and Design, Copenhagen, 2015.

86. Llano-Torre, A.; Serna, P.; Zerbino, R.; Martí-Vargas, J.R. Effect of initial crack opening on flexural creep behavior of FRC specimens. In: RILEM Proceedings

PRO 116 - 9th RILEM International Symposium on Fiber Reinforced Concrete: The Modern Landscape, BEFIB 2016. Vancouver, 2016, 117–126.

87. Llano-Torre, A.; Serna, P.; López, J.A. Flexural and compressive long term behaviour of UHPFRC Specimens. In: RILEM Proceedings PRO 116 - 9th RILEM International Symposium on Fiber Reinforced Concrete: The Modern Landscape, BEFIB 2016. Vancouver, Canada, 2016, 141–152

88. Llano-Torre, A.; López, J.A.; Martí-Vargas, J.R.; Serna, P. Comportamiento diferido en estado fisurado de elementos de UHPFRC a flexotracción. In: Proceedings of the V Congreso Iberoamericano de Hormigón Autocompactante y Hormigones Especiales HAC2018. Valencia, Spain, 2018, 361-372. (in Spanish) DOI: 10.4995/HAC2018.2018.6144

89. Llano-Torre, A.; Martí-Vargas, J.R.; Serna, P. Flexural and compressive creep behavior of UHPFRC specimens. Constr. Build. Mater. 2020, 244, 118254. DOI: 10.1016/j.conbuildmat.2020.118254

90. Abrishambaf, A.; Barros, J.; Cunha, V. Creep Behaviour of cracked Steel Fibre Reinforced Self-Compacting Concrete: from micro-mechanics to composite behaviour. In: Proceedings of the BEFIB 2016, 9th RILEM International Symposium on Fiber Reinforced Concrete. Vancouver, Canada, 2016, 102–116

91. Cunha, V.M.; Barros, J.A.; Abrishambaf, A. Time-Dependent Flexural Behaviour of SFRSCC Elements. In: Serna, P., Llano-Torre, A., Cavalaro, S. (eds) Creep Behaviour in Cracked Sections of Fibre Reinforced Concrete: Proceedings of the International RILEM Workshop FRC-CREEP 2016. RILEM Bookseries, vol 14. Springer, Dordrecht, 2017. DOI: 10.1007/978-94-024-1001-3_11

92. Babafemi, A.; Boshoff, W.P. Creep response of polypropylene macro Fibre Reinforced Concrete under sustained flexural loads. In: Proceedings of the BEFIB 2016, 9th RILEM International Symposium on Fiber Reinforced Concrete. Vancouver, Canada, 2016, 189–188

93. Babafemi, A.J.; Boshoff, W.P. Testing and modelling the creep of cracked macro-synthetic fibre reinforced concrete (MSFRC) under flexural loading. Mater. Struct. 2016, 49(10), 4389–4400. DOI: 10.1617/s11527-016-0795-7

94. Zerbino, R.; Monetti, D.H.; Giaccio, G. Creep behaviour of cracked steel and macro-synthetic fibre reinforced concrete. Mater. Struct. 2016, 49(8), 3397–3410. DOI: 10.1617/s11527-015-0727-y

95. Zerbino, R.; Monetti, D.H.; Giaccio, G.; Gettu, R. Creep en estado fisurado en hormigones reforzados con fibras. In: Proceedings of the VII Congreso Internacional, 21ª Reunión Técnica, Asociación Argentina de Tecnología del Hormigón, AATH. Salta – Argentina, 2016, 1(T2-62), 235-242. ISBN 978-987-21660-9-0. (in Spanish)

96. Zerbino, R.L.; Giaccio, G.M.; Monetti, D.H.; Torrijos, M.C. Effect of Beam Width on the Creep Behaviour of Cracked Fibre Reinforced Concrete. In: Serna, P., Llano-Torre, A., Cavalaro, S. (eds) Creep Behaviour in Cracked Sections of Fibre Reinforced Concrete: Proceedings of the International RILEM Workshop FRC-CREEP 2016. RILEM Bookseries, vol 14. Springer, Dordrecht, 2017. DOI: 10.1007/978-94-024-1001-3_14

97. Daviau-Desnoyers, D.; Charron, J-P.; Massicotte, B.; Rossi, P.; Tailhan, J-L. Characterization of the Propagation of a Macrocrack under Sustained Loading in Steel Fibre Reinforced Concrete. Mater. Struct. 2016, 49(3), 969-982. DOI: 10.1617/s11527-015-0552-3

98. Daviau-Desnoyers, D.; Charron, J-P.; Massicotte, B.; Rossi, P.; Tailhan, J-L. Creep Behavior of a SFRC Under Service and Ultimate Bending Loads. In: Serna, P., Llano-Torre, A., Cavalaro, S. (eds) Creep Behaviour in Cracked Sections of Fibre Reinforced Concrete: Proceedings of the International RILEM Workshop FRC-CREEP 2016. RILEM Bookseries, vol 14. Springer, Dordrecht, 2017. DOI: 10.1007/978-94-024-1001-3_18

99. Pham, T.D.; Sorelli, L.; Fafard, M.; Grassl, P. Modeling Nonlinear Creep of Steel Fiber Reinforced Concrete by Means of Hydro-Mechanical Coupling. In: Proceedings of the Sixth Biot Conference on Poromechanics. 2017, 1083-1090. DOI: 10.1061/9780784480779.135

100. Nishiwaki, T.; Kwon, S.; Otaki, H.; Igarashi, G.; Shaikh, F.U.; Fantilli, A.P. Experimental Study on Time-Dependent Behavior of Cracked UHP-FRCC Under Sustained Loads. In: Serna, P., Llano-Torre, A., Cavalaro, S. (eds) Creep Behaviour in Cracked Sections of Fibre Reinforced Concrete: Proceedings of the International RILEM Workshop FRC-CREEP 2016. RILEM Bookseries, vol 14. Springer, Dordrecht, 2017. DOI: 10.1007/978-94-024-1001-3_9

101. Nishiwaki, T.; Otaki, H.; Igarashi, G.; Kwon, S.; Shaikh, F.; Fantilli, A. Experimental study on the tensile and bending creep behavior of cracked UHP-FRCC. In: Hao, H. and Zhang, C. (eds), Proceedings of the 24th Australasian Conference on the Mechanics of Structures and Materials (ACMSM24). Perth, Australia, 2016, 149-154.

102. Pujadas, P.; Blanco, A.; Cavalaro, S.H.P.; de la Fuente, A.; Aguado, A. Flexural Post-cracking Creep Behaviour of Macro-synthetic and Steel Fiber Reinforced Concrete. In: Serna, P., Llano-Torre, A., Cavalaro, S. (eds) Creep Behaviour in Cracked Sections of Fibre Reinforced Concrete: Proceedings of the International RILEM Workshop FRC-CREEP 2016. RILEM Bookseries, vol 14. Springer, Dordrecht, 2017. DOI: 10.1007/978-94-024-1001-3_7

103. Pujadas, P.; Blanco, A.; Cavalaro, S.; de la Fuente, A.; Aguado, A. The need to consider flexural post-cracking creep behavior of macro-synthetic fiber reinforced

concrete. Constr. Build. Mater. 2017, 149, 790–800. DOI: 10.1016/j.conbuildmat.2017.05.166

104. Van Bergen, S.; Pouillon, S.; Vitt, G. Experiences from 14 Years of Creep Testing of Steel and Polymer Fiber Reinforced Concrete. In: Serna, P., Llano-Torre, A., Cavalaro, S. (eds) Creep Behaviour in Cracked Sections of Fibre Reinforced Concrete: Proceedings of the International RILEM Workshop FRC-CREEP 2016. RILEM Bookseries, vol 14. Springer, Dordrecht, 2017. DOI: 10.1007/978-94-024-1001-3_4

105. Casucci, D.; Thiele, C.; Schnell, J. Behaviour of Cracked Cross-Section of Fibre Reinforced UHPFRC Under Sustained Load. In: Serna, P., Llano-Torre, A., Cavalaro, S. (eds) Creep Behaviour in Cracked Sections of Fibre Reinforced Concrete: Proceedings of the International RILEM Workshop FRC-CREEP 2016. RILEM Bookseries, vol 14. Springer, Dordrecht, 2017. DOI: 10.1007/978-94-024-1001-3_8

106. Löber, P.; Heiden, B.; Holschemacher, K. Creep behaviour of macro glass fibre reinforced concrete beams. IOP Conf. Ser.: Mater. Sci. Eng. 2017, 246(1), 012028. DOI: 10.1088/1757-899X/246/1/012028

107. Monetti, D.H.; Torrijos, M.C.; Giaccio, G.; Zerbino, R. La estabilidad bajo condiciones de servicio de hormigón reforzado con fibras en estado fisurado. VIII CONGRESO INTERNACIONAL, 22ª Reunión Técnica AATH. Olavarría, Argentina, 2018, T051:361-370. (in Spanish)

108. Lima, V.N.; Cardoso, D.C.T.; de Silva, F. A. Flexural creep behavior of steel and polypropylene fiber reinforced concrete." In: Proceedings of the FraMCoS-X: Fracture Mechanics of Concrete and Concrete Structures. Bayonne, France, 2019. DOI: 10.21012/FC10.234778

109. Lima, V.N.; Cardoso, D.C.T.; de Silva, F. A. Creep mechanisms in precracked polypropylene and steel fiber–reinforced concrete. J. Mater. Civ. Eng. 2021, 33(8): 04021187. DOI: 10.1061/(ASCE)MT.1943-5533.0003775

110. Llano-Torre, A.; Serna, P.; Cavalaro, S.H.P. International Round Robin Test on creep behavior of FRC supported by the RILEM TC 261-CCF. In: RILEM Proceedings PRO 116 - 9th RILEM International Symposium on Fiber Reinforced Concrete: The Modern Landscape, BEFIB 2016. Vancouver, Canada, 2016, 127-140.

111. Llano-Torre, A.; Serna, P.; Cavalaro, S.H.P. International Round-Robin Test on Creep Behaviour of FRC - Part 2: An Overview of Results and Preliminary Conclusions. In: Serna, P., Llano-Torre, A., Martí-Vargas, J.R., Navarro-Gregori, J. (eds) Fibre Reinforced Concrete: Improvements and Innovations II (BEFIB 2021). RILEM Bookseries, vol 36. Springer, 2022. DOI: 10.1007/978-3-030-83719-8_26

112. Del Prete, C.; Buratti, N.; Mazzotti, C. Experimental analysis of time dependent phenomena and temperature effects on macro-synthetic fibre reinforced concretes in different loading conditions. Constr. Build. Mater. 2022, 326, 126904. DOI: 10.1016/j.conbuildmat.2022.126904

113. Del Prete, C.; Buratti, N.; Mazzotti, C. Experimental Investigation on the Influence of Temperature Variations on Macro-synthetic Fibre Reinforced Concrete Short and Long Term Behaviour. In: Serna, P., Llano-Torre, A., Martí-Vargas, J.R., Navarro-Gregori, J. (eds) Fibre Reinforced Concrete: Improvements and Innovations II (BEFIB 2021). RILEM Bookseries, vol 36. Springer, 2022. DOI: 10.1007/978-3-030-83719-8_29

114. Hunger, M.; Bokern, J.; Cleven, S.; Vrijdaghs, R. Creep in FRC – From Material Properties to Composite Behavior. In: Serna, P., Llano-Torre, A., Martí-Vargas, J.R., Navarro-Gregori, J. (eds) Fibre Reinforced Concrete: Improvements and Innovations (BEFIB 2020). RILEM Bookseries, vol 30. Springer, 2021. DOI: 10.1007/978-3-030-58482-5_37

115. Tošić, N.; de la Fuente, A. Short and Long Term Behaviour of Polypropylene Fibre Reinforced Concrete Beams with Minimum Steel Reinforcement. In: Serna, P., Llano-Torre, A., Martí-Vargas, J.R., Navarro-Gregori, J. (eds) Fibre Reinforced Concrete: Improvements and Innovations II (BEFIB 2021). RILEM Bookseries, vol 36. Springer, 2022, 342-353. DOI: 10.1007/978-3-030-83719-8_30

116. Vrijdaghs, R.; di Prisco, M.; Vandewalle, L. Sectional analysis of the flexural creep of cracked fiber reinforced concrete. Struct. Concr. 2021, vol 22(3), 1817–1830. DOI: 10.1002/suco.202000559

117. Vrijdaghs, R.; di Prisco, M.; Vandewalle, L. A Computational Sectional Approach for the Flexural Creep Behavior of Cracked FRC. In: Serna, P., Llano-Torre, A., Martí-Vargas, J.R., Navarro-Gregori, J. (eds) Fibre Reinforced Concrete: Improvements and Innovations (BEFIB 2020). RILEM Bookseries, vol 30. Springer, 2021, 347–358. DOI: 10.1007/978-3-030-58482-5_32

118. DAfStb: Guideline steel fibre reinforced concrete (in German Richtlinie Stahlfaserbeton). Beuth-Verlag, Berlin, 2012.

119. OBV (Austrian Society for Construction Technology): Guideline Fibre Reinforced Concrete (in German: Richtlinie Faserbeton). Vienna, 2008.

120. Llano-Torre, A.; Serna, P.; Garcia-Taengua, E.; Vrijdaghs, R.; Pauwels, H.; del Prete, C.; Buratti, N.; Zerbino, R.L.; Kusterle, W.; Bernard, E.S. Analysis of the RRT Results. In: Llano-Torre, A., Serna, P. (eds) Round-Robin Test on Creep Behaviour in Cracked Sections of FRC: Experimental Program, Results and Database Analysis. RILEM State-of-the-Art Reports, vol 34. Springer, 2021. https://doi.org/10.1007/978-3-030-72736-9_8

121. Purkiss, J.A.; Blagojevic P. Comparison between the short and long term behaviour of fibre reinforced and unreinforced concrete beams. Compos. Struct. 1993, 25, 45-49

122. Tan, K.H.; Paramasivam, P.; Tan, K.C. Creep and Shrinkage Deflections of RC Beams with Steel Fibers. J. Mater. Civ. Eng. 1994, 6(4), 474-494.

123. Tan, K.H.; Paramasivam, P.; Tan, K.C. Cracking Characteristics of Reinforced Steel Fiber Concrete Beams under Short- and Long-Term Loadings. Adv. Cem. Based Mater. 1995, 2, 127-137.

124. Tan, K.H.; Paramasivam, P.; Tan, K.C. Instantaneous and Long-Term Deflections of Steel Fiber Reinforced Concrete Beams. ACI Struct. J. 1994, 91(4), 384-393.

125. Tan, K.H., Saha, M.K. Ten-year study on Steel fiber-reinforced concrete beams under sustained loads. ACI Struct. J. 2005, 102(3) 472-480.

126. Kaminski, M.; Bywalski, C. Influence of creep deformations on value of long-term deflections of steel fiber-reinforced concrete beams. In: Proceedings of the 8th International Conference on Creep, Shrinkage and Durability of Concrete and Concrete Structures. Ise-Shima, Japan, 2008, 1, 729–734.

127. Buratti, N.; Mazzotti, C. Long term behaviour of self-compacting fibre-reinforced concrete beams. In: 2nd International Symposium on Design, Performance and Use of Self Consolidating Concrete. RILEM Publications. 2009, 551-561. ISSN/ISBN: 978-2-35158-073-8

128. Buratti, N.; Mazzotti, C.; Savoia, M. Long-term behaviour of steel- and macrosynthetic-fibre reinforced concrete beams. CONCRETE TECHNOLOGY, CPI - Concrete Plant International 5, 2010.

129. Buratti, N.; Mazzotti, C.; Savoia, M.; Rossi, P. Temperature and loading level effect on the long-term behaviour of MSFRC and SFRC. In: Proceedings of the 6th International Conference of Fibre Concrete. Prague, Czech Republic, 2011, 101-110.

130. Buratti, N.; Mazzotti, C. Temperature effect on the long term behaviour of macro–synthetic– and steel–fibre reinforced concrete. In: RILEM PRO88, Proceedings of the 8th RILEM international symposium on fibre reinforced concrete: Challenges and Opportunities (BEFIB 2012). Guimarães, Portugal, 2012, 715-725.

131. Buratti, N.; Mazzotti, C.; Savoia, M. Long-Term Behaviour of Fiber-Reinforced Self-Compacting Concrete Beams". In: Khayat, K., Feys D. (eds) Design, Production and Placement of Self-Consolidating Concrete. RILEM Bookseries, vol 1. Springer, Dordrecht, Montreal, 2010, 439-450

132. Buratti, N.; Mazzotti, C.; Savoia, M. Long-term behaviour of cracked SFRC beams exposed to aggressive environment. In: Proceedings of FraMCoS-7. 2010, 1512-1517.

133. Buratti, N.; Mazzotti, C.; Savoia, M. Long–Term Behavior of Cracked SFRC Elements Exposed to Chloride Solutions. ACI Special Publications. 2011, 280, 63-75. ISSN/ISBN: 0193-2527

134. Vasanelli, E.; Micelli, F.; Aiello, M.A.; Plizzari, G. Long term behaviour of fiber reinforced concrete beams in bending. In: RILEM PRO88, Proceedings of the 8th RILEM international symposium on fibre reinforced concrete: Challenges and Opportunities (BEFIB 2012). Guimarães, Portugal, 2012, 635-647.

135. Vasanelli, E.; Micelli, F.; Aiello, M.A.; Plizzari, G. Long term behavior of FRC flexural beams under sustained load. Eng. Struct. 2013, 56, 1858-1867.

136. Vasanelli, E.; Micelli, F.; Aiello, M.A.; Plizzari, G. Crack width prediction of FRC beams in short- and long-term bending condition. Mater. Struct. 2014, 47, 39–54.

137. Candido, L.; Micelli, F.; Aiello, M. A.; Plizzari, G. Cracking Behaviour of FRC Beams under Long-Term Loading. In: Proceedings of the 10th International Conference on Creep, Shrinkage, and Durability of Concrete and Concrete Structures CONCREEP 10. Vienna, Austria, 2015, 1147–1156.

138. Candido, L.; Micelli, F.; Vasanelli, E.; Aiello, M.; Plizzari, G. Durability of FRC Beams Exposed for Long-Term Under Sustained Service Loading. In: Serna, P., Llano-Torre, A., Cavalaro, S. (eds) Creep Behaviour in Cracked Sections of Fibre Reinforced Concrete: Proceedings of the International RILEM Workshop FRC-CREEP 2016. RILEM Bookseries, vol 14. Springer, Dordrecht, 2017. DOI: 10.1007/978-94-024-1001-3_19

139. Micelli, F.; Candido, L.; Vasanelli, E.; Aiello, M.A.; Plizzari, G. Effects of Short Fibers on the Long-Term Behavior of RC/FRC Beams Aged under Service Loading. Appl. Sci. 2019, 9, 2540.

140. Nakov, D.; Markovski G. Time dependant behavior of SFRC elements under sustained loads. In: RILEM PRO88, Proceedings of the 8th RILEM international symposium on fibre reinforced concrete: Challenges and Opportunities (BEFIB 2012). Guimarães, Portugal, 2012, 796 - 808.

141. Nakov, D.; Markovski, G.; Arangjelovski, T.; Mark, P. Creeping Effect of SFRC Elements Under Specific Type of Long Term Loading. In: Serna, P., Llano-Torre, A., Cavalaro, S. (eds) Creep Behaviour in Cracked Sections of Fibre Reinforced Concrete: Proceedings of the International RILEM Workshop FRC-CREEP 2016. RILEM Bookseries, vol 14. Springer, Dordrecht, 2017. DOI: 10.1007/978-94-024-1001-3_17

142. Nakov, D.; Markovski, G.; Arangjelovski, T.; Mark, P. Influence of the Residual Tensile Strength on the Factor for Quasi-permanent Value of a Variable Action ψ_2. In: Serna, P., Llano-Torre, A., Martí-Vargas, J.R., Navarro-Gregori, J. (eds)

Fibre Reinforced Concrete: Improvements and Innovations (BEFIB 2020). RILEM Bookseries, vol 30. Springer, 2021. DOI: 10.1007/978-3-030-58482-5_35

143. Aslani, F.; Nejadi, S.; Samali, B. Long-term flexural cracking control of reinforced self-compacting concrete one way slabs with and without fibres. Comput. Concr. 2014, 14(4), 419–444. DOI: 10.12989/CAC.2014.14.4.419

144. Buratti, N.; Mazzotti, C. An experimental and numerical study on the long-term behaviour of cracked fibre-reinforced self-compacting concrete beams. In: Proceedings of the 7th RILEM Symposium on Self-Compacting Concrete. Paris, France, 2013.

145. Park, Y.; Abolmaali, A.; Attiogbe, E.; Lee, S.-H. Time-Dependent Behavior of Synthetic Fiber–Reinforced Concrete Pipes under Long-Term Sustained Loading. Transp. Res. Rec. 2014, 2407(1), 71–79. DOI: 10.3141/2407-07

146. Attiogbe, E.; Abolmaali, A.; Park, Y. Polypropylene fiber-reinforced concrete pipes under sustained loading. In: Proceedings of the 9th RILEM International Symposium on Fiber Reinforced Concrete (BEFIB 2016). Vancouver, BC, Canada, 2016, 1128–1138

147. Daviau-Desnoyers, D.; Charron, J.-P.; Massicotte, B.; Rossi, P.; Tailhan, J.-L. Influence of reinforcement type on macrocrack propagation under sustained loading in steel fibre-reinforced concrete. Struct. Concr. 2016, 17, 736-746. DOI: 10.1002/suco.201500069

148. Altoubat, S.; Rieder, KA.; Junaid, M.T. Short- and long-term restrained shrinkage cracking of fiber reinforced concrete composite metal decks: an experimental study. Mater. Struct. 2017, 50(2), 1-15. DOI: 10.1617/s11527-017-1011-0

149. Galeote, E.; Blanco, A.; de la Fuente, A.; Cavalaro, S.H. Creep Behaviour of Cracked High Performance Fibre Reinforced Concrete Beams Under Flexural Load. In: Serna, P., Llano-Torre, A., Cavalaro, S. (eds) Creep Behaviour in Cracked Sections of Fibre Reinforced Concrete: Proceedings of the International RILEM Workshop FRC-CREEP 2016. RILEM Bookseries, vol 14. Springer, Dordrecht, 2017. DOI: 10.1007/978-94-024-1001-3_10

150. Bouziadi, F.; Boulekbache, B.; Haddi, A.; Djelal, C. Experimental and finite element analysis of creep behaviour of steel fibre reinforced high strength concrete beams. Constr. Build. Mater. 2018, 173, 101-110. DOI: 10.1016/j.conbuildmat.2018.04.013

151. Neutov, S.; Sydorchuk, M.; Surianinov, M. Experimental Studies of Reinforced Concrete and Fiber-Reinforced Concrete Beams with Short-Term and Long-Term Loads. In: Materials Science Forum. Trans Tech Publications, Ltd. 2019, 968, 227–233. DOI: 10.4028/www.scientific.net/msf.968.227

152. Al Rikabi, F.T.; Sargand, S.M.; Khoury, I.; Kurdziel, J. A new test method for evaluating the long-term performance of fiber-reinforced concrete pipes. Adv. Struct. Eng. 2020, 23, 1336–1349. DOI: 10.1177/1369433219894243

153. Al Rikabi, F. T.; Sargand, S.M.; Kurdziel, J.; Khoury, I. Performance of Thin-Wall Synthetic Fiber–Reinforced Concrete Pipes under Short and Long-Term Loading. J. Test. Eval. 2020, 48(5), 3713–3733. DOI: 10.1520/JTE20180369

154. Kassimi, F.; Khayat, K.H. Flexural Creep and Recovery of Fiber-Reinforced SCC - Testing Methodology and Material Performance. J. Adv. Concr. Technol. 2021, 19 (1), 67-81. DOI: 10.3151/jact.19.67

155. Al Marahla, R.H.; Garcia-Taengua, E. Cracking Behaviour of FRC Members Reinforced with GFRP Bars under Sustained Loads. In: Serna, P., Llano-Torre, A., Martí-Vargas, J.R., Navarro-Gregori, J. (eds) Fibre Reinforced Concrete: Improvements and Innovations II (BEFIB 2021). RILEM Bookseries, vol 36. Springer, 2022. DOI: 10.1007/978-3-030-83719-8_28

156. Watts, M.J.; Amin, A.; Gilbert, R.I.; Kaufmann, W.; Minelli, F. Simplified prediction of the time dependent deflection of SFRC flexural members. Mater. Struct. 2020, 53(3), 1-11. DOI: 10.1617/s11527-020-01479-8

157. Watts, M.; Amin, A.; Ian Gilbert, R.; Kaufmann, W. Time Dependent Deflection of FRC Members Under Sustained Axial and Flexural Loading. In: Serna, P., Llano-Torre, A., Martí-Vargas, J.R., Navarro-Gregori, J. (eds) Fibre Reinforced Concrete: Improvements and Innovations (BEFIB 2020). RILEM Bookseries, vol 30. Springer, 2021. DOI: 10.1007/978-3-030-58482-5_34

158. Watts, M.; Amin, A.; Ian Gilbert, R.; Kaufmann, W; Minelli, F. Simplified time-dependent crack width prediction for fiber reinforced concrete flexural members. Struct. Concr. 2021, vol 22(3), 1549-1560. DOI: 10.1002/suco.202000683

159. Boshoff, W.P.; van Zijl, G.P.a.G. Time-dependent response of ECC: Characterisation of creep and rate dependence. Cem. Concr. Res. 2007, 37(5), 725–734. DOI: 10.1016/j.cemconres.2007.02.001

160. Boshoff, W.P.; van Zijl, G.P.a.G. Time-dependent response of ECC: Characterisation and modelling of creep and creep fracture. In: RILEM International Workshop on High Performance Fiber Reinforced Cement-Based Composites (HPFRCC) in Structural Applications. Honolulu, Hawaii, 2005, 125-134. DOI: 10.1617/2912143942.014

161. Mouton, C.J.; Boshoff, W.P. Initial study on the tensile creep of cracked steel fibre reinforced concrete. In: RILEM PRO88, Proceedings of the 8th RILEM international symposium on fibre reinforced concrete: Challenges and Opportunities (BEFIB 2012). Guimarães, Portugal, 2012, 326 - 337.

162. Zhao, G.; di Prisco, M.D.; Vandewalle, L. Experimental research on uni-axial tensile creep behaviour of pre-cracked steel fibre reinforced concrete. In: RILEM PRO88, Proceedings of the 8th RILEM international symposium on fibre reinforced concrete: Challenges and Opportunities (BEFIB 2012). Guimarães, Portugal, 2012, 760 - 771.

163. Zhao, G.; Di Prisco, M.; Vandewalle, L. Experimental Research and Numerical Simulation of Post-Crack Creep Behavior of SFRC Loaded in Tension', Mechanics and Physics of Creep, Shrinkage, and Durability of Concrete. In: Proceedings of the Ninth International Conference on Creep, Shrinkage, and Durability Mechanics (CONCREEP-9). Cambridge, Massachusetts, 2013, 340–347.

164. Zhao, G.; di Prisco, M.; and Vandewalle, L. Experimental investigation on uniaxial tensile creep behavior of cracked steel fibre reinforced concrete. Mater. Struct. 2015, 48(10), 3173–3185.

165. Boshoff, W.P.; Adendorff, C.J., van Zijl, G.P.a.G. Creep of cracked strain hardening cement-based composites. In: Proceedings of International Conference on Creep, Shrinkage and Durability Mechanics of Concrete and Concrete Structures (CONCREEP-8). Japan, 2008, p 723–728.

166. Boshoff, W.P.; Adendorff, C.J. Effect of sustained tensile loading on SHCC crack widths. Cem. Concr. Compos. 2013, 37, 119-125.

167. Babafemi, A.J.; Boshoff, W.P. Preliminary creep behaviour of polypropylene fibre reinforced concrete (PPFRC) under a high tensile stress. In: Advances in Cement and Concrete Technology, Proceedings of the International Conference ACCTA. Johannesburg, South Africa, 2013, 887–895.

168. Babafemi, A.J.; Boshoff, W.P. Time-dependent behaviour of pre-cracked polypropylene fibre reinforced concrete (PFRC) under sustained loading. Research and Applications in Structural Engineering, Mechanics and Computation. In: Proceedings of the Fifth International Conference on Structural Engineering, Mechanics and Computation (SEMC 2013). Cape Town, South Africa, 2013, 1593-1598.

169. Babafemi, A.J.; Boshoff, W.P. Tensile creep of macro-synthetic fibre reinforced concrete (MSFRC) under uni-axial tensile loading. Cem. Concr. Compos. 2015, 55, 62–69. DOI: 10.1016/j.cemconcomp.2014.08.002

170. Babafemi, A.; Boshoff, W. Macro-Synthetic Fibre Reinforced Concrete: Creep and Creep Mechanisms. In: Serna, P., Llano-Torre, A., Cavalaro, S. (eds) Creep Behaviour in Cracked Sections of Fibre Reinforced Concrete: Proceedings of the International RILEM Workshop FRC-CREEP 2016. RILEM Bookseries, vol 14. Springer, Dordrecht, 2017. DOI: 10.1007/978-94-024-1001-3_15

171. Boshoff, W.P. Cracking Behavior of Strain-Hardening Cement-Based Composites Subjected to Sustained Tensile Loading, ACI Mater. J. 2014, 111, 553-559.

172. Vrijdaghs, R.; di Prisco, M.; Vandewalle, L. Creep of cracked polypropylene Fiber Reinforced Concrete. In: Proceedings of the BEFIB 2016, 9th RILEM International Symposium on Fiber Reinforced Concrete. Vancouver, Canada, 2016, 199–208

173. Vrijdaghs, R.; di Prisco, M.; Vandewalle, L. (2016). Creep of cracked polymer fiber reinforced concrete under sustained tensile loading. In: Proceedings of 9th International Conference on Fracture Mechanics of Concrete and Concrete Structures FraMCOS 0. Berkley, USA, 2016. DOI: 10.21012/FC9.059

174. Vrijdaghs, R.; di Prisco, M.; Vandewalle, L. Creep Deformations of Structural Polymeric Macrofibers. In: Serna, P., Llano-Torre, A., Cavalaro, S. (eds) Creep Behaviour in Cracked Sections of Fibre Reinforced Concrete: Proceedings of the International RILEM Workshop FRC-CREEP 2016. RILEM Bookseries, vol 14. Springer, Dordrecht, 2017. DOI: 10.1007/978-94-024-1001-3_5

175. Vrijdaghs, R.; di Prisco, M.; Vandewalle, L. Uniaxial tensile creep of a cracked polypropylene fiber reinforced concrete. Mater. Struct. 2018, 51, 5. DOI: 10.1617/s11527-017-1132-5

176. Vrijdaghs, R.; di Prisco, M.; Vandewalle, L. A Numerical Model for the Creep of Fiber Reinforced Concrete. In: D.A. Hordijk and M. Luković (eds.), High Tech Concrete: Where Technology and Engineering Meet, Springer. 2018, 366-373. DOI: 10.1007/978-3-319-59471-2_44

177. Vrijdaghs, R.; di Prisco, M.; Vandewalle, L. Creep of polymeric fiber reinforced concrete: A numerical model with discrete fiber treatment. Computers & Structures, vol 233, 2020, 106233. DOI: 10.1016/j.compstruc.2020.106233

178. Boshoff, W.; Nieuwoudt, P. Tensile Creep of Cracked Steel Fibre Reinforced Concrete: Mechanisms on the Single Fibre and at the Macro Level. In: Serna, P., Llano-Torre, A., Cavalaro, S. (eds) Creep Behaviour in Cracked Sections of Fibre Reinforced Concrete: Proceedings of the International RILEM Workshop FRC-CREEP 2016. RILEM Bookseries, vol 14. Springer, Dordrecht, 2017. DOI: 10.1007/978-94-024-1001-3_6

179. Nieuwoudt, P.D.; Babafemi, A.J.; Boshoff, W.P. The response of cracked steel fibre reinforced concrete under various sustained stress levels on both the macro and single fibre level. Constr. Build. Mater. 2017, 156, 828-843

180. Del Prete, C.; Boumakis, I.; Wan-Wendner, R.; Buratti, N.; Mazzotti, C. Creep of Macro Synthetic Fibre Reinforced Concrete: Experimental Results and Numerical Model Calibration. In: Serna, P., Llano-Torre, A., Martí-Vargas, J.R., Navarro-Gregori, J. (eds) Fibre Reinforced Concrete: Improvements and Innovations II (BEFIB 2021). RILEM Bookseries, vol 36. Springer, 2022. DOI: 10.1007/978-3-030-83719-8_37

181. EN 14488-5:2006. Testing sprayed concrete - Part 5: Determination of energy absorption capacity of fibre reinforced slab specimens, Residual), CEN - European Committee for Standardization, Brussels, 2006.

182. Zollo, R.F. Analysis of Support Apparatus for Flexural Load-Deflection Testing: Minimizing Bias Caused by Arching Forces. J. Test. Eval. 2013, 41(1), 63–68.

183. Bernard, E.S. Influence of Friction in Supporting Rollers on the Apparent Flexural Performance of Third-Point Loaded Fiber Reinforced Concrete Beams. Adv. Civ. Eng. Mater. 2014, 3(1), 1–12.

184. ASTM C1550-12a, Standard Test Method for Flexural Toughness of Fiber Reinforced Concrete (Using Centrally Loaded Round Panel), ASTM International, West Conshohocken, PA, 2012. DOI: 10.1520/C1550-12A

185. Bernard, E.S. Influence of Fiber Type on Creep Deformation of Cracked Fiber-Reinforced Shotcrete Panels. ACI Mater. J. 2010, 107(5), 474-480.

186. Bernard, E.S. The Influence of Creep on Relative Creep Deformations in Shotcrete Linings. Shotcrete. 2012, 52-57.

187. BEKAERT. Creep test for EN 14488-5 plates: Confirmation of Creep behavior plastic fibres in concrete plates. BEKAERT Technical Report, 2009.

188. Kaufmann, J.; Manser, M. Durability performance of bi-component polymer fibres under creep and in aggressive environments. Proceeding of the seventh International Symposium on Ground Support in Mining and Underground Construction, Perth, Australia, 2013.

189. Reinhold, M.; Wetzig, V. Long-term behaviour of synthetic fibre-reinforced shotcrete in underground construction. In: Proceedings of ITA-AITES World Tunnel Congress 2012: tunneling and underground space for a global society. Bangkok, Thailand, 2012.

190. de Rivaz, B. EFNARC Creep test procedure description for sprayed concrete and test results with steel and synthetic fibres. Conference Proceedings of Spritzbeton-Tagung, Alpbach, Tirol, 2015.

191. Larive, C.; Rogat, D.; Chamoley, D.; Welby, N.; Regnard, A. Creep behaviour of fibre reinforced sprayed concrete, SEE Tunnel: Promoting Tunneling in SEE Region. In: ITA WTC 2015 Congress and 41st General Assembly, Dubrovnik, Croatia, 2015.

192. Larive, C.; Rogat, D.; Chamoley, D.; Regnard, A.; Pannetier, T.; Thuaud, C. Influence of fibres on the creep behaviour of reinforced sprayed concrete. In: Proceedings of the World Tunnel Congress (WTC 2016). San Francisco, California, USA, 2016, 3, 1657-1666. ISSN/ISBN: 9781510822627

193. Larive, C.; Rogat, D.; Chamoley, D.; Regnard, A.; Pannetier, T.; Thuaud, C. Mid-term Behaviour of Fibre Reinforced Sprayed Concrete Submitted To Flexural Loading. In: Serna P., Llano-Torre A., Cavalaro S. (eds) Creep Behaviour in Cracked Sections of Fibre Reinforced Concrete: Proceedings of the International RILEM Workshop FRC-CREEP 2016. RILEM Bookseries, vol 14. Springer, Dordrecht, 2017. DOI: 10.1007/978-94-024-1001-3_13

194. Bernard, E.S. Influence of Fiber Geometry and Type on Creep Rupture of Cracked Fiber-Reinforced Shotcrete Mixtures. ACI Mater. J. 2021, 118(2), 3-12. DOI: 10.14359/51730410

195. Llano-Torre, A.; Cavalaro, S.H.; Kusterle, W.; Moro, S.; Zerbino, R.L.; Gettu, R.; Pauwels, H.; Nishiwaki, T.; Parmentier, B.; Buratti, N.; Toledo Filho, R.D.; Charron, J-P.; Larive, C.; Boshoff, W.P.; Bernard, E.S.; Kompatscher, M. Equipment and Procedure Description. In: Llano-Torre, A., Serna, P. (eds) Round-Robin Test on Creep Behaviour in Cracked Sections of FRC: Experimental Program, Results and Database Analysis. RILEM State-of-the-Art Reports, vol 34. Springer, 2021. DOI: 10.1007/978-3-030-72736-9_5

196. Arango, SE. Fluencia a flexión del hormigón reforzado con fibras de acero (SFRC) en estado fisurado. Universitat Politècnica de València, PhD thesis, 2010. DOI: 10.4995/Thesis/10251/8508

197. Llano-Torre, A.; Serna, P.; Cavalaro, S.H.P. Data and Parameter Definition. In: Llano-Torre, A., Serna, P. (eds) Round-Robin Test on Creep Behaviour in Cracked Sections of FRC: Experimental Program, Results and Database Analysis. RILEM State-of-the-Art Reports, vol 34. Springer, 2021. 10.1007/978-3-030-72736-9_6

198. Llano-Torre, A.; Serna Ros, P.; Cavalaro, S.; Kusterle, W.; Moro, S.; Zerbino, R.L.; Gettu, R.; Pauwels H.; Nishiwaki T.; Parmentier B.; Buratti N.; Toledo Filho R.D.; Charron J.P.; Larive C.; Boshoff W.P.; Bernard, E.S.; Kompatscher M. Database of the Round-Robin Test on Creep Behaviour in Cracked Sections of Fibre Reinforced Concrete organised by the RILEM Technical Committee 261-CCF, 2021. DOI: 10.4995/Dataset/10251/163221

199. Vrijdaghs R; Van Itterbeeck P; De Smedt M; Vandewalle L. Experimental study into the location of the neutral axis in fiber-reinforced concrete prisms. Struct. Concr. 2021, vol 22(1), 285–297. DOI: 10.1002/suco.201900397

200. Vrijdaghs, R. Creep of Synthetic Fiber Reinforced Concrete: A Multi-scale and Two Phased Approach. KU Leuven, PhD thesis, 2019.

Appendix A:
Creep experimental programmes

Many experimental flexure creep test programmes on fibre-reinforced concrete (FRC) in the cracked state were carried out during the PhD duration. This Appendix summarises the experimental programmes to support the reader in following the evolution of the flexure methodology improvements presented in this document. Relevant information about the creep test duration, the studied FRC matrix, and the number of specimens tested are collected in Table A.1.

Table A.1. Flexure creep experimental programmes developed during the PhD.

Year	Reference	Duration (days)	Mix	Nº Frames	Nº Specimens creep	Shrinkage
2015	WP1	180	SyFRC	2	6	-
			SFRC	2	6	-
2015	NAE-1	180	SFRC	1	1	-
2016	RRT	360	SyFRC	2	6	-
			SFRC	2	6	-
2017	WP2	180	SFRC	6	16	2
2017	OC2	390	GFRC	2	6	2
2019	FN2	540	SyFRC	2	2	1
			SFRC	2	2	1
2021	FN3	270	SyFRC	2	2	1
			SFRC	2	2	1

Table A.2 summarises the creep programmes which results were used to assess and determine the different parameters and improvements along the PhD.

Table A.2. Goals and new parameters assessment on the PhD experimental programmes.

Objectives	Experimental programmes						
	WP1	NAE1	RRT	WP2	OC2	NAE2	NAE3
Pre-crack level	X			X			
Creep index I_c				X			
Delayed recovery			X	X[*]	X		
Improved boundary conditions			X		X	X	X
Loading process duration t_{ci}						X	
Short-term deformation			X				
Shrinkage				X	X	X	X
Compressive strains	X					X	X
Neutral axis		X				X	X

[*] Delayed recovery was only assessed in the creep stage.

A full description of each experimental creep programme is provided in the following Appendices.

Appendix B:
WP1 creep experimental programme and results

The WP1 experimental programme aimed to assess the influence of the pre-cracking level $CMOD_p$ (named w_p in the starting methodology presented in Chapter 3) on the long-term response of FRC specimens. To this purpose, two FRC series were cast with the same concrete matrix shown in Table B.1. Series A consists of synthetic fibre-reinforced concrete (SyFRC) with 9 kg/m³. Series B consists of steel fibre-reinforced concrete (SFRC) with 40 kg/m³. The properties of fibres are described in Table B.2

Table B.1. WP1 concrete matrix composition in kg/m³.

Component	SyFRC	SFRC
	Series A	Series B
Cement CEM I 52.5 R	350	350
Water, w/c = 0.50	175	175
Aggregate 1 (6/10)	450	450
Aggregate 2 (4/6)	350	350
Crushed sand	900	900
filler	50	50
Superplasticizer	3.75	
Fibres	9	40

Table B.2. Fibre properties and dosage of WP1 experimental programme.

Series	Mix	Fibre		Dosage
		Brand	Length	(kg/m³)
Series A	SyFRC	Sikafiber M-48	48	9
Series B	SFRC	Dramix 3D 65/35 BG	35	40

Appendix B presents the main experimental results obtained on each creep test phase (characterisation, pre-crack, creep and post-creep) of the WP1 experimental programme.

B.1. FRC matrix characterisation tests results

Three specimens per series were tested in flexure for characterisation purposes following the EN 14651 standard in the 3-point bending test (3PBT) setup. The residual performance obtained in characterisation tests is presented in Figure B.1, and the experimental results are collected in Table B.3.
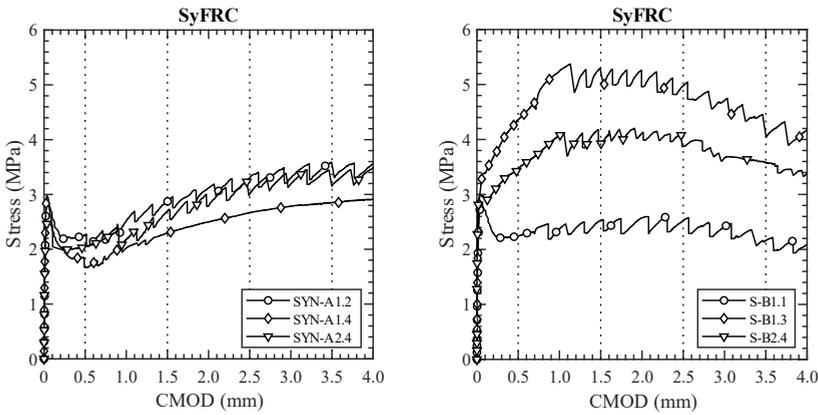
Figure B.1. Stress-CMOD curves from WP1 characterisation tests.

Table B.3. Flexure characterisation tests.

Series	Specimen	f_L (MPa)	$f_{R,1}$ (MPa)	$f_{R,2}$ (MPa)	$f_{R,3}$ (MPa)	$f_{R,4}$ (MPa)
A	A1	2.85	2.26	2.86	3.30	3.59
	A2	2.97	1.67	2.30	2.67	2.86
	A3	2.49	2.05	2.71	3.01	3.17
	Average	2.77	1.99	2.62	2.99	3.21
	CV	9.0	15.0	11.1	10.5	11.4
B	B1	2.81	2.24	2.53	2.53	2.16
	B2	3.21	4.36	4.99	4.98	4.04
	B3	2.99	3.46	3.93	3.87	3.59
	Average	3.00	3.35	3.82	3.79	3.26
	CV	6.7	31.7	32.3	32.3	30.1

B.2. Pre-cracking stage

Specimens were pre-cracked in a 4-point bending test (4PBT) setup with 450 mm support span until 0.2, 0.5, 0.8, 1.2, 1.5 and 2.0 mm $CTOD_p$. and then unloaded. Crack mouth opening deformations (CMOD) were monitored with an LVDT placed in the bottom face, whereas the compressive strains were registered using a 50 mm in length strain gauge in the top face of the specimen. Delayed recovery deformations after the unloading process were not registered since this procedure was later established.Figure B.2 presents the pre-cracking test Stress-CTOD curves for each specimen. Table B.4 collects the residual strength experimentally obtained and the average values for each mix.
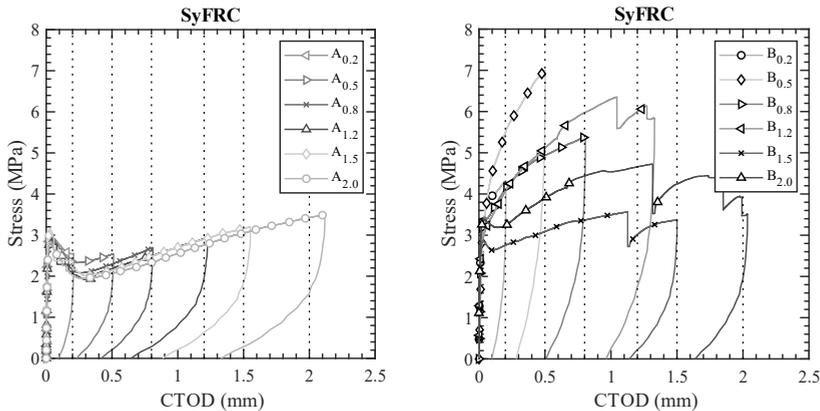
Figure B.2. Stress-CTOD curves from WP1 pre-cracking tests.

Table B.4. WP1 pre-cracking tests experimental results.

Series	Specimen	f_L (MPa)	$f_{R,1}$ (MPa)	$f_{R,2}$ (MPa)	$f_{R,3}$ (MPa)	$CTOD_p$ (mm)	$CMOD_p$ (mm)	$CMOD_{pri}$* (mm)
A	$A_{0.2}$	2.94				209	255	115
	$A_{0.5}$	3.01	2.43			513	627	294
	$A_{0.8}$	2.98	2.19			812	984	496
	$A_{1.2}$	2.91	2.08			1,231	1,483	797
	$A_{1.5}$	3.14	2.06	2.94		1,552	1,856	1,076
	$A_{2.0}$	2.84	1.99	2.81	3.47	2,117	2,490	1,589
B	$B_{0.2}$	3.31				202	263	126
	$B_{0.5}$	3.36	6.56			502	637	343
	$B_{0.8}$	3.44	4.76			806	964	589
	$B_{1.2}$	3.03	4.88	6.02		1,328	1,661	1,184
	$B_{1.5}$	2.86	2.97	3.10		1,500	1,808	1,352
	$B_{2.0}$	3.37	3.67	4.66	3.61	2,034	2,497	2,014

*Delayed recovery assessment was not realised in this experimental programme

B.3. Creep stage

Creep tests were carried out in a multi-specimen setup with three specimens per frame. The 4PBT setup with a 450 mm support span was used to improve the stability of the stacked specimens. Note that, in this WP1 experimental programme, the creep index was defined as 45% of the average $f_{R,1}$ obtained by each mix instead of the individual $f_{R,p}$ since not all the specimens reached 0.5 mm CMOD at pre-cracking tests. This fact implied a wider variation of the creep index. Delayed CMOD and compressive strains were recorded for 180 days. Specimens were unloaded and delayed recovery deformations were recorded for 30 days. Since the shrinkage assessment was established later, shrinkage flexure specimens were not used in the WP1 experimental programme. Table B.5 provides the relative position of each specimen in the creep frame and the applied load.

Table B.5. WP1 relative position of specimens on the creep frames.

Position	Frame			
	F2	F3	F4	F5
Top	$A_{1.5}$	$A_{2.0}$	$B_{1.5}$	$B_{2.0}$
Middle	$A_{0.2}$	$A_{0.5}$	$B_{0.2}$	$B_{0.5}$
Bottom	$A_{0.8}$	$A_{1.2}$	$B_{0.8}$	$B_{1.2}$
I_n (% of $f_{R,1}$)	45	45	45	45
$F_{R,c}$ (4PBT)	5.18	5.18	10.07	10.07

Delayed CMOD deformation curves for SyFRC and SFRC mixes are depicted in Figure B.3. The long-term experimental results for SyFRC and SFRC mixes are collected in Table B.6.
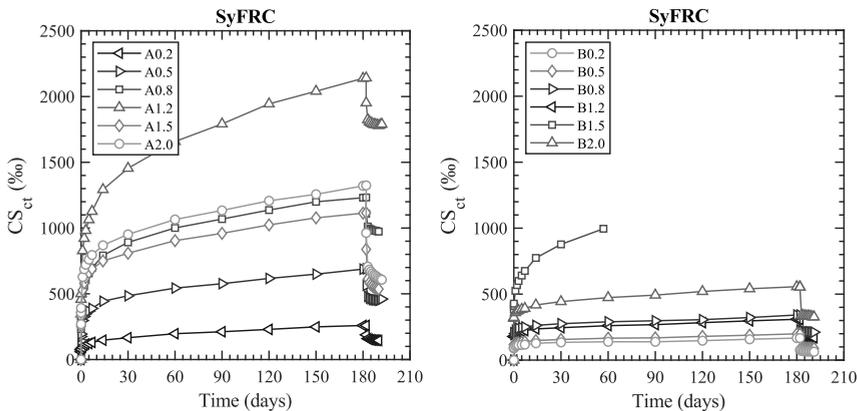
Figure B.3. WP1 programme CMOD delayed deformations in creep tests.

Table B.6. Delayed CMOD (in μm) in WP1 experimental programme.

Parameter [1]	SyFRC						SFRC					
	$A_{0.2}$	$A_{0.5}$	$A_{0.8}$	$A_{1.2}$	$A_{1.5}$	$A_{2.0}$	$B_{0.2}$	$B_{0.5}$	$B_{0.8}$	$B_{1.2}$	$B_{1.5}$	$B_{2.0}$
I_c (%)	--	45.1	55.0	57.8	48.0	49.7	--	30.7	44.5	43.50	64.2	52.0
$CMOD_{ci}$	58	141	225	341	245	251	89	116	194	178	380	317
$CMOD_{cd}^{14}$	147	444	792	1294	751	871	128	148	264	236	775	418
$CMOD_{cd}^{30}$	166	485	891	1457	808	953	135	156	276	246	878	444
$CMOD_{cd}^{60}$	196	542	1000	1655	903	1063	138	165	290	260	--	472
$CMOD_{cd}^{90}$	211	577	1068	1792	960	1134	138	169	298	269	--	493
$CMOD_{cd}^{120}$	230	618	1136	1940	1025	1207	148	179	309	283	--	519
$CMOD_{cd}^{150}$	248	648	1200	2039	1077	1255	157	188	322	298	--	541
$CMOD_{cd}^{180}$	258	688	1231	2140	1113	1320	167	199	343	309	--	557

[1] $CMOD_{ct}$ deformations are not compensated with shrinkage in this experimental programme since the use of shrinkage flexure specimens was later established.

Delayed compressive strain deformation curves for SyFRC and SFRC mixes are depicted in Figure B.4. The long-term experimental results for SyFRC and SFRC mixes are collected in Table B.7.
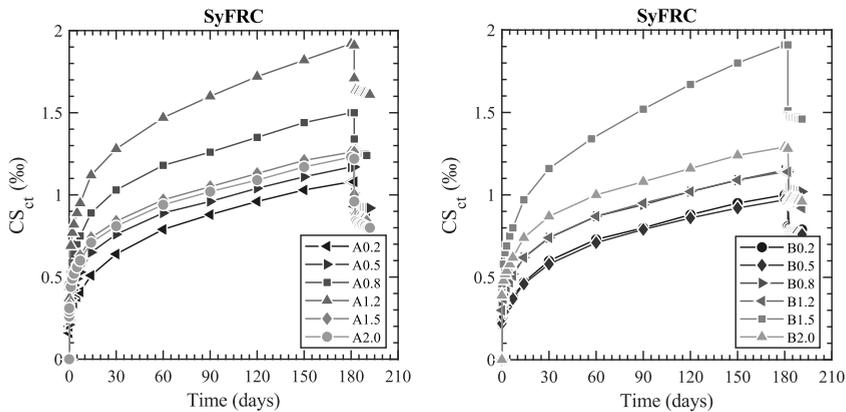
Figure B.4. WP1 compressive strains delayed deformations in creep tests.

Table B.7. Delayed compressive strains (in ‰) in WP1 experimental programme.

Parameter [1]	SyFRC						SFRC					
	$A_{0.2}$	$A_{0.5}$	$A_{0.8}$	$A_{1.2}$	$A_{1.5}$	$A_{2.0}$	$B_{0.2}$	$B_{0.5}$	$B_{0.8}$	$B_{1.2}$	$B_{1.5}$	$B_{2.0}$
CS_{ci}	0.16	0.21	0.28	0.36	0.26	0.25	0.21	0.22	0.32	0.30	0.42	0.39
CS_{cd}^{14}	0.51	0.65	0.89	1.12	0.74	0.71	0.47	0.46	0.62	0.62	0.97	0.74
CS_{cd}^{30}	0.64	0.77	1.03	1.28	0.84	0.82	0.60	0.58	0.74	0.74	1.16	0.87
CS_{cd}^{60}	0.79	0.89	1.17	1.47	0.97	0.94	0.72	0.70	0.86	0.87	1.36	1.00
CS_{cd}^{90}	0.88	0.96	1.26	1.60	1.05	1.02	0.80	0.79	0.94	0.95	1.52	1.08
CS_{cd}^{120}	0.96	1.04	1.35	1.72	1.13	1.10	0.88	0.86	1.02	1.02	1.68	1.16
CS_{cd}^{150}	1.03	1.10	1.44	1.82	1.21	1.16	0.95	0.92	1.09	1.09	1.78	1.24
CS_{cd}^{180}	1.08	1.17	1.50	1.92	1.26	1.23	1.00	0.97	1.15	1.14	1.91	1.29

The temperature and relative humidity in the climate room where the WP1 long-term tests were conducted are depicted in Figure B.5.
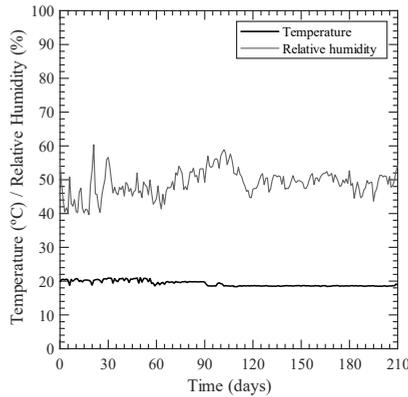
Figure B.5. Environmental conditions during WP1 long-term test.

B.4. Post-creep stage

Post-creep flexure tests followed the same flexure setup as pre-cracking tests. The assembled complete creep test curves (including the pre-cracking, creep and post-creep stages) are presented in Figure B.6. The post-creep residual strengths are collected in Table B.8. Note that some CMOD reference values for the residual performance were achieved during either the creep phase or the post-creep loading process. As explained in Section 6.1.3, the residual strengths obtained in those cases (marked in Table B.8) are not considered for the average residual stress calculation in the creep test report.
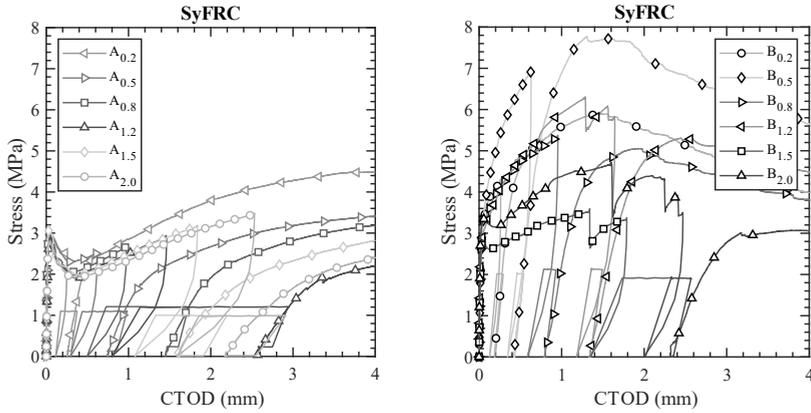
Figure B.6. WP1 post-creep test results.

Table B.8. WP1 post-creep performance.

Mix	Specimen	f_L (MPa)	$f_{R,1}$ (MPa)	$f_{Post-creepR,2}$ (MPa)	$f_{Post-creep,R,3}$ (MPa)	$f_{Post-creep,R,4}$ (MPa)
SyFRC	$A_{0.2}$	2.94	2.25	3.36	4.08	4.43
	$A_{0.5}$	3.01	2.43	2.25*	2.98	3.32
	$A_{0.8}$	2.98	2.19	-	2.47*	3.05
	$A_{1.2}$	2.91	2.08	-	-	1.93*
	$A_{1.5}$	3.14	2.06	-	1.93*	2.61*
	$A_{2.0}$	2.84	1.99	-	-	2.14*
	Average	2.97	2.17	3.36	3.53	3.60
SFRC	$B_{0.2}$	3.31	4.60	5.89	5.14	4.25
	$B_{0.5}$	3.36	6.56	7.70	6.83	6.03
	$B_{0.8}$	3.44	4.76	4.73*	4.66	4.00
	$B_{1.2}$	3.03	4.88	-	5.26	4.71
	$B_{1.5}$	2.86	2.97	-	-	-
	$B_{2.0}$	3.37	3.67	-	-	3.01
	Average	3.23	4.57	4.57	6.80	5.47

*Residual strength values achieved during the post-creep loading process.

Appendix C:
NAE1 creep experimental programme and results

The first experimental programme focused on assessing the neutral axis evolution (NAE) used on specimen SFRC of the WP1 programme. Then, the concrete matrix of the tested specimens is the same as that presented in Table B.1. To assess the NAE during both monotonic and long-term tests, five LVDTs were mounted as defined in Figure 113.

Appendix C presents the main experimental results obtained on each creep test phase (characterisation, pre-crack, creep and post-creep) of the NAE1 experimental programme.

C.1. FRC matrix characterisation tests results

The characterisation results of the SFRC mix correspond to the previously presented in Figure B.1 (right) and Table B.3.

C.2. Pre-cracking stage

The specimen was pre-cracked in a 4-point bending test (4PBT) setup with a 450 mm support span until 0.5 mm $CTOD_p$ and then unloaded. Crack mouth opening deformations (CMOD) were monitored with an LVDT placed in the bottom face, whereas the compressive strains with a 50 mm in length strain gauge in the top face of the specimen. Four additional LVDTs were side mounted in the specimen to record crack opening deformations at CTOD and 25 mm from the top face. Delayed recovery deformations after the unloading process were not registered since this procedure was later established.

Figure C.1 presents the pre-cracking test Stress-CTOD curves for the specimen. Table C.1 collects the experimental residual strength obtained.
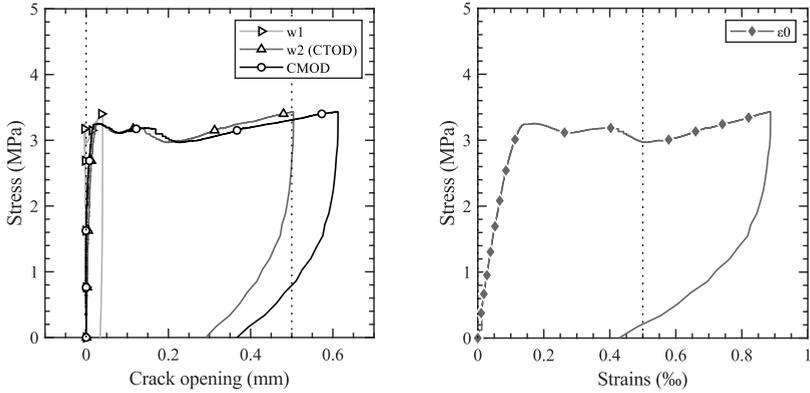
Figure C.1. Stress-CTOD and Stress-Strains curves of NAE1 pre-cracking test.

Table C.1. NAE-1 pre-cracking tests experimental results.

Specimen	f_L	$f_{R,1}$	$CTOD_p$	$CMOD_p$	$CMOD_{pri}$	$CMOD_{prd}$*
	(MPa)	(MPa)	(µm)	(µm)	(µm)	(µm)
NAE1-B2.2	3.25	3.31	504.1	612.5	366.9	-

* Delayed recovery assessment was not realised in this experimental programme

C.3. Creep stage

Single-specimen creep test was carried out in a 4PBT setup with a 450 mm support span due to the presence of the strain gauge. The applied stress ($f_{R,c}$) represented a creep index of 50% of the residual strength at pre-cracking tests ($f_{R,p}$). The specimen was unloaded after 180 days, and delayed recovery deformations were recorded for 30 days. No shrinkage specimen was used for this experimental programme. The evolution of $CMOD_{ct}$ and compressive strains during the long-term test is presented in Figure C.2.
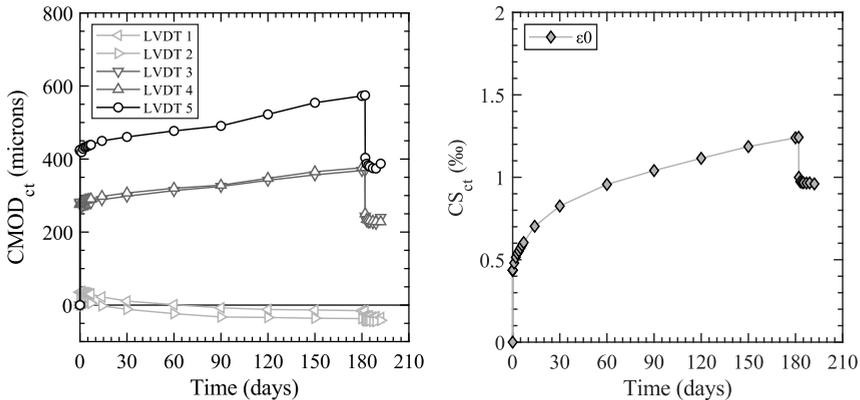
Figure C.2. NAE1 delayed CMOD and compressive strain in creep tests.

Table C.2 provides relevant data on the instantaneous deformation ($CMOD_{ci}$), total deformations ($CMOD_{ct}{}^{j}$) at different j days and unloading process recovery ($CMOD_{cri}$ and $CMOD_{crd}{}^{j}$). Compressive strain deformations are also provided at the same steps and time lapses.

Table C.2. NAE1 delayed deformations in creep tests of SyFRC specimens.

Parameter	Frame 1	Parameter	Frame 1
	NAE1-B2.2		NAE1-B2.2
$CMOD_{ci}$	422.3	CS_{ci}	0.435
$CMOD_{ci}{}^{10'}$	424.3	$CS_{ci}{}^{10'}$	0.436
$CMOD_{ci}{}^{30'}$	425.1	$CS_{ci}{}^{30'}$	0.437
$CMOD_{ct}{}^{1}$	380.8	$CS_{ct}{}^{1}$	0.480
$CMOD_{ct}{}^{2}$	389.2	$CS_{ct}{}^{2}$	0.515
$CMOD_{ct}{}^{3}$	393.4	$CS_{ct}{}^{3}$	0.538
$CMOD_{ct}{}^{5}$	395.9	$CS_{ct}{}^{5}$	0.571
$CMOD_{ct}{}^{7}$	399.1	$CS_{ct}{}^{7}$	0.604
$CMOD_{ct}{}^{14}$	408.9	$CS_{ct}{}^{14}$	0.703
$CMOD_{ct}{}^{30}$	418.8	$CS_{ct}{}^{30}$	0.826
$CMOD_{ct}{}^{60}$	433.8	$CS_{ct}{}^{60}$	0.957
$CMOD_{ct}{}^{90}$	446.2	$CS_{ct}{}^{90}$	1.041
$CMOD_{ct}{}^{120}$	474.9	$CS_{ct}{}^{120}$	1.115
$CMOD_{ct}{}^{150}$	503.9	$CS_{ct}{}^{150}$	1.186
$CMOD_{ct}{}^{180}$	522.5	$CS_{ct}{}^{180}$	1.243
$CMOD_{cri}$	366.8	CS_{cri}	1.000
$CMOD_{crd}{}^{1}$	352.0	$CS_{crd}{}^{1}$	0.974
$CMOD_{crd}{}^{2}$	347.9	$CS_{crd}{}^{2}$	0.970
$CMOD_{crd}{}^{3}$	345.2	$CS_{crd}{}^{3}$	0.967
$CMOD_{crd}{}^{5}$	341.0	$CS_{crd}{}^{5}$	0.965
$CMOD_{crd}{}^{7}$	340.1	$CS_{crd}{}^{7}$	0.966
$CMOD_{crd}{}^{10}$	352.3	$CS_{crd}{}^{30}$	0.960

Appendix D:
RRT creep experimental programme and results

The RILEM Technical Committee organised an international Round-Robin Test on creep. The RRT creep experimental programme is the contribution of my PhD to the RRT. The goal of the RRT was to determine the variability of creep results obtained by different procedures developed by international laboratories. The concrete matrix composition is defined in Table D.1. Fibre properties are described in Table D.2.

Table D.1. RRT concrete matrix composition in kg/m^3.

Component	SyFRC	SFRC
Cement CEM I 42.5 R	350	350
Water, w/c = 0.50	175	175
Aggregate 1 (12/20)	118	118
Aggregate 2 (6/12)	591	591
Sand 1	482	482
Sand 2	482	482
Sand 3	168	168
Superplasticizer	3.75	2.50
Fibres	10	30

Table D.2. Fibre properties and dosage of RRT experimental programme.

Mix	Series	Fibre		Dosage
		Brand	Length	(kg/m^3)
SyFRC	M-B1	Unknown	40	10
	M-B2			
SFRC	S-B1	50% 3D 65/60BG /50 % HE 90-60	60	30
	S-B2			

D.1. FRC matrix characterisation tests results

RRT characterisation tests followed the EN 14651 standard in a 3-point bending test (3PBT) with a 500 mm span. Although characterisation tests were performed for the RRT programme at different ages, this appendix only presents results at 28 days. The characterisation tests Stress-CMOD curves are shown in Figure D.1 and the residual stress values are collected in Table D.3.
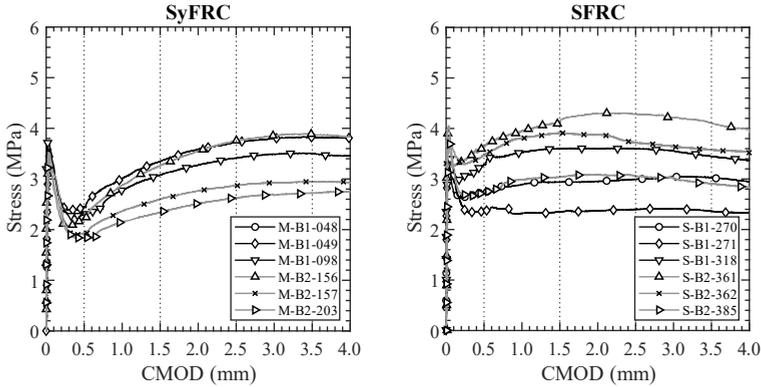
Figure D.1. Stress-CMOD chart form characterisation test of RRT programme.

Table D.3. RRT flexure characterisation tests results.

Batch	Specimen	f_L (MPa)	$f_{R,1}$ (MPa)	$f_{R,2}$ (MPa)	$f_{R,3}$ (MPa)	$f_{R,4}$ (MPa)
M-B1	M-B1-048	--	--	--	--	--
	M-B1-049	3.58	2.45	3.35	3.72	3.82
	M-B1-098	3.72	2.30	3.08	3.42	3.50
	Average	3.65	2.37	3.21	3.57	3.66
M-B2	M-B2-156	3.32	2.22	3.26	3.75	3.88
	M-B2-157	3.52	1.93	2.61	2.87	2.94
	M-B2-203	3.52	1.83	2.34	2.63	2.72
	Average	3.45	1.99	2.74	3.08	3.18
S-B1	S-B1-270	3.55	2.74	2.93	2.99	3.02
	S-B1-271	3.32	2.37	2.35	2.40	2.37
	S-B1-318	3.44	3.28	3.59	3.60	3.45
	Average	3.44	2.80	2.96	3.00	2.94
S-B2	S-B2-361	3.94	3.64	4.13	4.29	4.11
	S-B2-362	4.06	3.46	3.90	3.72	3.58
	S-B2-385	3.71	2.74	3.04	3.06	2.91
	Average	3.90	3.28	3.69	3.69	3.53

D.2. Pre-cracking stage

Specimens were pre-cracked in the 3PBT setup with a 500 mm support span until 0.5 mm $CMOD_p$. and then unloaded, and delayed recovery deformations were registered for 10 minutes after the unloading process. Crack mouth opening deformations (CMOD) were monitored with an LVDT placed in the bottom face of the specimen.

Figure D.2 presents the pre-cracking test Stress-CTOD curves for each specimen. Table D.4 collects the residual strength experimentally obtained and the average values for each mix.
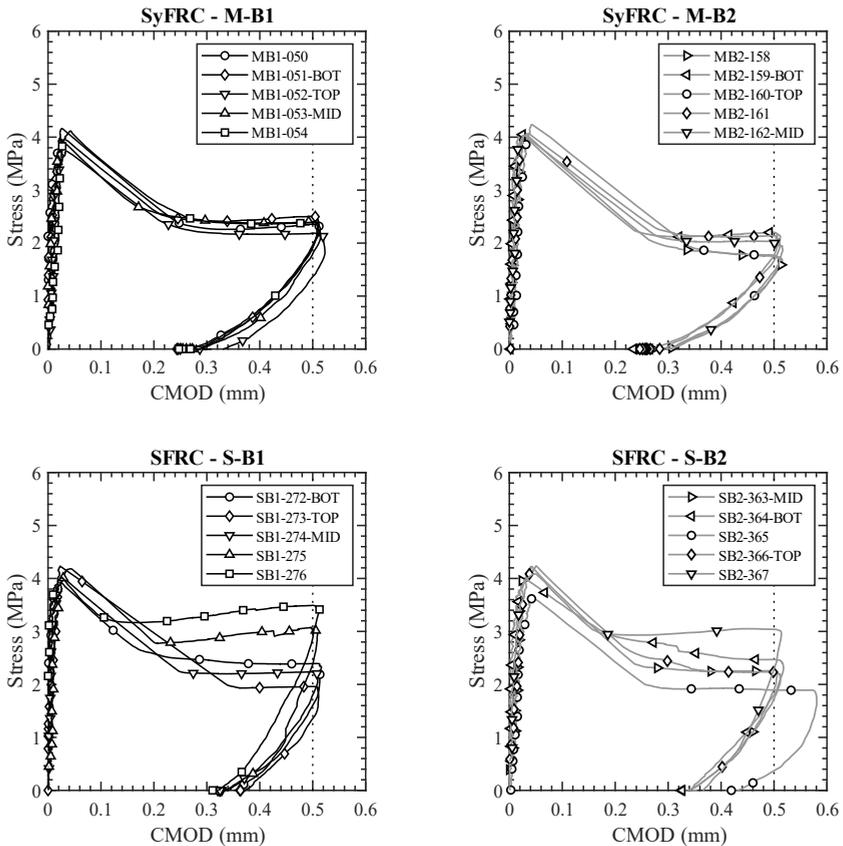
Figure D.2. Pre-cracking test Stress-CMOD chart of RRT experimental programme.

Table D.4. RRT pre-cracking tests experimental results.

Mix	Batch	Specimen	f_L	$f_{R,1}$	$CMOD_p$	$CMOD_{pri}$	$CMOD_{prd}$
			(MPa)	(MPa)	(µm)	(µm)	(µm)
SyFRC	M-B1-	050	4.19	2.36	514.4	276.4	221.6
		051	3.98	2.51	511.4	287.1	242.0
		052	3.75	2.19	523.1	337.7	282.6
		053	3.98	2.40	515.2	293.9	249.4
		054	4.13	2.39	509.8	292.3	248.7
		Average	4.01	2.37	514.8	297.5	248.9
	M-B2-	158	4.09	1.75	515.7	306.9	254.6
		159	4.07	2.21	511.8	277.0	233.4
		160	4.25	1.77	509.9	311.8	261.1
		161	4.09	2.13	511.1	291.4	253.6
		162	4.05	2.04	516.5	307.6	254.9
		Average	4.11	1.98	513.0	298.9	251.5
SFRC	S-B1-	272	3.94	2.39	516.5	357.1	340.1
		273	4.26	1.96	511.2	375.2	365.9
		274	4.04	2.24	511.3	345.2	323.7
		275	4.20	3.02	509.4	338.3	324.8
		276	4.04	3.50	514.4	326.8	307.1
		Average	4.09	2.62	512.6	348.5	332.3
	S-B2-	363	4.24	2.26	506.7	341.8	313.3
		364	4.00	2.47	518.0	344.3	322.8
		365	3.63	1.89	580.7	437.7	412.7
		366	4.23	2.23	512.2	344.6	322.2
		367	4.11	3.04	514.1	373.5	349.2
		Average	4.04	2.38	526.3	368.4	344.1

D.3. Creep stage

Creep tests were carried out in a multi-specimen setup with three specimens per frame. The 4PBT setup with a 450 mm support span was used to improve the stability of the stacked specimens. One LVDT at the bottom face of the specimen recorded delayed CMOD deformations during the test duration. Specimens were loaded to 45% of $f_{R,1}$ creep index. After 360 days of sustained load, specimens were unloaded, and recovery capacity was recorded for 30 days. Shrinkage flexure specimens were not used in the RRT experimental programme. Table D.5 provides the relative position of each specimen in the creep frame, as well as the applied load.

Table D.5. RRT relative position of specimens on the creep frames.

Position	Frame			
	F1	F2	F3	F4
Top	M-B1-052	M-B2-160	S-B1-273	S-B2-366
Middle	M-B1-053	M-B2-162	S-B1-274	S-B2-363
Bottom	M-B1-051	M-B2-159	S-B1-272	S-B2-364
I_n (% of $f_{R,1}$)	45	45	45	45
$F_{R,c}$ (4PBT)	5.68	4.72	5.25	5.50

Delayed CMOD deformation curves for SyFRC and SFRC mixes are depicted in Figure D.3. The long-term experimental results for SyFRC and SFRC mixes are collected in Table D.6 and Table D.7, respectively.
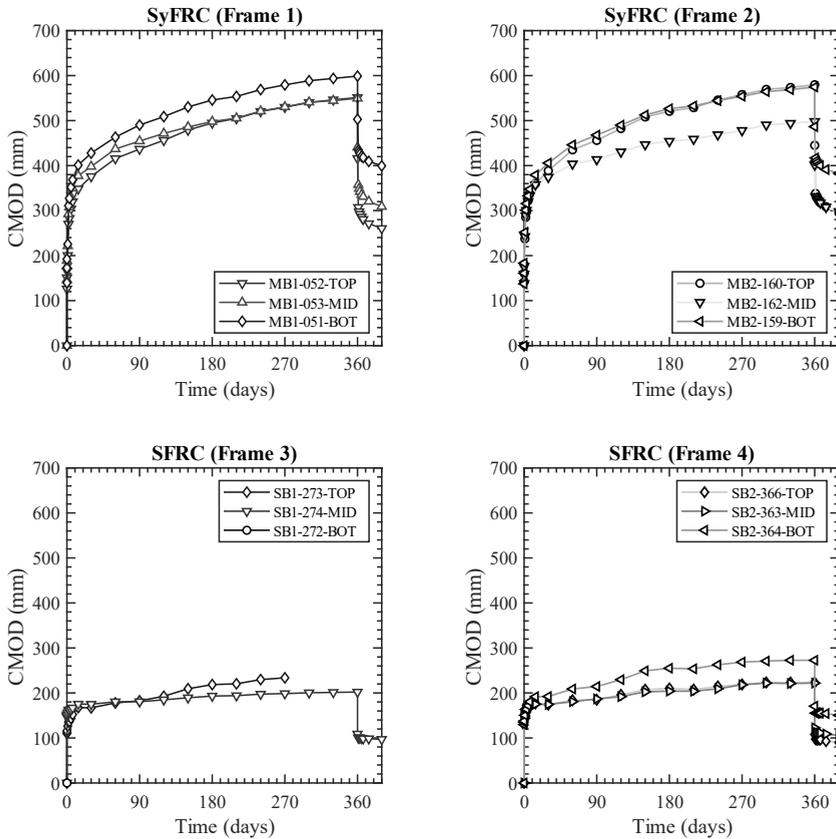
Figure D.3. RRT delayed deformations in creep tests of SyFRC specimens.

Table D.6. RRT delayed experimental results of SyFRC specimens.

Parameter	Frame 1			Frame 2		
	M-B1-052	M-B1-053	M-B1-051	M-B2-160	M-B2-162	M-B2-159
$CMOD_{ci}$	126.0	146.4	139.8	141.5	138.2	137.3
$CMOD_{ci}^{10'}$	150.9	176.4	172.6	160.9	159.2	161.1
$CMOD_{ci}^{30'}$	166.1	189.0	192.1	180.6	176.3	183.3
$CMOD_{ct}^{1}$	200.3	221.6	225.5	237.3	242.5	252.0
$CMOD_{ct}^{2}$	270.2	292.3	311.0	285.1	288.7	301.1
$CMOD_{ct}^{3}$	283.0	307.7	327.3	299.7	300.7	315.7
$CMOD_{ct}^{5}$	303.6	330.0	352.1	322.0	320.4	332.8
$CMOD_{ct}^{7}$	320.1	349.9	368.5	337.6	333.5	347.5
$CMOD_{ct}^{14}$	348.3	377.3	401.1	359.8	357.5	379.2
$CMOD_{ct}^{30}$	375.8	398.0	427.8	388.5	374.3	405.6
$CMOD_{ct}^{60}$	415.6	437.0	463.2	435.2	403.8	446.2
$CMOD_{ct}^{90}$	436.6	454.5	490.1	456.1	413.6	467.8
$CMOD_{ct}^{120}$	456.1	471.5	508.8	482.5	430.6	490.0
$CMOD_{ct}^{150}$	479.0	485.8	530.3	508.2	446.8	512.5
$CMOD_{ct}^{180}$	494.6	497.9	545.7	520.7	454.1	526.5
$CMOD_{ct}^{210}$	504.7	505.5	553.7	528.9	458.8	532.5
$CMOD_{ct}^{240}$	520.3	521.1	568.9	545.6	468.6	544.4
$CMOD_{c}^{270}$	529.7	530.4	579.4	557.7	478.2	554.2
$CMOD_{ct}^{300}$	540.2	540.9	588.6	569.3	490.5	564.4
$CMOD_{ct}^{330}$	546.2	544.3	593.7	573.6	493.9	568.7
$CMOD_{ct}^{360}$	551.3	549.5	598.9	579.6	498.2	574.7
$CMOD_{cri}$	416.0	440.7	502.9	445.1	401.4	486.4
$CMOD_{crd}^{1}$	307.2	357.6	434.4	338.0	331.2	417.1
$CMOD_{crd}^{2}$	297.8	349.0	430.1	330.3	327.8	411.1
$CMOD_{crd}^{3}$	291.8	342.2	425.8	327.7	324.3	406.8
$CMOD_{crd}^{5}$	286.0	335.5	420.8	321.9	321.1	402.6
$CMOD_{crd}^{7}$	280.7	331.0	418.1	318.3	317.5	399.9
$CMOD_{crd}^{14}$	271.0	320.5	409.4	308.7	307.9	391.2
$CMOD_{crd}^{30}$	260.3	309.0	399.4	295.4	298.0	382.9

Table D.7. RRT delayed experimental results of SFRC specimens.

Parameter	Frame 3		Frame 4			
	S-B1-273 [1]	S-B1-274	S-B1-272 [2]	S-B2-366	S-B2-363	S-B2-364
$CMOD_{ci}$	110.1	146.7	-	129.2	143.2	129.8
$CMOD_{ci}^{10'}$	111.3	149.0	-	134.3	146.7	134.9
$CMOD_{ci}^{30'}$	115.9	151.7	-	137.9	149.3	137.6
$CMOD_{ct}^{1}$	126.4	156.1	-	148.2	156.2	150.5
$CMOD_{ct}^{2}$	135.5	161.5	-	159.6	164.7	163.3
$CMOD_{ct}^{3}$	136.4	162.3	-	159.6	164.7	164.1
$CMOD_{ct}^{5}$	143.2	164.0	-	165.6	169.0	171.8
$CMOD_{ct}^{7}$	152.0	166.7	-	170.8	170.8	180.6
$CMOD_{ct}^{14}$	167.4	175.3	-	176.8	175.1	191.7
$CMOD_{ct}^{30}$	167.0	175.0	-	174.1	174.5	192.2
$CMOD_{ct}^{60}$	177.8	180.4	-	183.8	180.7	208.9
$CMOD_{ct}^{90}$	182.6	180.6	-	184.9	186.9	214.4
$CMOD_{ct}^{120}$	192.6	184.8	-	195.9	191.9	229.6
$CMOD_{ct}^{150}$	209.3	189.3	-	207.3	202.6	249.3
$CMOD_{ct}^{180}$	218.6	193.2	-	210.1	204.1	255.0
$CMOD_{ct}^{210}$	220.3	194.0	-	207.6	203.9	253.7
$CMOD_{ct}^{240}$	229.7	197.5	-	214.4	209.3	262.7
$CMOD_{c}^{270}$	233.6	198.6	-	218.9	218.2	268.6
$CMOD_{ct}^{300}$	-	200.4	-	223.3	221.9	270.9
$CMOD_{ct}^{330}$	-	201.3	-	223.3	221.1	272.6
$CMOD_{ct}^{360}$	-	202.0	-	223.3	221.9	272.6
$CMOD_{cri}$	-	108.8	-	107.6	122.6	170.7
$CMOD_{crd}^{1}$	-	100.2	-	97.4	111.4	155.3
$CMOD_{crd}^{2}$	-	100.2	-	97.4	111.4	155.3
$CMOD_{crd}^{3}$	-	100.2	-	96.5	111.4	156.1
$CMOD_{crd}^{5}$	-	99.5	-	96.6	110.7	155.5
$CMOD_{crd}^{7}$	-	98.5	-	96.5	111.4	155.3
$CMOD_{crd}^{14}$	-	98.4	-	93.0	108.8	154.2
$CMOD_{crd}^{30}$	-	96.9	-	89.8	105.5	150.3

[1] Transducer failed at 270 days of test; [2] transducer corrupted

The temperature (in ºC) and relative humidity (in %) recorded in the climate room where the RRT long-term tests were conducted are depicted in Figure D.4.
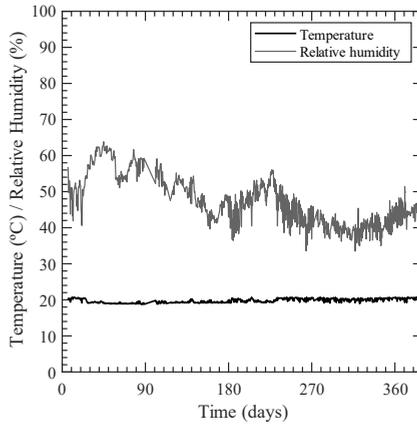
Figure D.4. Environmental conditions during RRT long-term test.

D.4. Post-creep stage

Post-creep flexure tests followed the same flexure setup as pre-cracking tests. The assembled complete creep test curves are presented in Figure D.5. The post-creep residual strengths are collected in Table D.8.
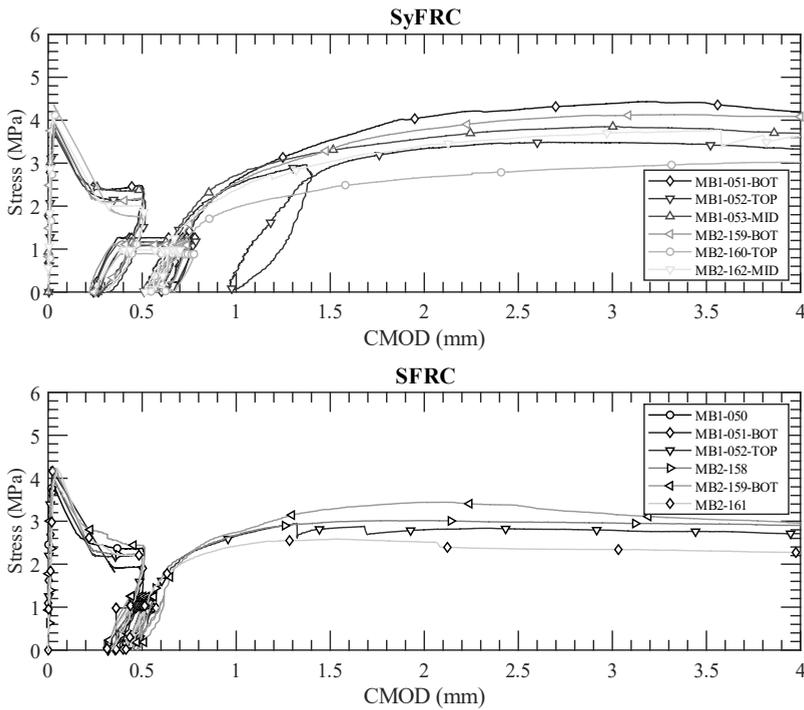
Figure D.5. RRT post-creep test results.

Table D.8. RRT post-creep performance.

Mix	Batch	Specimen	f_L (MPa)	$f_{R,1}$ (MPa)	$f_{Post-creepR,2}$ (MPa)	$f_{Post-creep,R,3}$ (MPa)	$f_{Post-creep,R,4}$ (MPa)
SyFRC	M-B1-	051	3.98	2.51	3.98	2.51	3.55
		052	3.75	2.19	3.75	2.19	2.91
		053	3.98	2.40	3.98	2.40	3.32
		Average	3.90	2.37	3.26	3.86	3.93
	M-B2-	159	4.07	2.21	3.34	4.05	4.18
		160	4.25	1.77	2.44	2.83	3.02
		162	4.05	2.04	3.06	3.63	3.79
		Average	4.12	2.01	2.95	3.50	3.66
SFRC	S-B1-	272	3.94	2.39	-	-	-
		273	4.26	1.96	-	-	-
		274	4.04	2.24	2.86	2.86	2.79
		Average	4.08	2.20	2.86	2.86	2.79
	S-B2-	363	4.24	2.26	3.01	3.02	2.97
		364	4.00	2.47	3.31	3.42	3.09
		366	4.23	2.23	2.60	2.38	2.34
		Average	4.16	2.32	2.97	2.94	2.80

Appendix E:
WP2 creep experimental programme and results

The WP2 experimental programme continues the WP1 programme, where the $CMOD_p$ is assessed. However, this experimental programme includes the influence of the creep index (I_c) assessment with 25, 35 and 35% applied creep index. Regarding the pre-cracking level ($CMOD_p$), this experimental programme considers low pre-cracking levels: 0.05, 0.1, 0.2, 0.3 and 0.5 mm. For this purpose, two batches from one SFRC series reinforced with 50 kg/m³ of steel fibres were cast with the same concrete matrix presented in Table E.1. The fibre properties are shown in Table E.2.

Table E.1. WP2 concrete matrix composition in kg/m³.

Component	Dosage
Cement CEM I 42.5 R	410
Water, w/c = 0.41	170
Coarse aggregate (6/12)	825
Sand	935
Superplasticizer	3.4
Fibres	50

Table E.2. Fibre properties of the WP2 experimental programme.

Mix	Fibre			Dosage
	Material	Length	Diameter	(kg/m³)
SFRC	Steel	50	1.0	50

This Appendix presents the main experimental results obtained on each creep test phase (characterisation, pre-crack, creep and post-creep) of the WP2 experimental programme.

E.1. FRC matrix characterisation tests results

Characterisation flexure tests were conducted in a 3-point bending test (3PBT) setup with a 500 mm support span until 3.5 mm CMOD to obtain the residual stresses defined in EN 14651. The characterisation tests Stress-CMOD curves are presented in Figure E.1 and the residual stress values are collected in Table E.3.
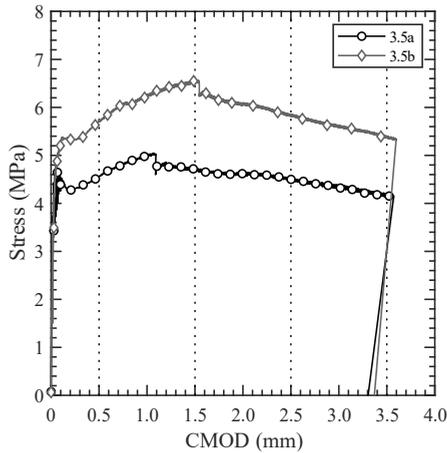
Figure E.1 WP2 characterisation tests experimental curves.

Table E.3. WP2 characterisation test results.

Batch	f_{ck} (MPa)	Specimen	f_L (MPa)	$f_{R,1}$ (MPa)	$f_{R,2}$ (MPa)	$f_{R,3}$ (MPa)	$f_{R,4}$ (MPa)
A	41.7	3.5a	3.74	4.56	4.72	4.53	4.62
B	39.2	3.5b	3.60	5.70	6.57	5.86	5.39
		Average	3.67	5.13	5.65	5.20	5.01

E.2. Pre-cracking stage

Specimens were pre-cracked in a 3PBT setup with a 500 mm support span until 0.05, 0.1, 0.2, 0.3 and 0.5 mm $CMOD_p$ and then unloaded. Crack opening deformations were monitored during the pre-cracking test with one clip gauge at the crack mouth opening displacement (CMOD) level crossing the notch. Delayed recovery deformations after the unloading process were not registered since this procedure was later established.

Figure E.2 presents the pre-cracking test Stress-CTOD curves for each specimen. Table E.4 collects the residual strength experimentally obtained and the average values for each mix.
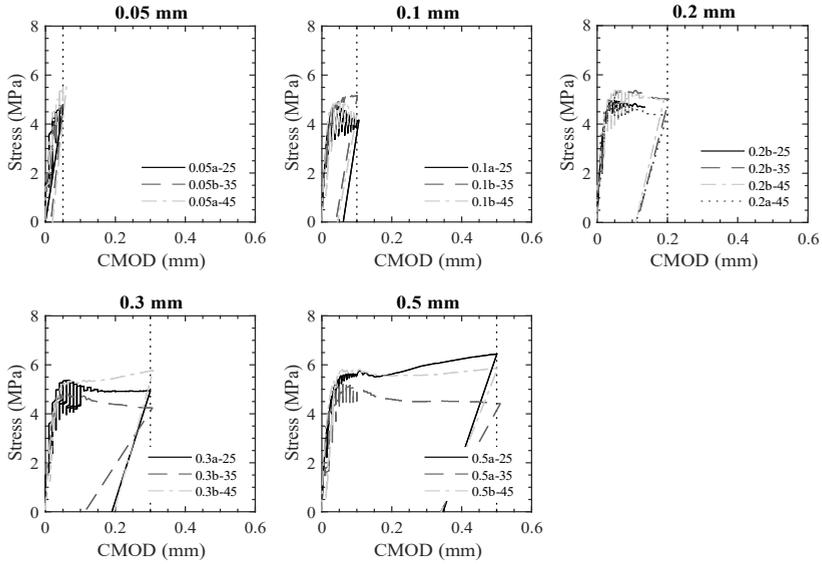
Figure E.2 WP2 pre-cracking tests experimental curves.

Table E.4. WP2 pre-cracking tests experimental results.

Specimen	f_L	$f_{R,p}$					$CMOD_p$	$CMOD_{pri}$
		0.05	0.1	0.2	0.3	0.5	(µm)	(µm)
0.05a-25	4.24	4.78					52	28
0.05b-35	3.90	4.79					51	15
0.05a-45	3.58	5.27					56	21
0.1a-25	4.00		4.04				106	61
0.1b-35	3.54		5.15				102	40
0.1b-45	4.66		4.35				100	45
0.2b-25	3.96			4.69[*]			137[*]	--[*]
0.2b-35	3.88			5.02			205	113
0.2a-45	3.72			4.39			205	114
0.2b-45	4.16			4.96			195	112
0.3a-25	4.20				4.94		300	191
0.3b-35	3.25				4.25		306	113
0.3b-45	4.27				5.75		308	195
0.5a-25	3.99					6.44	501	347
0.5a-35	4.41					4.42	512	340
0.5b-45	5.35					5.85	503	341
Average	4.03	4.95	4.51	4.77	4.98	5.39	--	--

E.3. Creep stage

Creep tests were carried out in a multi-specimen setup with two or three specimens per frame. Table E.5 provides the relative position of each specimen in the creep frame, as well as the applied load. The 4-point bending test (4PBT) setup with 450 mm support span was used to improve the stability of the stacked specimens. Dial gauges at the CMOD level were used to register crack opening deformations of each specimen during creep tests. Three creep indexes referred to the residual strength at pre-cracking tests ($f_{R,p}$) were applied: 25, 35 and 45%. Two creep frames were destined per creep index. One shrinkage flexure specimen per mix was tested simultaneously. The long-term test duration was 180 days. Specimens were unloaded and delayed recovery deformations recorded for 30 days.

Table E.5. WP2 relative position of specimens on the creep frames.

Position	Frame					
	F1	F2	F3	F4	F5	F6
Top	0.05a-25	0.3b-35	0.2b-25	0.05b-35	0.05a-45	0.3b-45
Middle	-	-	0.3a-25	0.5a-35	0.1b-45	0.5b-45
Bottom	01a-25	0.2b-35	0.5a-25	0.1b-35	0.2b-45	0.2a-45
I_n (% of $f_{R,1}$)	25	35	25	35	45	45
$F_{R,c}$ (4PBT)	6.3	8.9	6.3	8.9	11.3	10.6

Delayed CMOD deformation curves are depicted in Figure E.3 and experimental results are collected in Table E.6, Table E.7 and Table E.8.
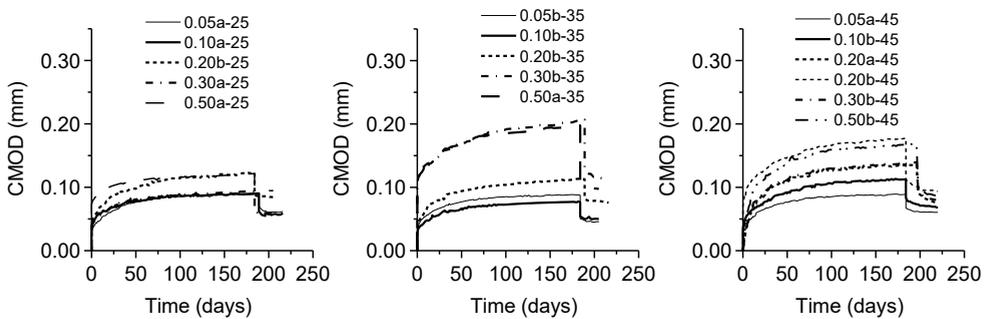

Figure E.3 WP2 delayed CMOD in the creep test.

Table E.6. WP2 long-term experimental results from specimens subjected to 25% creep index.

Parameter	Specimen				
	0.05a-25	0.1a-25	0.2b-25	0.3a-25	0.5a-25
$f_{R,c}$	1.3	1.35	1.31	1.35	1.38
I_c (% of $f_{R,1}$)	24.1	25.0	24.3	25.0	25.6
I_c (% of $f_{R,p}$)	27.2	33.3	27.7	27.3	21.4
$CMOD_{ci}$	21.0	31.0	35.0	32.0	32.0
$CMOD_{cts}^{14}$	52.2	60.4	67.5	55.1	89.5
$CMOD_{cts}^{30}$	62.0	66.3	81.2	65.9	97.6
$CMOD_{cts}^{60}$	73.6	75.8	91.0	72.8	102.6
$CMOD_{cts}^{90}$	79.2	80.1	100.9	78.3	105.3
$CMOD_{cts}^{120}$	80.2	81.6	103.3	79.5	106.5
$CMOD_{cts}^{150}$	80.7	83.1	105.0	81.5	107.0
$CMOD_{cts}^{180}$	81.1	84.6	106.2	82.5	107.8
$CMOD_{cris}$	59.1	53.6	71.7	51.5	42.8
$CMOD_{crds}^{30}$	49.1	48.6	66.7	46.5	39.8

Table E.7. WP2 long-term experimental results from specimens subjected to 35% creep index.

Parameter	Specimen				
	0.05b-35	0.1b-35	0.2b-35	0.3b-35	0.5a-35
$f_{R,c}$	1.8	1.9	1.9	1.8	2.0
I_c (% of $f_{R,1}$)	33.7	35.0	34.9	33.7	36.2
I_c (% of $f_{R,p}$)	38.0	36.7	37.5	42.8	44.1
$CMOD_{ci}$	17.0	22.0	30.0	98.0	90.0
$CMOD_{cts}^{14}$	53.0	44.1	70.6	135.4	134.6
$CMOD_{cts}^{30}$	60.7	55.9	77.7	155.3	151.4
$CMOD_{cts}^{60}$	69.0	60.8	91.9	169.3	170.3
$CMOD_{cts}^{90}$	71.4	62.3	97.6	183.6	174.8
$CMOD_{cts}^{120}$	71.7	63.1	102.0	191.1	179.7
$CMOD_{cts}^{150}$	72.0	64.2	105.1	195.8	183.8
$CMOD_{cts}^{180}$	72.2	64.9	107.0	199.6	186.0
$CMOD_{cris}$	45.7	49.5	86.0	123.6	96.5
$CMOD_{crds}^{30}$	38.7	44.5	76.0	90.6	82.5

Table E.8. WP2 long-term experimental results from specimens subjected to 45% creep index.

Parameter	Specimen					
	0.05a-45	0.1b-45	0.2a-45	0.2b-45	0.3b-45	0.5b-45
$f_{R,c}$	2.3	2.3	2.3	2.5	2.3	2.5
I_c (% of $f_{R,1}$)	42.1	43.4	43.4	47.1	43.4	45.6
I_c (% of $f_{R,p}$)	42.7	53.5	53.3	51.1	40.7	42.1
$CMOD_{ci}$	25.0	25.0	49.0	65.0	51.0	71.0
$CMOD_{cts}^{14}$	54.9	68.3	74.9	116.3	83.6	99.9
$CMOD_{cts}^{30}$	68.4	80.1	98.3	133.1	104.9	119.8
$CMOD_{cts}^{60}$	79.5	95.2	115.8	149.7	125.1	143.8
$CMOD_{cts}^{90}$	84.7	103.9	125.6	164.9	133.2	156.6
$CMOD_{cts}^{120}$	85.8	107.5	129.5	171.0	138.1	161.0
$CMOD_{cts}^{150}$	86.4	110.0	133.0	174.0	141.2	164.5
$CMOD_{cts}^{180}$	88.4	112.3	135.5	176.3	143.2	167.0
$CMOD_{cris}$	67.4	83.8	95.0	114.3	101.7	97.5
$CMOD_{crds}^{30}$	61.4	67.8	78.0	93.3	86.7	82.5

The temperature and relative humidity in the climate room where the WP2 long-term tests were conducted are depicted in Figure E.4.
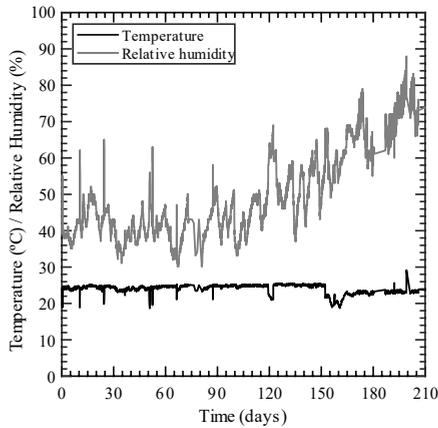

Figure E.4 Environmental conditions during WP2 long-term test.

E.4. Post-creep stage

Post-creep flexure tests were carried out following the same flexure setup as the pre-cracking tests. The post-creep residual strengths are collected in Table E.9. The assembled complete creep test curves are presented in Figure E.5.

Table E.9. WP2 post-creep performance.

| Specimen	f_L (MPa)	$f_{R,p}$ (MPa)	$f_{R,1}$ (MPa)	$f_{Post-creep,R,1}$	$f_{Post-creep,R,2}$ (MPa)	$f_{Post-creep,R,3}$ (MPa)	$f_{Post-creep,R,4}$ (MPa)
0.05a-25	4.24	4.78	-	4.66	5.72	5.1	4.59
0.05b-35	3.90	4.79	-	6.28	6.98	7.18	6.71
0.05a-45	3.58	5.27	-	7.99	9.08	8.36	7.68
0.1a-25	4.00	4.04	-	4.13	4.83	4.99	4.81
0.1b-35	3.54	5.15	-	6.13	6.94	6.89	6.61
0.1b-45	4.66	4.35	-	4.54	4.54	4.89	4.19
0.2b-25	3.96	4.69[*]	-	5.11	5.81	5.55	4.85
0.2b-35	3.88	5.02	-	6.02	7.23	7.59	7.24
0.2a-45	3.72	4.39	-	5.62	6.31	6.10	5.84
0.2b-45	4.16	4.96	-	4.95	6.41	6.61	6.15
0.3a-25	4.20	4.94	-	4.94	5.77	5.54	4.88
0.3b-35	3.25	4.25	-	4.63	5.41	5.58	4.88
0.3b-45	4.27	5.75	-	6.4	7.96	8.44	8.01
0.5a-25	3.99	-	6.44	-	8.51	8.22	7.57
0.5a-35	4.41	-	4.42	-	5.12	5.45	5.28
0.5b-45	5.35	-	5.85	-	7.38	8.05	7.29
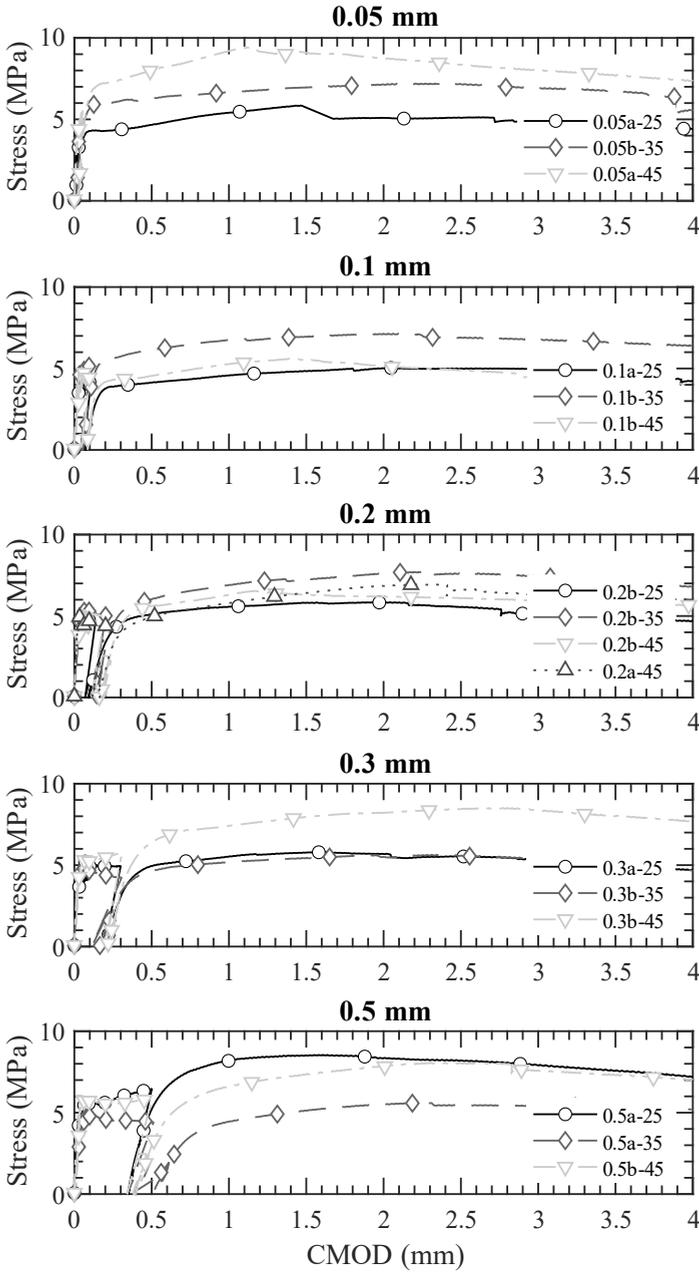
Figure E.5 WP2 post-creep test results.

Appendix F:
OC2 creep experimental programme and results

The OC2 experimental programme consists of three series of concrete: plain concrete (series A), GFRC with 10 kg /m^3 (Series B) and GFRC with 20 kg /m^3 (Series C). The concrete matrix composition is given in Table F.1. This experimental programme aimed to assess the long-term behaviour of GFRC. The shrinkage procedure was defined, and one shrinkage flexure specimen per mix was used for the first time. Fibre properties are described in Table F.2.

Table F.1. OC2 concrete matrix composition in kg/m^3.

Component	Series		
	A	B	C
Cement CEM I 42.5 R	400	400	400
Water, w/c = 0.50	200	200	200
Aggregate 1 (7/12)	500	500	500
Aggregate 2 (4/6)	250	250	250
Sand	900	900	900
Filler	70	70	70
Superplasticizer	2.2	2.8	2.8
Fibres	0	10	20

Table F.2. Fibre properties and dosage of OC2 experimental programme.

Series	Mix	Fibre		Dosage
		Material	Length	(kg/m^3)
B	GFRC	Glass	43	10
C	GFRC	Glass	43	20

F.1. FRC matrix characterisation tests results

FRC matrix characterisation tests followed the EN 14651 standard in a 3-point bending test (3PBT) with a 500 mm span. The characterisation tests Stress-CMOD curves are presented in Figure F.1, and the residual stress values are collected in Table F.3.
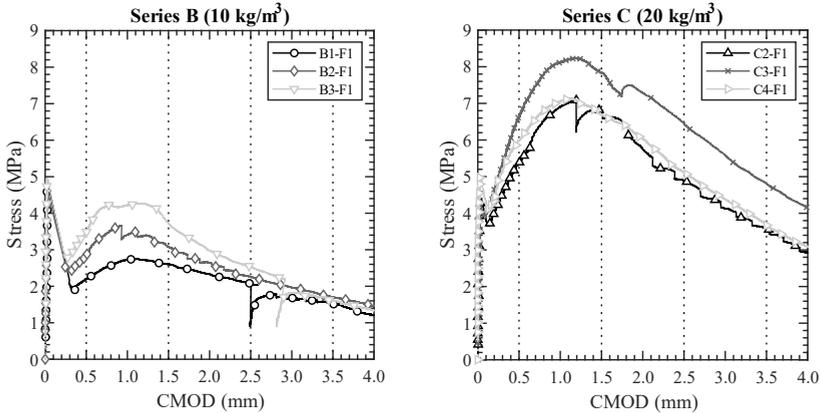

Figure F.1. Stress-CMOD chart form characterisation specimens of OC2 experimental programme.

Table F.3. OC2 characterization test results.

Series	f_{ck} (MPa)	Specimen	f_L (MPa)	$f_{R,1}$ (MPa)	$f_{R,2}$ (MPa)	$f_{R,3}$ (MPa)	$f_{R,4}$ (MPa)
A	65.4	A1-F1	5.09	--	--	--	--
		A1-F2	5.55	--	--	--	--
		A1-F3	5.10	--	--	--	--
		Average	5.25	--	--	--	--
B	60.6	B1-F1	4.73	2.19	2.60	2.07	1.55
		B2-F1	4.62	2.83	3.07	2.25	1.71
		B3-F1	4.94	3.47	3.72	2.54	1.61
		Average	4.76	2.83	3.13	2.29	1.62
C	61.2	C2-F1	4.31	5.38	6.80	4.89	3.58
		C3-F1	4.31	6.64	7.84	6.45	4.81
		C4-F1	4.99	5.98	6.70	5.11	3.68
		Average	4.54	6.00	7.11	5.48	4.02

F.2. Pre-cracking stage

Specimens were pre-cracked in a 3PBT setup with a 500 mm support span until 0.5 mm $CMOD_p$. and then unloaded and delayed recovery deformation after the unloading process was registered for 10 minutes. Crack mouth opening deformations (CMOD) were monitored using an LVDT placed in the bottom face of the specimen. Figure F.2 presents the pre-cracking test Stress-CTOD curves for each specimen. Table F.4 collects the residual strength experimentally obtained and the average values for each mix.
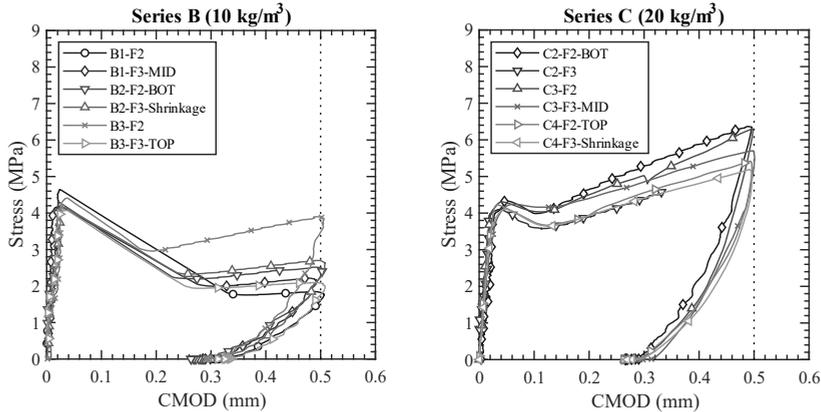

Figure F.2. Pre-cracking test Stress-CMOD chart of OC2 programme.

Table F.4. OC2 pre-cracking test results.

Series	Specimen	f_L (MPa)	$f_{R,1}$ (MPa)	$CMOD_p$ (µm)	$CMOD_{pri}$ (µm)	$CMOD_{prd}^{10'}$ (µm)
B	B1-F2	4.67	1.85	510.4	332.5	312.4
	B1-F3	4.21	2.22	497.6	313.4	276.0
	B2-F2	4.32	2.52	510.1	300.0	273.0
	B2-F3	4.16	2.71	512.9	333.8	308.4
	B3-F2	4.44	3.91	514.6	316.7	291.8
	B3-F3	4.08	2.10	514.8	341.9	313.2
	Average	4.31	2.55	510.1	323.0	295.8
C	C2-F2	4.36	6.38	507.2	292.3	266.5
	C2-F3	4.18	--	--	--	--
	C3-F2	4.33	6.32	503.3	296.8	266.9
	C3-F3	4.19	5.72	506.4	319.8	291.3
	C4-F2	4.28	5.45	503.6	294.3	266.3
	C4-F3	4.14	5.23	504.9	300.4	266.8
	Average	4.25	5.82	505.1	300.7	271.6

F.3. Creep stage

Creep tests were carried out in a multi-specimen setup with three specimens per frame. Table F.5 provides the relative position of each specimen in the creep frame, as well as the applied load. The 4-point bending test (4PBT) setup with 450 mm support span was used to improve the stability of the stacked specimens. One LVDT was used to record delayed deformations during the creep test. A creep index of 50% of $f_{R,p}$ at 0.5 mm $CMOD_p$ was applied. One shrinkage flexure specimen per mix was tested simultaneously. The long-term test duration was 390 days and then specimens were unloaded, and delayed recovery deformations recorded for 30 days.

Table F.5. OC2 relative position of specimens on the creep frames.

Position	Frame	
	F1	F2
Top	B3-F3	C4-F2
Middle	B1-F3	C3-F3
Bottom	B2-F2	C2-F2
I_n (% of $f_{R,1}$)	50	50
$F_{R,c}$ (4PBT)	5.51	15.06

Delayed CMOD deformation curves for SyFRC and SFRC mixes are depicted in Figure F.3. The long-term experimental results for SyFRC and SFRC mixes are collected in Table F.6 and Table F.7, respectively.
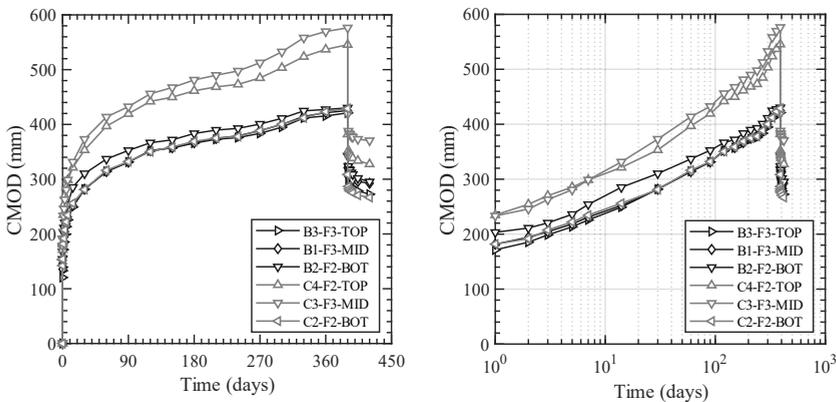

Figure F.3. OC2 delayed deformations in creep tests.

Table F.6. OC2 delayed experimental results of Series B.

Parameter	Serie B			
	B3-F3	B1-F3	B2-F2	Mean (CV)
$CMOD_{ci}$	118.2	134.1	153.1	135.1 (13.0)
$CMOD_{cts}^{14}$	249.1	252.0	285.2	262.1 (7.6)
$CMOD_{cts}^{30}$	281.7	281.8	310.2	291.2 (5.6)
$CMOD_{cts}^{60}$	314.3	313.9	336.8	322.7 (4.1)
$CMOD_{cts}^{90}$	331.4	331.1	352.5	338.3 (3.6)
$CMOD_{cts}^{120}$	351.6	352.2	366.5	357.8 (2.4)
$CMOD_{cts}^{150}$	357.1	357.5	371.8	362.2 (2.3)
$CMOD_{cts}^{180}$	365.8	366.6	383.4	372.0 (2.7)
$CMOD_{cts}^{210}$	372.8	374.5	389.7	379.0 (2.4)
$CMOD_{cts}^{240}$	375.9	379.2	392.8	383.6 (2.3)
$CMOD_{cts}^{270}$	383.6	388.6	400.6	391.0 (2.2)
$CMOD_{cts}^{300}$	394.9	400.0	411.1	402.0 (2.1)
$CMOD_{cts}^{330}$	411.7	414.5	424.7	417.0 (1.6)
$CMOD_{cts}^{360}$	415.4	421.5	427.3	421.4 (1.4)
$CMOD_{cts}^{390}$	421.0	425.2	430.2	425.5 (1.1)

Table F.7. OC2 delayed experimental results of Series C.

Parameter	Serie C			
	C4-F2	C3-F3	C2-F2	Mean (CV)
$CMOD_{ci}$	171.3	178.5	140.6	163.4 (12.3)
$CMOD_{cts}^{14}$	321.3	331.5	256.1	303.0 (13.5)
$CMOD_{cts}^{30}$	353.3	373.0	281.1	335.8 (14.4)
$CMOD_{cts}^{60}$	396.9	413.6	316.3	375.6 (13.8)
$CMOD_{cts}^{90}$	419.4	432.5	332.1	394.7 (13.8)
$CMOD_{cts}^{120}$	442.0	455.9	350.4	416.1 (13.8)
$CMOD_{cts}^{150}$	449.8	467.4	358.9	425.4 (13.7)
$CMOD_{cts}^{180}$	461.5	481.2	368.9	437.2 (13.7)
$CMOD_{cts}^{210}$	468.5	489.8	375.0	444.4 (13.7)
$CMOD_{cts}^{240}$	473.1	497.6	378.0	449.6 (14.0)
$CMOD_{cts}^{270}$	484.8	512.5	388.5	461.9 (14.1)
$CMOD_{cts}^{300}$	503.5	532.6	400.2	478.8 (14.5)
$CMOD_{cts}^{330}$	523.7	558.1	412.0	497.9 (15.3)
$CMOD_{cts}^{360}$	537.0	569.6	423.3	510.0 (15.1)
$CMOD_{cts}^{390}$	544.8	576.4	428.9	516.7 (15.0)

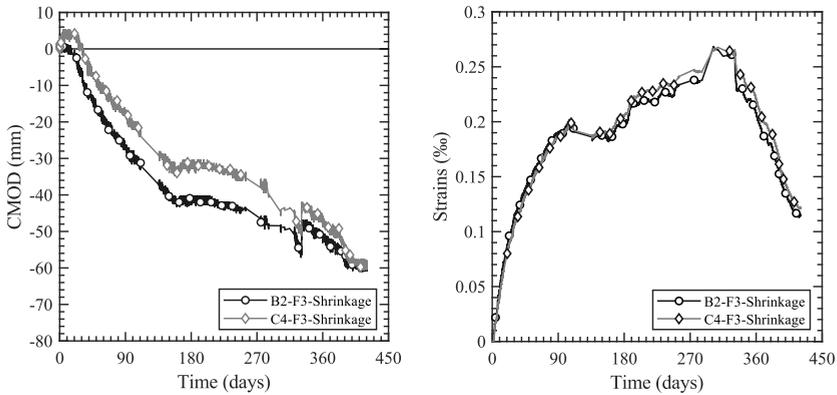The shrinkage flexure test results are presented in Figure F.4.

Figure F.4. OC2 shrinkage flexure specimens.

The temperature and relative humidity in the climate room where the OC2 long-term tests were conducted are depicted in Figure F.5.
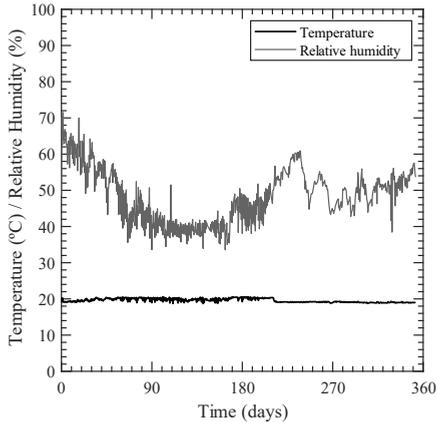

Figure F.5. Environmental conditions during OC2 long-term test.

F.3. Post-creep stage

Post-creep flexure tests followed the same flexure setup as pre-cracking tests. The assembled complete creep test curves are presented in Figure F.6. The post-creep residual strengths are collected in Table F.8.
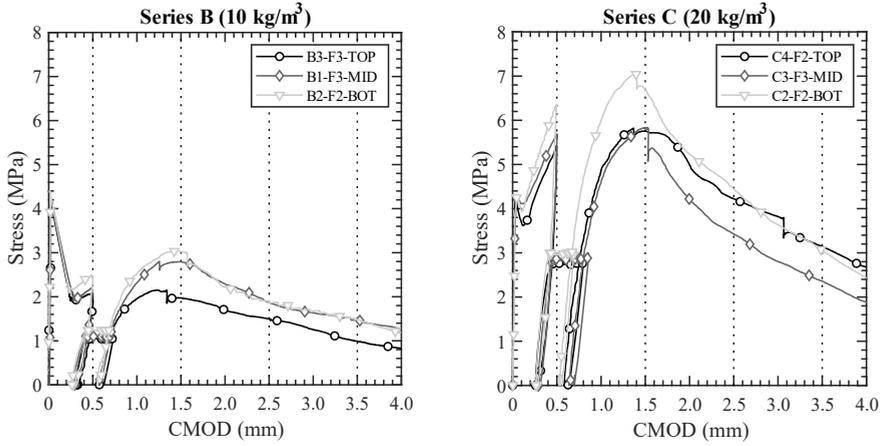
Figure F.6. OC2 post-creep test results.

Table F.8. OC2 post-creep performance.

Series	Specimen	f_L (MPa)	$f_{R,1}$ (MPa)	$f_{Post-creepR,2}$ (MPa)	$f_{Post-creep,R,3}$ (MPa)	$f_{Post-creep,R,4}$ (MPa)
B	B3-F3	4.08	2.10	2.00	1.52	1.01
	B1-F3	4.21	2.19	2.83	1.91	1.49
	B2-F2	4.32	2.43	3.07	1.93	1.53
	Average	4.20	2.24	2.63	1.79	1.34
C	C4-F2	4.28	5.45	5.82	4.30	3.21
	C3-F3	4.19	5.72	5.90	3.50	2.42
	C2-F2	4.36	6.35	6.82	4.55	3.15
	Average	4.28	5.84	6.18	4.12	2.92

Appendix G:
NAE2 creep experimental programme and results

The NAE2 experimental programme is focused on assessing the neutral axis evolution (NAE) considering one SyFRC and one SFRC matrix. Five LVDTs and one strain gauge were mounted, as defined in Figure 113, to determine the NAE during both monotonic and long-term test. The concrete matrix composition is presented in Table G.1.

Table G.1. NAE2 concrete matrix composition in kg/m³.

Component	SyFRC	SFRC
Cement CEM I 42.5 R	350	350
Water, w/c = 0.50	175	175
Aggregate 1 (12/20)	118	118
Aggregate 2 (6/12)	591	591
Sand 1	482	482
Sand 2	482	482
Sand 3	168	168
Superplasticizer	4.66	2.5
Fibres	10	30

G.1. FRC matrix characterisation tests results

Characterisation flexure tests were conducted in a 3-point bending test (3PBT) setup with a 500 mm support span until 4.0 mm CMOD to obtain the residual stresses defined in EN 14651. The characterisation tests Stress-CMOD curves are presented in Figure G.1 and the residual stress values are collected in Table G.2.
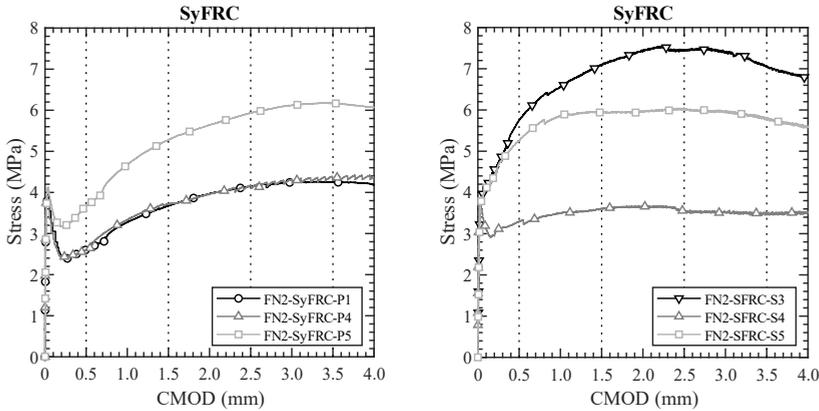
Figure G.1. NAE2 characterisation tests experimental curves.

Table G.2. NAE2 characterization test results.

Mix	f_{ck}	Specimen	f_L	$f_{R,1}$	$f_{R,2}$	$f_{R,3}$	$f_{R,4}$
	(MPa)		(MPa)	(MPa)	(MPa)	(MPa)	(MPa)
SyFRC	54.5	FN2-P1	4.00	2.61	3.67	4.15	4.26
		FN2-P4	3.92	2.60	3.72	4.17	4.30
		FN2-P5	4.12	3.67	5.28	5.93	6.17
		Average	4.02	2.96	4.22	4.75	4.91
SFRC	50.7	FN2-S3	3.89	5.75	7.08	7.45	7.04
		FN2-S4	3.70	3.29	3.61	3.56	3.52
		FN2-S5	3.83	5.26	5.95	6.01	5.82
		Average	3.81	4.77	5.55	5.67	5.46

G.2. Pre-cracking stage

Specimens were pre-cracked in a 4-point bending test (4PBT) setup with a 450 mm support span until 0.5 mm $CMOD_p$ and then unloaded. Five LVDTs and one strain gauge were used to determine the NA position, as defined in Figure 113. Delayed recovery deformations after the unloading process were recorded for 15 minutes. After the pre-cracking tests, LVDTs were not removed, and specimens were moved to the creep frames with the transducers.

Figure G.2 presents the pre-cracking test Stress-CTOD curves for each SyFRC specimen, whereas Figure G.3 presents the SFRC specimens. Table G.3 collects the residual strength experimentally obtained and the average values for each mix.
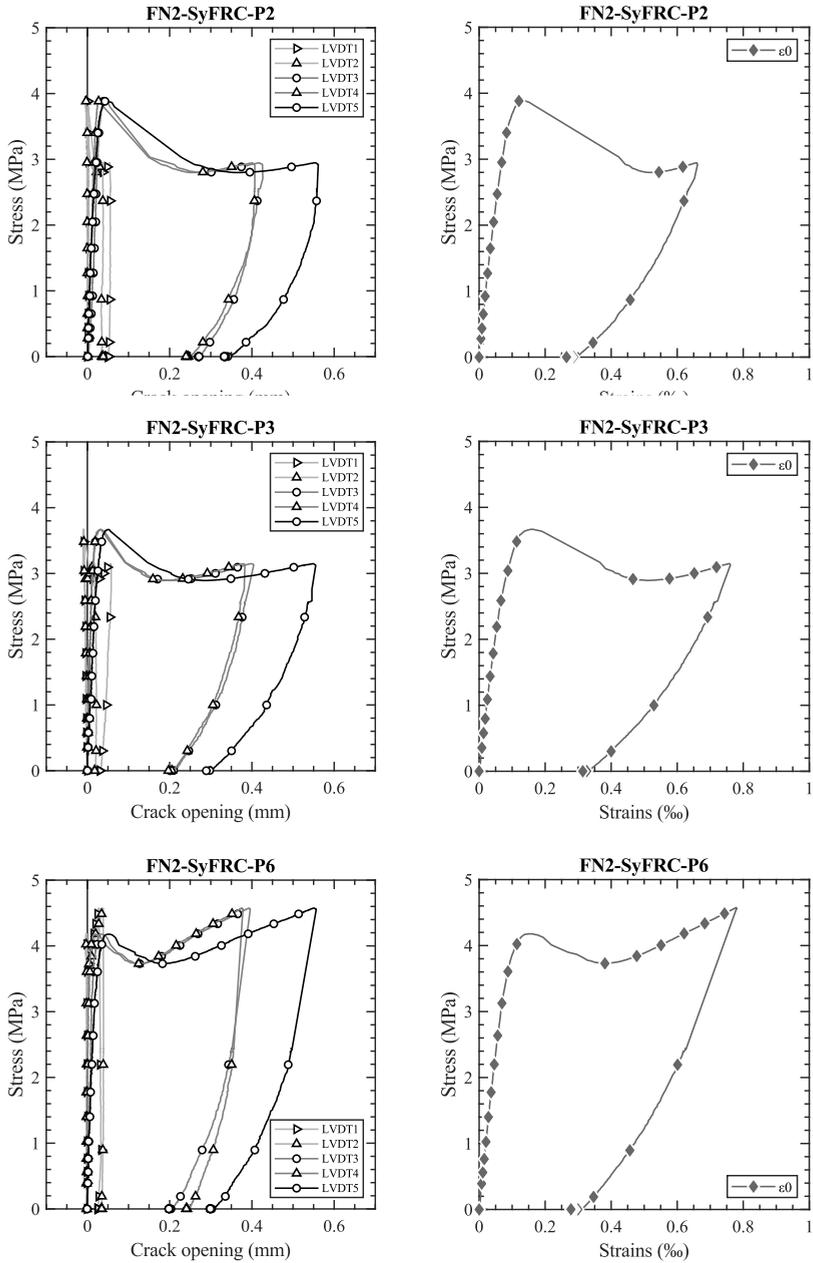
Figure G.2. Stress-CMOD and Stress-strains curves of SyFRC specimens of NAE2 pre-cracking tests.
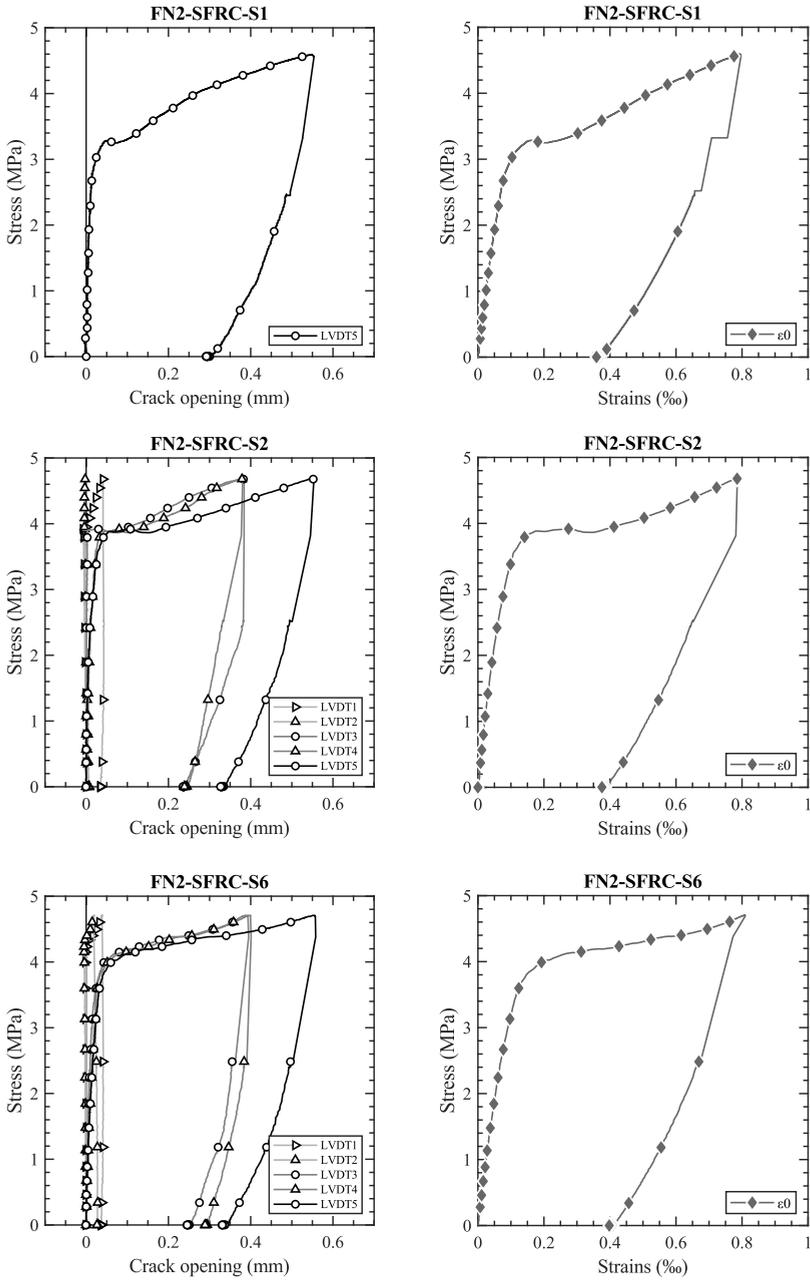
Figure G.3. Stress-CMOD and Stress-strains curves of SFRC specimens of NAE2 pre-cracking tests.

Table G.3. NAE2 pre-cracking tests experimental results.

Mix	Specimen	f_L (MPa)	$f_{R,1}$ (MPa)	$CMOD_p$ (µm)	$CMOD_{pri}$ (µm)	$CMOD_{prd}$ (µm)
SyFRC	FN2-P2	3.89	2.94	511.1	308.8	302.6
	FN2-P3	3.67	3.15	504.7	268.2	255.0
	FN2-P6	4.18	4.57	506.9	275.7	271.0
	Average	3.91	3.55	507.6	284.2	276.2
SFRC	FN2-S1	3.29	4.59	503.7	272.8	265.0
	FN2-S2	3.88	4.69	503.4	301.7	297.9
	FN2-S6	3.95	4.71	507.9	306.0	301.3
	Average	3.71	4.66	505.0	293.5	288.1

G.3. Creep stage

Creep tests were carried out in a single-specimen setup using the 4PBT setup with a 450 mm support span due to the presence of a strain gauge centred in the top face of the specimen. The same five LVDTs and the strain gauge used in the pre-cracking tests are used now to determine the NA position during creep stage. The applied stress ($f_{R,c}$) represented a 50% creep index of the residual strength at pre-cracking tests ($f_{R,p}$). One shrinkage flexure specimen per mix was tested simultaneously. The long-term test duration was 540 days. Specimens were unloaded and delayed recovery deformations were recorded for 20 days. The distribution of the specimens in the creep frames is provided in Table G.4.

Table G.4. NAE-2 distribution of specimens on the creep frames.

Position	Frame				Shrinkage	
	F1	F2	F3	F4	S1	S2
Top	FN2-P2	FN2-P3	FN2-S2	FN2-S6	FN2-P6	FN2-S1
I_n (% of $f_{R,1}$)	50	50	50	50	0	0
$F_{R,c}$ (4PBT)	7.60	8.06	12.30	12.27	-	-

Delayed CMOD and compressive strains deformation curves are depicted in Figure G.4. Table G.5
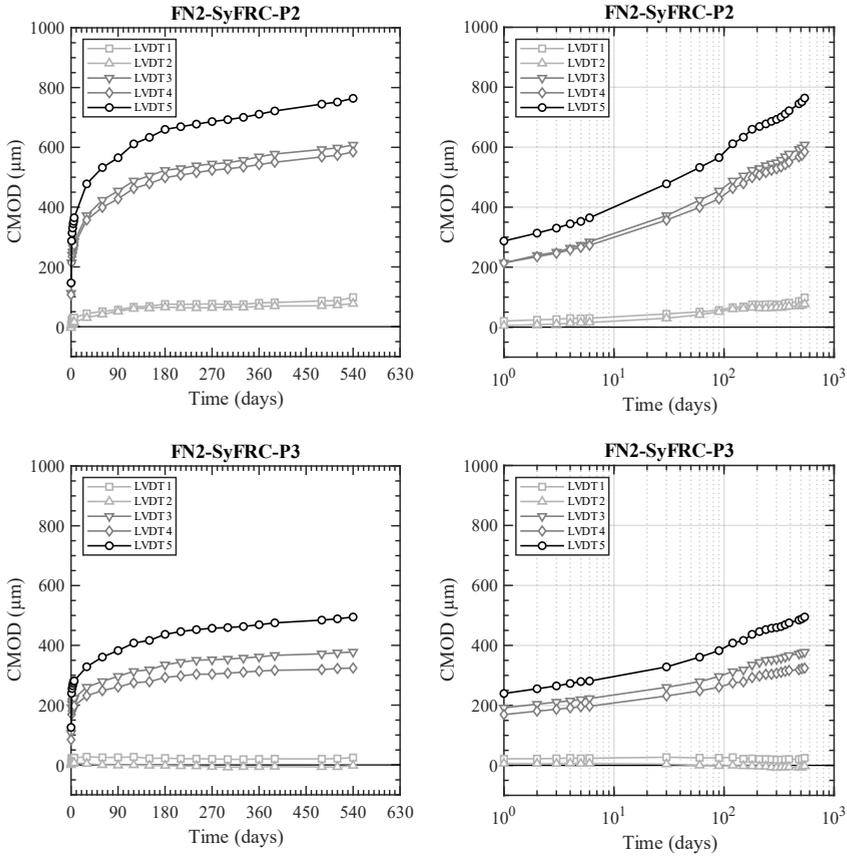
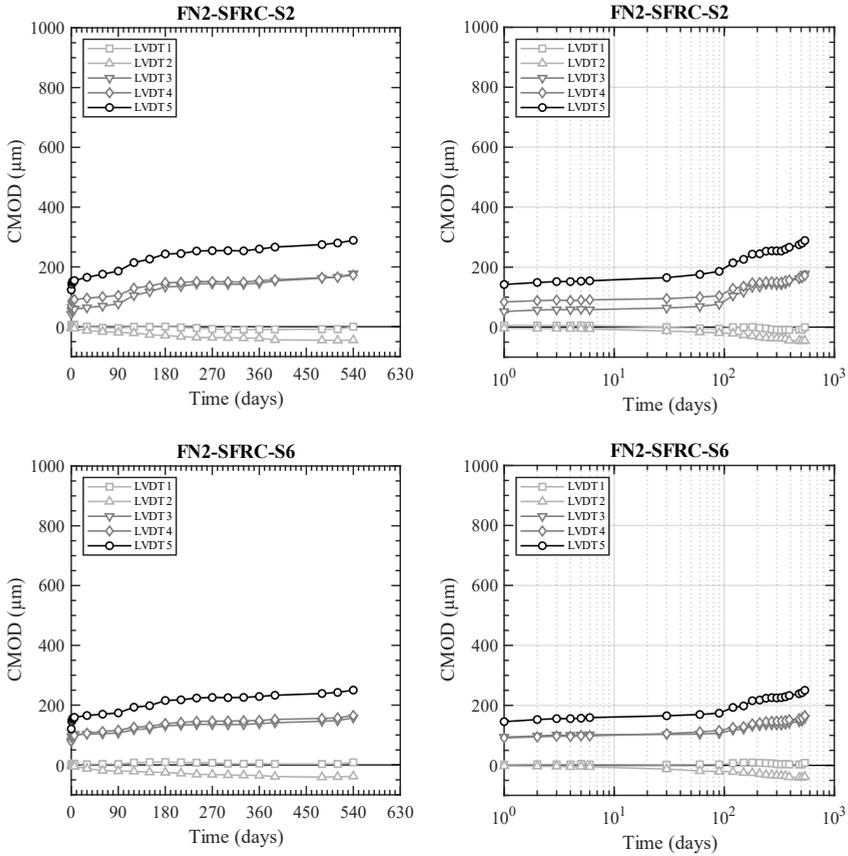**Figure G.4. Delayed CMOD of SyFRC specimens from NAE2.**

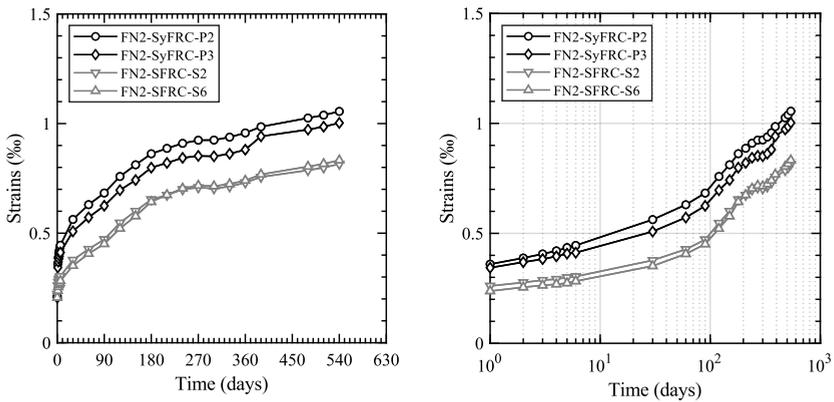**Figure G.5. Delayed CMOD of SFRC specimens from NAE2.**

Figure G.6. Delayed strains long-term experimental results of NAE2.

Table G.5. NAE3 long-term experimental results.

Parameter	Specimen			
	FN2-P2	FN2-P3	FN2-S2	FN2-S6
$CMOD_{ci}$	133.2	114.1	112.1	109.7
$CMOD_{cts}^{1}$	261.1	217.8	129.3	132.6
$CMOD_{cts}^{2}$	285.1	232.2	135.4	139.2
$CMOD_{cts}^{3}$	300.3	240.8	138.1	141.8
$CMOD_{cts}^{5}$	320.6	254.0	139.3	143.1
$CMOD_{cts}^{7}$	340.1	-	143.6	145.7
$CMOD_{cts}^{14}$	-	-	-	-
$CMOD_{cts}^{30}$	434.4	298.5	150.1	150.4
$CMOD_{cts}^{60}$	484.2	328.1	159.8	154.4
$CMOD_{cts}^{90}$	514.0	347.8	169.2	158.3
$CMOD_{cts}^{120}$	556.0	370.8	194.9	175.7
$CMOD_{cts}^{150}$	576.0	378.6	205.5	180.3
$CMOD_{cts}^{180}$	600.1	397.1	221.2	196.2
$CMOD_{cts}^{210}$	608.5	405.5	222.4	198.2
$CMOD_{cts}^{240}$	616.3	411.5	230.2	203.7
$CMOD_{cts}^{270}$	624.1	415.6	231.1	205.4
$CMOD_{cts}^{300}$	629.9	417.8	231.3	204.7
$CMOD_{cts}^{330}$	636.9	420.9	230.5	205.5
$CMOD_{cts}^{360}$	646.5	426.4	236.2	208.2
$CMOD_{cts}^{390}$	656.4	432.0	242.1	212.1
$CMOD_{cts}^{410}$	664.9	435.9	246.0	216.0
$CMOD_{cts}^{450}$	-	-	-	-
$CMOD_{cts}^{480}$	677.2	440.4	249.7	217.4
$CMOD_{cts}^{510}$	683.5	444.3	254.6	220.6
$CMOD_{cts}^{540}$	694.6	450.7	262.0	227.4
$CMOD_{cri}$	514.9	284.7	146.3	121.7
$CMOD_{crd}^{1}$	485.6	257.8	142.0	118.9
$CMOD_{crd}^{7}$	467.5	241.8	138.5	114.7
$CMOD_{crd}^{14}$	461.3	235.2	135.8	112.1
$CMOD_{crd}^{20}$	459.7	232.3	135.2	110.7

The shrinkage flexure test results are presented in Figure G.7.
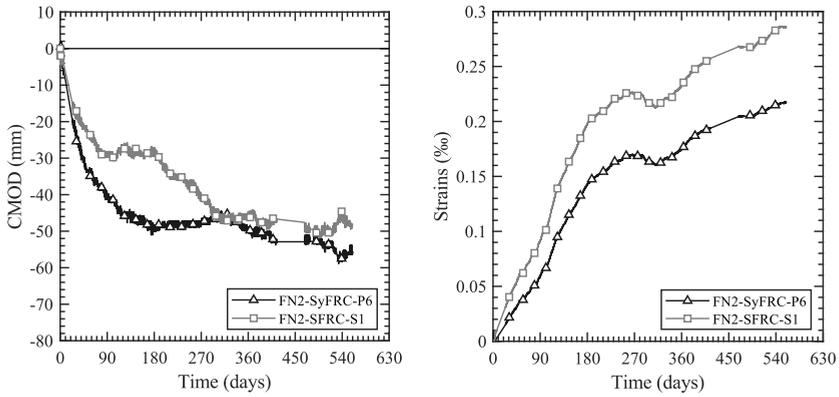
Figure G.7. Shrinkage experimental results of NAE2.

The temperature and relative humidity in the climate room where the NAE2 long-term tests were conducted are depicted in Figure G.8.
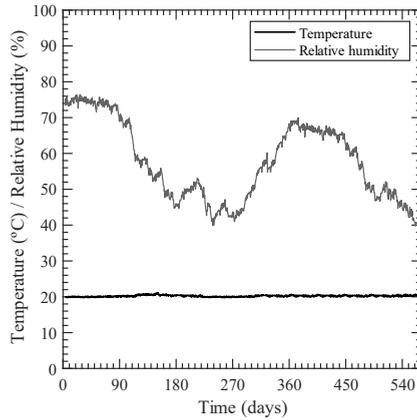

Figure G.8. Environmental conditions during NAE2 long-term test.

Appendix H:
NAE3 creep experimental programme and results

The NAE3 experimental programme focused on assessing the neutral axis evolution (NAE) considering one SyFRC and one SFRC matrix reinforced with 10 and 30 kg/m^3 of fibres, respectively. Five LVDTs were mounted, as defined in Figure 113. The concrete matrix composition is presented in Table H.1. Fibres properties are described in Table H.2.

Table H.1. NAE3 concrete matrix composition in kg/m^3.

Component	SyFRC	SFRC
Cement CEM I 42.5 R	280	280
Water, w/c = 0.50	175	175
Aggregate 1 (16/20)	183	183
Aggregate 2 (8/16)	415	415
Aggregate 2 (4/8)	146	146
Sand 1	895	895
Sand 2	211	211
Superplasticizer	4.2	3.36
Fibres	10	30

Table H.2. Fibre properties and dosage of NAE3 experimental programme.

Mix	Fibre			Dosage
	Brand	Length	Diameter	(kg/m^3)
SyFRC	Masterfiber 249	48	0.85	10
SFRC	HE 90-60	60	0.90	30

H.1. FRC matrix characterisation tests results

Characterisation flexure tests were conducted in a 3-point bending test (3PBT) setup with a 500 mm clear support span until 4.0 mm CMOD. One LVDT was mounted at the bottom face of the specimen to record CMOD deformations. Figure H.1 depicts the characterisation Stress-CMOD curves and Table H.3 collects the residual stress values.
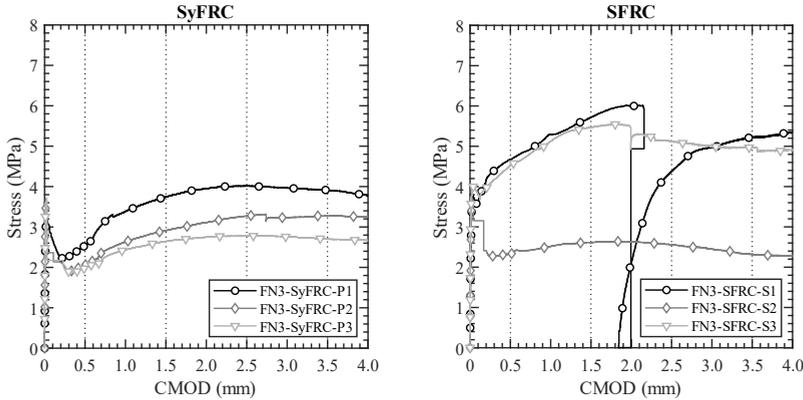

Figure H.1. NAE3 characterisation tests experimental curves.

Table H.3. NAE3 characterization test results.

Mix	f_{ck}	Specimen	f_L	$f_{R,1}$	$f_{R,2}$	$f_{R,3}$	$f_{R,4}$
	(MPa)		(MPa)	(MPa)	(MPa)	(MPa)	(MPa)
SyFRC	42.6	FN3-P1	3.18	2.55	3.74	4.01	3.91
		FN3-P2	3.56	2.06	2.91	3.27	3.27
		FN3-P3	3.70	1.98	2.65	2.78	2.70
		Average	3.48	2.20	3.10	3.35	3.30
SFRC	43.9	FN3-S1	3.78	4.67	5.72	-	5.21
		FN3-S2	3.70	2.33	2.61	2.56	2.32
		FN3-S3	4.03	4.53	5.47	5.11	4.96
		Average	3.84	3.84	4.60	3.83	4.16

H.2. Pre-cracking stage

Specimens were pre-cracked using a 3PBT setup with a 500 mm support span until 0.5 mm $CMOD_p$. and then unloaded. The strain gauge was not used in pre-cracking tests to allow the 3PBT setup. Five LVDTs were used to determine the NA position during monotonic pre-cracking tests, as defined in Figure 113. Delayed recovery deformations were recorded for 15 minutes. After the pre-cracking tests, LVDTs were not removed, and specimens were moved to the creep frames with the transducers. Figure H.2 presents the Stress-CMOD curves for each specimen and Table H.4 collects the residual strengths.
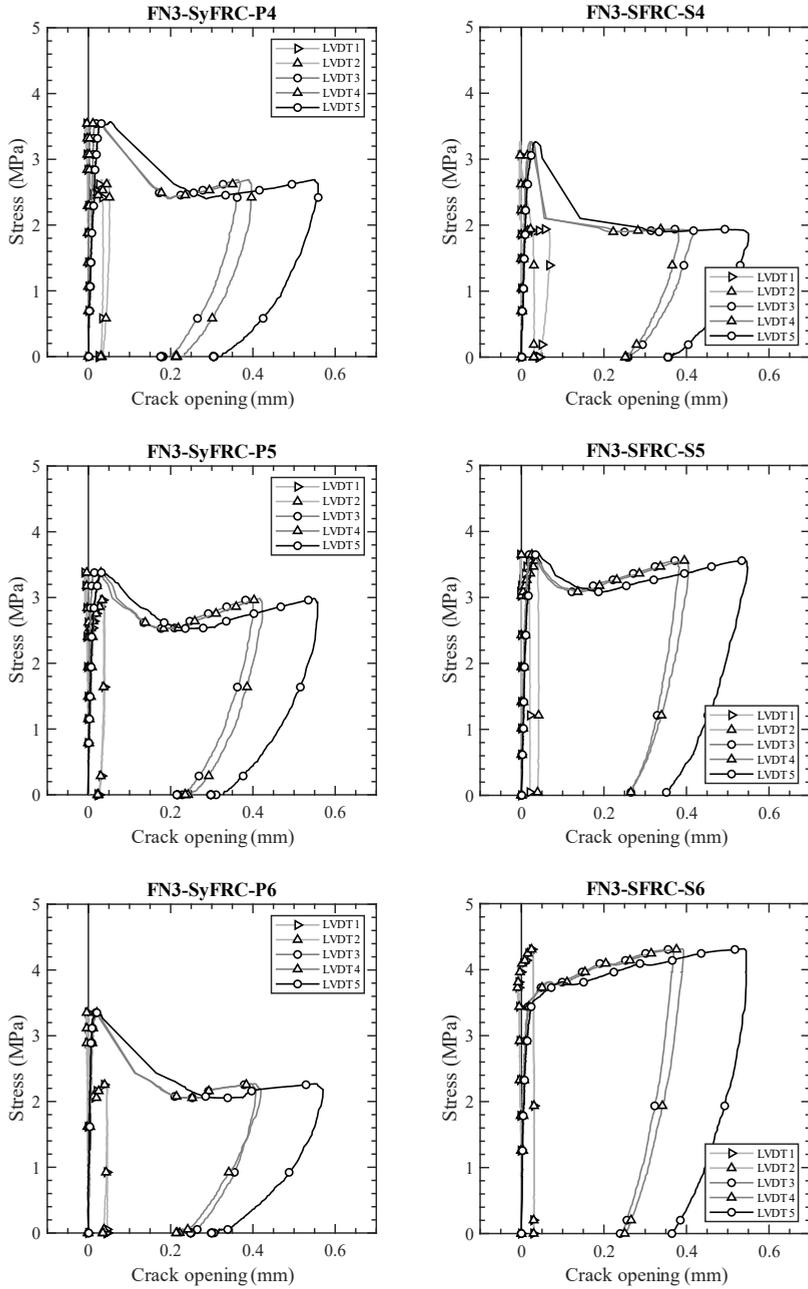
Figure H.2. Stress-CMOD and Stress-strains curves of NAE3 pre-cracking tests: SyFRC (left column) and SFRC (right column).

Table H.4. NAE3 pre-cracking tests experimental results.

Mix	Specimen	f_L (MPa)	$f_{R,1}$ (MPa)	$CMOD_p$ (μm)	$CMOD_{pri}$ (μm)	$CMOD_{prd}$ (μm)
SyFRC	FN3-P4	3.57	2.69	508.5	294.4	277.2
	FN3-P5	3.39	2.99	507.9	298.4	268.9
	FN3-P6	3.37	2.27	520.6	289.9	271.3
	Average	3.44	2.65	512.3	294.2	272.4
SFRC	FN3-S4	3.26	1.88	500.9	329.3	324.4
	FN3-S5	3.68	3.46	499.4	313.1	306.9
	FN3-S6	3.66	4.29	496.1	336.0	332.5
	Average	3.54	3.21	498.8	326.1	321.3

H.3. Creep stage

After the pre-cracking tests, one strain gauge was mounted on the top face of each specimen to monitor the compressive strain evolution during the creep tests. Creep tests were carried out in a single-specimen setup using the 4-point bending test (4PBT) setup with a 450 mm support span due to the strain gauge centred in the top face. The distribution of the specimens in the creep frames is provided in Table H.5. The same five LVDTs and the strain gauge used in the pre-cracking tests are used now to determine the NA position during creep stage. The applied stress ($f_{R,c}$) represented a creep index of 50% of the residual strength at pre-cracking tests ($f_{R,p}$). One shrinkage flexure specimen per mix was tested simultaneously. The long-term tests of the NAE experimental programme are still ongoing. The delayed results until 270 days are included in this PhD thesis.

Table H.5. NAE-3 distribution of specimens on the creep frames.

Position	Frame				Shrinkage	
	F1	F2	F3	F4	S1	S2
Top	FN3-P4	FN3-P5	FN3-S5	FN3-S6	FN3-P6	FN3-S4
I_n (% of $f_{R,1}$)	50	50	50	50	0	0
$F_{R,c}$ (4PBT)	7.48	8.27	9.55	11.49	-	-

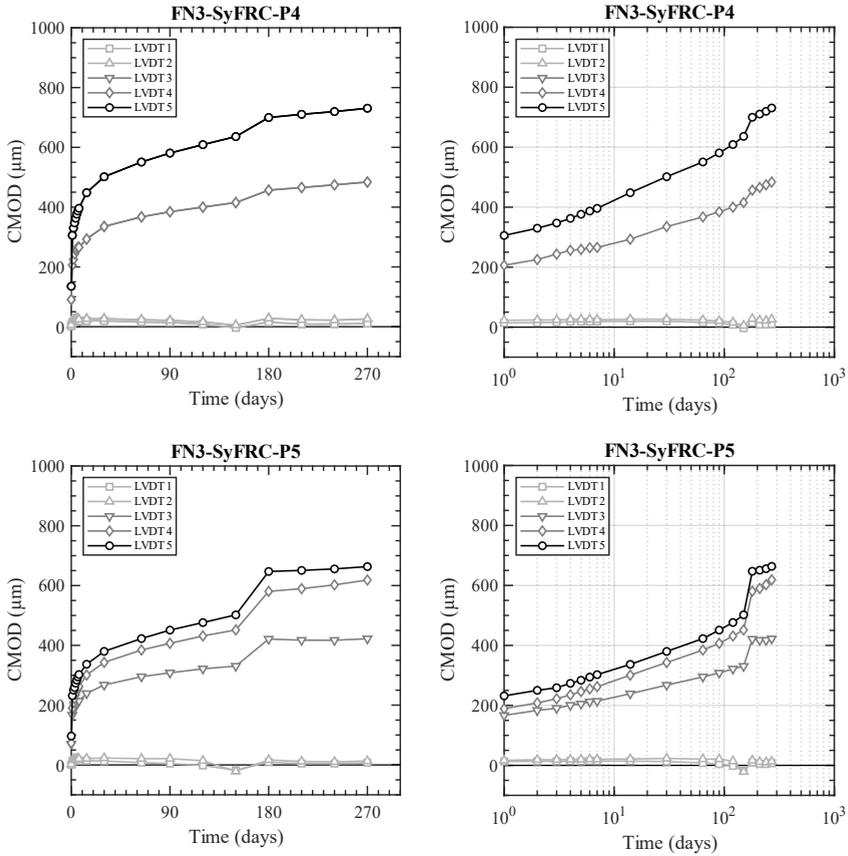Delayed CMOD and compressive strain deformation curves are depicted in Figure H.3.

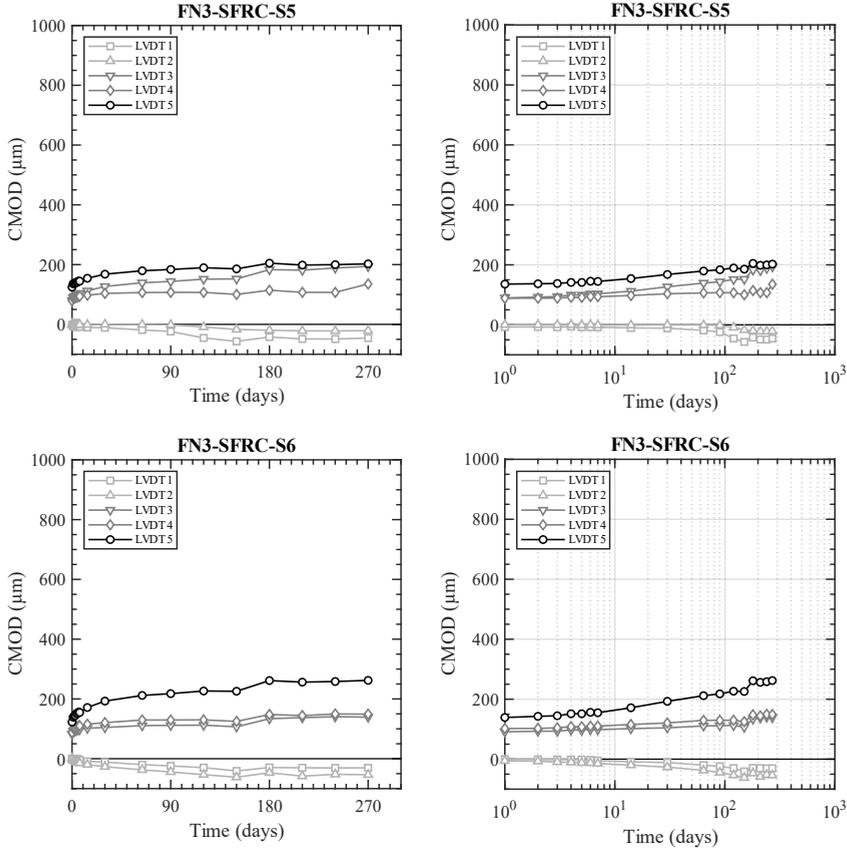**Figure H.3. NAE-3 delayed deformations in creep tests.**

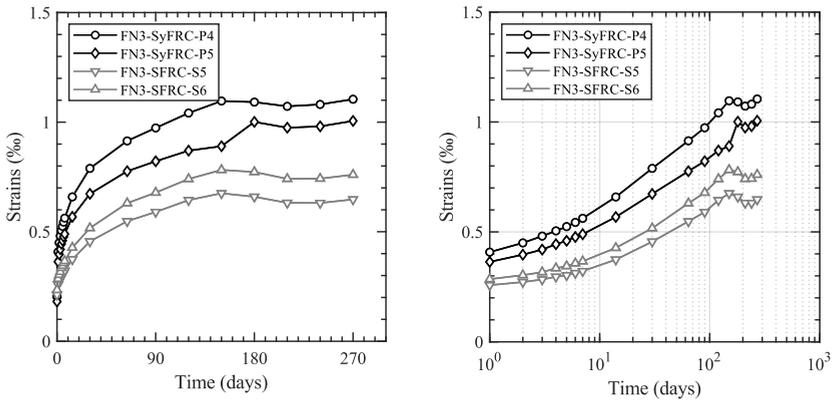**Figure H.4. NAE-3 delayed deformations in creep tests.**

Figure H.5. Delayed strains long-term experimental results of NAE3.

Table H.6. NAE3 long-term experimental results.

Parameter	Specimen			
	FN3-P4	FN3-P5	FN3-S5	FN3-S6
$CMOD_{ci}$	123.1	87.9	113.6	111.8
$CMOD_{cts}^{1}$	278.2	211.0	123.7	126.6
$CMOD_{cts}^{2}$	300.3	227.7	124.8	130.1
$CMOD_{cts}^{3}$	316.0	235.6	125.7	131.8
$CMOD_{cts}^{5}$	342.6	258.3	128.8	137.9
$CMOD_{cts}^{7}$	360.5	275.3	131.8	141.0
$CMOD_{cts}^{14}$	408.1	306.6	140.5	156.0
$CMOD_{cts}^{30}$	456.6	345.8	153.0	175.6
$CMOD_{cts}^{60}$	501.4	384.9	163.4	192.8
$CMOD_{cts}^{90}$	528.7	410.6	167.3	198.3
$CMOD_{cts}^{120}$	554.3	433.7	172.7	206.4
$CMOD_{cts}^{150}$	578.9	457.0	169.1	205.5
$CMOD_{cts}^{180}$	637.0	589.3	186.6	238.1
$CMOD_{cts}^{210}$	646.7	592.5	180.8	233.3
$CMOD_{cts}^{240}$	655.1	597.0	182.1	235.3
$CMOD_{cts}^{270}$	665.2	604.1	184.4	238.7

The shrinkage flexure test results of both the crack opening and compressive strains deformations are presented in Figure H.6.
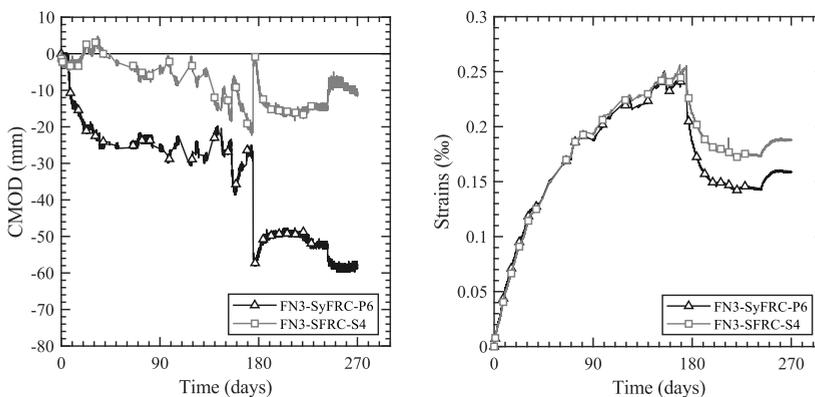

Figure H.6. Shrinkage experimental results of NAE3.

The temperature and relative humidity in the climate room where the NAE3 long-term tests were conducted are depicted in Figure H.7.
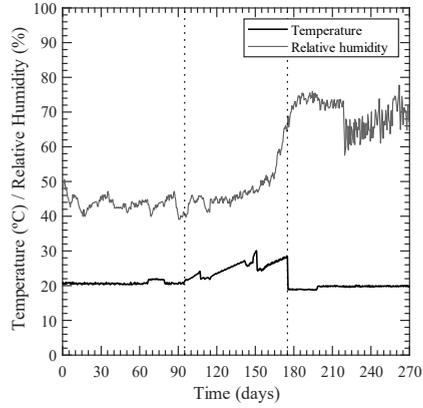

Figure H.7. Environmental conditions during NAE3 long-term test.

List of Publications

Articles in internationally peer-reviewed scientific journals

1. Llano-Torre, A.; Serna, P. Recommendation of RILEM TC 261-CCF: test method to determine the flexural creep of fibre reinforced concrete in the cracked state. Mater. Struct. 2021, 54, 124. DOI: 10.1617/s11527-021-01675-0

2. Monetti, D.H.; Llano-Torre, A.; Torrijos, M.C.; Giaccio, G.; Zerbino, R.; Martí-Vargas, J.R.; Serna, P. Long-term behavior of cracked fiber reinforced concrete under service conditions. Constr. Build. Mater. 2019, 196, 649–658. DOI: 10.1016/j.conbuildmat.2018.10.230

3. Llano-Torre, A.; Martí-Vargas, J.R.; Serna, P. Flexural and compressive creep behavior of UHPFRC specimens. Constr. Build. Mater. 2020, 244, 118254. DOI: 10.1016/j.conbuildmat.2020.118254

Articles presented at international conferences and symposia

1. Llano-Torre, A.; Serna, P.; Cavalaro, S.H.P. International Round-Robin Test on Creep Behaviour of FRC - Part 2: An Overview of Results and Preliminary Conclusions. In: Serna, P., Llano-Torre, A., Martí-Vargas, J.R., Navarro-Gregori, J. (eds) Fibre Reinforced Concrete: Improvements and Innovations II (BEFIB 2021). RILEM Bookseries, vol 36. Springer, 2022. DOI: 10.1007/978-3-030-83719-8_26

2. Llano-Torre, A.; López, J.A.; Martí-Vargas, J.R.; Serna, P. Comportamiento diferido en estado fisurado de elementos de UHPFRC a flexotracción. In: Proceedings of the V Congreso Iberoamericano de Hormigón Autocompactante y Hormigones Especiales HAC2018. Valencia, Spain, 2018, 361-372. (in Spanish) DOI: 10.4995/HAC2018.2018.6144

3. Llano-Torre, A.; Serna, P.; Zerbino, R.; Martí-Vargas, J.R. Effect of initial crack opening on flexural creep behavior of FRC specimens. In: RILEM Proceedings PRO 116 - 9th RILEM International Symposium on Fiber Reinforced Concrete: The Modern Landscape, BEFIB 2016. Vancouver, 2016, 117–126.

4. Llano-Torre, A.; Serna, P.; López, J.A. Flexural and compressive long term behaviour of UHPFRC Specimens. In: RILEM Proceedings PRO 116 - 9th RILEM International Symposium on Fiber Reinforced Concrete: The Modern Landscape, BEFIB 2016. Vancouver, Canada, 2016, 141–152

5. Llano-Torre, A.; Serna, P.; Cavalaro, S.H.P. International Round Robin Test on creep behavior of FRC supported by the RILEM TC 261-CCF. In: RILEM Proceedings PRO 116 - 9th RILEM International Symposium on Fiber Reinforced Concrete: The Modern Landscape, BEFIB 2016. Vancouver, Canada, 2016, 127-140.

6. Serna, S.; Serna Ros, P.; Pelufo Carbonell, M.J.; Orero, V.; Llano-Torre, A. Shotcrete reinforced with recycled fibers from secondary waste of end of life tires. In: Second International Conference on Concrete Sustainability (ICCS 16). Madrid, 2016, 212-222. ISSN 978-84-945077-7-9

7. Serna, P.; Llano-Torre, A.; Garcia-Taengua, E.; Marti-Vargas, J.R. Database on the Long-Term Behaviour of FRC: A Useful Tool to Achieve Overall Conclusions. In: Proceedings of the 10th International Conference on Mechanics and Physics of Creep, Shrinkage, and Durability of Concrete and Concrete Structures, Vienna, 2015, 1544-1553.

8. Gayarre, F. L.; Blanco Viñuela, R.; Serna Ros, P.; Llano Torre, A.; Lopez-Colina, C. Influence of Mixed Recycled Aggregates on deformational properties of concrete used in precast prestressed components. In: Proceedings of the International Conference on Sustainable Structural Concrete, La Plata, Argentina, 2015, 204-213. ISBN 978-987-3838-02-6

9. Llano-Torre, A.; Garcia-Taengua, E.; Marti-Vargas, J.R.; Serna, P. Compilation and study of a database of tests and results on flexural creep behaviour of fibre reinforced concrete specimens. Proceedings of the FIB Symposium Concrete Innovation and Design, Copenhagen, 2015.

10. Gayarre, F.L.; Blanco Viñuela, R.; Serna, P.; Lopez-Colina, C.; Llano-Torre, A. Deformation properties of Recycled Concrete with Mixed Recycled Aggregates, Focused On Precast Prestressed Products. In: Proceedings of the 30th International Conference on Solid Waste Technology and Management, Philadelphia, PA, USA. 2015, 712-721. ISBN/ISSN: 1091-8043

Book chapters

1. Llano-Torre, A.; Serna, P.; Cavalaro, S.H.; Buratti, N.; Bernard, E.S.; Boshoff, W.P.; Zerbino, R.L.; Pauwels, H.; Kusterle, W.; Garcia-Taengua, E.; Vrijdaghs, R.; del Prete, C.; dos Santos, K.F.; Parmentier, B.; Mazzotti, C. Statements and Conclusions. In: Llano-Torre, A., Serna, P. (eds) Round-Robin Test on Creep Behaviour in Cracked Sections of FRC: Experimental Program, Results and Database Analysis. RILEM State-of-the-Art Reports, vol 34. Springer, 2021. DOI: 10.1007/978-3-030-72736-9_9

2. Llano-Torre, A.; Serna, P.; Garcia-Taengua, E.; Vrijdaghs, R.; Pauwels, H.; del Prete, C.; Buratti, N.; Zerbino, R.L.; Kusterle, W.; Bernard, E.S. Analysis of the RRT Results. In: Llano-Torre, A., Serna, P. (eds) Round-Robin Test on Creep Behaviour in Cracked Sections of FRC: Experimental Program, Results and Database Analysis. RILEM State-of-the-Art Reports, vol 34. Springer, 2021. https://doi.org/10.1007/978-3-030-72736-9_8

3. Llano-Torre, A.; Serna, P. Round-Robin Test Results. In: Llano-Torre, A., Serna, P. (eds) Round-Robin Test on Creep Behaviour in Cracked Sections of FRC: Experimental Program, Results and Database Analysis. RILEM State-of-the-Art Reports, vol 34. Springer, 2021. DOI: 10.1007/978-3-030-72736-9_7

4. Llano-Torre, A.; Serna, P.; Cavalaro, S.H.P. Data and Parameter Definition. In: Llano-Torre, A., Serna, P. (eds) Round-Robin Test on Creep Behaviour in Cracked Sections of FRC: Experimental Program, Results and Database Analysis. RILEM State-of-the-Art Reports, vol 34. Springer, 2021. 10.1007/978-3-030-72736-9_6

5. Llano-Torre, A.; Cavalaro, S.H.; Kusterle, W.; Moro, S.; Zerbino, R.L.; Gettu, R.; Pauwels, H.; Nishiwaki, T.; Parmentier, B.; Buratti, N.; Toledo Filho, R.D.; Charron, J-P.; Larive, C.; Boshoff, W.P.; Bernard, E.S.; Kompatscher, M. Equipment and Procedure Description. In: Llano-Torre, A., Serna, P. (eds) Round-Robin Test on Creep Behaviour in Cracked Sections of FRC: Experimental Program, Results and Database Analysis. RILEM State-of-the-Art Reports, vol 34. Springer, 2021. DOI: 10.1007/978-3-030-72736-9_5

6. Llano-Torre, A.; Serna, P.; Boshoff, W.P.; Buratti, N.; dos Santos, K.F.; Bernard, E.S. General Procedure of Creep Test. In: Llano-Torre, A., Serna, P. (eds) Round-Robin Test on Creep Behaviour in Cracked Sections of FRC: Experimental Program, Results and Database Analysis. RILEM State-of-the-Art Reports, vol 34. Springer, 2021. DOI: 10.1007/978-3-030-72736-9_4

7. Llano-Torre, A.; Serna, P. Fibre Reinforced Concrete Characterization. In: Llano-Torre, A., Serna, P. (eds) Round-Robin Test on Creep Behaviour in Cracked Sections of FRC: Experimental Program, Results and Database Analysis. RILEM State-of-the-Art Reports, vol 34. Springer, 2021. DOI: 10.1007/978-3-030-72736-9_3

8. Llano-Torre, A.; Serna, P.; Cavalaro, S.H.P. Round-Robin Test Program and Execution. In: Llano-Torre, A., Serna, P. (eds) Round-Robin Test on Creep Behaviour in Cracked Sections of FRC: Experimental Program, Results and Database Analysis. RILEM State-of-the-Art Reports, vol 34. Springer, 2021. DOI: 10.1007/978-3-030-72736-9_2

9. Llano-Torre, A.; Serna, P.; Cavalaro, S.H.; Buratti, N.; Bernard, E.S.; Boshoff, W.P.; Zerbino, R.L.; Pauwels, H.; Kusterle, W.; Garcia-Taengua, E.; Vrijdaghs, R.; del Prete, C.; dos Santos, K.F.; Parmentier, B.; Mazzotti, C. Introduction and Background. In: Llano-Torre, A., Serna, P. (eds) Round-Robin Test on Creep Behaviour in Cracked Sections of FRC: Experimental Program, Results and Database Analysis. RILEM State-of-the-Art Reports, vol 34. Springer, 2021. DOI: 10.1007/978-3-030-72736-9_1

10. Llano-Torre A.; Arango, S.E.; García-Taengua, E.; Martí-Vargas, J.R.; Serna, P. Influence of Fibre Reinforcement on the Long-Term Behaviour of Cracked Concrete. In: Serna P., Llano-Torre A., Cavalaro S. (eds) Creep Behaviour in Cracked Sections of Fibre Reinforced Concrete: Proceedings of the International RILEM Workshop FRC-CREEP 2016. RILEM Bookseries, vol 14. Springer, Dordrecht, 2017. DOI: 10.1007/978-94-024-1001-3_16

11. Garcia-Taengua, E.; Llano-Torre, A.; Marti-Vargas, J.R.; Serna, P. Effect of Residual Strength Parameters on FRC Flexural Creep: Multivariate Analysis. In: Serna, P., Llano-Torre, A., Cavalaro, S. (eds) Creep Behaviour in Cracked Sections of Fibre Reinforced Concrete: Proceedings of the International RILEM Workshop FRC-CREEP 2016. RILEM Bookseries, vol 14. Springer, Dordrecht, 2017. DOI: 10.1007/978-94-024-1001-3_12

Edited books

1. Serna P.; Llano-Torre A.; Martí Vargas J.R.; Navarro-Gregori J. (eds) Fibre Reinforced Concrete: Improvements and Innovations II. RILEM Bookseries, 2022, vol 36. Springer, Dordrecht. DOI: 10.1007/978-3-030-83719-8

2. Llano-Torre A.; Serna P. (eds) Round-Robin test on creep behaviour in cracked sections of FRC: experimental program, results and database analysis. RILEM State-of-the-Art Reports. Springer. DOI: 10.1007/978-3-030-72736-9

3. Serna P.; Llano-Torre A.; Martí Vargas J.R.; Navarro-Gregori J. (eds) Fibre Reinforced Concrete: Improvements and Innovations. RILEM Bookseries, 2021, vol 30. Springer, Dordrecht. DOI: 10.1007/978-3-030-58482-5

4. Llano-Torre, A.; Martí-Vargas, J.R.; Serna Ros. P. (eds) V Congreso Iberoamericano de Hormigón Autocompactante y Hormigones Especiales

HAC2018: Libro de Comunicaciones. Editorial Universitat Politècnica de València, ISBN: 978-84-9048-591-0 DOI: 10.4995/HAC2018.2018.8274

5. Llano-Torre, A.; Serna, P.; Cavalaro, S.H.P. (eds) Creep Behaviour in Cracked Sections of Fibre Reinforced Concrete. Proceedings of the International RILEM Workshop FRC-CREEP 2016. ISBN: 978-94-024-1000-6 DOI: 10.1007/978-94-024-1001-3

Database

1. Llano-Torre, A.; Serna Ros, P.; Cavalaro, S.; Kusterle, W.; Moro, S.; Zerbino, R.L.; Gettu, R.; Pauwels H.; Nishiwaki T.; Parmentier B.; Buratti N.; Toledo Filho R.D.; Charron J.P.; Larive C.; Boshoff W.P.; Bernard, E.S.; Kompatscher M. Database of the Round-Robin Test on Creep Behaviour in Cracked Sections of Fibre Reinforced Concrete organised by the RILEM Technical Committee 261-CCF. 2021. DOI: 10.4995/Dataset/10251/163221

Master thesis

1. Llano Torre, A. Fluencia en estado fisurado de Hormigones Reforzados de Fibras (HRF). Aplicación a Hormigones de Muy Alto Rendimiento (HMAR) y Hormigones Reforzados con Fibras de Vidrio (GFRC). Universitat Politècnica de València, MSc tesis, 2010. DOI: 10251/51320

Awards

Achievement Award for Top-10 Most-Downloaded Articles in 2021 for the article "Recommendation of RILEM TC 261-CCF: test method to determine the flexural creep of fibre reinforced concrete in the cracked state", Materials and Structures (2021) 54:124 by A. Llano-Torre & P. Serna